

**TARGETING K-RAS, PAK-1, AND MCL-1
FOR THE TREATMENT OF CANCER**

by

Craig Matthew Goodwin

Dissertation

Submitted to the Faculty of the
Graduate School of Vanderbilt University
in partial fulfillment of the requirements
for the degree of

DOCTOR OF PHILOSOPHY

in

Pharmacology

December 2015

Nashville, Tennessee

Approved:

Carlos Arteaga, MD.

Stephen Fesik, Ph.D.

Craig Lindsley, Ph.D. (Chair)

Brian Wadzinski, Ph.D.

David Weaver, Ph.D.

To Megan, my loving wife,
Matthew, my precocious son,
And my parents, for their unending support,
This work is dedicated.

ACKNOWLEDGEMENTS

I would first like to gratefully acknowledge and sincerely thank Stephen W. Fesik for his support and guidance throughout my graduate studies. The education I received in Steve's lab was unparalleled, and I could not have asked for a more thoughtful and dedicated mentor. The example that Steve provides as a successful and passionate scientist is highly valuable to all the students that he has trained, and I count myself lucky to be among them. This work would not have been possible without Steve's commitment to my education, and I am extremely grateful for that commitment.

I also would like to extend many thanks to Olivia Rossanese for her daily mentorship and guidance. I was always thankful, and sometimes awestruck, by Olivia's uncanny ability to make sense of my seemingly intractable data, and I can't thank her enough for the numerous impromptu conferences in her office. I would not be the scientist that I am today without her training and example. I would also like to especially thank Edward Olejniczak for his support during my time in the Fesik lab. I relied heavily on Ed for experimental design, data interpretation, and scientific training, and I appreciate the effort he put forward to make sure my projects and my graduate student career were successful.

Drug discovery is a highly collaborative endeavor, and the work described in these pages would not have been possible without contributions from many dedicated scientists. I would like to thank the members of the K-Ras Team during my time on that project. Alex Waterson, Taekyu Lee, and Edward Olejniczak led chemistry and structural biology efforts, Jason Phan and Qi Sun conducted NMR and x-ray crystallography, and chemistry was conducted by R. Nathan Daniels, Jason Burke, J. Phil Kennedy, Nick Pelz, and James Patrone. For the Pak-1 project, I am indebted

to Olivia Rossanese and Alex Waterson for their leadership, and to Jason Burke and Bin Zhao for chemical synthesis and x-ray crystallography, respectively. In particular, I would like to again thank Alex for his singular dedication to the chemistry on this project. Our success in fragment extension were due, in no small part, to his intellectual and technical contributions. Finally, I would like to gratefully acknowledge and thank those who contributed to the Mcl-1 drug discovery project. Leadership was provided by Edward Olejniczak and Taekyu Lee. Chemistry was conducted by Subrata Shaw, Zhiguo Bian, Johannes Belmar, James “Chris” Tarr, and Nick Pelz. Crystallography was conducted by Bin Zhao. Our cell biology team was led by Olivia Rossanese, with Carrie Browning, DeMarco Camper, Allison Arnold, and John Sensintaffer conducting the routine biochemical and cellular assays. Many thanks should also be extended to Natalia Smothers for causing our administrative functions to run so smoothly.

I was blessed to work in close proximity with accomplished scientists who provided innumerable assistance in my experiments, but who also became close friends. To Jen “Destroyer” Howes, Dom Vigil, Hai-Young Kim, and Feng Wang: you have provided me an example of what a successful post-doctoral fellow can be, and I was lucky to work alongside you. To my fellow graduate students in the Fesik lab: Mike Burns, Qi Sun, Laura Keigher, and Evan Perry, I’m glad to have studied together with you. To those of you who have already graduated: good luck on your future career. To those just starting on their journey at Vanderbilt, I wish you the best of luck! To my friends at Vanderbilt: our adventures together meant the world to me, and I am so lucky to have met each of you. I feel no small amount of regret as we all graduate and move away, and I will always look back fondly at our time together in Nashville.

Finally, I would like to thank my loving family for their support. My parents have helped me achieve my dreams at every stage in my life, and I could not have arrived at Vanderbilt without them standing behind me. To my wife and my son, thank you for your patience and tolerance for the late nights, early mornings, and my grumpy demeanor when the experiments failed. I would finally like to thank my grandparents, Clarence and Flora Byrd, for their remarkable commitment to seeing that my education is a success.

I realize these acknowledgements can only scratch the surface in listing all those individuals who have contributed to this work or to my life while a student at Vanderbilt University. So to those who I have not mentioned by name, you are gratefully acknowledged and abundantly thanked.

This research was financially supported by a National Institutes of Health Training in Pharmacological Sciences grant, T32 (GM07628) and the National Cancer Institute Breast Specialized Programs of Research Excellence (SPORE) grant at Vanderbilt University (grant number 2P50CA098131-11). Flow Cytometry experiments were performed in the Vanderbilt Medical Center (VMC) Flow Cytometry Shared Resource. The VMC Flow Cytometry Shared Resource is supported by the Vanderbilt Ingram Cancer Center (P30 CA68485) and the Vanderbilt Digestive Disease Research Center (DK058404).

TABLE OF CONTENTS

ACKNOWLEDGEMENTS.....	iii
LIST OF FIGURES.....	viii
LIST OF TABLES.....	xii
LIST OF ABBREVIATIONS	xiii
Chapter	
1. General Introduction.....	1
1.1 Cancer as a disease.....	1
1.2 Oncogene addiction and targeted therapeutics	2
1.3 Scope of this thesis.....	4
2. Discovery of K-Ras Inhibitors	6
2.1 Introduction.....	6
2.1.1 The Ras protein superfamily functions as molecular switches.....	6
2.1.2 Structure and function of the p21/Ras isoforms	8
2.1.3 K-Ras drives tumor formation and progression in human cancers.....	13
2.1.4 K-Ras inhibitors for the treatment of cancer	16
2.1.5 Efforts to directly target Ras proteins with small-molecule inhibitors.....	19
2.1.6 Scope of this thesis chapter	23
2.2 Results	23
2.2.1 K-Ras purification and nucleotide exchange.....	23
2.2.2 First-site Fragment Screen	25
2.2.3 Hit characterization.....	27
2.3 Discussion.....	33
2.4 Methods	36
3. Discovery of Pak-1 inhibitors	39
3.1 Introduction.....	39
3.1.1 Structure and function of the Pak family kinases	39
3.1.2 Pak kinases promote cancer progression and metastasis	43
3.1.3 Serine/Threonine kinase domain structure and common inhibitor features.....	47
3.1.4 Publicly disclosed Pak inhibitors	49
3.1.5 Suitability of FBDD to kinase inhibitor development.....	52
3.2 Results	53
3.2.1 Expression and purification of the Pak-1 kinase domain.....	53
3.2.2 Attempted optimization of HSQC-NMR spectra for Pak-1-KD.....	54
3.2.3 Saturation Transfer Difference (STD)-NMR First-site Fragment screen.....	56
3.2.4 Development of a biochemical assay to measure compound activity	60
3.2.5 Development of a selectivity counterscreen against Pak-4	64
3.2.6 X-ray crystallography revealed fragment binding orientations on Pak-1-KD	66
3.2.7 An ILNOE-NMR screen identified fragments bound to a second site.....	69
3.2.8 Fragments and designed compounds bind Pak-1-KD with low micromolar affinities.....	71
3.2.9 Discovery of inhibitors with selectivity for Pak-1 over Pak-4.....	73
3.2.10 A fragment growing strategy successfully increased compound activity.....	78

3.2.11	Pak-1 inhibitors active in breast cancer cell lines.....	82
3.3	Discussion.....	85
3.4	Methods.....	88
4.	Discovery of Mcl-1 inhibitors and identification of sensitive cancer types.....	92
4.1	Introduction.....	92
4.1.1	Mechanisms of cell death.....	92
4.1.2	The Bcl-2 family of proteins regulate the intrinsic apoptotic pathway.....	96
4.1.3	BH3-only proteins activate apoptosis in response to diverse stimuli.....	97
4.1.4	Pro-survival Bcl-2 family members sequester pro-apoptotic proteins.....	100
4.1.5	Mcl-1 protein overexpression is implicated in cancer cell survival.....	102
4.1.6	Therapeutic use of an Mcl-1 specific inhibitor.....	104
4.1.7	Publicly disclosed BH3-mimetic Mcl-1 inhibitors.....	106
4.2	Results.....	109
4.2.1	Optimized a fluorescence-based assay to measure Mcl-1 inhibitors.....	109
4.2.2	Discovery of slow-binding compounds.....	111
4.2.3	Development of assays to measure picomolar-affinity compound interactions.....	114
4.2.4	BH3 profiling used to measure Mcl-1 dependency of cancer cell lines.....	122
4.2.5	Developed assays to discriminate on-target and off-target activity in cells.....	124
4.2.6	Mcl-1 protects a subset of TNBC cell lines from apoptosis.....	130
4.2.7	BH3 profiling confirms the specific dependency on Mcl-1 for survival.....	136
4.2.8	Mcl-1 sequesters more Bim than Bcl-xL in Mcl-1 dependent cell lines.....	138
4.2.9	Mcl-1 knockdown overcomes resistance to Bcl-xL small-molecule inhibitors.....	140
4.2.10	Mcl-1 inhibitors powerfully synergize with Bcl-2 family inhibition.....	142
4.2.11	Bcl-2 family member mRNA or protein levels do not predict Mcl-1 dependency.....	143
4.2.12	A combined index of Bcl-2 family proteins better predicts Mcl-1 dependency.....	146
4.3	Discussion.....	150
4.4	Methods.....	156
5.	General conclusions.....	164
	Appendix A.....	167
	Appendix B.....	172
	Appendix C.....	173
	REFERENCES.....	190

LIST OF FIGURES

Figure	Page
1-1: The leading causes of death in the United States	2
2-1: Ras superfamily proteins function as “molecular switches”	8
2-2: The Ras GTPase domain structure.....	9
2-3: Ras proteins are at the center of a broad interaction network	11
2-4: Activated Ras effects a broad range of cellular changes.....	13
2-5: Common Ras mutations in human cancer	14
2-6: Fragment optimization through a linking approach.....	21
2-7: K-Ras (G12D) alters conformation upon binding a first-site fragment hit.	22
2-8: Expression and purification of K-Ras (G12D).....	24
2-9: NMR confirms the successful loading of K-Ras with GppNHP	25
2-10: K-Ras-GTP selective compounds	27
2-11: Compounds that non-selectively bind GDP- and GTP-bound Ras.....	27
2-12: HSQC-NMR spectrum of ¹⁵ N-K-Ras in the presence of VU0430640-1	29
2-13: HSQC-NMR spectrum of ¹⁵ N-K-Ras in presence of VU0447313-1.....	30
2-14: HSQC-NMR spectrum of ¹⁵ N-K-Ras in the presence of VU0406331-1	31
2-15: Determination of compound dissociation constants by NMR	32
2-16: Examples of selective indole-containing compounds	33
2-17: Examples of selective catechol-containing compounds.....	33
3-1: Pak kinases are classified into two groups	40
3-2: Pak kinases regulate cellular motility, proliferation, and survival	42

3-3: Crystal structure of the Pak-1 kinase domain	47
3-4: Chemical structures of key reported Pak inhibitors discussed in this chapter	51
3-5: Purification of the human Pak-1 kinase domain (Pak-1-KD)	54
3-6: Attempted optimization of HSQC-NMR for Pak-1-KD	55
3-7: Two NMR ¹ H spectra are measured for an STD-NMR experiment	57
3-8: STD-NMR difference spectrum for adenosine binding to Pak-1-KD	58
3-9: Example fragments identified in the Pak-1-KD first-site fragment screen	59
3-10: Example fragment hits from the designed hinge library.....	60
3-11: Validation of a fluorescence anisotropy assay to detect Pak-1 inhibition	61
3-12: LANCE <i>Ultra</i> TR-FRET schematic.....	62
3-13: Optimization of the Pak-1 TR-FRET assay.....	63
3-14: Pak-1-KD activity assay validated with external measurements.....	64
3-15: Development and optimization of the Pak-4 activity assay	65
3-16: Example x-ray crystal structures for Pak-1-KD fragment hits	67
3-17: Optimization of an ILNOE-NMR second-site fragment screen.....	70
3-18: Representative fragment hits from a second-site screen	71
3-19: Example dose-response inhibition curves in the kinase activity assay	72
3-20: Investigating fragment selectivity for specific Pak kinase isoforms.....	74
3-21: X-ray structure explains the exquisite Pak-1 selectivity of Neratinib	76
3-22: Ternary crystal structure showing two fragments bound to Pak-1-KD.....	79
3-23: An example of structure-guided fragment merging opportunities	80
3-24: Fragment growing approach to reach the selectivity pocket of Pak-1 kinase	81

3-25: X-ray structure confirms orientation of extended fragment	82
3-26: Pak-1 inhibitors demonstrate mechanistic activity in breast cancer cells	84
4-1: Apoptosis consists of the extrinsic, intrinsic, and perforin/granzyme pathways	95
4-2: The Bcl-2 family of proteins regulates the intrinsic apoptotic cascade	97
4-3: Sequences of the BH3-motif of BH3-only proteins.	98
4-4: BH3-domain interactions among Bcl-2 family proteins	99
4-5: Structure of BH3 interactions with anti-apoptotic Bcl-2 proteins	100
4-6: Mcl-1 is uniquely regulated through its N-terminus	102
4-7: Compounds discussed in this introduction with reported Mcl-1 activity	107
4-8: Optimization of the Mcl-1 FPA assay.....	111
4-9: Some Mcl-1 inhibitors bind time-dependently	112
4-10: Summary of the SAR for time-dependent compound binding.....	114
4-11: Schematic for the AlphaScreen assay.....	115
4-12: Biotin-Bim2 peptide has unsuitably slow binding kinetics.....	116
4-13: The Alphascreen assay requires detergent to produce signal	118
4-14: Development and optimization of the FPA/Bim6 assay.....	120
4-15: The FPA/Bak and FPA/Bim6 assays similarly measure most compounds.....	121
4-16: 'BH3 profiling' was used to determine Mcl-1 dependency status	123
4-17: Mcl-1 inhibitors cause dose-dependent mitochondrial depolarization.....	125
4-18: Mcl-1 inhibitors dose-dependently induce Caspase cleavage and cell death	126
4-19: VU0657538 inhibits binding of biotin-MS-1 to Mcl-1 in cell lysates	127
4-20: VU0516301-1 fails to disrupt Noxa or Bim in H929 cells	128

4-21: High affinity Mcl-1 inhibitors potently displace Noxa from cellular Mcl-1	128
4-22: High affinity inhibitor VU0659158 potently displaces Noxa from Mcl-1	129
4-23: Duolink PLA assay visualizes disruption of Mcl-1/Bim complexes in live cells.....	130
4-24: Mcl-1 and Bcl-xL protein expression silenced by siRNA transfection	131
4-25: A subset of TNBC cell lines are solely dependent on Mcl-1 to evade apoptosis	133
4-26: Mcl-1 protein silencing induces caspase activation	134
4-27: Annexin V-positive cells increases in Mcl-1 dependent lines after knockdown	135
4-28: BH3 profiling confirms Mcl-1 dependency status	137
4-29: Mcl-1, but not Bcl-xL, primarily sequesters mitochondrial Bim	139
4-30: Bcl-2 and Bcl-xL inhibitors in combination with Mcl-1 silencing	141
4-31: Mcl-1 inhibitors powerfully synergize with Bcl-2/Bcl-xL inhibitor ABT-263.....	143
4-32: mRNA expression levels do not correlate with MCL-1 sensitivity.....	144
4-33: Bcl-2 family protein expression levels in the TNBC cell line panel.....	145
4-34: Bcl-2 family protein expression does not strongly correlate with Mcl-1 sensitivity	145
4-35: A combined index predicts sensitivity to Mcl-1 knockdown.....	147
4-36: Bak most heavily contributes to the prediction algorithm	148
4-37: Prediction of Mcl-1 dependency in the CCLE	150
4-38: Mcl-1 program compound progression chart	152

LIST OF TABLES

Table	Page
3-1: Cancers in which Pak-1 and Pak-4 are commonly overexpressed or amplified.....	43
3-2: SAR table for the 3-Aminopyrazole designed series	73
3-3: Pak selectivity for the 3-aminopyrazole series.....	75
4-1: Bim peptide sequences developed for use in the AlphaScreen assay	117
4-2: Percent knockdown of Mcl-1 and Bcl-xL for experiments in Figure 4-25	134

LIST OF ABBREVIATIONS

AID	Auto-inhibitory domain
ATP	Adenosine tri-phosphate
Bcl-2	B-cell lymphoma
Bcl-xL	BCL2-like 1 isoform 1
CCL	Cancer Cell Line Encyclopedia
CMC	Critical micelle concentration
CML	Chronic myeloid leukemia
COSMIC	Catalog of Somatic Mutations in Cancer
Da	Dalton
K_D	Dissociation constant
K_d	Kinetic off rate
EC_{50}	Half maximal effective concentration
EGFR	Epidermal growth factor receptor
ER	Estrogen receptor
FPA	Fluorescence polarization anisotropy
TR-FRET	Time-resolved fluorescence resonance energy transfer
GAP	GTPase-activating protein
GDP	Guanosine diphosphate
GEF	Guanine nucleotide exchange factors
GppNHp	Guanosine 5'-[β,γ -imido]triphosphate
GST	Glutathione S-transferase
GTP	guanosine triphosphate
HER2	human epidermal growth factor receptor 2
HIS6	Hexahistidine-tag
HSQC	Heteronuclear Single Quantum Correlation
IAP	Inhibitor of Apoptosis Proteins
IC_{50}	Half maximal inhibitory concentration
ILNOE	Inter-Ligand Nuclear Overhauser Effect (NMR technique)

IPTG	Isopropyl β -D-1-thiogalactopyranoside
MBP	Maltose-binding protein
MCL-1	Myeloid cell leukemia-1
NMR	Nuclear magnetic resonance
NSCLC	Non-small cell lung cancer
Pak	p21-Activated Kinase
Pak-1-KD	Kinase domain of Pak-1 protein
PAR4	Prostate Apoptosis Response homolog 4
PBD	Protein binding domain
PLA	Proximity ligation assay
Ras	rat sarcoma viral oncogene
RNAi	Ribonucleic acid interference
RTK	Receptor Tyrosine Kinase
SAR	Structure-activity relationship
siRNA	Small interfering RNA
SOS	Son of Sevenless
SPR	Surface plasmon resonance
STD	Saturation transfer difference NMR
TNBC	Triple-negative breast cancer

Chapter 1

General Introduction

1.1 Cancer as a disease

Malignant cancers are the second leading cause of death in the United States. Projections by the National Cancer Institute estimate that new cancer diagnoses this year will top 1.6 million, and almost 600,000 patients are expected to eventually succumb to this disease, accounting for almost 23% of all deaths (Figure 1-1).¹ Despite these grim statistics, medical treatment for cancer has achieved remarkable progress in the last 60 years. Our understanding of cancer initiation, its progression, and treatment with rational therapies has advanced enormously. The death rate for children ages 0-4 years has been reduced by 80% compared to 1950, reductions of at least 50% are seen for all Americans under 45 years of age, and 5-year survival rates have dramatically increased for all cancer types.¹ Yet despite these significant improvements in outcome for younger and middle-aged patients, an aging American population increasingly succumbs to this disease. Increases in life expectancy (and a concomitant decrease in cardiac-related deaths) have increased overall cancer incidence rates. As a result, diagnoses are projected to increase 45% by the year 2030 from a 2010 baseline.² Medicine must continue to seek new therapies to maintain pace with an ageing population that increasingly depends upon these discoveries for survival.

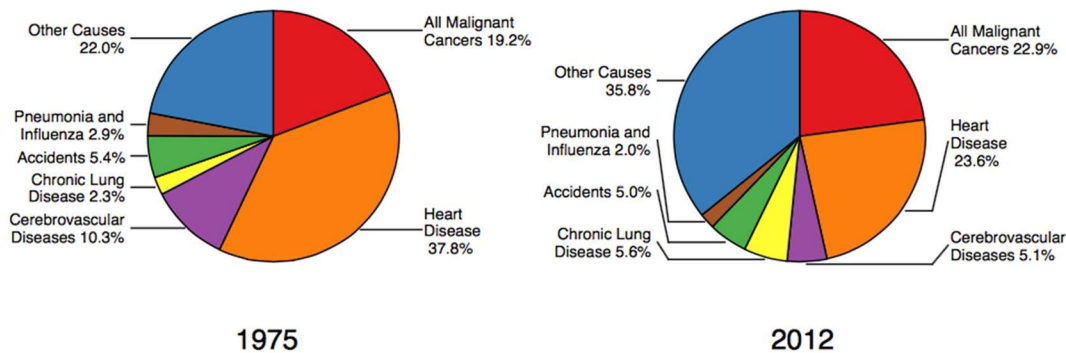


Figure 1-1: The leading causes of death in the United States

Shown is the percent of all causes of death for both sexes in 1975 and 2012, the most recent year that data was available. Malignant cancers remain the second largest contributor to mortality, and reductions in heart disease mortality have outpaced gains made in cancer survival. Figure adapted from Howlader 2015.¹

1.2 Oncogene addiction and targeted therapeutics

Pharmacological agents for treating cancer have improved significantly in the past two decades. Many traditional therapies achieved selectivity for cancer cells by focusing on interfering with cellular division. These therapies, such as etoposide and taxol, can be effective at slowing tumor growth or inducing cell death but are poorly selective for tumor cells and exert significant toxicity against rapidly dividing non-cancerous human cells. More specific next-generation cancer therapeutics are designed to be more selectively lethal to cancer cells by taking advantage of specific innate differences between cancer cells and the host. The selective toxicity of these “targeted therapeutics” could take many forms, including restricting cancer cell proliferation, inhibiting metastasis, or activating the apoptotic mechanism. The best inhibitors may target several pathways simultaneously.

Identification and validation of these selectively lethal targets is a grand challenge in the field. Cancers frequently rely on particular proteins for survival and growth that are dispensable in normal cells.³ This specific dependency, termed “oncogene addiction” by Bernard Weinstein in 2000,⁴ provides a key new source of cancer-specific targets for inhibition. Clinical response to specific inhibitors of these proteins can be remarkable. The discovery of Imatinib (Gleevec), an inhibitor of the BCR-ABL tyrosine kinase fusion oncogene, was an early powerful example of a rationally developed targeted therapeutic for the treatment of chronic myeloid leukemia (CML).⁵ Consider, too, the remarkable clinical outcomes seen with directed therapies against the human epidermal growth factor receptor 2 (Her2)/ErbB2 receptors in breast cancer,⁶ or the response to Epidermal growth factor receptor (EGFR) blockade in EGFR-mutant non-small cell lung cancer.⁷ These and many other examples showcase the powerful efficacy of pharmacologic inhibition brought to bear against an appropriate target.

Problematically, predicting oncogenic dependency is not trivial. Many proteins are upregulated or downregulated in cancer cells, and of these, a smaller number have been vetted for anti-proliferative activity or other detrimental effects selective for cancer cells after inhibition. Overexpression of a protein does not necessarily correlate with dependency in any cancer, nor are all cancers of a particular subtype dependent on frequently overexpressed oncogenes or other proteins.³ Put another way, we must carefully discriminate a “passenger” mutation that arises by chance and does not provide any selective benefit to cancer, from the critical “driver” mutations that provide a selective advantage to cancer cells by aiding in tumor initiation, growth, metastasis, and other changes.⁸ Only these driver mutations have the potential to be effective therapeutic targets, and even these must be carefully selected for targeted therapy by following

both *in vitro* and *in vivo* experimental evidence to verify whether the protein is required for survival at a particular stage of progression, and whether its inhibition will be detrimental to non-cancerous cells.⁹ Ultimately, a positive clinical response is the strongest evidence to validate a particular rationally-selected target,¹⁰ though of course the absence of a positive clinical outcome does not guarantee that a target is invalid, but only that the tested inhibitor, method of administration, patient population, and other considerations were insufficient to yield a beneficial outcome.

1.3 Scope of this thesis

This thesis encompasses efforts to discover small-molecule targeted inhibitors for three proteins: K-Ras, Pak-1 kinase, and Mcl-1. While these proteins differ significantly in structure and function, each plays a key role in cancer progression, and each has been extensively validated pre-clinically as objectives for targeted therapy. Despite the wealth of evidence suggesting a positive therapeutic benefit for inhibiting these proteins in human patients, no inhibitors for these proteins have been discovered that are in clinical trials.

In Chapter 2, I will describe a fragment-based screen of the GTP-bound form of K-Ras. Because of its role as a key promoter of cell growth, survival, motility, and other pathways crucial to cancer maintenance and progression, K-Ras is one of the most well-validated anti-cancer targets but has proven to be especially challenging to chemically modulate. The GTP-bound form directly binds and activates various effector proteins; to discover an inhibitor capable of disrupting these interactions, I conducted an NMR fragment-based screen and identified a number of compounds that bind to K-Ras.

In Chapter 3, I will describe the discovery of Pak-1 kinase inhibitors. This serine/threonine kinase regulates a wide variety of pathways implicated in cancer progression, including survival, growth, and motility. Our goal was to discover a potent Pak-1 inhibitor with selectivity over other kinases, including other Pak isoforms. Towards this end, I conducted a first- and second-site fragment-based NMR screen, developed robust *in vitro* activity assays to measure compound affinities to guide chemical optimization, and measured the effects of in-house synthesized compounds in cells. Our best compound had a 300nM K_i and inhibited Pak-1 kinase activity in cells.

In Chapter 4, I will discuss my contributions to the discovery of Mcl-1 inhibitors and to the understanding of which cancers are dependent on Mcl-1 for survival. Mcl-1 is an anti-apoptotic Bcl-2 family member that prevents apoptosis by binding and sequestering pro-apoptotic Bcl-2 family members. It is commonly upregulated in many cancer types, including breast carcinomas. My contributions to this project are threefold: first, I enabled the understanding of compound SAR through the development of highly sensitive biochemical assays capable of measuring picomolar affinities; second, I developed assays to determine the on-mechanism actions of these compounds in cells; and third, I defined and predicted the molecular mechanisms of Mcl-1 sensitivity in triple-negative breast cancer and other cancer types.

Finally, in the last chapter, I will conclude with general thoughts on the accomplishments obtained in my studies and discuss future directions.

Chapter 2

Discovery of K-Ras Inhibitors

2.1 Introduction

Activating Ras mutations occur in up to 30% of all human cancers, and over 30 years of research has demonstrated the oncogenic power of these key signaling molecules to endow healthy cells with the “hallmarks of cancer.”¹¹ Numerous *in vitro* and *in vivo* models have strongly suggested that inhibition of Ras signaling will provide therapeutic benefit in human patients. However, discovering a Ras inhibitor has proven to be immensely challenging, and to date, no Ras inhibitor has achieved clinical testing. In this chapter, I will review the tumorigenic role that Ras plays in cancer biology and will detail our efforts to discover K-Ras-GTP small-molecule inhibitors.

2.1.1 *The Ras protein superfamily functions as molecular switches*

The Ras superfamily comprises over 150 proteins in five distinct subfamilies (Ras, Rho, Rab, Ran, and Arf) which regulate numerous and varied cellular processes, including cell growth, motility, and death.¹² Each subfamily contains shared structural features and regulatory functions, and are distinguished by unique methods of activation, regulation, and transduction of biological signals in response to extra- or intra-cellular stimuli.¹³ Despite wide variances in structure, regulation, and method of activation, each Ras superfamily protein contains a highly conserved GTPase domain that binds guanosine nucleotides and enzymatically catalyzes the hydrolysis of guanosine triphosphate (GTP) to guanosine diphosphate (GDP). Nucleotide binding occurs through the presence of several conserved “G box” sequences. Multiple hydrophobic,

hydrogen bonding, and charge-charge interactions (including interactions involving an obligatory Mg^{2+} ion) contribute to form an extremely tight (picomolar) interaction between Ras proteins and GTP.¹⁴ Hydrolysis of GTP to GDP is accompanied by a defined conformational shift in the tertiary structure of the protein, altered binding kinetics to other proteins, and significant alterations in Ras localization, activity, and function. By carefully controlling GTP/GDP binding and the rate of GTP catalysis, cells have organized these simple “molecular switches” into complex networks capable of regulating nearly every aspect of gene expression, cellular division, movement, and death.¹⁵

Ras superfamily proteins are inactive when bound to GDP, and are therefore unable to activate downstream signaling pathways (the molecular switch is “off”). Activation requires nucleotide exchange of the GDP molecule for GTP (Figure 2-1). However, Ras proteins lack a mechanism to efficiently accomplish this task, and due to the lengthy off-rate (K_d) for GDP, the intrinsic exchange rate of GDP for GTP is physiologically irrelevant despite a 10-fold cytosolic molar excess of GTP (the off-rate of GDP on H-Ras is just $3.4 \times 10^{-4} \text{ s}^{-1}$, for example).¹⁴ In practice, the catalyzed exchange of GDP for GTP is the rate-limiting step in activating Ras superfamily proteins and depends entirely on external regulation.^{16,17} This process is catalyzed by guanine nucleotide exchange factors (GEFs), such as Son of Sevenless (SOS), which cause Ras proteins to release guanine nucleotides by weakening their affinity for GDP.¹⁸ The aforementioned molar excess of GTP over GDP in the cell ensures that a large proportion of nucleotide that binds Ras upon GEF release is GTP.¹⁹ There are numerous GEFs, some of which act on multiple RAS superfamily proteins,¹⁵ and this diversity enables granular control over which members are activated in response to distinct biological stimuli.

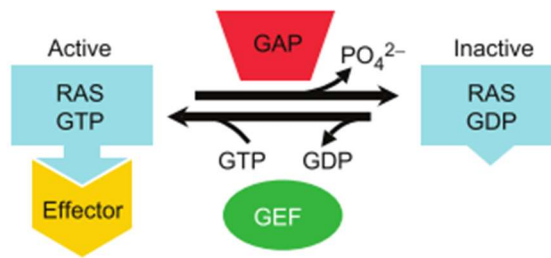


Figure 2-1: Ras superfamily proteins function as “molecular switches”

These small GTPases selectively bind to GTP (active state) or to GDP (inactive state) in response to biological signals. Only the GTP-bound form of Ras interacts with effector proteins in high affinity. Guanine-exchange factors (GEFs), such as SOS, cause dissociation of GDP, allowing cytosolic GTP to bind. In contrast, GTPase Activating Proteins (GAPs) increase the rate of GTP hydrolysis to deactivate signaling. Tight control of GEF and GAP activity regulates RAS activity in the cell. Figure from Colicelli *et al*, 2004.¹⁴

The intrinsic rate of GTP hydrolysis is too slow to be physiologically meaningful for regulation (the rate for H-Ras is just $4.2 \times 10^{-4} \text{ s}^{-1}$), thus favoring a persistently active GTP-bound form.²⁰ Therefore, in practice cells utilize GTPase-activating proteins (GAPs) to increase this rate.^{21,22} Like the GEFs described above, GAP activity is tightly regulated in a tissue and context-specific manner to offer granular control over Ras protein activation and signalling.²³⁻²⁷

2.1.2 Structure and function of the p21/Ras isoforms

The p21/Ras isoforms are the founding members of the Ras superfamily. These isoforms include three genes encoding for H-Ras, N-Ras, and two splice variants of K-Ras (4A and 4B).²⁸ Each is composed entirely by their GTPase domain and lack the additional regulatory domains commonly found in other Ras superfamily proteins.¹⁴ First identified as oncogenes in acutely transforming retroviruses, these small (approximately 21-kDa) proteins are now known to play a critical role in fundamental cellular processes, including proliferation, survival, motility, normal cell differentiation, and organ development.²⁹⁻³²

Ras isoforms are globular proteins containing a single GTPase domain of five α -helices and six β -strands (Figure 2-2).³³ First crystallized in 1989, the conserved GTPase binding domain is now understood to contain five nucleotide-binding regions (G1-G5) surrounding a centrally bound guanosine nucleotide.³⁴ A well-defined conformational shift primarily involving two “switch” regions occurs upon the conversion from the GDP to GTP bound state.¹⁶ These switch regions are highly flexible and, upon loss of hydrogen-bond interactions between conserved threonine and glycine residues and the γ -phosphate on GTP, Ras will naturally relax into a looser conformational shape.³⁵

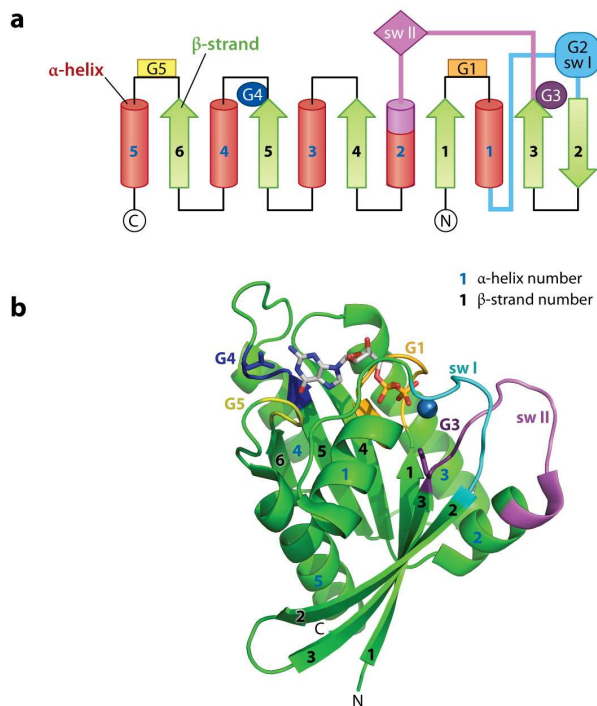


Figure 2-2: The Ras GTPase domain structure

(A) Ras proteins are composed almost entirely of a nucleotide-binding domain consisting of five α -helices and six β -strands that is highly conserved among isoforms. In addition, Ras contains a hypervariable C-terminal region, which is post-translationally isoprenylated to allow for plasma membrane localization. **(B)** Shown is a crystal structure of K-Ras bound to the GTP-analog, GppNHp. α -helices (cyan) and β -strands (purple) are numbered as indicated. Figure adapted from Wittinghoffer *et al*, 2011.³⁶

Ras isoforms significantly differ only in their unstructured hypervariable C-terminal region, which controls membrane localization³⁷ and is absolutely required for intrinsic or transforming Ras activity.^{38,39} A conserved CAAX motif is post-translationally modified by the attachment of a farnesyl isoprenoid lipid by the enzyme farnesyl transferase (FTase).^{40,41} Isoprenylation is followed by the proteolytic cleavage of the AAX sequence catalyzed by Ras-converting enzyme-1 (RCE1) and subsequent carboxymethylation of the cysteine C-terminal residue by isoprenylcysteine carboxymethyltransferase-1 (ICMT1) to facilitate membrane targeting.³² H-, N-, and K-Ras-4A are also palmitoylated at an upstream Cys residue near the C-terminus, while K-Ras-4B contains a series of positively charged lysine residues to facilitate tighter plasma membrane attachment through charge-charge interactions.³² However, localization of the protein can also be aided by other mechanisms. Various proteins, including calmodulin⁴² and galectin-1⁴³ have been reported to bind the C-terminal region of Ras proteins, and these interactions also play a role in a functional distinction between Ras isoforms. For example, calmodulin is responsible for shuttling K-Ras-4B from the plasma membrane to the Golgi apparatus in hippocampal neurons in response to calcium signaling, but has no effect on K-Ras-4A or H-Ras localization.⁴⁴

As a central signaling component to an extremely diverse set of cellular pathways, Ras signals downstream by activating dozens of effector proteins, and Ras activation is carefully controlled by a large assortment of diverse regulatory proteins (Figure 2-3).¹⁵ This regulation occurs primarily (though not exclusively) through the modulation of GTP/GDP binding by carefully controlling GEF and GAP activation and localization.

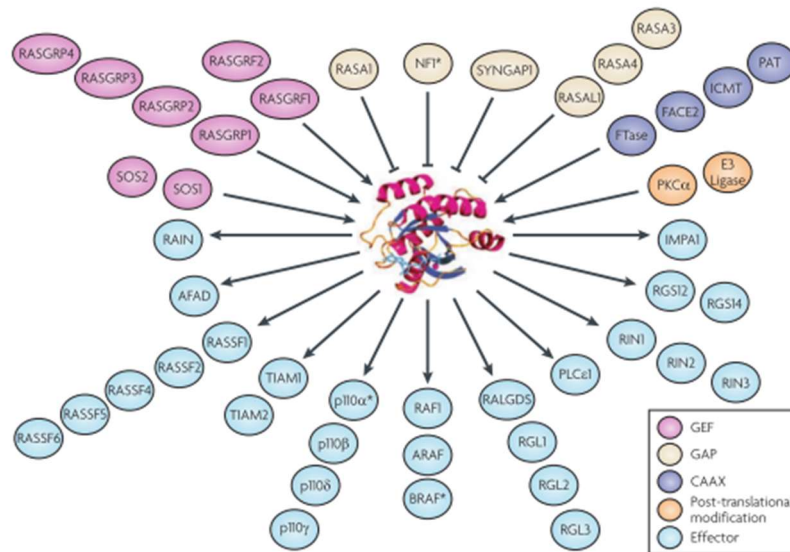


Figure 2-3: Ras proteins are at the center of a broad interaction network

Ras proteins are regulated by several families of GEF (pink) and GAP (beige) proteins to control GTP-binding, CAAX motif regulation to control isoprenylation and membrane localization (purple), and ubiquitination to induce protein degradation (orange). Ras effectors (blue) number in the dozens and are activated only through binding to active (GTP-bound) Ras. Figure from Vigil *et al*, 2010.¹⁵

Ras activation occurs through nucleotide exchange catalyzed by GEFs, including SOS, RasGRF, and RasGRP. Two domains (CDC25 and the Ras Exchange Motif (REM) domains) are required for GEF activity and are expressed in all three GEF families.⁴⁵ Canonically and most commonly exemplified, growth factor binding activates transmembrane Receptor Tyrosine Kinases (RTKs), allowing Grb2 to bind and recruit a GEF, such as SOS, to the membrane, where it can then activate the membrane-localized Ras. RasGRF and RasGRP activation are Ca²⁺ dependent and play more specialized roles in the brain and T-cell development, respectively.^{46,47}

Active Ras signals downstream via protein–protein interactions with effector proteins.^{32,48} Effectors contain one of several different Ras-binding domains, preferentially bind the GTP-bound form of Ras, and are biologically activated by this binding interaction. Methods of activation differ among effectors, but follow at least one of three mechanisms: (1) altered

subcellular localization of the effector; (2) altered intrinsic catalytic activity (allosteric regulation); or (3) altered interaction with other signaling components (complex formation).^{49,50} The effector-binding region was first identified on H-Ras by selective mutations between amino acids 32-40 that precluded transforming activity but did not destabilize the protein structure or membrane localization. The first Ras effector to be identified was Raf1 (now known more commonly as c-Raf) in 1993, a discovery that directly linked Ras activation and the Mitogen Activated Protein Kinase (MAPK) cascade, an event that ultimately leads to altered gene transcription.⁵¹ Phosphatidylinositol 4,5 bisphosphate 3-kinase (PI3K), a lipid kinase which is activated by binding active Ras through its Ras binding domain (RBD), was the second Ras effector to be identified.⁵² Elevated kinase activity increases the rate of PIP₂ to PIP₃ generation on the plasma membrane, and hence elevated recruitment of PH-domain containing proteins such as AKT1 and PDK1. Ras effectors are not restricted to kinases. For example, GEF effectors such as TIAM1 activate downstream Ras superfamily members like Rac1. Loss of TIAM1 in mice prevents carcinogen-induced tumorigenesis, suggesting a critical role for this Ras effector (and the small GTPase Rac1) in cell transformation.⁵³ Other GEF effectors include RalGDS, which activates the Ral small GTPases. To date, over thirty effectors have been identified (Figure 2-4).^{15,54}

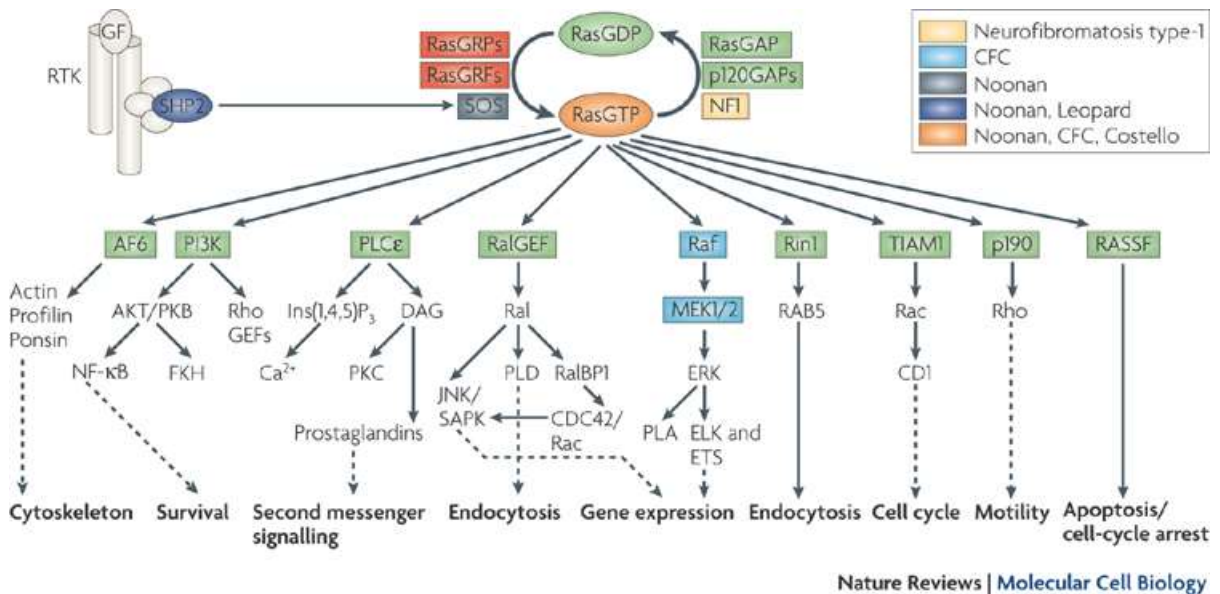


Figure 2-4: Activated Ras effects a broad range of cellular changes

RTKs activated through the binding of extracellular ligands (or induced oncogenic dimerization) bind to and activate RTKs such as EGFR, inducing Grb2 recruitment, SOS binding, and Ras GDP-to-GTP nucleotide exchange. Active Ras-GTP can then bind and activate various effector proteins, which then regulate diverse cellular pathways such as cytoskeletal rearrangement, endocytosis, motility, and apoptosis. Adapted from Karnoub *et al*, 2008.³²

2.1.3 K-Ras drives tumor formation and progression in human cancers

Ras was first identified in 1982 as a transduced oncogene in acutely transforming retroviruses, and constitutively active mutant forms were subsequently isolated from human tumor cells.¹⁴ The Ras pathway is one of the most commonly deregulated pathways in human cancer,³² and K-Ras mutant cancers are more refractory to therapy.⁵⁵ Indeed, Ras is the most highly mutated oncogene (occurring in up to 30% of all human cancers).⁵⁶ The highest incidence of Ras mutations occur in carcinomas of the pancreas (63–90%), colon (36–50%), and lung (19–30%), which constitute three of the four most lethal cancers in the United States.⁵⁷

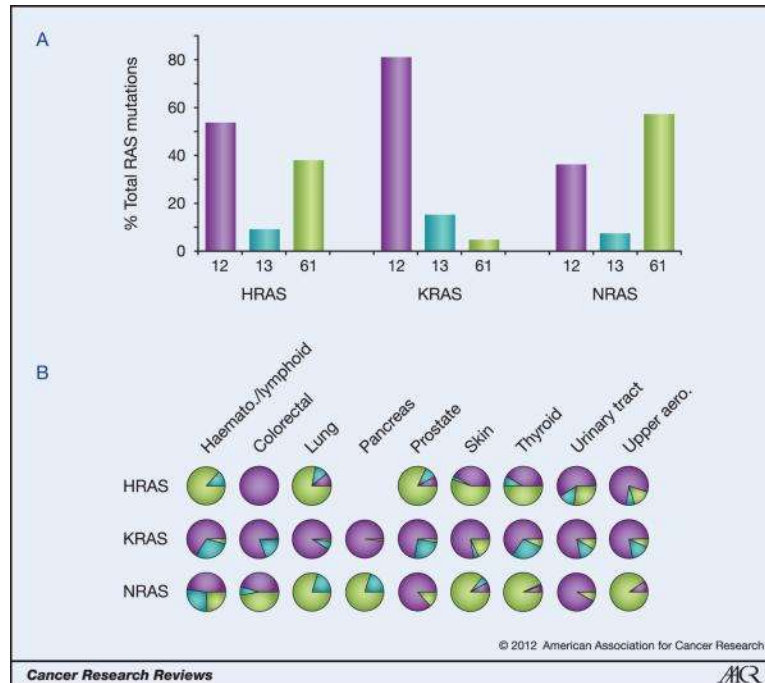


Figure 2-5: Common Ras mutations in human cancer

(A) Ras isoforms are commonly mutated only at three positions: amino acids 12, 13, and 61 (in this figure, color-coded as purple, cyan, and green, respectively). Ras isoforms have distinct codon preferences for mutations at each site when averaged across all human cancers. **(B)** Isoform-specific mutations also depend on the cancer type in which they occur. These preferences appear to have biological significance to Ras signaling. Adapted from Prior *et al*, 2012.⁵⁸

Activating Ras mutations prevent GAP-mediated GTP hydrolysis⁵⁹ and significantly slow intrinsic hydrolysis,⁶⁰ thus resulting in the constitutive activation of downstream effector pathways in the absence of extracellular stimuli. These activating mutations most commonly occur at amino acid positions 12, 13, and 61 (just 0.8% of mutations occur outside these three sites) (Figure 2-5A).³² Mutations at position 12 and 13 prevent insertion of the “arginine finger” due to a steric clash between the Ras amino acid side chain and the GAP. These mutants most commonly include G12C, G12D, G12V, and G13D. While all four exemplified mutations block GAP activity, their occurrence is not uniformly distributed; G12D mutations occur 20-times as often as G12C in pancreatic cancers, while G12C is 2.5-times more common than G12D in lung cancers

(Figure 2-5B).³⁷ These differences reflect, in part, the genotypic insults observed by each cancer. G12C commonly occurs in response to carcinogens present in tobacco smoke. These mutations also provide insight into the dependencies of these cancers on downstream Ras effectors. G12D mutations, through their particular alterations on Ras conformational structure, preferentially activate the B-Raf/MAPK and PI3K pathways, which suggests a particular dependency on these pathways in cancers heavily dependent on this mutation (i.e. colorectal, pancreatic, and others).³⁷ Conversely, mutations at position 61 block glutamine-mediated stabilization of the arginine finger and transition state stabilization.⁵⁸ Mutations at position 61 are unique because they do not block binding of GAP proteins, merely their function, and so could theoretically sequester otherwise active GAP proteins. Further, intrinsic hydrolysis of Q61 mutants is further slowed when bound to Raf1 kinase (but not other effectors), leading to preferential activation of Raf1/MAPK pathway effectors – a common occurrence in melanoma, a cancer also commonly driven by B-Raf mutations.^{37,60,61}

Oncogenic Ras activation is not limited to Ras mutations. Amplification of upstream Ras activators (commonly RTKs, such as Her2/neu amplification in breast cancer), or less commonly, loss of GAP function can also lead to deregulated signaling and the potential for cancer even with wild-type Ras expression. Loss of expression or inactivating mutations in the Ras GAP protein neurofibromin occurs in 14% of glioblastomas, 13%–14% of melanomas, 8%–10% of lung adenocarcinomas, and single-digit frequencies in most other cancers.³⁷

Activated Ras is a critical oncogene for both tumor initiation and tumor maintenance,¹¹ including the ability to proliferate, evade programmed cell death, alter metabolism, induce angiogenesis, increase invasion and metastasis, and evade immune destruction.⁵⁷ Induced

expression of Ras *in vitro* in murine and human cells, and *in vivo* in various murine tissues, leads to tumorigenesis, and has been reviewed extensively.^{32,57,62} As discussed above, K-Ras activation is most highly correlated with cancers of the lung, pancreas, and colon, and the induced expression of mutationally active K-Ras in these tissues is sufficient to produce neoplasia.⁶³⁻⁶⁵ Aberrant activation of key Ras effector pathways, including Raf1/MAPK, PI3K, and TIAM1/Rac1, are critical for cancer transformation. Cell proliferation is rapidly increased through cell cycle blockade evasion through transcriptional upregulation of growth factors (such as TGF α , HBEGF, and AREG), growth factor receptors and the downregulation of growth inhibitors such as TGF β and cyclin-dependent kinase inhibitors (CDKIs). Apoptosis is suppressed by upregulation of PI3K, by downregulation of BAK expression, and upregulation of Caspase inhibitors and the Inhibitors of Apoptosis Proteins (IAPs). Raf activation leads to transcriptional repression of prostate apoptosis response-4 (PAR4) and upregulation of Bcl-2, an anti-apoptotic protein, and phosphorylation of BAD, a pro-apoptotic protein inactive in the phosphorylated state.

2.1.4 *K-Ras inhibitors for the treatment of cancer*

Inactivation of oncogenic Ras reverses the transformed phenotype of cells both *in vitro* and *in vivo*, and results in the dramatic regression of tumors in murine xenograft models.^{66,67} Thus, K-Ras inhibition represents an attractive therapeutic strategy for many cancers. Indeed, discovering a clinically suitable inhibitor has been considered the “holy grail” of cancer drug discovery. Yet despite the well-validated role that Ras isoforms play in tumor initiation, progression, and survival, development of a small-molecule inhibitor has proven to be challenging, and no direct inhibitor has reached the clinic. Ras activation and signaling is

accomplished primarily through protein-protein interactions, and such interfaces typically lack well-defined binding pockets on the protein surface for which a small molecule inhibitor could bind.⁶⁸ These challenges have led some to consider that direct targeting of Ras will be impossible.⁶⁹

However, there have been attempts to indirectly block Ras signaling. These include three distinct approaches: (1) blocking membrane localization by inhibiting Ras isoprenylation; (2) indirectly inhibiting Ras by targeting downstream effectors; and (3) inhibiting other proteins that are synthetically lethal only with mutant Ras expression.⁶⁹

Ras proteins are subject to post-translational modification by isoprenylation (attachment of a farnesyl or geranylgeranyl group) at a C-terminal cysteine residue. This modification is critical for determining subcellular membrane localization. In fact, loss of isoprenylation precludes Ras trafficking to the membrane and prevents activation, effector binding, and Ras-mediated transformation.^{38,40,70} Isoprenylation inhibitors (farnesyl-transferase inhibitors, or FTIs) that inhibit FTase activity initially showed significant activity in H-Ras-driven murine tumors. Two FTIs (lonafarnib and Tipifarnib) reached Phase III clinical trials but failed due to lack of efficacy in pancreatic and colon cancers. In these cancers, K-Ras and N-Ras isoforms play a more significant role than H-Ras. K-Ras and H-Ras both support alternative geranylgeranylation and thereby circumvent FTase inhibition.^{62,71,72}

Attempts to indirectly inhibit K-Ras have also been achieved by the modulating activity of downstream effectors known to be crucial for cancer progression or maintenance, such as kinases in the Raf/Mek/Erk MAPK or PI3K pathways. These targets, primarily encompassing proteins that are easier to inhibit with small-molecules, have achieved significantly greater pre-

clinical and clinical success than have inhibitors of K-Ras itself. Primary attention was initially placed on the Raf/Mek/Erk pathway. This work has led to a number of Raf, Mek, and Erk inhibitors have reached pre-clinical evaluation,⁷³ and some, such as the Raf inhibitor Sorafenib and MEK inhibitor Trametinib, are FDA-approved for human therapy. PI3K inhibitors are also under active development, although their single-agent anti-cancer activity has been disappointing. Understanding the therapeutic benefit of these inhibitors is complicated, as Ras mediates its oncogenic role through the activation of multiple effector families. Separately inhibiting one pathway may ultimately prove insufficient to strongly restrict cancer growth and survival. A combination therapy of multiple Ras effector inhibitors may be necessary to revert the transformed phenotype. Moreover, downstream signaling pathways are characterized by multiple levels of feedback regulation. Inhibiting kinase activity within these pathways prevents feedback inhibition and may further lead to pathway activation. Overcoming this process may again require multiple inhibitors for a single pathway (such as combined Raf/Mek inhibitors, for example). In conclusion, combination therapy of two or more inhibitors will probably be required to achieve the same therapeutic benefit as single-agent inhibition of Ras itself.

Finally, Ras-dependent cells might be indirectly targeted through the careful identification and inhibition of proteins that are synthetically lethal only with mutant Ras. The metabolic and signaling changes induced by oncogenic Ras activation are enormous and might conceivably lead to survival dependency on the continued expression and activity of other proteins that are dispensable in healthy cells. In principle, inhibition of these protein(s) would cause cell death only in cells which harbor activating Ras mutations. Synthetic lethality has been observed in both lower organisms and humans and is exploited in cancer therapy. For example, poly(ADP-ribose)

polymerase (PARP) inhibitors, which repair single-stranded DNA breaks, are highly potent in breast cancers with mutations in DNA recombination repair protein breast cancer susceptibility gene (BRCA).⁶⁹ However, despite many screens for such proteins,⁷⁴ no inhibitor has proven as effective as Ras inhibition at reducing viability, and surprisingly, relatively few genes are found in common among the various screens.⁶⁹

2.1.5 Efforts to directly target Ras proteins with small-molecule inhibitors

Despite the inherent challenges to binding and inhibiting Ras proteins, a number of small molecules have been reported to directly bind to Ras and block effector binding.⁶⁹ The most well characterized molecules are the non-steroidal anti-inflammatory sulindac sulfide compound and analogues. More recently, a covalent inhibitor selective for K-Ras G12C mutants has been reported.⁷⁵ These inhibitors universally have poor binding affinities, unknown off-target toxicities, and none have advanced into the clinic. Alternatively, a Ras inhibitor might block activation by preventing Ras-GEF interaction. As mentioned above, GEF activity is required even in mutant Ras cell lines to overcome intrinsic GTP hydrolysis. Two inhibitors^{76,77} have been published to date that bind to an induced pocket between the switch I and switch II region of GDP-bound Ras and sterically occlude SOS1 GEF binding.

A technique uniquely suited to discovering small-molecule inhibitors of protein-protein interactions is fragment-based drug discovery (FBDD).⁷⁸⁻⁸⁰ FBDD has been highly successful at identifying inhibitors of other proteins, such as the clinically-approved B-Raf inhibitor Vemurafenib,⁸¹ HSP90 inhibitor AT13387,⁸² and Bcl-2 and Bcl-xL, and Bcl-w inhibitor ABT-737.⁸³ This approach consists of screening a small library of hundreds or thousands of small molecular

“fragments” (less than 250Da) for direct binding to a target protein, of which binding affinities of hundreds of micromolar are expected.⁸⁴ This contrasts with conventional high-throughput screens in which large libraries of molecules (more than 10^6) with molecular weights typically between 400 and 600Da are used. These molecules are expected to bind in the low micromolar range or better to trigger the screen.⁸⁵ Yet because fragments are much smaller than full-size compounds, even small screens necessarily cover a larger percentage of chemical space.^{85,86} As a result, fragments are typically better suited with scaffold and functional groups substitutions to bind a target,⁸⁷ thus ensuring better complementarity to the receptor and higher ligand efficiency ($\Delta G_{\text{bind}}/\text{heavy atom count}$).⁸⁸ Finally, small fragments may bind in the smaller and broader binding sites present on protein-protein interaction targets.⁸⁹

Due to their small size and weak binding affinity, fragment hits must be improved through one of several approaches:⁸⁴ (1) fragment growing, where an anchor fragment is iteratively expanded by additional chemical matter; (2) merging, where two or more fragments shown by crystallographic studies to overlap in space may be merged into a single compound encompassing all binding sites;⁹⁰ and (3) linking, where two fragments in close proximity may be covalently linked. A linked compound binds with an affinity described as $K_D = K_D(1\text{st}) * K_D(2\text{nd}) * L$, where K_D is the binding constant for each ligand, and L is a constant to account for linking. While a primary fragment screen may identify two adjacent and non-overlapping fragments, more commonly a second fragment screen with a saturating concentration of the first site-ligand is used to identify second-site hits (Figure 2-6).

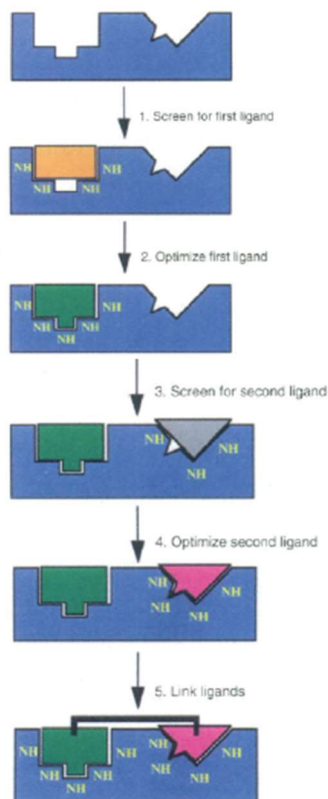


Figure 2-6: Fragment optimization through a linking approach

A “first-site” fragment screen identifies a fragment that binds in an available site on the protein surface (1). After identifying the tightest-binding fragments, SAR and chemical modification are conducted to optimize binding affinity and modality of this first site ligand (2). A second fragment screen is conducted in the presence of saturating concentrations of the optimized first-site ligand to detect “second-site” binding compounds (3). Identified second-site ligands are then optimized for binding affinity (4) and chemically linked to the first site using a flexible linker (methylene, ether, etc) (5) with the goal of discovering a linked ligand with micromolar or better affinity. Adapted from Shuker *et al*, 1996.⁹¹

Our group previously reported on the discovery of over 140 compounds identified in a fragment-based screen that bound to K-Ras-GDP (G12D).⁷⁶ Many of these hits also bound wild-type K-Ras, an alternative mutant form of K-Ras (G12V), and H-Ras. Crystallographic and NMR-based studies revealed that these compounds bind in an induced pocket formed by a conformational change whereby the $\alpha 2$ helix of switch II moves away from the central β sheet of the protein (Figure 2-7). Further, the side chain of Y71 breaks the hydrogen bond network present

in the ligand-free form by rotating to open a primarily hydrophobic pocket where the indole moiety binds. The M67 side chain additionally rotates out of the way to form a shallow electronegative binding cleft adjacent to the primary binding pocket. In total, these conformational changes create a binding site for small molecules that is not present in the apo-K-Ras “closed” form.

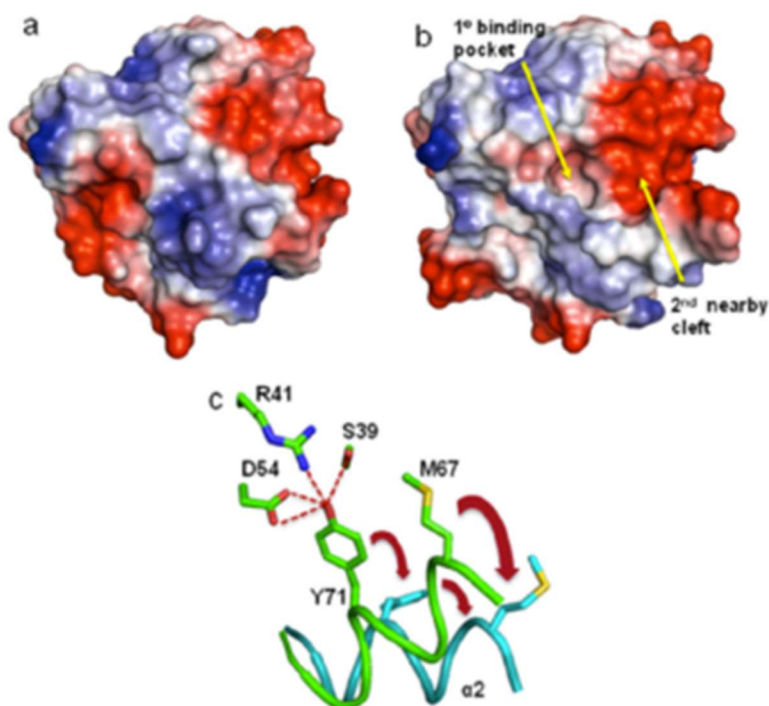


Figure 2-7: K-Ras (G12D) alters conformation upon binding a first-site fragment hit.

Electrostatic surface representations of GDP-K-Ras **(A)** in the “closed” form absent a bound ligand, and **(B)** the “open” form with indole series ligand bound. Note the presence of primary and secondary binding sites. **(C)** Schematic demonstration of Y71 and M67 movements in the transition from “closed” (green) to “open” (cyan) K-Ras conformations induced by ligand binding. Adapted from Sun *et al*, 2012.⁷⁶

These compounds function as activation inhibitors by blocking SOS-catalyzed nucleotide exchange in an *in vitro* biochemical system by preventing SOS-K-Ras interaction through a steric clash between compound and the α H helix of SOS.⁷⁶ As of this writing, it remains unclear whether

this effect occurs in a cellular environment, whether other Ras GEFs can bind to compensate for loss SOS activity, or how Ras activation and downstream signaling is altered.

2.1.6 Scope of this thesis chapter

An alternative approach to inhibiting K-Ras for the treatment of cancer is to block effector binding to the active, GTP-bound form. As discussed above, K-Ras undergoes conformational changes in the switch I and switch II regions when bound to GTP, which may alter compound binding. Therefore, we reasoned that a fragment-based screen could also identify fragments that bind to the GTP-bound form of K-Ras and directly block effector binding. Moreover, we could counterscreen GTP-bound K-Ras against those compounds that were identified in the original GDP-K-Ras screen in order to ascertain binding specificities between the forms. Herein I report the discovery of small-molecule K-Ras inhibitors through a fragment screening approach that bind to the active, GTP-bound form.

2.2 Results

2.2.1 K-Ras purification and nucleotide exchange

K-Ras is the most highly mutated Ras isoform in human cancer, and the glycine to aspartic acid mutation at residue 12 (G12D) is commonly utilized in human cancers to activate Ras signaling. For these reasons, we chose to conduct our fragment-based screen against this mutant isoform. To generate the protein needed for this fragment screen, monoisotopically ¹⁵N labeled K-Ras (G12D) was expressed in *E. coli* and purified using nickel-affinity and size-exclusion chromatography (Figure 2-8A).

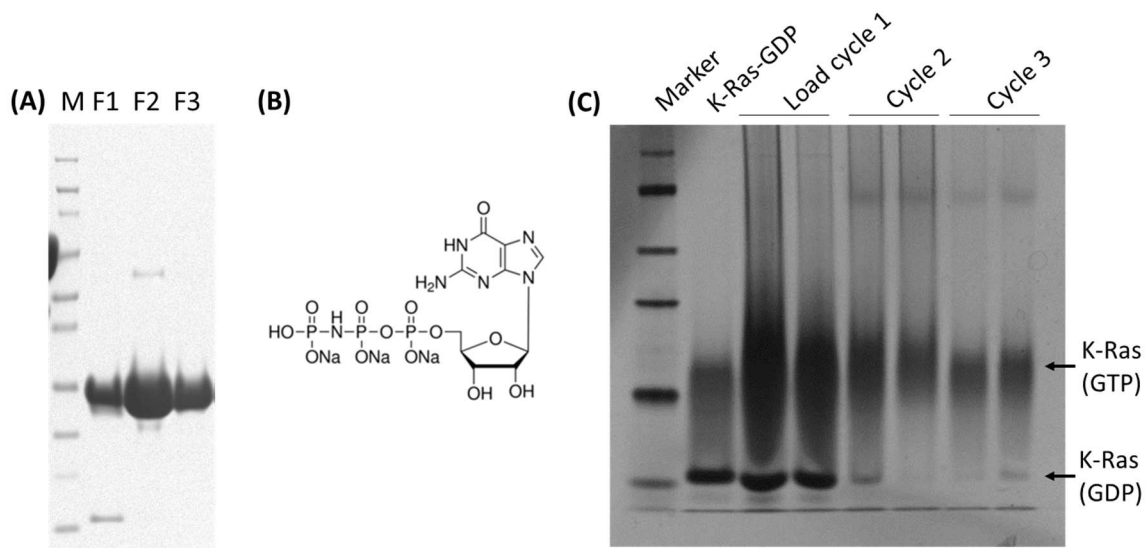


Figure 2-8: Expression and purification of K-Ras (G12D)

HIS6-MBP-K-Ras was expressed in *E. coli* and purified on a nickel-affinity column. TEV protease was used to cleave off the MBP tag, and K-Ras was isolated on a Superdex-100 size-exclusion chromatography column. Elution fractions containing the most highly pure K-Ras samples were used (labeled F1-F3, **A**). Due to intrinsic GTP hydrolysis, purified K-Ras uniformly binds GDP. We exchange to a non-hydrolyzable analog of GTP (GppNHp, **B**) by three successive loading cycles. EDTA destabilized GDP-binding by chelating Mg^{2+} and the enzyme Apyrase hydrolyzed GDP to the weaker affinity GMP molecule. GTP-PNP (1mM) was then added to competitively bind K-Ras. Each load cycle resulted in a more uniform K-Ras-GTP population as visualized on a Tris-glycine native gel (**C**), characterized here by a slower migrating band and the removal of the faster migrating K-Ras-GDP band seen in the untreated sample.

Despite significantly reduced intrinsic GTPase activity compared to wild-type protein, K-Ras (G12D) is fully GDP-bound after purification. Moreover, this intrinsic rate of hydrolysis precludes screening with GTP-bound protein due to gradual hydrolysis at a non-trivial rate. Therefore, we forcibly loaded K-Ras with the non-hydrolyzable GTP analog Guanosine 5'-[β,γ -imido]triphosphate (GppNHp). To accomplish this, GDP-binding was destabilized by chelating magnesium with EDTA, and the enzyme Apyrase was added to hydrolyze the α - β phosphate on GDP to form GMP. GppNHp (1mM) was then incubated at 30°C for 30 minutes to allow competitive binding to K-Ras. After a buffer exchange, this process was repeated two additional times to ensure complete loading (Figure 2-8C). Finally, Mg^{2+} ion was added to lock K-Ras in its

new GTP-PNP bound conformation. Subsequent measurements days or weeks later confirmed that GppNHP remains bound to K-Ras and is not hydrolyzed by enzymatic activity.

We measured the $^1\text{H}/^{15}\text{N}$ HSQC spectra of GTP-loaded K-Ras (Figure 2-10A), which is highly similar to the published spectrum of H-Ras-GTP.⁹² We compared the spectra to K-Ras-GDP (Figure 2-9B). As expected, a distinct shift is noted for many peaks after loading with the GTP analog. NMR signals for the P-loop and Switch I & II regions of K-Ras-GTP are often missing due to conformational exchange and polysterism; indeed, we observed fewer peaks in the GTP-bound form.^{92,93}

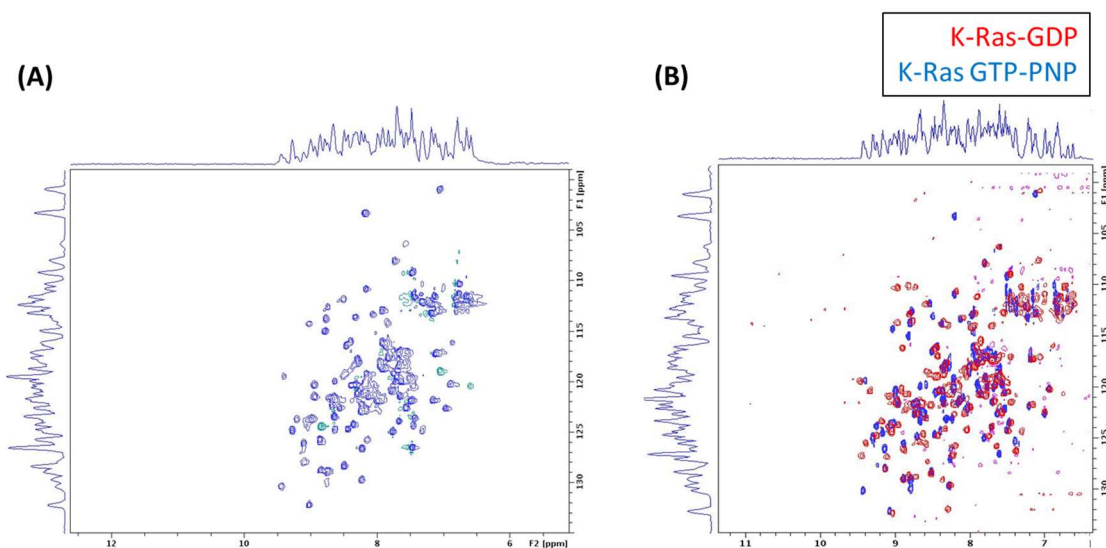


Figure 2-9: NMR confirms the successful loading of K-Ras with GppNHP
(A) $^1\text{H}/^{15}\text{N}$ HSQC spectra for purified K-Ras-GTP-PNP. (B) A distinct peak shift is observed between the GDP (Red) and GTP-PNP (Blue) loaded forms of K-Ras, indicating a successful analog exchange accompanied by a general conformational change.

2.2.2 First-site Fragment Screen

Because K-Ras lacks a well-defined ligand binding pocket, and due to the success of the K-Ras-GDP fragment screen discussed in the introduction, we sought to discover a K-Ras-GTP

inhibitor by using a similar fragment screening approach. We conducted a first-site fragment screen to identify compounds that bind to K-Ras-GTP. Because fragments typically bind weakly with 100 – 1000 μ M affinities, the technique used to detect fragment binding must be able to observe weak binding and tolerate high compound concentrations (on the order of 500 μ M or greater) without measurement artifacts, for which NMR is ideally suited. An NMR-spectroscopy-based screen of 11,000 fragments yielded 72 fragments that bind to GTP-bound K-Ras (hit rate=0.65%) as determined by changes of ^1H and ^{15}N chemical shifts in $^1\text{H}/^{15}\text{N}$ HSQC spectra. Representative examples of some of the hits that were identified in the fragment-based screen are depicted in Figure 2-10 and Figure 2-11. All of the hits are shown in Appendix A. Fragment hits were assigned a SCORE from 0-3, with a higher number indicating a larger magnitude ppm peak shift which is suggestive of a higher affinity interaction. Additionally, a counterscreen was conducted against all highly scored (SCORE=3) fragments and synthesized compounds which has been identified to bind K-Ras-GDP.⁷⁶ This counterscreen allowed us to gain insight into the SAR behind selectivity for GTP or GDP-bound forms of K-Ras. Thirty-nine additional hits were identified in this counterscreen, for a total of 110 fragments and synthesized compounds identified. Fifty-four fragments were SCORE=1; thirty-four were SCORE=2; and twenty-two were SCORE=3.

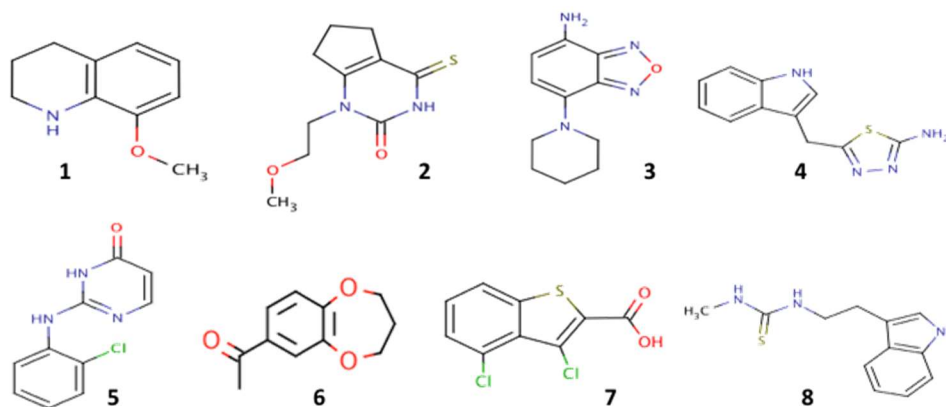


Figure 2-10: K-Ras-GTP selective compounds

These compounds were identified in the fragment-based screen against K-Ras-GTP but were not observed to bind to K-Ras-GDP.

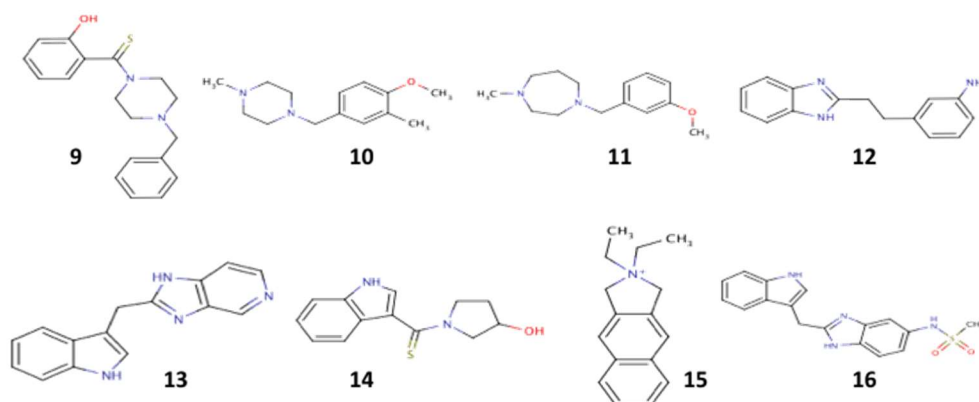


Figure 2-11: Compounds that non-selectively bind GDP- and GTP-bound Ras

The majority of compounds identified in the K-Ras-GTP fragment screen also bound to K-Ras-GDP. Shown here are several examples. A complete list of hits is provided in Appendix A.

2.2.3 Hit characterization

Fragments identified in the primary screen were classified into six series based on common structural features: indoles, catechols, halobenzenes, sulfonamides, phenols, benzimidazoles, and singleton compounds of various chemotypes.

Commonalities in the HSQC spectra for each compound were noted to provide insight into shared binding modes. Alterations in peak location necessarily indicate a change in the

electronic shielding of the H and N nuclei being measured, and may occur for several reasons. Binding of the ligand may directly perturb the chemical shifts of residues in close proximity to the binding interface and/or the added ligand may induce structural/conformational changes in the protein, which can also cause chemical shift changes. One cannot *a priori* determine the reason for the changes in chemical shift since the directionality and intensity of these peak differences is caused by several non-exclusive events. For example, atoms moved out the plane of an aromatic system will be shifted upfield, as will weakening or breaking a hydrogen bond interaction.⁹⁴ Despite these differences, we could use the HSQC-NMR spectra to classify compounds based on similar chemical structures and observed peak shifts. Because the backbone assignments have been published for both the GDP⁹⁵ and GTP⁹⁶ forms of K-Ras, we were able to specify which regions were affected by ligand binding.

The indole series of compounds were the most heavily investigated after the K-Ras-GDP fragment screen published in Sun et al, 2012, and many indole-containing fragments also bound to the GTP-bound form of K-Ras. VU0430640-1 is representative of the many compounds in this series that bind to K-Ras-GTP. When bound, a characteristic rightward shift is seen for G75 as indicated in Figure 2-12. Chemical shift changes were also observed for both C80 and V81.

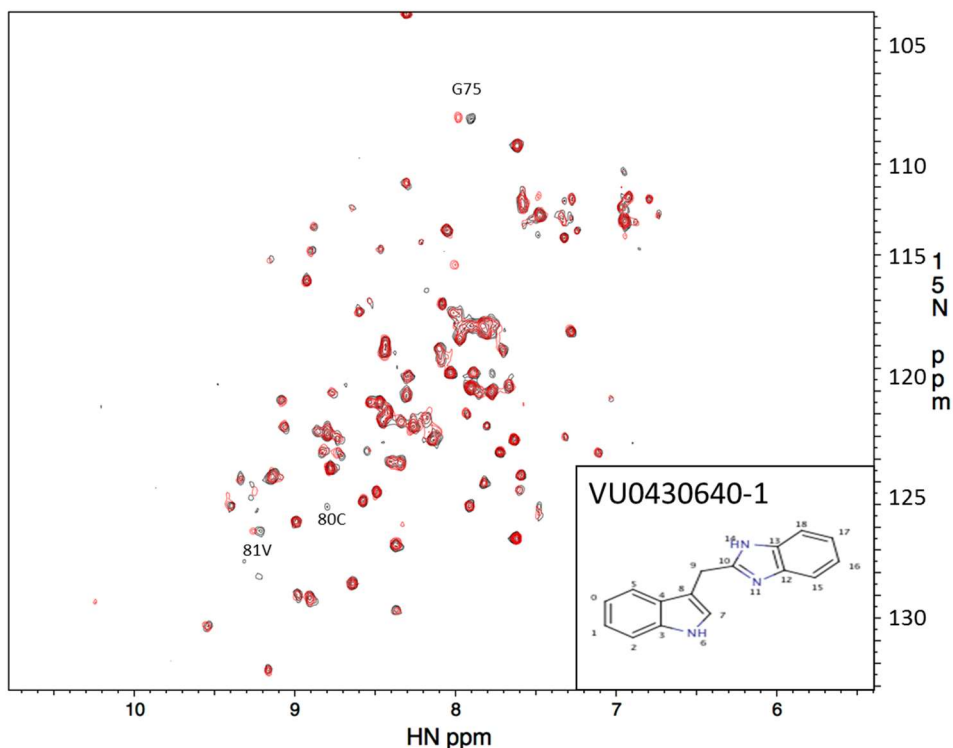


Figure 2-12: HSQC-NMR spectrum of ^{15}N -K-Ras in the presence of VU0430640-1

The spectrum of K-Ras-GTP (red) when incubated with $800\mu\text{M}$ VU0430640-1 is overlaid with a reference apo-spectrum (black). Note the rightward shift of G75 peak caused by ligand binding, as well as shifts in both C80 and V81.

While crystal structures were not determined for the hits obtained in the screen when bound to K-Ras-GTP, it is highly likely that these compounds bind in an analogous way to Compound 4 exemplified in Sun *et al*, for which X-ray crystallographic data were published (Figure 2-7).⁷⁶

While the peak shift pattern exemplified in Figure 2-13 is typical for the indole series of compounds, other patterns were observed. For example, Figure 2-15 exemplifies a pattern in which the G75 peak disappears, but C80 and V81 shift in similar magnitude and direction to that observed in Figure 2-13.

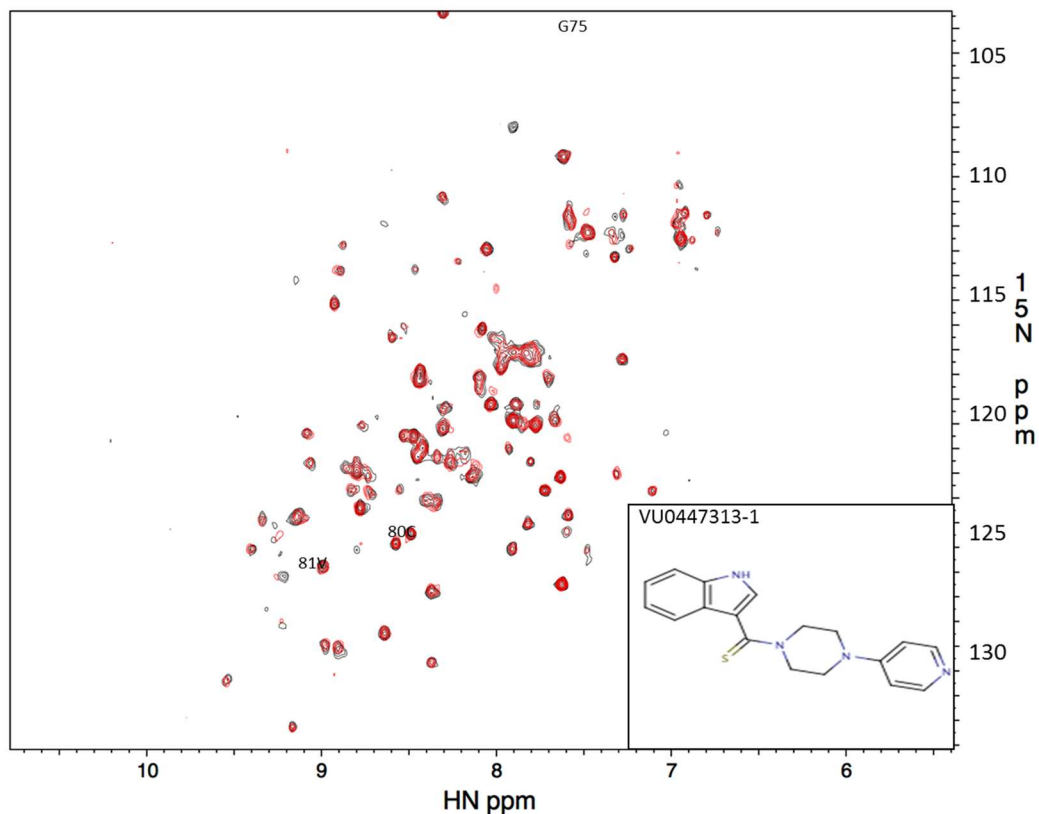


Figure 2-13: HSQC-NMR spectrum of ^{15}N -K-Ras in presence of VU0447313-1

The spectrum of K-Ras-GTP (red) when incubated with $800\mu\text{M}$ VU0447313-1 is overlaid with a reference apo-spectrum (black). Note the disappearance of G75 peak caused by ligand binding.

Other compound series, such as the benzoamide compounds (Figure 2-14), show a quite distinct shift pattern. The G75 peak shifts in an opposite direction to that seen for indole compound exemplified above, and both the quantity and intensity of peak shifts are unparalleled for any other series. Amino acids are affected not only near the induced pocket mentioned above, but in helices and loops across the entire protein.

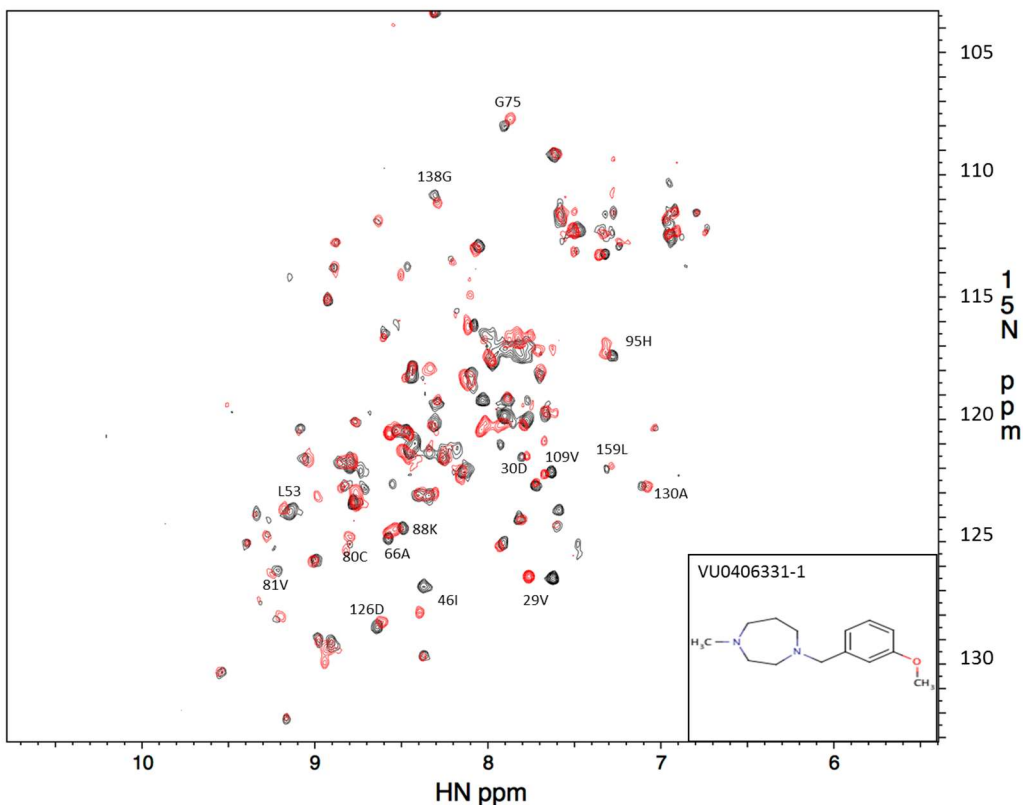


Figure 2-14: HSQC-NMR spectrum of ^{15}N -K-Ras in the presence of VU0406331-1

The spectrum of K-Ras-GTP (red) when incubated with $800\mu\text{M}$ VU0406331-1 is overlaid with a reference apo-spectrum (black). More peaks shifted with this series of compounds than for any other identified in the fragment screen.

To determine the binding dissociation constants for compounds bound to K-Ras-GTP, a saturation-binding curve was measured for four fragment hits and 36 compounds that had been synthesized for the K-Ras-GDP inhibitor program. I used HSQC-NMR to measure the compound-mediated, dose-dependent shift of the G75 peak (Figure 2-15). Fragment screening hits bound to K-Ras-GTP (G12D) with affinities of $0.4\text{-}2\text{mM}$, and synthesized compounds were measured to bind with affinities as low as $178\mu\text{M}$. These results are tabulated in Appendix B.

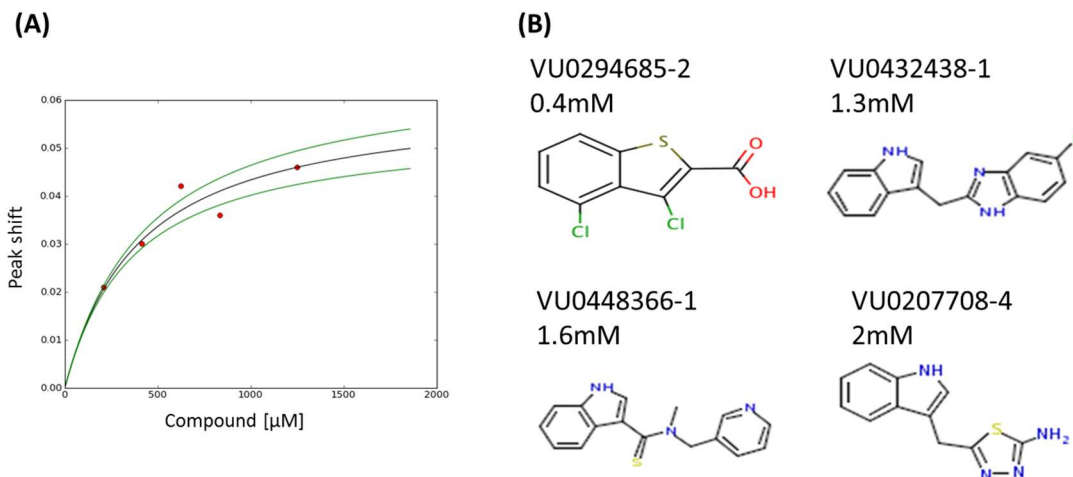


Figure 2-15: Determination of compound dissociation constants by NMR

(A) Peak shifts in HSQC-NMR spectra were measured for compounds at a variety of concentrations. The K_D is determined by plotting relative peak shift from the DMSO control vs. the compound concentration used and fitting a nonlinear regression curve. Shown is an example curve for VU0294685-2. The K_D was determined to be 0.4mM. **(B)** Four compounds with NMR-determined affinity are shown. A complete list is provided in Appendix B.

To identify the unique chemical features for binding between the GDP- and GTP-bound forms of K-Ras, SCORES for each compound identified in the K-Ras-GTP counterscreen were compared to the SCORES for GDP-bound K-Ras (results tabulated in Appendix A). Overall, the GTP-bound form generally binds fragments weaker than GDP-K-Ras, as evidenced by fewer primary hits in the fragment screen, fewer SCORE=3 compounds, and weaker K_D values for compounds measured against both GDP- and GTP-bound forms.

As mentioned above, the indole series of compounds identified in both the fragment screen and elaborated by chemists in the group bind similarly in both the GDP- and GTP-bound forms. The indole appears to occupy the same induced binding pocket in both forms, as seen by similar peak shift patterns. Moreover, the extended binding cleft occupied by the benzimidazole in Figure 2-7 appears to be similar between K-Ras forms, lengthy fragments with several heterocyclic rings connected in series are tolerated. However, indole binding was not uniform.

For example, some members of the indole series of compounds bind to GTP-K-Ras but demonstrate little binding to the GDP-bound form, such as VU0207708 and VU0412845 in Figure 2-16.

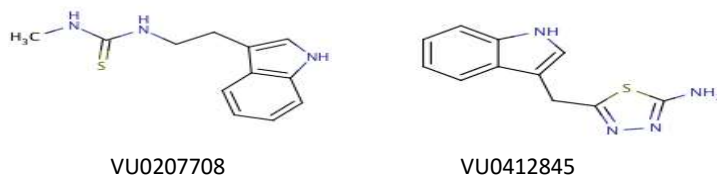


Figure 2-16: Examples of selective indole-containing compounds

Indole-containing compounds with SCORE=3 against K-Ras-GTP but which do not bind K-Ras-GDP.

Unlike the indole series, catechols preferentially bind to K-Ras-GTP. Several compounds, exemplified in Figure 2-17, bind tightly to the GTP-bound form but not to the GDP-bound form. The sulfonamide series, which showed distinct promise as a nucleus for a GDP-K-Ras inhibitor program, were largely inactive against GTP-bound K-Ras.

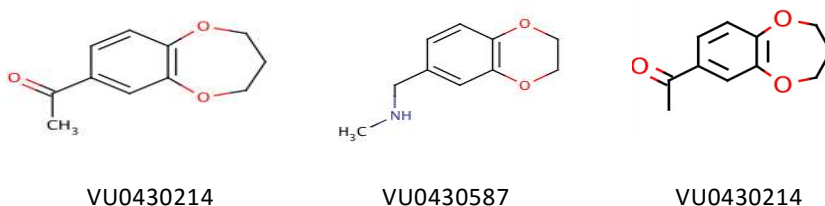


Figure 2-17: Examples of selective catechol-containing compounds

Exemplified catechol compounds that bind to K-Ras-GTP but not to K-Ras-GDP

2.3 Discussion

K-Ras is one of the most commonly mutated oncogenes in human cancer.³² Ras pathway activations contribute to tumor initiation, maintenance,¹¹ increased proliferation, evasion of programmed cell death, altered metabolism, induced angiogenesis, increased invasion and metastasis, and evasion of immune destruction.⁵⁷ Moreover, K-Ras mutant cancers correlate with

decreased response to therapy.⁵⁵ In contrast, inactivation of oncogenic Ras reverses the transformed phenotype of cells both *in vitro* and *in vivo*, and results in the dramatic regression of tumors in murine xenograft models.^{66,67} Yet despite the preponderance of evidence linking Ras to cellular transformation, and its inhibition to a reversion of that transformed phenotype, no Ras inhibitor has yet achieved clinical testing. Ras is a technically challenging protein for which to develop a small-molecule inhibitor, and some believed that inhibiting this “undruggable” protein was impossible.⁶⁹ In light of the challenges inherently present in directly targeting Ras, alternative strategies have been developed to inhibit Ras indirectly by modulating other proteins in the Ras effector pathway. Several of these attempts, such as inhibitors of downstream effector proteins Raf by Sorafenib and Mek by Trametinib, have achieved FDA approval for clinical use. Nevertheless, direct Ras inhibition would be preferable in both the breadth of downstream targets effected and the avoidance of feedback inhibitory mechanisms which confound downstream inhibitor activity. Therefore, a direct Ras inhibitor remains a highly challenging but extremely important anti-cancer target in drug discovery.⁶⁹

Despite these hurdles, a prior fragment-based screen of the inactive GDP-bound form of K-Ras identified over one hundred fragment hits. Subsequent NMR studies, x-ray crystallography, and dedicated compound synthesis resulted in compounds which bound in the low hundreds of micromolar and inhibited nucleotide exchange by SOS-GEF.⁷⁶ As described here, a fragment screen was also conducted for the active, GTP-bound form of K-Ras and revealed differences in binding preferences between the two forms. These results could potentially lead to an inhibitor that directly blocked effector activation. I identified 72 compounds that caused distinct ¹H and ¹⁵N chemical shifts in ¹H/¹⁵N HSQC spectra when bound to K-Ras-GTP, and further

counterscreened all high-affinity compounds from our K-Ras-GDP inhibitor project to ascertain specificity. In total, 110 compounds were detected to bind to the GTP-bound form of K-Ras, which corresponds to less than 1% hit rate. However, a previous analysis of fragment-based screens suggests that protein targets with a hit rate of at least 0.1% can result in the design of high affinity, drug-like molecules against the target.⁹⁷ Therefore, K-Ras in both the GDP and GTP bound forms could be a druggable protein, albeit a significantly challenging one.

It remains unclear whether fragments identified in our K-Ras-GTP screen also bind to other Ras isoforms. Given the complimentary binding profiles seen for K-Ras-GDP compounds also binding to these other Ras isoforms, this suggests a similar complementarity for GTP-bound forms.

The biological activity of these compounds was not investigated for this dissertation. Mutating residues in the switch II region of Ras, or otherwise altering the conformation of that region, can block effector binding in a cellular context.^{75,98} Therefore, it is possible that the fragments discovered in this chapter may block effector binding to K-Ras-GTP if they bind in a similar way to the fragments identified in the K-Ras-GDP screen. Alternatively, a compound could be extended from its anchor point in the induced pocket at tyrosine 71 to physically occlude effector binding.

Primary fragment hits often bind weakly (hundreds to thousands of μM), as was the case in this screen. Discovery of potent (nM) affinity compounds using fragment-based drug discovery requires linking or merging a first-site fragment with a second fragment occupying an adjacent site, or iteratively growing the first-site fragment to occupy additional pockets and binding interfaces on the protein surface. These techniques are significantly aided by x-ray

crystallography to determine the binding location and orientation of fragments and to suggest the most appropriate ways to grow, merge, or link fragment hits. While Qi Sun and Jason Phan solved multiple co-crystal structures of fragments bound to K-Ras-GDP, they were unable to discover conditions suitable for K-Ras-GTP/fragment co-crystallization. This significantly impeded the discovery effort.

Despite these challenges, these molecules represent a starting point for obtaining probe molecules useful in elucidating new insights into Ras signaling and for discovering K-Ras inhibitors for the treatment of cancer. The Fesik group has recently begun a collaboration with Boehringer Ingelheim to continue the discovery of K-Ras inhibitors, primarily focused on the GTP-bound form. Chemical optimization conducted by an active team at Boehringer Ingelheim has initially focused on synthesizing analogs based on the fragment hits described in this chapter. Their second key contribution is the ability to co-crystallize K-Ras-GTP with a bound ligand, thus providing key structural information needed to fully elucidate compound SAR. Thus, it may now be possible to discover high affinity ligands capable of inhibiting K-Ras-GTP activity. A K-Ras-GTP inhibitor should disrupt effector binding *in vitro*, reduce signaling through Ras-modulated pathways, and inhibit cancer cell growth in culture and *in vivo*. These predictions await confirmation upon the discovery of high-affinity K-Ras-GTP inhibitors.

2.4 Methods

Cloning, expression, and purification

The GTPase domain (residues 1-169) of oncogenic mutant K-Ras (G12D C118S) was cloned, expressed, and purified as previously described.⁷⁶ Briefly, a pDEST construct containing

the sequence for maltose binding protein (MBP) fused to the K-Ras expression sequence using a tobacco etch viral protease (TEV) recognition sequence linker. This vector was transformed into Rosetta 2 (DE3) E. coli and expressed in a BioFlow 415 fermentor (New Brunswick Scientific) in minimal media (4g/L KH₂PO₄, 6g/L K₂HPO₄, 1g/L NA₂SO₄, 1g/L K₂SO₄, 1g/L Yeast Extract, 1mL/L Glycerol, 5mL/L K12 trace metals solution, 0.2mL/L Antifoam, 20g/L glucose, 2mL/L 1M MgCl₂, 0.1mL/L CaCl₂, 1mg/L Thiamine, 10mL/L 100x MEM vitamins, 1.0g/L ¹⁵NH₄Cl, and ampicillin, at pH 7.0 with a dissolved oxygen of 35-65% and 10% O₂ after induction. Expression was induced with 1 mM IPTG at a cell density corresponding to an absorbance of OD₆₀₀=1.0. The fusion protein was purified on a Ni-IDA (ProBond from Invitrogen) column in buffer containing 20mM Tris-HCL, 150mM NaCl, and 1mM DTT. A 1:20 molar ratio of TEV protease was used to cleave the MBP fusion protein, and the mixture was separated by flowing over an Ni-NTA column, and the K-Ras protein was collected in the flow through and exchanged into a low salt buffer. Purified proteins were concentrated with Amicon ultra centrifugal columns (Millipore).

K-Ras in vitro nucleotide exchange

Purified K-Ras-GDP at 10mg/mL is added to Exchange Buffer (5mM EDTA, 2mM CaCl₂, 1mM GTP-PNP, 3U/mL Apyrase). This solution is incubated at 30°C for 30 minutes, buffer exchanged into fresh Exchange Buffer, and repeated an additional two times. The final solution is buffer exchanged into buffer containing 25mM Tris-HCl pH 7.0, 50mM NaCl, and 1mM MgCl₂.

Fragment library composition

A proprietary collection of small molecule “fragments” was assembled as previously described.⁷⁶ Briefly, 11,000 chemically diverse compounds representing more than 700 distinctive ring systems were purchased from major chemical supply manufacturers which fit certain criteria ($MW \leq 300$, $cLogP \leq 3.0$, no more than 3 hydrogen bond donors, and no more than 4 rotatable bonds). Compounds were preferentially selected with bias towards compounds containing rings and functional group substitutions that are known in the literature to show high affinity for protein binding, especially at the interface for protein-protein interactions. Compounds with functional groups known to react under physiological conditions were excluded.

Fragment-based screen

The fragment-based screen was conducted using two-dimensional sensitivity-enhanced $^1H/^{15}N$ - HSQC spectra collected on a Bruker DRX500 spectrometer equipped with a cryoprobe and a Bruker Sample Jet sample changer. Each sample contained 50 μ M GTP-bound K-Ras (G12D) protein and 12 fragments at a concentration of 650 μ M. Positive hits were deconvoluted by testing samples containing a mixture of four compounds, then individually testing positive hits from those samples. Screening data were processed using Bruker TOPSPIN and analyzed by comparing spectra with and without compounds. Dissociation constants were obtained for selected compounds in fast exchange by monitoring the chemical shift changes of resonances as a function of compound concentration using standard fitting software.

Chapter 3

Discovery of Pak-1 inhibitors

3.1 Introduction

p21-Activated Kinase-1 (Pak-1) is the founding member of the Pak family of kinases, and regulates a wide variety of cellular processes including cell motility, actin rearrangement, proliferation, and apoptosis. Its role in driving tumor growth, survival, and metastasis has been demonstrated in multiple pre-clinical cell-based and animal studies, and human clinical data suggest a link between its expression and a higher tumor grade and lower overall survival in several cancer types. In this chapter, we will review the tumorigenic role Pak-1 plays in cancer biology and our efforts to discover specific Pak-1 small-molecule inhibitors.

3.1.1 *Structure and function of the Pak family kinases*

The Pak family of Sterile 20 (Ste20) serine/threonine kinases contains six isoforms divided into two groups: Pak 1-3 comprise Group I and Pak 4-6 comprise Group II.⁹⁹ Structure, function, and expression profiles differ substantially for Pak family members, especially between Group I and II Paks. Pak-2 and Pak-4 are ubiquitously expressed in adult human tissues, while Pak-1 is highly expressed in the brain, muscle, and spleen.¹⁰⁰ Indeed, Pak-1, 3, 5, and 6 all play an important role in neuronal tissues where deregulation may contribute to mental retardation, Alzheimer's, and Huntington's disease.¹⁰¹ Pak-2 and Pak-4 are ubiquitously expressed and their loss is embryonically lethal in mice due to defects in vascularization and heart development, respectively. Pak-1 null mice are viable¹⁰² but manifest various defects in the central nervous

system, immunity, metabolism,^{103,104} and most severely, alterations in cardiac ion regulation and actinomyosin function.¹⁰⁵ These defects cause Pak-1-deficient mice to become more vulnerable to cardiac hypertrophy and failure under sustained load.⁴

All six Pak proteins contain a catalytic kinase domain of traditional structure. Protein sequence homology is extremely high within members of a group; sequence similarity exceeds 90 percent among the Group I Paks, and is 79 percent or more homologous among the Group II Paks. Sequence homology between group members is lower (between 50 and 60 percent).¹⁰⁶ The key distinctive feature that separates Pak proteins from other kinases is their N-terminal regulatory region, which contains multiple domains contributing to Pak auto-regulation, localization, scaffolding, and effector activation. This region also forms the key differentiator between Group I & II Paks, with groups differing substantially in domains expressed, their method of auto-regulation, and scaffolding functionality (Figure 3-1).

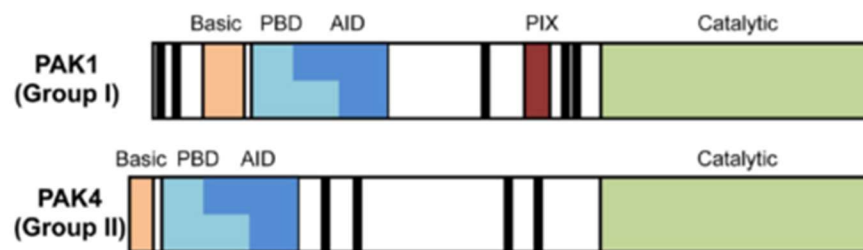


Figure 3-1: Pak kinases are classified into two groups

Pak groups I & II are differentiated by the composition and arrangement of domains within the N-terminal regulatory region. These differences have profound effects on protein localization, activation, and scaffolding of other signaling components. However, all Pak kinase isoforms contain a conserved catalytic subunit at the C-terminal end of the protein. Figure from Rudolph *et al*, 2015.¹⁰⁶

Group I Paks are constitutively auto-inhibited by trans-dimerization, a distinguishing feature among serine/threonine kinases.¹⁰⁷ Activation of Group I Paks occurs due to three N-terminal regulatory regions: a proline-rich SH3-binding domain, GTPase protein binding domain

(PBD), and a regulatory auto-inhibitory domain (AID).¹⁰⁸ In cells, Pak-1 forms an auto-inhibited homodimer via the AID (in contrast to tyrosine kinase family receptors, which are activated by dimerization). Group I Paks in healthy or cancerous cells require activation via binding of the p21-proteins Rac1 or Cdc42 to the PBD.^{100,109} This in turn causes dissociation of Pak dimers, auto-phosphorylation of T402 and T423,^{107,110,111} and constitutive kinase activation. Activator proteins can then dissociate without impeding activity, although may remain bound to be localized to the cellular leading edge.¹⁰⁹ Grb2 or Nck SH3-mediated binding to Pak proline rich regions induces activation in a p21-independent process. These proteins localize Group I Paks to the plasma membrane near active receptor tyrosine kinases (RTKs) such as EGFR. These RTKs can then in turn directly phosphorylate Pak to activate it.¹¹² Alternatively, Nck mediates localization to focal adhesions and the co-recruitment of Pak-1-interacting exchange factor (PIX) to Pak-1 through an SH3/proline-rich region interaction. PIX activates Pak-1 indirectly through its GEF activity for Rac1 and CDC42.^{113,114} Nck-mediated recruitment to the plasma membrane also enables Pak activation via sphingolipid-mediated disruption of the Pak homodimer,¹¹⁵ though Rac1/CDC42-mediated activation is by far the most commonly employed method to control Group I Pak activity.

In contrast to the well-studied activation functions of the Group I Pak N-terminal region, this region of the Group II Paks has only recently been elucidated. While Rac1/CDC42 binding via the PBD has long been observed, initial reports indicated that binding did not alter Group II Pak activity. In fact, they appeared to be constitutively active.¹¹⁶ However, recently it has been suggested that Pak-4 does contain an auto-inhibitory domain, though no consensus has been reached on the mechanism by which Rac1/CDC42 binding activates the protein.^{117,118} These studies suggest that Pak-4 catalytic activity (and, possibly, the group II Paks in general) is

regulated by conformational changes in the N-terminal region rather than phosphorylation in the kinase domain activation loop (Ser474), as is seen for Group I Paks.¹¹⁹ Regardless of the specific mechanisms, all Pak isoforms require activation by one of these processes (Rac1/CDC42 binding, RTK-mediated phosphorylation, or membrane recruitment).

Pak kinases function to transduce signaling from cell-cycle regulators (via CDC42), cell-surface receptors (via Rac1), and cellular damage sensors (via Caspase-3) to downstream effectors controlling cellular motility, proliferation, cell cycle, and survival (Figure 3-2).¹⁰⁰ Substrates for Pak kinases number in the dozens; some substrates are phosphorylated by multiple Pak isoforms, while others (such as MEK1 at serine 298) are phosphorylated solely by a single Pak isoform.¹⁰⁹ Pak proteins also rely on extensive protein scaffolding functionality in their N-terminal region to control the activity of cellular processes independent of catalytic kinase activity, such as by co-localizing MEK and Raf1 to increase downstream ERK activation¹²⁰ or by enabling PI3K-mediated signaling by co-localizing PDK-1 to Akt.¹²¹

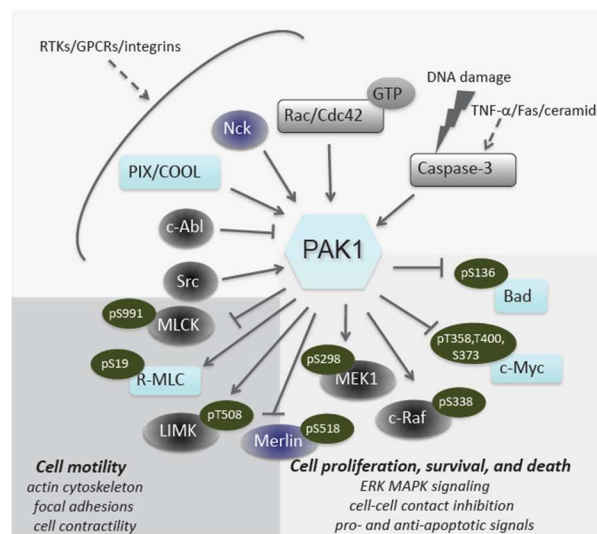


Figure 3-2: Pak kinases regulate cellular motility, proliferation, and survival

Pak-1 interaction partners are shown with indicated phosphorylation sites. Pak-1 requires upstream activation by one of several processes, though most commonly by Rac1 and CDC42 binding. Once active, Pak-1 directly phosphorylates a wide range of substrates regulating motility,

survival, and proliferation. Shown here are the most notable substrates regulated by Pak-1 including MLCK, Merlin, MEK, c-Raf, and Bad. Adapted from Ong *et al*, 2011.¹²²

3.1.2 Pak kinases promote cancer progression and metastasis

All Pak isoforms have been implicated in cancer progression.¹¹⁹ Pak-1 and Pak-4 are the most commonly overexpressed isoforms, while the other isoforms are more rarely overexpressed. Cancers for which Pak-1 in particular is commonly overexpressed include breast, colon, brain, prostate, and ovarian, and recent literature indicates an important role in lung cancer as well.^{109,122} In breast cancer, PAK1 is amplified in 9% and overexpressed in 55% of patients and correlates with HER2+, ER+ breast cancer, and a poor prognosis.¹²³ Higher Pak-1 expression also correlates with increased lymph node invasion, and is more frequently observed in nodal metastases than in primary tumor samples.¹⁰⁶ Pak-4 is also commonly overexpressed in various cancers including pancreatic, breast, and colon cancers.^{119,123} Increased expression correlates with higher tumor grade, invasiveness, and a worse overall prognosis.¹²⁴

Cancer type	Pak isoform	Type of alteration	References
Breast	PAK1	55% protein overexpression	18
Breast	PAK1	Protein overexpression and tamoxifen resistance	33
Colon	PAK1	Protein overexpression	117
Ovarian	PAK1	30% gene amplification; 85% protein overexpression	118
Bladder	PAK1	Gene amplification	H. Nishiyama and O. Ogawa, personal communication
Pancreas	PAK4	Gene amplification; protein overexpression	12
Brain	PAK1	Protein overexpression	Y. Kondo and K. D. Aldape, personal communication
Neurofibromatosis	PAK1	Protein stabilization	24
T-cell lymphoma	PAK1	Gene amplification	119

Table 3-1: Cancers in which Pak-1 and Pak-4 are most commonly overexpressed or amplified
Figure from Kumar, et al.¹²³

Despite their immutable requirement for external activation to overcome constitutive homodimerization, activating mutations are rare in Pak kinases. Mutations of any sort for Pak-1 occur in just 100 of 22,000 cases in the COSMIC database.¹²⁵ Activating point mutations have only been reported in Pak-4 and Pak-5 in colon and lung cancers, though whether these contribute to tumor formation is currently unknown.^{126,127} In the absence of activating mutations, Paks still require external activation to overcome intrinsic inhibition: this may occur through simultaneous increases in Rac1/CDC42 activity (such as for Ras-mutant cancers discussed in Chapter II), or by relying on basal p21 activity to activate a larger molar quantity of Pak kinase.¹²⁸

These clinical observations linking Pak expression to invasive carcinomas and a worse prognosis have a solid molecular underpinning. Pak-1 plays three key roles in cancer progression. First, Pak promotes cell proliferation^{109,123,129} through direct phosphorylation and activation of Mek1 and Raf1,^{130,131} by activating the Akt and Wnt pathways,¹²⁸ through regulation of Aurora Kinase A and Polo-like kinase 1 (PLK1), and regulation of the nuclear hormone estrogen receptor that promotes its activation and signaling through Cyclin D1.¹³² Loss of Pak-1 expression through RNAi-based approaches reverses these phenotypes.¹⁰⁰

Second, Pak-1 drives cancer invasion and metastasis in late-stage tumors. Metastasis is an invasion-driven process whereby cells must attach to a matrix, enzymatically degrade it using matrix metalloproteinases (MMPs), and move across.¹³³ Pak-1 is known to drive cell motility and control filopodia at the leading edge and promote invadopodia.¹³⁴ The literature reports a host of cell-motility substrates that are phosphorylated by Pak-1 including LIM kinase, myosin light chain kinase, merlin, filamin A, p41-ARC, and Op18/stathmin,¹³⁵ and these pathways are likely utilized in cancer for metastasis. Furthermore, Pak-1 is recruited to cortical actin structures upon

cellular exposure to PDGF, insulin, and several other stimuli,¹³⁶ and Pak-1 activity is essential for invadopodia formation in the A375MM melanoma cell line.¹³⁴ Pak-1 regulates MMP expression and activity¹²⁸ to such an extent that mouse embryonic fibroblasts altered to prevent CDC42-mediated Pak activation were unable to remodel extracellular matrix.¹³⁷ These data indicate Pak-1 plays an important role in regulating and/or promoting cell motility and cancer metastasis.

Third, Pak-1 increases survival by blocking apoptosis through several mechanisms. Raf1 is phosphorylated at S338 to induce translocation to the mitochondria, where it binds Bcl-2 and phosphorylates BAD, thus preventing BAD-mediated induction of apoptosis.⁹⁹ Pak-1 can also phosphorylate BAD directly to prevent its antagonism of pro-death Bcl-2 family members.¹³⁸ Pak-1 also increases NF κ B pathway activation through an unknown mechanism,¹²⁸ and inhibits pro-apoptotic FKHR transcription.¹⁰⁹

Pak-1 activation drives human breast cancer progression. Synthetic Pak-1 activation *in vitro* increases cell growth and proliferation,¹⁰⁰ leads to anchorage-independent growth, and radically alters signaling throughout the cell.¹³⁹ Synthetic overactivation *in vivo* causes malignant mammary tumor development.^{123,140,141} Most significantly, inhibition of Pak-1 restricts cancer cell growth and metastasis but has no effect in non-cancerous tissue, thus supporting the hypothesis that Pak-1-amplified cells can become “addicted” to expression and would be susceptible to small-molecule Pak-1 inhibition.^{139,122} Moreover, several commonly activated oncogenes require Pak-1 to transform cells. Inhibition of Pak-1 can effectively silence Ras-induced cell transformation.^{142,143}

Finally, an inhibitor of Pak-1 would augment current therapies. For example, 70% of breast cancers express Estrogen Receptor alpha (E α) and are susceptible to estrogen receptor

antagonism by tamoxifen. Yet Pak-1 expression is predictive of tamoxifen resistance: active Pak-1 causes constitutive estrogen receptor activity and resistance to antagonism by phosphorylating $E\alpha$ at S305. Inhibition of this phosphorylation could restore tamoxifen resistance and improve patient outcome.^{144,145} Further, a screen conducted in NSCLC revealed potent drug-drug synergism with Pak-1 knockdown with several targeted therapeutics including BV6 (IAP antagonist), Erlotinib, and Gefitinib (demonstrating a 57-, 15-, and 13-fold change in EC_{50} coincident with Pak-1 knockdown).¹²² These pre-clinical and clinical data strongly suggest that a Pak-1 inhibitor would positively benefit patient survival in breast and other cancers. Importantly, a Pak-1 inhibitor should be selectively toxic for at least a subset of cancer patients. Knocking down Pak-1 expression in non-cancerous adult tissues gives no observable phenotype and the pan-Pak inhibitor PF-3758309 (discussed below) is not toxic to healthy tissues.

While the above discussion has focused exclusively on Pak-1, Group II Paks do contribute to tumorigenesis and cancer proliferation,¹⁰⁰ and RNAi-based inhibition restricts cell growth and survival.^{119,126} Of the Group II Paks, Pak-4 is the most widely studied, overexpressed, and important for tumorigenic signaling. Pak-4 is neither overexpressed as widely as Pak-1,¹¹⁹ nor relied upon as heavily for cancer cell transformation and progression.^{99,109} For example, motility and proliferation in prostate cancer cells is substantially reduced after Pak-1 knockout and is not rescued by the Group II Paks 4 and 6 despite high overexpression.¹⁴⁶ In summary, Pak-1 and Pak-4 each contribute to tumorigenesis in particular cancers, but Pak-1 inhibition will be more broadly applicable than inhibition of Pak-4.

3.1.3 Serine/Threonine kinase domain structure and common inhibitor features

Serine/threonine kinases share a conserved tertiary structure divided into an N-terminal and C-terminal lobe that is connected by an unstructured, flexible “hinge” loop region. ATP binds within the cleft formed between these two lobes, and the substrate protein receiving the transferred phosphate moiety binds adjacent to the ATP molecule (Figure 3-3). This structure is conserved in the Pak kinases, though they are distinguished by a larger-than-average ATP-cleft and a highly flexible N-terminal domain.^{106,147}

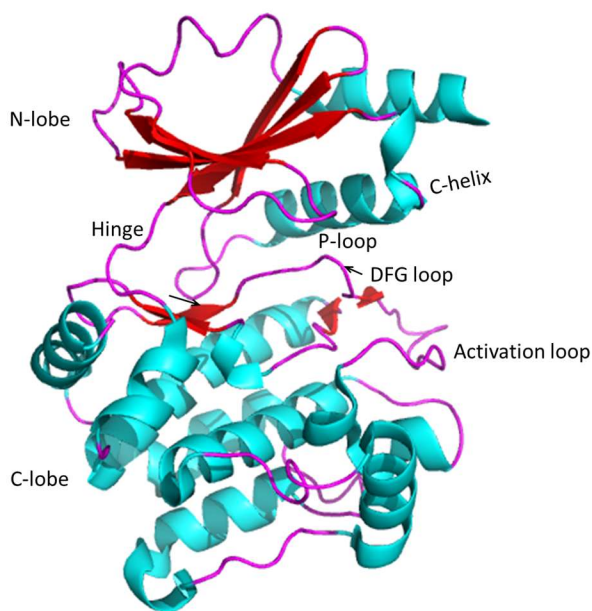


Figure 3-3: Crystal structure of the Pak-1 kinase domain

Notations indicate conserved features of serine/threonine kinase domains (PDB 1YHW).¹⁴⁸

Published kinase inhibitors are most commonly ATP-competitive, or more rarely, allosteric in action.¹⁴⁹ ATP-competitive inhibitors directly occlude ATP binding to prevent activity. A “hinge binding” motif is universally present on ATP-competitive kinase inhibitors and serves a key role in providing affinity through multiple hydrogen bond interactions with the “hinge region” of the kinase amide and carboxy protein backbone, and as a central core from which additional

substitutions may be added to improve pharmacokinetic and pharmacodynamic properties.¹⁵⁰ Many structures which satisfy this hinge-binding criteria have been identified and published.¹⁵¹⁻¹⁵³ These generally contain a flat heterocycle such as an aminopyridine or pyrimidine, a heteroatom in the meta or para position of a ring (i.e. morpholine), or contain a heteroatom at the end of a long alkyl chain (i.e. cyano group) unless a large substitution or bulky ring adjacent to hinge-binding moiety could sterically occlude the hydrogen-bonding interaction.

Because hundreds of serine/threonine and tyrosine kinases also bind ATP, engineering selectivity for a particular kinase is challenging. ATP-competitive inhibitors gain kinase selectivity using several mechanisms. First, an inhibitor may occupy regions of the ATP cleft that are not bound by ATP itself and where inter-kinase amino acid differences are more pronounced. One possibility is to push through a “gatekeeper residue” deep within the cleft to gain access into a “selectivity pocket.”^{154,155} Other regions commonly accessed by ATP-competitive inhibitors include the “P loop” and a hydrophobic pocket adjacent to the C-helix typically occupied by a conserved phenylalanine. The size, shape, and binding electronics of these pockets differ among kinase families and, quite often, within isoforms of kinase families themselves (as will be discussed below for the Pak kinases).¹⁵³

A second method to gain selectivity is to force a conformational change that is preferred by a particular kinase/inhibitor pairing but inaccessible to other kinases bound to the same inhibitor. In practice, this most commonly means transition into the inactive “DFG out” conformation. The DFG triad is a series of conserved catalytic residues in a loop near the ATP cleft that contribute to Mg²⁺ complexation. For example, the Gleevec-analog STI-571 potently inhibits Abl but not the closely related Src despite nearly identical binding sites. This selectivity is partially

explained by conformational changes in Abl that are unfavorable in Src.¹⁵³ Whether a kinase is favored to alter its conformation is likely influenced by overall protein dynamics and amino acid differences in disparate regions of the kinase and not just the ATP-binding site.¹⁵⁶ Predicting *a priori* what chemical structures will achieve this is not simple.

Finally, an allosteric inhibitor would bind to an alternative site on the kinase and somehow prevent its enzymatic activity. For example, the MEK1/2 noncompetitive inhibitor CI-1040 binds to a site adjacent to the ATP cleft and locks the kinase in an inactive conformation.¹⁵⁷ Allosteric inhibitors are typically more selective because sequence homology is reduced outside of the ATP cleft.¹⁵⁸

3.1.4 Publicly disclosed Pak inhibitors

No potent Pak-1-specific small molecule inhibitor had been publicly disclosed prior to the start of this project in 2011. Several compounds were known to inhibit Pak-1 quite effectively, such as the pan-kinase inhibitor staurosporine and its derivatives (with sub-nanomolar binding affinity),^{159,160} including ruthenium complexes based on a staurosporine-derived scaffold (such as (R)-DW-12, 83nM affinity).¹⁶⁰ For obvious toxicity and safety concerns, neither inhibitor was ever publicly considered for clinical development, nor is either compound selective against the Group II Paks.

Pfizer pioneered the discovery of clinically suitable pan-Pak inhibitors based on two scaffolds identified in a high-throughput screen,¹⁶¹ and had published multiple patents on further modified compounds. PF-3758309, a derivative of their earlier work based on the pyrrolopyrazole structure but with improved affinity and pharmacokinetic properties, entered Phase I clinical

trials for advanced/metastatic solid tumors. It blocks Pak-mediated signaling in an *in vitro* context and prevents tumor growth in xenografts derived from multiple cancer types including colon, breast, lung, melanoma, and stomach cancers.¹⁶² However, this inhibitor is equipotent for Pak-1, and its cellular activity is potentially also mediated through inhibition of multiple cell-cycle control kinases such as CDK7 ($IC_{50} = 7nM$).¹⁰⁶ Therefore, ascribing its cellular efficacy to a particular Pak kinase or to the Pak family in general is premature. PF-3758309 failed in Phase I studies due to low bioavailability and several adverse events, including grade 4 neutropenia and gastrointestinal issues.¹⁰⁶

In 2013, the biotechnology company Afraxis disclosed the first highly potent Pak-1-selective inhibitor FRAX597.¹⁶³ This inhibitor, based on a prior disclosed and patented pyrimidine-7-one series and now licensed by Genentech,¹⁶⁴ binds to Pak-1 with an affinity of 7.7nM and Pak-4 at $>10\mu M$, and demonstrates clear cellular effects on Pak-1-substrate phosphorylation and cell proliferation. However, this compound substantially inhibits many receptor tyrosine kinases and, intriguingly, causes a reduction in Pak-1 expression through a proteasome-mediated process.¹²⁸ This compound series has been further refined in subsequent publications to improve DMPK properties and kinome selectivity, and the most recently published example (FRAX-1036) addresses some of the selectivity concerns of FRAX-597 while retaining exquisite Pak-1/Pak-4 selectivity.^{165,166} Prior publicly available patent applications filed by Afraxis did not exemplify these selective compounds and, indeed, those structures listed in these patents are non-selective for Group I or II Paks.¹⁶⁷

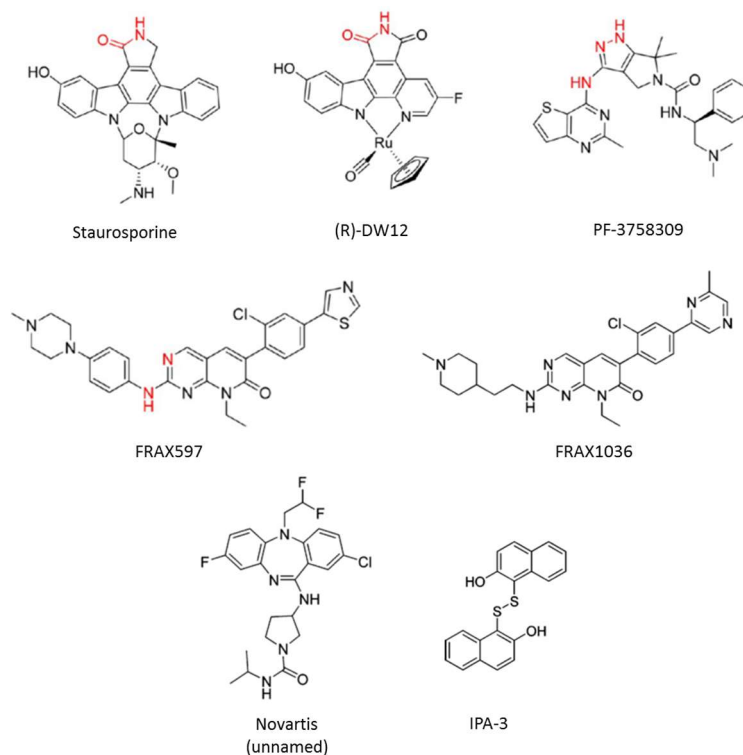


Figure 3-4: Chemical structures of key reported Pak inhibitors discussed in this chapter

Genentech also reported in 2013 a highly ligand-efficient Pak-1 inhibitor with 1.6nM affinity but no reported specificity for Pak-1 over Pak-4.¹⁶⁸ An azaindole-containing compound published in 2014 by AstraZenica is both potent and specific for Pak-1 (IC₅₀ 20nM, 30-fold Pak-1/Pak-4 specific), though it inhibited a wide range of other kinases.¹⁶⁹ Pak-4-specific inhibitors have also recently been published, and are reviewed elsewhere.¹⁰⁶

Allosteric kinase inhibitors are highly attractive because they impart immediate selectivity over other kinases by avoiding the conserved ATP-binding sites.¹⁵⁸ In particular, extensive N-terminal regulatory and activation regions represent appealing targets for which to develop an allosteric inhibitor. The first non-competitive allosteric inhibitor disclosed for the Group I Paks was IPA-3, a disulfide containing compound which covalently binds the regulatory domain of inactive Pak-1 and prevents subsequent Rac1/CDC42-mediated activation.¹⁷⁰ These disulfide

bonds are obligatory for function and would be a significant liability in the chemically reducing cellular environment (and completely inappropriate for a clinical setting). A 2013 oral presentation by Novartis disclosed their discovery of a Pak-1-specific inhibitor in a fragment-based screen. Their initial hit was subsequently improved to 100nM potency and greater than 100-fold selectivity against other Pak isoforms, including highly similar the Group I Paks.¹⁰⁶ X-ray crystallography revealed that the inhibitor binds to the “back pocket” of Pak-1, where more selectivity can be obtained, and forced the kinase into the inactive “DFG-out” conformation.

3.1.5 Suitability of FBDD to kinase inhibitor development

Introducing kinase selectivity is a primary challenge of any kinase drug discovery program. We reasoned that a fragment-based approach offered unique benefits to gain novel selectivity that other kinase inhibitors known to us at the time had failed to include (notably, PF-3758309). Firstly, because fragment hits can bind to smaller pockets that larger compounds would miss, a fragment screen might identify allosteric Pak modulators. Second, the large chemical space covered in a fragment screen might identify unique binding opportunities within the ATP-cleft to provide kinase selectivity. Third, a fragment screen might identify a novel mechanism of binding within the ATP cleft, either by avoiding hinge-binding, or using novel chemical structures that are more easily patentable. Finally, a fragment-based approach is demonstrably successful. BRAF kinase inhibitor Vemurafenib was the first clinically approved drug to be started from a fragment-based screen.¹⁷¹

In summary, Pak-1 serves a critical role in tumorigenesis, metastasis, and survival in breast and other cancer types. No Pak-1-specific inhibitor had been published at the genesis of this

project in 2011, but Pak protein knockout and pan-Pak inhibitor PF-309 powerfully reduced cell growth, motility, and survival in an *in vitro* or *in vivo* setting. Finally, while cancers seemingly depend more commonly on Pak-1 than Pak-4 for transformation, no tool compound existed to fully elucidate the individual contributions of each family member to tumorigenesis and cancer progression. Therefore, we sought to discover Pak-1-selective small molecule inhibitors using a fragment-based approach, test their efficacy in breast cancer cell lines, and to investigate the contributions of individual Pak family members to normal and cancer biology.

3.2 Results

3.2.1 Expression and purification of the Pak-1 kinase domain

Enzymatic Pak-1 kinase functionality promotes cell survival, proliferation, and motility, and both pre-clinical and clinical observations suggest that Pak-1 kinase contributes to tumorigenesis and cancer progression. Therefore, we sought to discover Pak-1-specific small-molecule inhibitors using a fragment-based approach to further validate this cancer target in a pre-clinical setting. To obtain the protein required for this screen, the kinase domain of Pak-1 (Pak-1-KD) comprising residues 249-545 was cloned, expressed, and purified in an *E. coli* expression system using glutathione-affinity and size-exclusion chromatography (Figure 3-5). Two mutations were introduced: K299R to make the kinase catalytically inactive and so prevent cytotoxicity to *E. coli* during expression, and a phospho-mimetic mutation on the activation loop (T423E) to mimic the Pak-1 active state whereby the activation loop transitions into a loose (free) conformation.¹⁰⁷

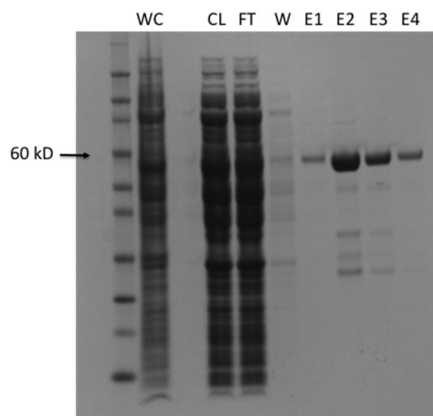


Figure 3-5: Purification of the human Pak-1 kinase domain (Pak-1-KD)

Pak-1-KD protein was expressed in *E. coli* cells and lysed with a homogenizer (whole-cell paste, WC). The paste was spun at 10,000 RPM to pellet unlysed cells and membrane, and the supernatant (clear lysate, CL), and was loaded onto a nickel-affinity purification column. Flow-through (FT), wash (W), and the early elution fractions (E1) were discarded. Later elution fractions (E2-E4) were retained. Precision Protease was then used to cleave the GST tag, and the protein was then purified again on the glutathione column and a sephacryl size-exclusion chromatography column.

3.2.2 Attempted optimization of HSQC-NMR spectra for Pak-1-KD

The protein-observed 2D HSQC-NMR technique is commonly used in fragment-based screens due to the wealth of information it provides on ligand-protein interactions, including affinity and predictions on binding mode or location. Indeed, this technique was used successfully in Chapter 2 to discover inhibitors of K-Ras-GTP. However, as a protein-observed technique, HSQC-NMR requires a high protein concentration (25-50 μ M is typical) in order to generate enough signal, and the protein must be monoisotopically labeled with 15 N. Moreover, the protein must be small enough in size to allow adequate peak resolution (typically less than 30-40kDa).⁸⁴ The Pak-1 kinase domain is 32kDa but in solution dimerizes to form a 64kDa molecule, and the N-lobe of the kinase domain is highly dynamic.¹⁰⁶ HSQC spectra generated from this molecule were of insufficient quality to conduct a fragment screen due to the very low percentage of amide

backbone residues that could be observed as individual peaks (Figure 3-6A). A screen conducted under these conditions would result in a large percentage of false-negatives because chemical shifts induced by ligand binding would not be detected.

The Pak-1 homodimer forms due to spontaneous interactions between the α G and α E helix (Figure 3-6B). To improve the HSQC spectra, we introduced a mutation (L449Q) on the α G helix to disrupt dimerization in solution by sterically occluding the dimer interface between α G and α E.¹⁷² However, this change failed to substantially improve the spectra, as seen in Figure 3-6C, and only a few indistinct peak shifts are noted when bound to the known interacting ligand VU0466177 (red) when compared to apo-Pak-1 (blue, Figure 3-6D). In summary, despite optimization of the HSQC protocol and mutagenesis of Pak-1 protein, this technique was unsuitable for a fragment-based screen.

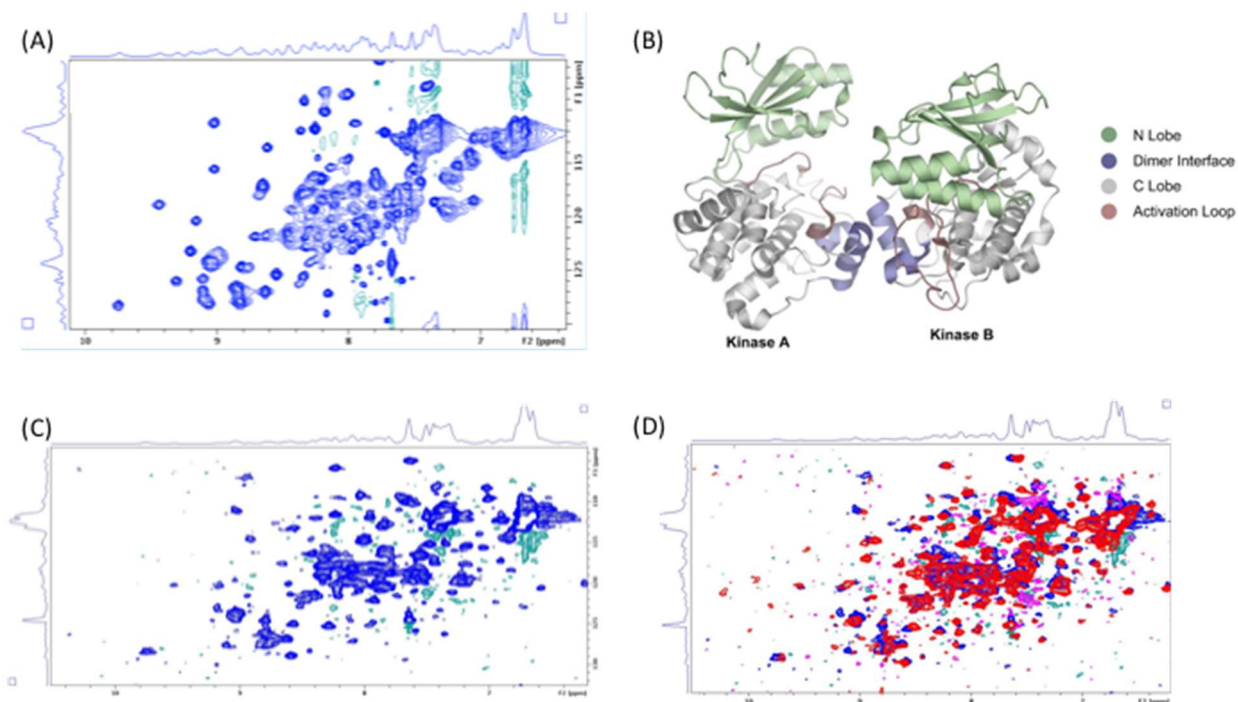


Figure 3-6: Attempted optimization of HSQC-NMR for Pak-1-KD

(A) HSQC-NMR spectrum for Pak-1-KD. Resolution was insufficient to screen using this methodology. Pak-1 dimerizes in solution through an α -helical interface (B, adapted from

Pirruccello, et al. ¹⁷²). To reduce the size of Pak-1 in solution (and therefore, hopefully improve the HSQC spectra), we blocked this interaction by introducing an L449Q mutation. **(C)** HSQC spectra of the mutated protein. While more peaks are visible, the quality is still not sufficient to conduct a fragment screen. **(D)** An overlay spectra of apo-Pak-1 (blue) with a known Pak-1 binding compound (VU0466177, 50 μ M, red) shows that, while some peaks do shift position, the quality is insufficient for a fragment-based screen.

3.2.3 Saturation Transfer Difference (STD)-NMR First-site Fragment screen

In contrast to HSQC-NMR, Saturation Transfer Difference (STD) NMR is a ligand-observed technique whereby an NMR spectrum is generated for the ligand rather than the protein.¹⁷³ Two spectra are measured in an STD-NMR experiment (Figure 3-7A). The first requires selectively saturating a resonance contained only by the protein and not overlapping with ligand whatsoever (typically, from 0ppm to -1ppm). Saturation will propagate from the irradiated receptor protons at that resonance frequency to other protons on the receptor via spin diffusion and, if ligand is bound, will then transfer to the ligand by cross relaxation at the ligand-receptor interface, which results in peak broadening. A reference spectrum is separately measured by saturating a region that does not contain signal for either protein or ligand. The difference spectrum of these two measurements will show only those resonances that have experienced saturation (i.e. the receptor and compound that bind to the receptor). Since the protein concentration is generally negligible compared to ligand concentration, its resonances are typically not visible in the difference spectrum.⁸⁵

As a ligand-observed NMR technique, STD-NMR requires only a small amount of non-isotopically labeled protein, and the technique is relatively unaffected by protein size or dynamics.¹⁷⁴ As with other NMR techniques, STD-NMR is insensitive to high ligand

concentrations, compound precipitation, or fluorescence. However, unlike HSQC, STD-NMR spectra cannot provide information on the ligand binding site and affinity.

To verify that this assay could detect ligand-protein interactions, I performed an STD-NMR experiment and obtained the on-resonance, off-resonance, and difference spectrum for a fragment that binds Pak-1, VU0456757 (Figure 3-7B). To further validate that STD-NMR can detect weakly interacting ligands, I measured the STD-NMR spectrum for adenosine. The resulting difference spectrum clearly demonstrated both expected ^1H peaks (Figure 3-8).

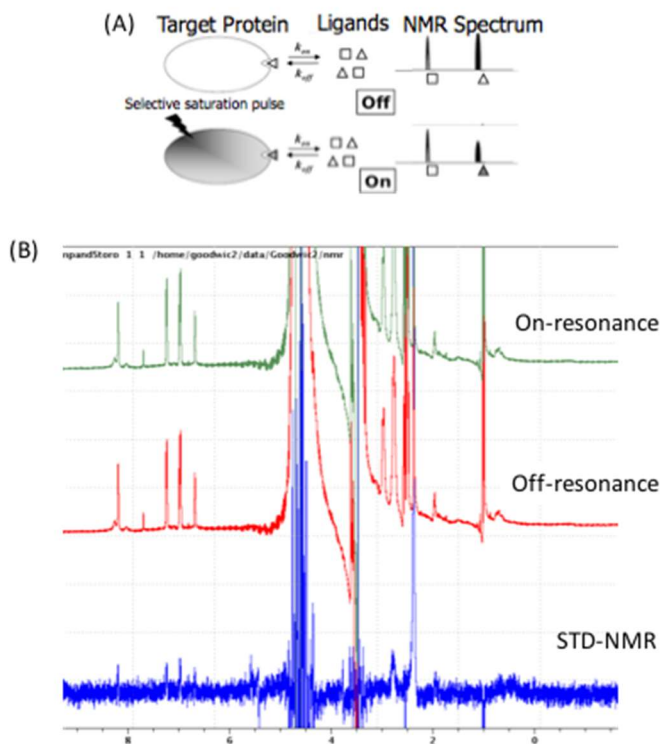


Figure 3-7: Two NMR ^1H spectra are measured for an STD-NMR experiment

(A) In an STD-NMR experiment, the protein is selectively pulsed at a resonance where ligand does not respond (on-resonance). This energy may transfer to bound ligand protons through cross-relaxation, thus causing peak broadening. A reference spectrum is generated by selectively pulsing where neither ligand nor protein respond (off-resonance). The difference of these spectra reveals only those peaks which were broadened and, therefore, those that are bound to the receptor. **(B)** Example on-resonance, off-resonance, and differences STD-NMR spectra for a fragment (VU0456757) bound to Pak-1-KD. Because of the large background water peak visible

around 4-5ppm, the easiest determination of ligand binding occurs for protons surrounding an aromatic ring (7-9ppm).

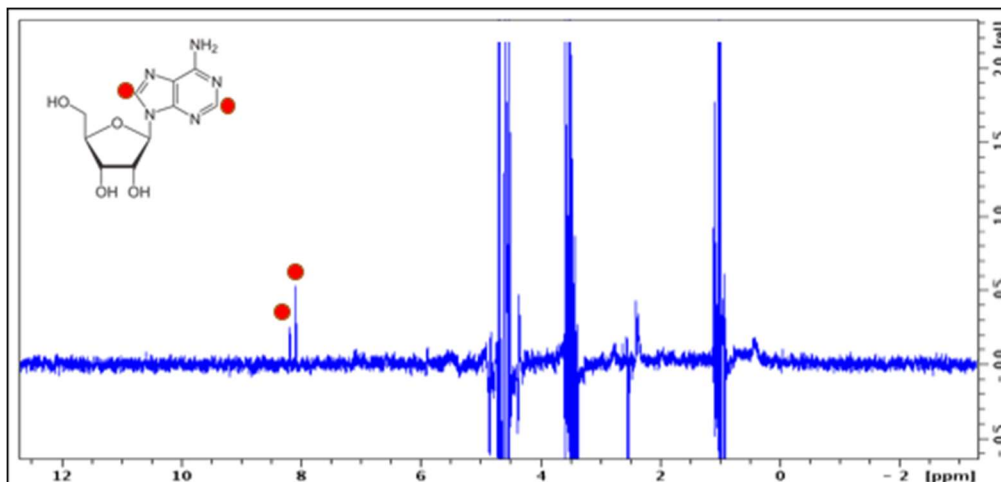


Figure 3-8: STD-NMR difference spectrum for adenosine binding to Pak-1-KD

Adenosine (inset, 500 μ M) is confirmed to bind Pak-1-KD in this difference STD-NMR spectrum. Both predicted ^1H protein peaks in the purine base are observed (designated here by red dots).

Pak-1-KD was then screened for binding to 14,000 fragments. Hits showing a detectible STD-NMR signal were validated in triplicate. In total, 193 compounds were identified (a 1.4% hit rate). Some of these compounds are exemplified in Figure 3-9, while the full list is found in Appendix C.

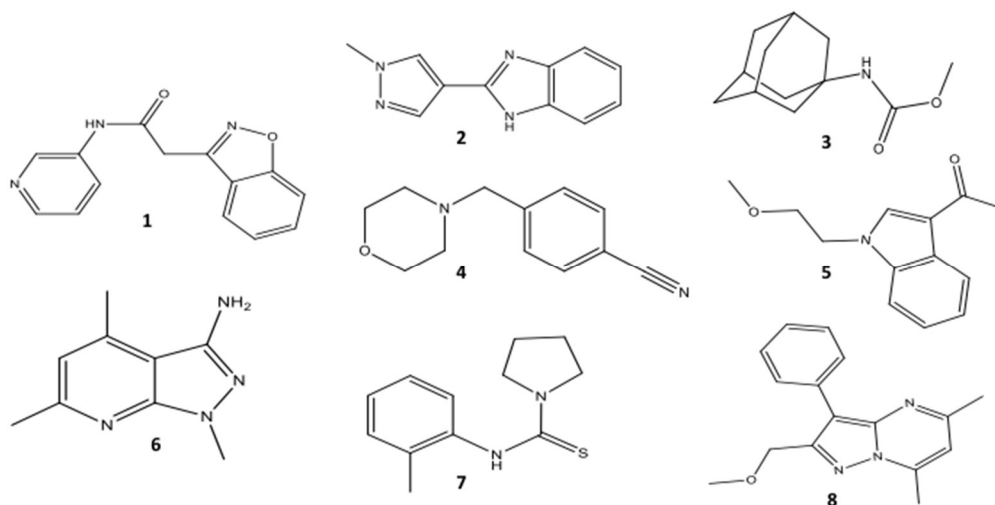


Figure 3-9: Example fragments identified in the Pak-1-KD first-site fragment screen
Results were verified in triplicate. The full list of fragments is included in Appendix C.

We additionally conducted a focused screen using rationally designed compounds built around three scaffolds (2-Aminopyrimidines, 3-Aminopyrazoles, and 5-Methyl-3-Aminopyrazoles) which utilize the generic hinge-binding motif commonly found in many published kinase structures. These structural features include a planar structure with multiple hydrogen bond donors/acceptors to amino- or carbonyl-groups on the protein backbone, most commonly provided by nitrogen-containing rings or NH groups.¹⁵⁰ These compounds, synthesized in the group by Alex Waterson and Jason Burke, were designed to provide rapid identification of generic and relatively high-affinity first-site fragment hits. While these structures are by definition not selective, they offer a powerful starting point for ATP-competitive inhibitors by providing a core scaffold to enable expansion into the distal portions of the ATP cleft, including the DFG loop and selectivity pocket.¹⁵⁰ Further, a potent hinge-binding motif from this library would also provide rapid identification of a first-site hit at a known binding location for progression to a second-site screen. In total, 81 compounds were synthesized for this library, of

which 59 were confirmed to bind Pak-1-KD (a 73% hit rate). Examples of these hits are shown in Figure 3-10, and the full list is included in Appendix C.

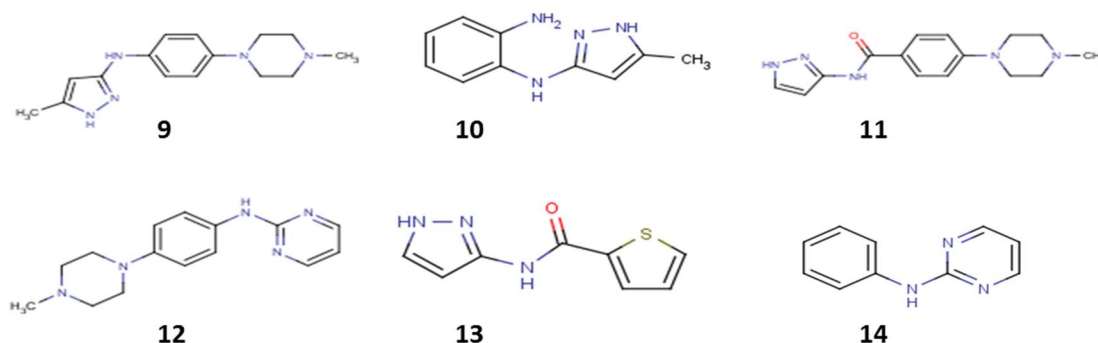


Figure 3-10: Example fragment hits from the designed hinge library

Note the generic hinge-binding motif present in each: a planar structure with multiple hydrogen bond donors/acceptors available for amino- or carbonyl-groups on the protein backbone.

3.2.4 Development of a biochemical assay to measure compound activity

Understanding compound SAR is challenging without measuring ligand affinity. Because STD-NMR is unable to directly measure binding affinities, I developed biochemical assays to measure inhibition constants against Pak-1 kinase. I first considered using a fluorescence polarization anisotropy (FPA) assay whereby binding of a fluorescently-labeled probe to a protein will slow rotational tumbling in solution and, therefore, raise its anisotropy.¹⁷⁵ Our probe, BODIPY-ATP, consisted of a BODIPY fluorophore covalently attached via a flexible linker to the 2' position on the ATP ribose ring. A saturation-binding curve consisting of varying concentrations of Pak-1-KD was titrated into buffer containing a fixed concentration of 100nM BODIPY-ATP probe, and the increase in anisotropy was measured. Based on these data, the binding constant (K_D) for this interaction is 122.8 μ M (Figure 3-11A). As a control, a high concentration (100 μ M)

of unlabeled ATP was able to displace BODIPY-ATP (Figure 3-11B). However, because the binding constant for BODIPY-ATP is so weak, this was found to be inappropriate for routinely measuring all but the weakest compounds.

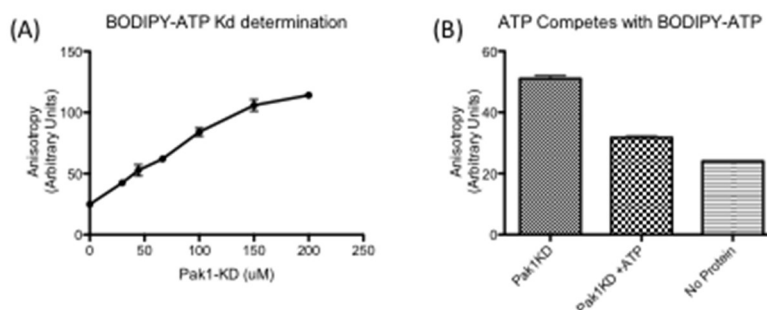


Figure 3-11: Validation of a fluorescence anisotropy assay to detect Pak-1 inhibition

(A) The affinity for ATP tagged with fluorescent molecule BODIPY was measured using a saturation binding experiment whereby Pak-1-KD was titrated into a fixed concentration of BODIPY-ATP (100nM). The affinity is measured at 122.8µM. **(B)** Unlabeled ATP is able to compete with BODIPY-ATP for Pak-1 binding, here shown as a decrease on anisotropy (middle column). Shown is the average of three independent experiments (error bars SD).

Alternatively, compound activity could be measured with an enzymatic assay; in theory, higher-affinity compounds are better able to displace unlabeled ATP and thus prevent phosphate transfer to a substrate in an *in vitro* setting. Phosphate group transfers may be detected quantitatively using the FRET-based LANCE Ultra kinase activity assay (Perkin-Elmer, Figure 3-12). In short, a FRET signal is generated only when a proprietary dye (ULight) and a europium-tagged antibody are brought into close proximity. Full-length Pak-1 will constitutively phosphorylate a short peptide in the presence of excess ATP, thus allowing a phospho-specific antibody to bind. A compound-mediated decrease in signal after pre-incubation demonstrates compound activity.

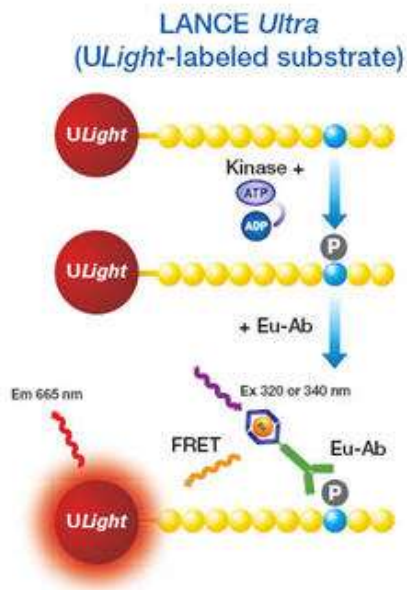


Figure 3-12: LANCE *Ultra* TR-FRET schematic
Figure provided by Perkin-Elmer.

This assay requires full-length Pak-1 because the active kinase domain alone cannot be purified in an E.coli system due to toxicity. Thus, full-length Pak-1 was commercially acquired (ProKinase). Full-length Pak-1 is activated only after auto-phosphorylation of T423 on the activation loop. In a cellular context this process is stimulated by CDC42 or Rac1 binding to the N-terminal protein-binding domain. To stimulate this process in an *in vitro* context, we pre-incubated Pak-1 with ATP to allow for gradual self-activation. Indeed, Pak-1 activity did increase in a time-dependent manner following pre-incubation with ATP, which stabilized at a maximal signal after 60 minutes of pre-incubation (Figure 3-13A). Pre-incubating Pak-4 with ATP did not similarly increase its activity, which is consistent with the known constitutive activity of the Pak-4 kinase domain.¹⁷⁶

Next, I optimized the protein concentration to ensure that subsequent experiments were conducted in the linear range of detection. Pak-1 titrated into a fixed concentration of 2nM ATP revealed an EC₅₀ point of 9nM. Next, the Michaelis-Menten constant (K_m) was calculated by

titrating in ATP to a fixed concentration (9nM) of Pak-1, and was found to be 4.3 μ M. This number is critical for converting from the inhibitory concentration-50 (IC₅₀) measured in dose-response curves to the K_i by the Cheng-Prusoff equation:
$$K_i = \frac{IC_{50}}{1 + \frac{[S]}{K_m}}$$
 where [S] is the ATP concentration used and K_m is the Michaelis-Menten constant measured in Figure 3-13C.¹⁵⁸ Finally, an inhibitory dose-response curve for pan-kinase inhibitor Staurosporine gives a K_i of 0.51nM, which is in agreement with published values.^{177,178}

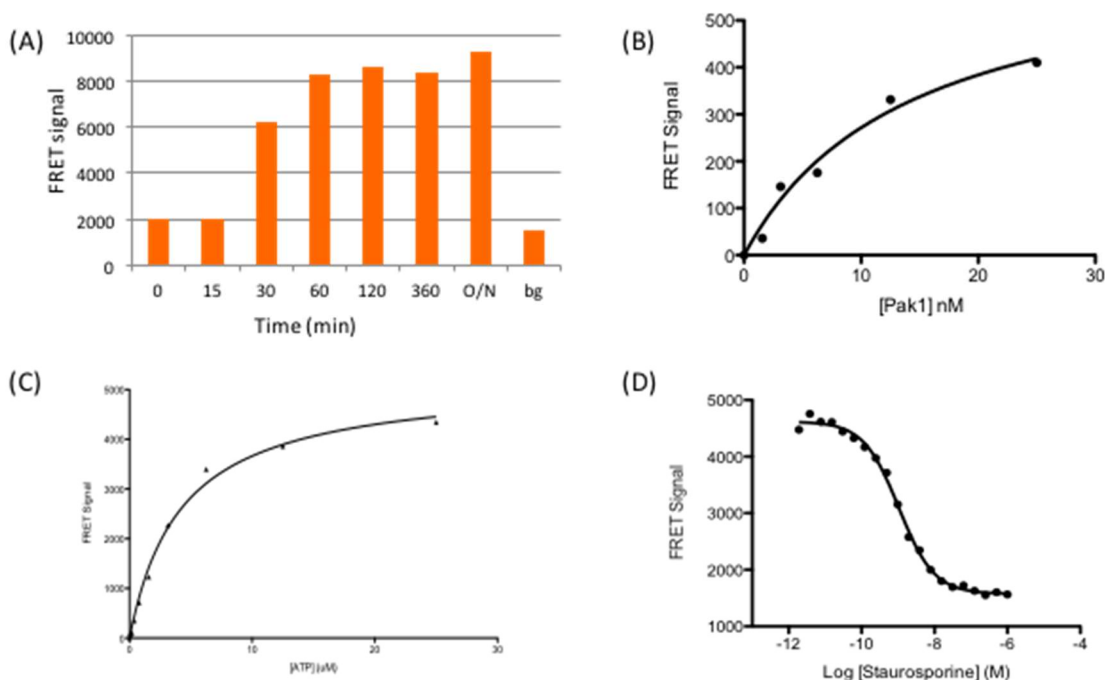


Figure 3-13: Optimization of the Pak-1 TR-FRET assay

(A) Pak-1 requires pre-incubation with ATP to allow activation by auto-phosphorylation. Activation is time-dependent and peaks after 60 minutes. (bg: assay background with no peptide added). **(B)** Saturation binding curve for Pak-1. Pak-1 was titrated in with a fixed concentration of ATP (2nM). **(C)** The Michaelis-Menten constant (K_m) was determined by titrating ATP into the assay buffer. **(D)** Inhibition dose-response curve for staurosporine, a pan-kinase inhibitor. The measured IC₅₀ is 0.51nM, which agrees favorably with literature values in the 1nM range.

To further validate that compound activities are correctly measured in this assay, we sent a select group of designed hinge binders for external measurement (at DiscoverX and Reaction

Biology). In both cases the K_D or K_i compared extremely well with the numbers measured in our assay (Figure 3-14).

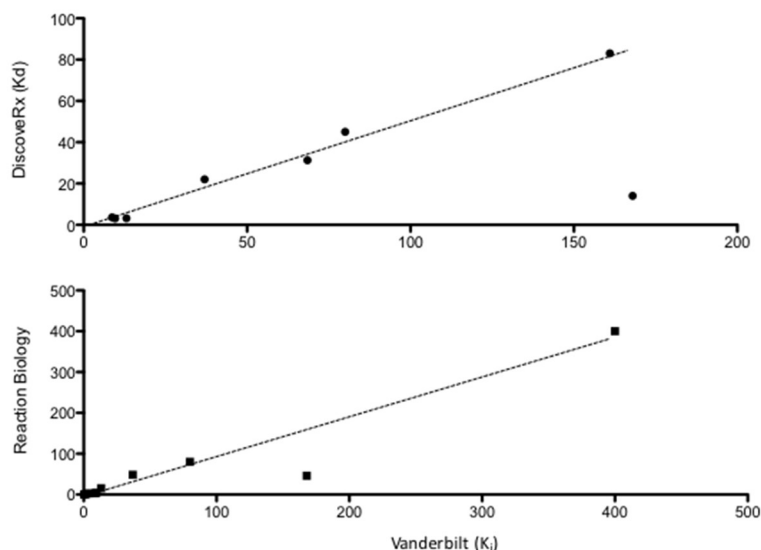


Figure 3-14: Pak-1-KD activity assay validated with external measurements

A select group of designed hinge-binding compounds were sent to two external contract companies for measurement against Pak-1. Results from both DiscoverRx and Reaction Biology compare favorably (linear correlation) with Vanderbilt results, with the notable exception of one compound that was consistently measured weaker than either external company.

3.2.5 Development of a selectivity counterscreen against Pak-4

One of the primary challenges in developing ATP-competitive kinase inhibitors is engineering selectivity over other kinases due to similarities in the ATP binding cleft. Therefore, introducing selectivity at an early stage of the drug discovery process is vital. Pak-4 is the most well characterized member of the Group II Paks, and sequence and structural similarities between Pak-1 and Pak-4 suggest that developing a selective inhibitor would be challenging. However, we hoped that subtle amino acid differences between Pak-1 and Pak-4 would allow a selective inhibitor to be engineered. We reasoned that obtaining selectivity between these nearly

identical kinases would correlate with increased selectivity against other kinases as well. Additionally, selectivity for Pak-1 over Pak-4 would allow us to ascertain the individual contributions of the Pak-1 isoform to cancer progression. By counter-screening these hits against Pak-4 using the LANCE TR-FRET assay, we could rank compounds by their selectivity for Pak-1. These data, combined with co-crystallization studies, might reveal the molecular differentiators for Pak-1 specificity over Pak-4.

The kinase domain of Pak-4 (Pak-4-KD) was purified as described for Pak-1-KD, and the Lance Ultra TR-FRET assay was re-optimized for this kinase (Figure 3-15). We chose to use a Pak-4 concentration of 15nM, and the $K_{M,ATP}$ was a highly potent 41nM. The measured Staurosporine K_i of 21.6nM agrees within 3-fold of literature values.¹⁷⁸

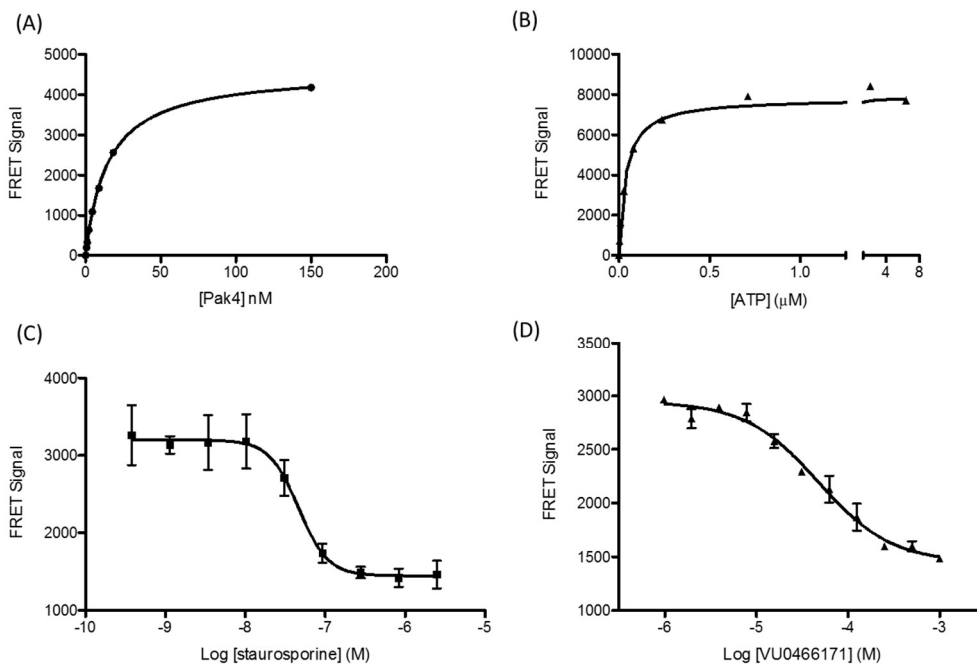


Figure 3-15: Development and optimization of the Pak-4 activity assay

(A) Pak-4 was titrated into the assay buffer with a fixed ATP concentration under standard assay conditions defined in methods. **(B)** To determine the enzymatic Michaelis-Menten constant $K_{M,ATP}$, ATP was titrated into the assay buffer at a fixed concentration of Pak-4. $K_{M,ATP} = 0.041\mu\text{M}$. **(C)** Pak-

4 inhibition by staurosporine was measured in triplicate for a K_i of 21.6nM. **(D)** Example inhibition curve for designed fragment VU171 (Error bars SD).

3.2.6 *X-ray crystallography revealed fragment binding orientations on Pak-1-KD*

Discovery of a potent inhibitor could be significantly aided by accurate knowledge of compound binding location and orientation. *A priori*, a compound could bind Pak-1 in one of three locations. It could bind outside the ATP-cleft (that is, allosterically), or within the cleft in a hinge-binding or non-hinge-binding orientation. To identify the compound binding location and orientation, Bin Zhao co-crystallized Pak-1-KD with many fragment hits and based on these structures, designed compounds with the chemists (exemplary structures in Figure 3-16).

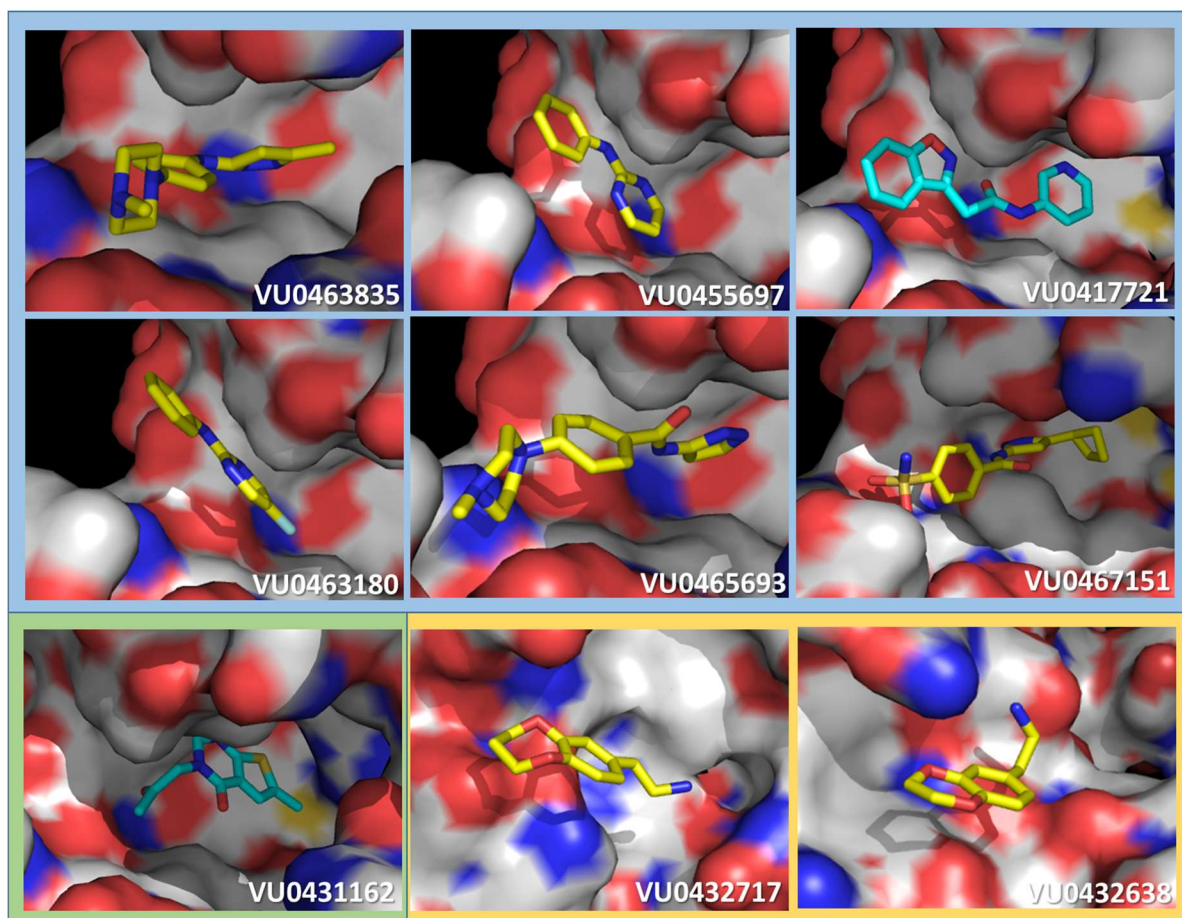


Figure 3-16: Example x-ray crystal structures for Pak-1-KD fragment hits

This subset of co-crystal structures solved by Bin Zhao illustrates the diverse binding modes of fragment hits. Blue background: compounds that bind to the hinge region in a traditional orientation. Green background: a compound that binds farther into the ATP cleft and only partially overlaps with the hinge-binding region. Orange background: compounds that bind outside the ATP cleft.

A large number of fragments identified in the screen have the characteristics typically seen in hinge-region binders (for example, compounds 1 and 6 in Figure 3-9). Many of these were co-crystallized with Pak-1-KD (Figure 3-16, blue background). In each case, the compounds bind to the “hinge” region of the kinase between the N- and C-terminal lobes. Each compound makes hydrogen bond interactions with the amide backbone of the hinge loop in a bidentate or tridentate fashion. For VU0463835, bidentate interactions occur between amine hydrogens in the linker amine and pyrazole ring and the amide oxygen on residues E345 and L347 on the

protein backbone. Tridentate hinge-binding compounds include an additional hydrogen-bond interaction pair. VU0463180 exhibits this type of binding arrangement, and includes interactions with the amide backbone at residue A348 and the carbonyl moiety. Hinge-binding compounds were forced to orient along the hinge loop such that one end of the molecule points into the ATP cleft and selectivity pocket, while the opposite end of the compound points out toward solvent. These fragments were of insufficient length to take advantage of potentially favorable interactions deep within the ATP cleft. A hydrophobic pocket proximally adjacent to the hinge was the most easily accessible location to expand the compound and gain affinity. None of these crystallized fragments fully utilized this binding site, though the cyclobutyl group on VU0467151 partially accessed this region.

Not all fragment hits crystallized in this hinge-binding orientation. Some, such as VU0431162 (green background), co-crystallized in a distinct binding mode deeper in the ATP cleft. In contrast to the hinge-binding fragments discussed above, this fragment occupies the hydrophobic pocket and expands partially beyond it towards the selectivity pocket and pushes aside the gatekeeper residues M319, though the methyl substituent does not extend far enough to pick up significant interactions in that region. This fragment partially overlaps with the hinge-binding compounds described above: for example, the ketone carbonyl on VU0431162 occupies a similar position to the amide carbonyl in VU693 and VU721.

Several fragments were co-crystallized outside of the ATP cleft entirely. For example, VU0432638 binds to the opposite side of the hinge region. It does not occupy a “pocket” in the traditional sense – the interaction surface is a shallow depression on the protein surface. A water-mediated hydrogen-bonding interaction is predicted for an oxygen in the 1,4-dioxane with Q294.

Expanding to replace the water molecule is an immediately available optimization strategy. Because this fragment does not occlude the ATP-cleft or block known Pak-1 protein-interaction surfaces, allosteric inhibition of kinase activity would require a global conformational change that is not seen with this fragment.

VU0432717 (and related fragment VU0430234, not shown) crystallized between helices H and I in Pak-1-KD in the C-terminal lobe. As with VU0432638, these compounds bind in a shallow surface depression (Figure 3-16, orange background). The terminal amine moiety is within hydrogen-bonding distance with several residues, but the fragments do not appear to be highly suited for this binding site: each is relatively hydrophobic yet this interaction interface is relatively hydrophilic in nature. No general conformational change was noted for either compound.

3.2.7 *An ILNOE-NMR screen identified fragments bound to a second site*

Fragments identified in a fragment-based screen are expected to only weakly bind to the protein because of their small size. One way to improve the binding affinity of fragments is to chemically link or merge them with a second fragment that binds in close proximity. A second-site fragment screen can be used to identify these proximal fragments. We chose to conduct this screen using Inter-Ligand Nuclear Overhauser Effect (ILNOE-NMR). The Nuclear Overhauser Effect (NOE) is the transfer of nuclear spin polarization from one nuclear spin population to another via cross-relaxation during the mixing period, with the spectrum containing diagonal peaks and cross peaks connecting resonances from nuclei that are spatially in close proximity. A saturating concentration of a carefully selected first-site ligand is used to occlude the first-site

binding pocket. ILNOE can discriminate between closely bound coincident ligands because signal can only transfer between ligands bound at the same time and within close proximity (around five angstroms).¹⁷⁹

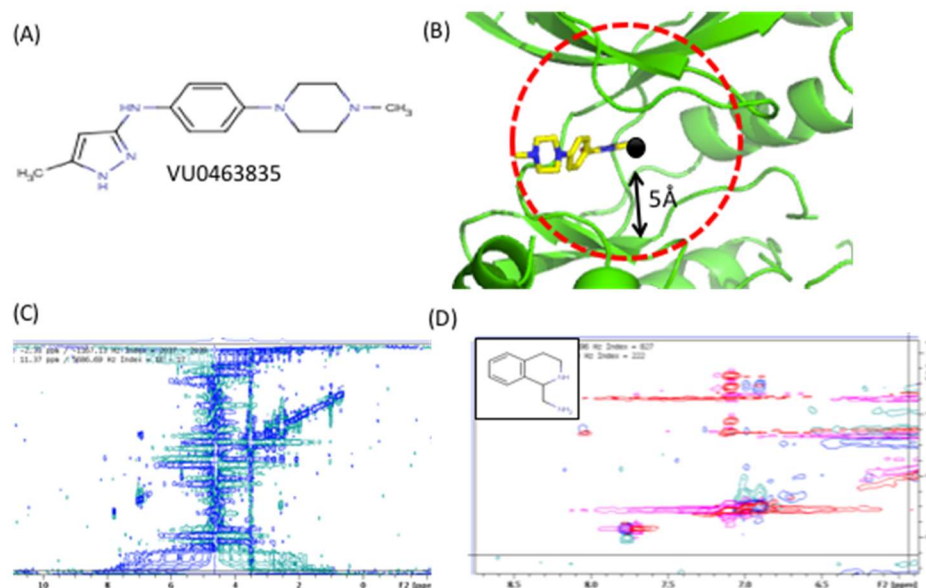


Figure 3-17: Optimization of an ILNOE-NMR second-site fragment screen

(A) A 3-aminopyrazole hinge-binding compound was chosen as a first-site ligand. A methyl group verified by x-ray crystallography to point into the ATP-cleft serves as a probe. (B) ILNOE will detect NOEs between ligands only if they are bound simultaneously and in close proximity (within roughly 5Å). (C) Reference NOESY spectra for the first-site ligand bound to Pak-1. (D) The ILNOE NOESY spectra for a second-site hit (red) bound to Pak-1, overlaid with the reference spectrum (blue).

The first-site ligand (VU0463835, Figure 3-17A) was chosen because it obstructs the hinge region but does not protrude down the ATP cleft towards the selectivity pocket or G-loop of the kinase. Therefore, no additional hinge-binding compounds would be identified – only compounds that bound farther down the ATP cleft could become “hits.” In addition, the first-site ligand has a relatively high affinity (40µM), high solubility, and contains a methyl substituent angled directly towards the selectivity pocket. A methyl group was important because second-site “hits” would be chosen based on an ILNOE to the methyl protons on the first-site ligand (Figure 3-17B). A

reference NOESY spectrum for VU0463835 bound to Pak-1-KD confirmed that the intra-ligand NOE for the methyl group extending from the pyrazole moiety is clearly resolved.

Some fragments are simply too bulky to occupy the back pockets of the ATP cleft. To enrich our library for smaller fragments that might bind with higher affinity, we conducted a virtual screen of the fragment library using GLIDE and selected the top 800 hits by GLIDE score. In addition, I also screened the 193 STD-NMR hits to determine whether any “second-site” hits had already been identified. Of these two screens, thirty-eight compounds (4.4% hit rate) were identified that gave a discernible inter-ligand NOE in comparison to the VU0463835 reference spectrum (Figure 3-17B), of which three had previously been identified in the STD-NMR screen. These structures were classified into three general categories: Sulfonamides, N-Acyl Indoles, and Aryl Lactams (Figure 3-18).

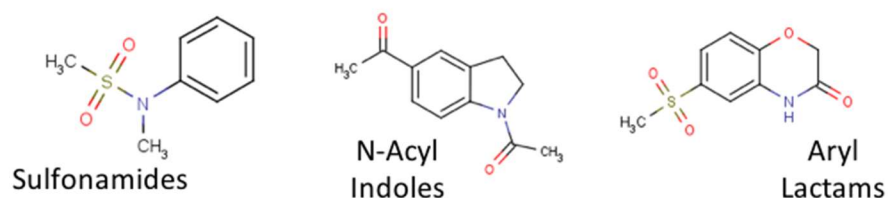


Figure 3-18: Representative fragment hits from a second-site screen

In total, thirty-eight fragments were identified to bind Pak-1-KD in close proximity to the first site ligand VU0463835. These hits classified into three distinct chemical series.

3.2.8 Fragments and designed compounds bind Pak-1-KD with low micromolar affinities

We measured the activity of each fragment in our biochemical kinase assay. Roughly one-fourth of STD-NMR hits showed statistically significant (4 SD, or at least 15.8%) inhibition of kinase activity compared to DMSO control at 1mM. Full dose-response curves were measured for each compound that had statistically significant inhibition at 1mM (example curve shown in

Figure 3-19A). Of these, only twenty-two had an IC_{50} below 1.5mM. The best fragment gives a K_i value for Pak-1 of 90.5 μ M.

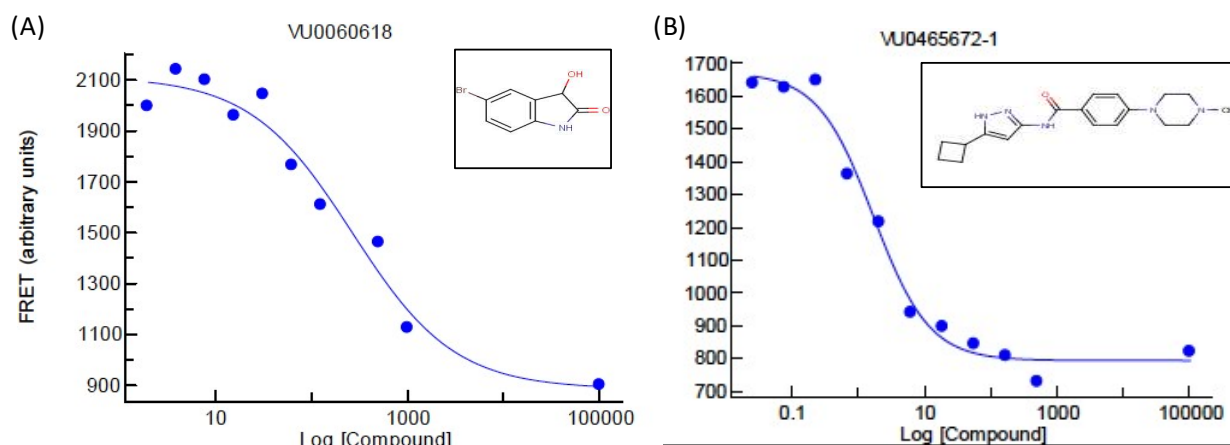


Figure 3-19: Example dose-response inhibition curves in the kinase activity assay

Example dose-response inhibition curves for a fragment (A) or designed compound (B) are shown for full-length Pak-1 in the TR-FRET assay.

In contrast, the designed hinge compounds bound with significantly tighter affinity (example dose-response curve in Figure 3-19B) and, somewhat surprisingly given their generic pattern, followed a clear SAR pattern (Table 3-2). While not exemplifying every compound, Table 3-2 clearly demonstrates the SAR trends evident in the 3-Aminopyrazoles designed series. First, larger or bulkier hydrophobic groups oriented inwards toward the ATP cleft were not tolerated. Second, a methylene or sulfate linker on the connected ring substituent virtually abrogates all binding. Third, the most favorable compounds contain a cyclobenzyl substituent that extends into the ATP cleft or a thiophene that extends towards solvent. The most potent compound in this series combines these features and inhibits Pak-1 with an IC_{50} of 1.7 μ M.

Expand out to solvent

Expand into ATP site							
		46 μ M (0.28 LE)	37 μ M (0.33 LE)	>400 μ M	23 μ M (0.46 LE)	>400 μ M	13 μ M (0.33 LE)
		9.6 μ M	8.7 μ M	>400 μ M	6.2 μ M		
		310 μ M	150 μ M	>400 μ M	250 μ M		
		5.0 μ M	3.6 μ M	380 μ M	1.7 μ M		
			>400 μ M		19 μ M (0.41 LE)		
			>400 μ M		160 μ M		
			>400 μ M		17 μ M (0.35 LE)		
		>400 μ M	89 μ M (0.24 LE)	350 μ M	304 μ M		
					41 μ M (0.30 LE)		

Table 3-2: SAR table for the 3-Aminopyrazole designed series

In general, Pak-1 does not tolerate bulky substituents leading into the ATP site, nor methylene or sulfate linkers on the connected ring substituents. The most favorable substitutions (cyclobutyl groups extending into ATP site, and thiophene extending towards solvent) give a 1.7 μ M K_i when combined.

3.2.9 Discovery of inhibitors with selectivity for Pak-1 over Pak-4

It is possible that selective compounds were already discovered in our first-site fragment screen. Therefore, all first-site hits from the fragment and designed hinge-binding libraries that gave measurable inhibition of Pak-1 at 1mM were counter-screened against Pak-4 in the biochemical kinase assay. In general, STD fragment hits were found to be nonselective, although

a handful of compounds were moderately selective (2-3 fold) for Pak-1 or Pak-4 (Figure 3-20A). In contrast, the designed hinge-binding library was found to be selective for Pak-4 almost exclusively; many compounds were at least 2-fold selective for Pak-4, and two compounds were 100-fold selective for Pak-4 (Figure 3-20B).

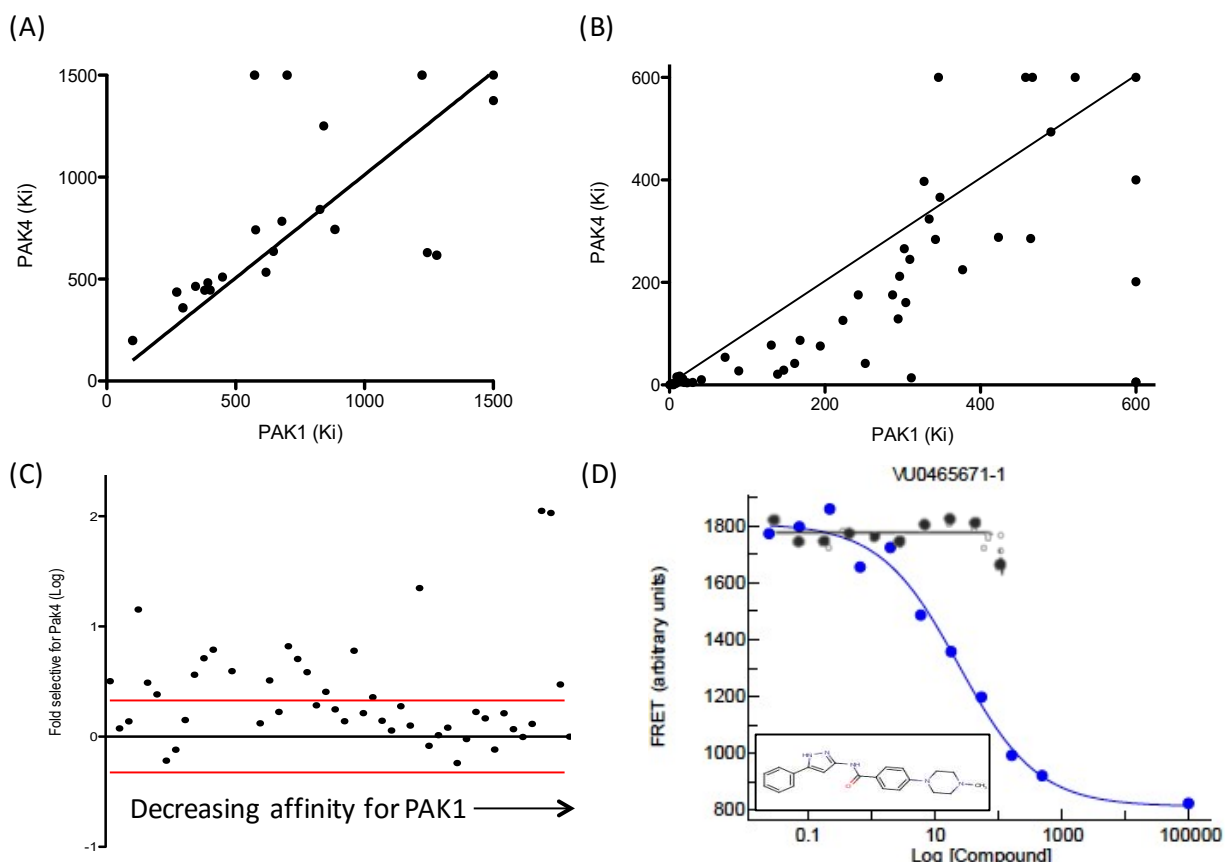


Figure 3-20: Investigating fragment selectivity for specific Pak kinase isoforms

(A) Scatter-plot of Pak-4 vs. Pak-1 K_i for first-site fragment hits that measurably inhibited Pak-1 at 1mM; the vast majority non-selectively bind either kinase. Linear trendline indicates a slope of 1. **(B)** In contrast, the designed fragment library was in general selective for Pak-4 by at least two fold, whereas several compounds exceeded a 10 or 100-fold binding preference for Pak-4. Linear trendline indicates a slope of 1. **(C)** Fold selectivity for Pak-4 is plotted on a log-scale. Note the large number of compounds 2-fold or more potent for Pak-4 (equal to 0.3 log units) above the red line. **(D)** Example dose-response curves for VU0465671 inhibiting Pak-1 (black) or Pak-4 activity (blue). No measurable Pak-1 inhibition is observed even at 400 μ M.

Selectivity for Pak-4 follows a clear SAR pattern. In Table 3-3, the 3-aminopyrazole SAR table has been amended to instead show fold-selectivity for Pak-1 (green) or Pak-4 (red). In

general, weaker binding for Pak-1 translates to weaker Pak-4 binding as well (the methylene and sulfate linkers on solvent-extending piece, for example). However, the general selectivity for Pak-4 over Pak-1 is clearly evident, and Pak-4 follows unique SAR trends. Bulky substituents extending back into the ATP cleft, such as phenyl or cyclohexyl groups, abrogated Pak-1 binding but are easily tolerated by Pak-4. Moreover, substitutions providing the highest Pak-1 activity, such as thiophene or cyclobutyl containing compounds, are the least selective.

Expand out to solvent

Expand into ATP site	Expand out to solvent						
Me-	1.9		NB	5	NB	1.3	
	1.65	2.4	NB	3			
	22	5	NB	6			
	12.5	1.4	1.7	1.25			
		NB		3.6			
		NB		3.9			
Ph-	>80	3.3	1.15	1.9			
Ph-				3.9			

Fold Pak1 specific
Fold Pak4 specific
NB: No binding; ND: No data

Table 3-3: Pak selectivity for the 3-aminopyrazole series

Fold-selectivity for Pak-1 (green) or Pak-4 (orange) is displayed for each compound. In general, Pak-4 binds these designed fragments tighter than Pak-1, and more readily tolerates bulky substituents extending into the ATP cleft.

Many published kinase inhibitors inhibit the Pak kinases accidentally due to poor kinase selectivity. We reasoned that some of these inhibitors may be selective for particular Pak

isoforms, and may provide hints for engineering selectivity into these series. Indeed, DiscoverX reported in 2011 on a screen of 72 kinase inhibitors against 442 separate kinases to comprehensively detail inhibitor selectivity.¹⁷⁸ All six Pak isoforms were included in this survey, and the dual HER2/EGFR receptor tyrosine kinase inhibitor HKI-272 “Neratinib” (Figure 3-21A) is highly Pak-1 selective. Reported Pak-1 inhibition is 210nM but no detectable Pak-4 inhibition was detected up to 10 μ M. These numbers were confirmed in the TR-FRET assay for both kinases (Figure 3-21B).

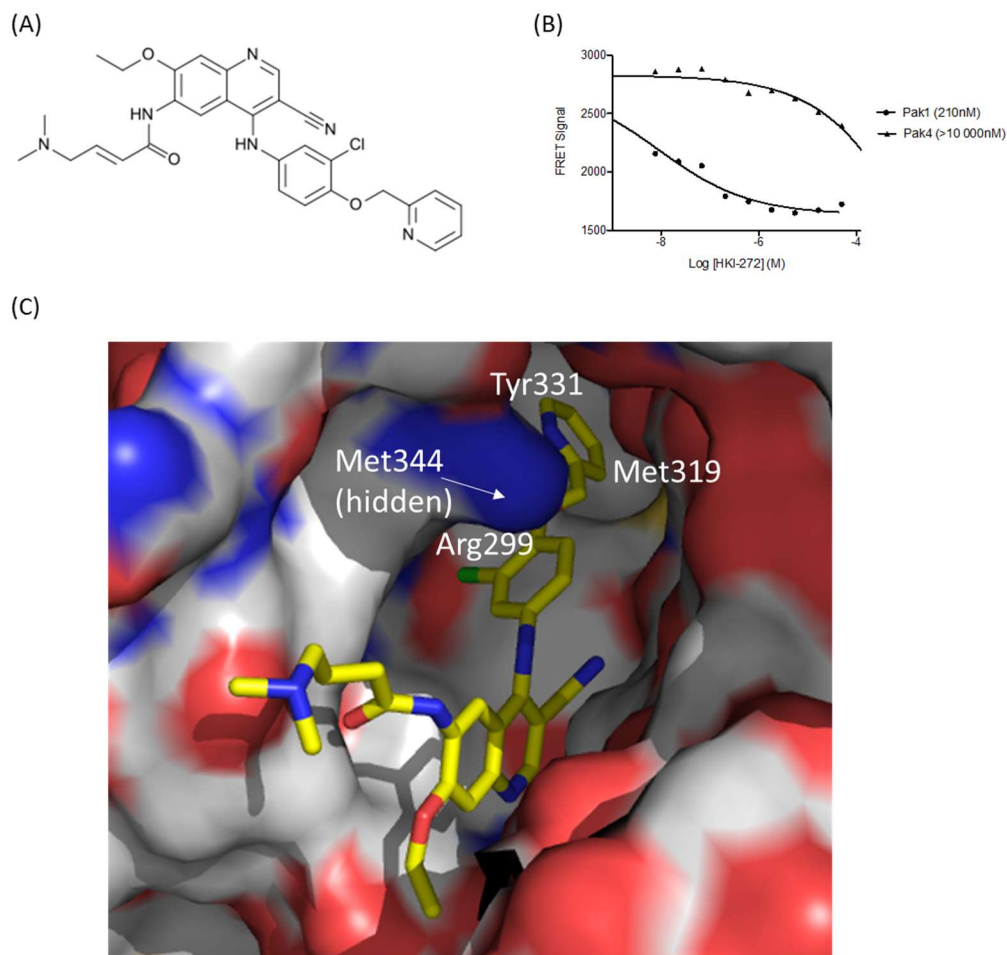


Figure 3-21: X-ray structure explains the exquisite Pak-1 selectivity of Neratinib

The dual EGFR/HER2 inhibitor HKI-272 “Neratinib” (A) inhibits Pak-1 with an IC₅₀ of 210nM in the kinase activity assay, but the IC₅₀ against Pak-4 is greater than 10 μ M K_i (B). (C) HKI-272 pushes

through the Met344 “gatekeeper” residue and causes Arg299 and Met319 side chains to swing away.

We sought to explain the selectivity between Pak-1 and Pak-4 using x-ray crystallography, and to use this knowledge to increase selectivity of our own compounds. Bin Zhao crystallized HKI-272 with Pak-1 (Figure 3-21C), which revealed several key binding contacts. HKI-272 occupies the hinge region as expected, but the extended functionalization from the quinoline 4-position and terminating in a pyridine ring extends deeply into the ATP-cleft past the gatekeeper Met344 residue to gain access to the selectivity pocket. As discussed in the introduction, extension into this pocket is commonly employed by kinase inhibitors to gain affinity and selectivity. Both Arg299 and Met319 rotated out of the way to provide room for the pyridine ring. Pak-4 possesses the same Met344 residue as in Pak-1 (in Pak-4, Met395); however, it is in a different conformation than that observed for Pak-1. Moreover, the back pocket of Pak-4 is distinctly smaller than that of Pak-1, possibly due to the presence of Y331 in Pak-1 that is rotated away from the pocket, while in Pak-4, Met381 is fully occupying the site. Other amino acid changes that may account for differences in binding specificity are I312 and I316 in Pak-1 that correspond to L363 and V367 in Pak-4. To summarize, multiple amino acid changes and differences in side chain position within the selectivity pocket suggest steric issues with bulky side chains in Pak-4 but not Pak-1, while an altered conformation of the gatekeeper residue between Pak-1 and Pak-4 could alter accessibility to this pocket by an inhibitor. That Pak-4 does not tolerate bulky ligands in the selectivity pocket stands in contrast to its preference for bulky substituents towards the hinge-binding region, as noted earlier.

The selectivity details described above were independently discovered by Afraxis for FRAX-597.¹⁶³ That group similarly proposed that Pak-4 is restricted from binding bulky side chains

in its back pocket, and further that Lys-350 is a key residue in Pak-4 that prevents binding. To test this hypothesis, they mutated Pak-1 Val-342 in the back pocket into the bulky amino acids phenylalanine (V342F) and tyrosine (V342Y), and indeed observed a sharp loss in FRAX-597 binding.

3.2.10 A fragment growing strategy successfully increased compound activity

Three strategies can be commonly used to improve fragment affinity from first or second-site screens: fragment linking, merging, and growing.⁸⁴ In a fragment linking approach, first- and second-site fragments are covalently joined using a flexible linker, such as several methylene units or ethers. If linked properly, the linked compound has affinity equal to the product of affinities for individual fragments. This technique requires accurate knowledge of the binding pose for each fragment. In our studies, the second-site fragment VU0053155 (the sulfonamide in Figure 3-18) was successfully crystallized in a ternary arrangement with Pak-1 and the first-site ligand (Figure 3-22). The phenyl substituent was found to be tucked under the kinase P-loop and the sulfonamide moiety on the second-site fragment was within linking distance from the pyrazole scaffold on VU0463835. Intriguingly, the Pak-1/4 inhibitor PF-3578309 contains a phenyl ring in precisely the same orientation under the P-loop.¹⁸⁰ That each group independently discovered this possibility further confirms the utility and accuracy of this second-site screening approach.

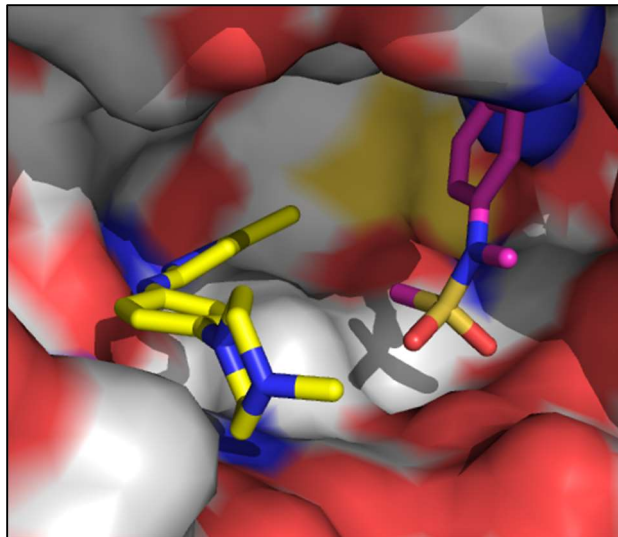


Figure 3-22: Ternary crystal structure showing two fragments bound to Pak-1-KD
Shown is Pak-1-KD, the first-site fragment VU0463835, and the second-site fragment VU0053155.

Fragment merging is another strategy to improve affinity that is highly supported by crystallography. For example, Bin Zhao co-crystallized two fragments (VU0417721 and VU0431162) with Pak-1-KD which both bind in non-traditional hinge-binding orientations (Figure 3-23). These compounds overlap only on the pyridine ring of VU0417721, and one could easily imagine removing that ring and directly linking the fragment into the central scaffold of VU0431162.

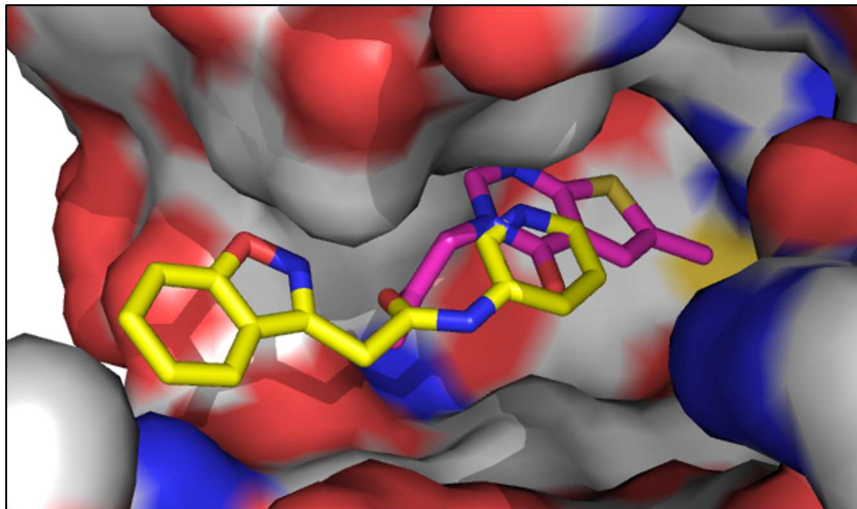


Figure 3-23: An example of structure-guided fragment merging opportunities

Here, crystal structures for VU0417721 and VU0431162 in non-traditional hinge-binding orientations are overlaid to show opportunities for merging these structures. Specifically, the pyridine ring on VU0417721 might be replaced by the central scaffold on VU0431162.

A third strategy to improve compound affinity is a fragment growing approach whereby x-ray crystallography drives iterative compound modifications to reach adjacent binding sites. This approach was readily adaptable to Pak-1 because of the large number of first-site fragment hits with co-crystal structures demonstrating binding orientation. Studies with HKI-272 proved that the selectivity pocket of Pak-1 was readily accessible by extended ATP-competitive inhibitors and would provide selectivity for Pak-1 over Pak-4. Based on that concept, Alex Waterson and Jason Burke iteratively extended VU0466177 ($K_i=1.7\mu\text{M}$) from the cyclobutyl moiety. Initial modifications to convert the cyclobutyl group to an azetidine was very unfavorable (100-fold drop in potency), but was necessary for subsequent chemical modifications. Addition of a carbonyl rescued the affinity by 10-fold, but the final addition of groups that could access the back pocket (here represented by a chloro-substituted indole linked on the 3-position) improved affinity by 100-fold. The final compound, VU0476647, inhibited Pak-1 with a K_i of 210nM.

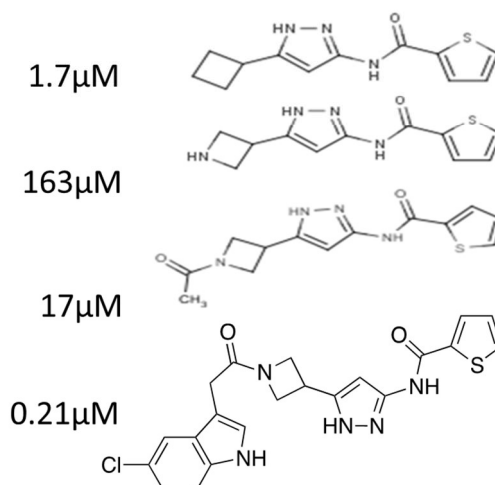
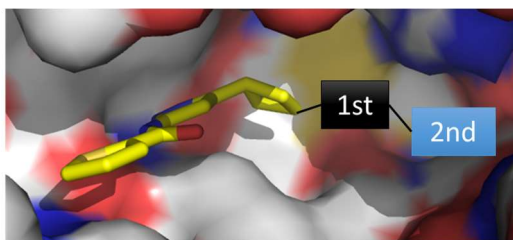


Figure 3-24: Fragment growing approach to reach the selectivity pocket of Pak-1 kinase

Starting from VU0466177 ($K_i=1.7\mu\text{M}$), a series of modifications were made to engineer an extended molecule that could occupy the Pak-1 selectivity pocket. One compound to achieve this goal (VU0476647-1) is shown here and binds with a K_i of 210nM. Not shown is VU0477448, a close analog with similar activity.

These compounds reached the selectivity pocket and bound with sub-micromolar affinity.

VU0476647 was successfully co-crystallized with Pak-1-KD by Bin Zhao (Figure 3-25A). This compound extends past the gatekeeper residue Met344 to access the selectivity pocket, which explains its selectivity for Pak-1 over Pak-4. Similarly to HKI-272, VU0476647 also intriguingly binds to both the open “DFG-in” and closed “DFG-out” form of Pak-1.

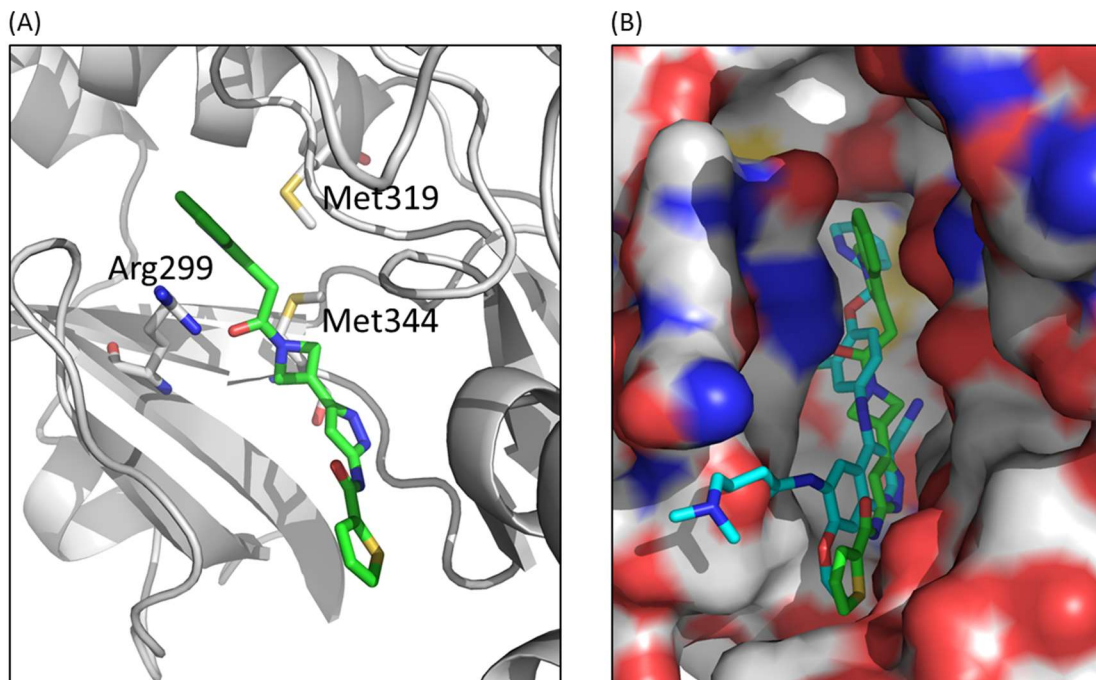


Figure 3-25: X-ray structure confirms orientation of extended fragment

(A) Crystal structure of elaborated molecule VU0476647 extending through back pocket gatekeeper Met344 to access the selectivity pocket. **(B)** Binding is similar to HKI-272 (cyan overlay).

3.2.11 Pak-1 inhibitors active in breast cancer cell lines

We next tested whether the Pak-1 inhibitors that we discovered would exhibit on-target mechanistic activity in breast cancer cell lines through inhibition of Pak-1-mediated phosphorylation. To test this hypothesis, we first analyzed a panel of ten breast cancer cell lines for Pak-1 activity. These cell lines comprise examples of luminal and basal-derived cell lines, and include ER+, Her2+, and triple-negative breast cancer (TNBC) subtypes. Pak-1 is only active when phosphorylated on T423; therefore, higher ratios of phospho-Pak-1(T423) to total Pak-1 indicates higher overall activity. HCC-1954 and MDA-MB-468 cell lines contained the highest amount of active Pak-1, while MDA-MB-453, MDA-MB-157, and SKBR-3 contain very low percentage of

active Pak-1. High Pak-1 activity did not correlate with basal or luminal subtype, nor with HER2+ or ER+ expression (Figure 3-26A).

I next assayed whether compounds could prevent Pak-1 phosphorylation. Pak-1 uniquely phosphorylates several proteins on specific residues, including MEK1 at S298¹⁸¹⁻¹⁸³ and MERLIN at S518.¹⁸⁴⁻¹⁸⁶ The rate at which pre-existing phosphate groups is lost is dependent on several factors, including the rate at which compound inhibits Pak-1 (dependent on compound entry into the cell and binding kinetics), the level of phosphatase activity, and speed of target protein turnover. To preliminarily measure the time it takes to reduce MEK S298 phosphorylation, I dosed MDA-MB-468 cells with a Pak kinase inhibitor discovered by Astex Pharmaceuticals (K_i reported to be less than 500nM and measured in-house to be 310nM).¹⁸⁷ This compound dose-dependently decreases MEK S298 phosphorylation just 5 minutes post-dosing, with sustained inhibition to 300 minutes (Figure 3-26B). The designed fragment VU0466177 ($K_i=1.7\mu\text{M}$) weakly reduces Pak-1-mediated phosphorylation with an IC_{50} of $>100\mu\text{M}$, while VU0476647 and VU0477448 inhibited with IC_{50} s of 4.3 and $14.7\mu\text{M}$, respectively (Figure 3-26C-D). These compounds were also tested to reduce Pak-1-mediated phosphorylation of MERLIN at S518 in a dose-dependent fashion (data not shown).

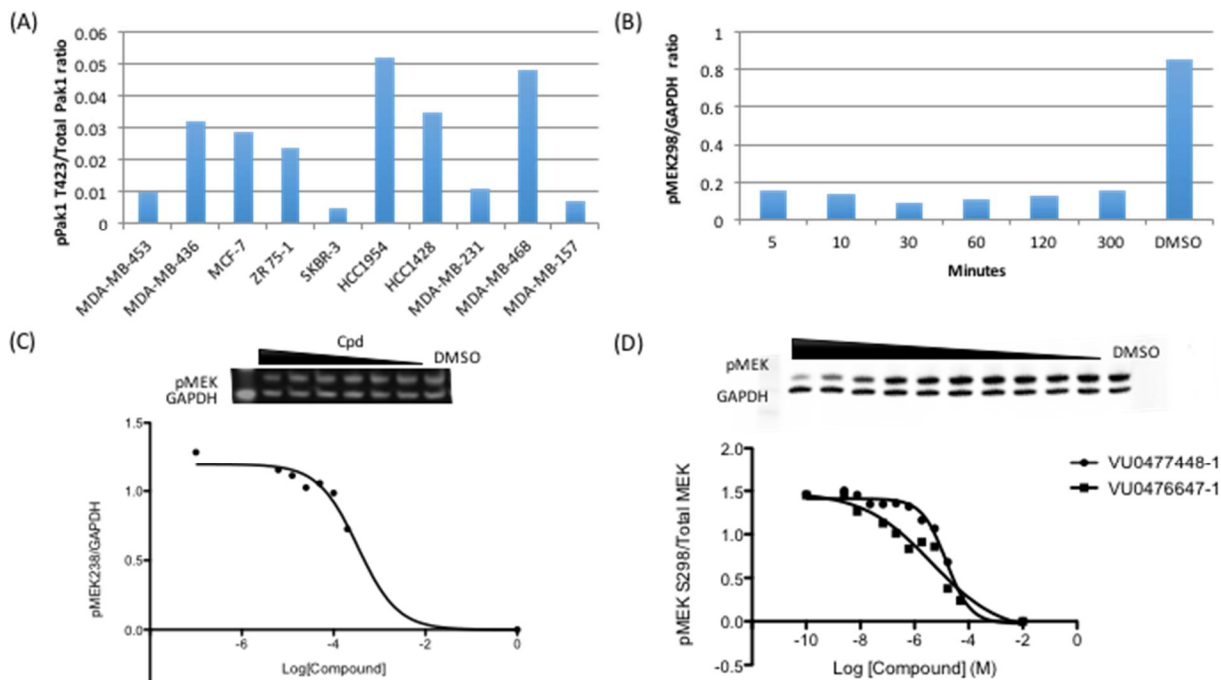


Figure 3-26: Pak-1 inhibitors demonstrate mechanistic activity in breast cancer cells

(A) Screening a panel of breast cancer cell lines for active Pak-1 (phospho-Pak-1 to total Pak-1 ratio). HCC1954 and MDA-MB-468 cells contain the most active Pak-1 kinase **(B)** Time-course of inhibition in cells at Pak-1-specific site MEK pS298 after treatment with a Pak-1 kinase inhibitor. Maximum inhibition is at 30 minutes post-dosing. Dose-response curves for VU0466177 **(C)** and VU0477448 and VU0476647 **(D)** to reduce phosphorylation at MEK phosphor-S298 in MDA-MB-468 cells are shown. The IC_{50} for VU0466177 is greater than $100\mu\text{M}$, while the IC_{50} is 4.3 and $14.7\mu\text{M}$ for VU0476647 and VU0477448, respectively.

ATP-competitive kinase inhibitors must compete with endogenous ATP (which ranges between $1\text{-}5\text{mM}$)¹⁸⁸ in a cellular environment; kinase activity is also dependent on the K_M for ATP ($K_{M, \text{ATP}}$), which for most kinases is in the low-to-mid micromolar range. Therefore, there is typically a 10-100 fold decrease in activity when progressing from K_i to IC_{50} in cells.¹⁵⁸ As expected, Pak-1 inhibitors with K_i values of 200-300nM show in-cell mechanistic activity of 5-15 μM (a 20-50 fold loss in activity). However, even single-digit micromolar IC_{50} in cells is inappropriate to accurately measure Pak-1's role in proliferation, motility, and survival due to confounding off-target effects produced by high compound concentrations.

3.3 Discussion

All Pak isoforms have been implicated in cancer progression in a wide range of cancer types.¹¹⁹ In particular, Pak-1 expression correlates with increased metastasis¹⁰⁶ and a poor clinical prognosis in breast cancer,^{123,124} though other cancers for which Pak-1 plays a significant role include colon cancer, ovarian cancer, and in neurofibromatosis.¹²³ Synthetic Pak-1 activation *in vitro* increases cell growth, proliferation,¹⁰⁰ and anchorage-independence,¹³⁹ while *in vivo* activation induces malignant mammary tumor development.^{123,140,141} Inhibition of Pak-1 reverses these phenotypes.^{122,139} Moreover, because Pak-1 is a common resistance factor for estrogen receptor therapies, inhibition of Pak-1 may restore sensitivity to ER α -targeted therapies. Yet no specific Pak-1 inhibitor had been published prior to the start of this project in 2011.

In light of the strongly suggestive pre-clinical and clinical validation for Pak-1 as an effective therapeutic target in the treatment of human cancer, we proposed to discover a Pak-1-selective tool molecule to further validate this kinase as a target for multiple cancer types, and to elucidate the individual contributions of Pak-1 to tumorigenesis and cancer progression. Towards this end, we identified over two hundred chemically diverse compounds from multiple series in two fragment-based NMR screens. Using biochemical assays to measure the inhibition of Pak-1 and Pak-4, we improved the activity and selectivity of our compounds through a fragment growing approach, and synthesized an inhibitor with *in vitro* K_i of 200nM. Our inhibitors blocked Pak-1-mediated phosphorylation of MEK1 at S298 and MERLIN at S518 in breast cancer cell lines. The reduction in activity between K_i and cellular IC₅₀ (here 25-50 fold) is consistent with previously published kinase inhibitors, and moreover, demonstrates that our inhibitors are soluble, chemically and metabolically stable in culture up to 300 minutes, and cell-permeable.

Although great progress was made on this project, our compounds require significant improvement to meet the objectives laid out in the introduction to this chapter. First, affinity would have to be improved by 10 to 100-fold such that cellular inhibition of Pak-mediated phosphorylation could be achieved using sub-micromolar concentrations. Secondly, these inhibitors must be tested *in vitro* for efficacy at reducing cancer cell growth, motility, and survival in breast cancer cell lines, and these effects must be in agreement with cellular sensitivity following Pak-1 RNAi silencing. Only when these compound validation steps have been accomplished can this inhibitor be used to answer the basic science issues raised in the Introduction.

VU0476647 and VU0477448 were the most potent and fully elaborated molecules synthesized for this program, but they failed to fully occupy available the space in the ATP cleft. For example, the Pak-1 back pocket extends further beyond the chloro-indole headpiece on VU0476647. In principle, filling these sites would result in further affinity improvements. Due to time and resource constraints, opportunities for compound linking or merging were not implemented.

We initiated this drug discovery program because of a severe deficit in the field of highly potent and selective Pak-1 inhibitors that could be used as tool molecules to validate inhibition of Pak-1 kinase activity as a therapeutic target.¹⁸⁹ However, after this project was initiated a number of Group I-selective inhibitors were published.¹⁰⁶ Several of these inhibitors were suitable as pre-clinical tool molecules, and the more advanced FRAX-series retains troubling kinome selectivity and DMPK issues that must be addressed before proceeding to the clinic. Nevertheless, because these groups maintained active discovery efforts with compounds more

potent than those we had discovered, our effort was not competitive, and we chose to discontinue this project.

Despite this setback, newly available Pak-1 inhibitors are beginning to answer basic questions about Pak-1 biology and to validate its role as an anti-cancer target. Consistent with the available pre-clinical evidence, a Pak-1-selective molecule can inhibit cancer cell proliferation *in vitro* and *in vivo*. FRAX597 reduced proliferation in transformed (Nf2-null) Schwann cells in culture, and in a model of schwannomas whereby Nf2-null schwann cells are implanted into a myelinated nerve, inhibitor significantly reduced the growth rate and burden compared to control animals. These phenotypes were recapitulated by treatment with pan-Pak inhibitor PF3758309, suggesting that this activity is mediated by the Group I Paks.¹⁶³ In breast cancer, single-agent Group I Pak inhibition by FRAX-1036 increased apoptosis and elevated Bim expression and powerfully synergized with the microtubule-destabilizing agent Docetaxel to induce apoptosis in luminal MDA-MB-175 and HCC2911 cells.¹⁶⁵ These early studies clearly demonstrate that inhibiting the kinase activity (but not scaffolding functionality) of Group I Paks is a valid therapeutic strategy in certain cancer types, that simultaneous inhibition of Group II Paks is not always necessary, and that these agents can synergize with other chemotherapeutics to reduce growth and induce apoptosis both *in vitro* and *in vivo*.

Many questions regarding Pak-1 inhibition remain unanswered. What are the genetic or molecular determinants of Group I Pak sensitivity, and what drives a cell to depend on Pak-1 for growth, survival, and motility? In breast cancer in particular, no study has investigated correlations between Pak-1 activation or dependency and HER2 or EGFR status, nor with activating mutations in the PI3K/Akt or Raf/Mek/Erk pathways. Can we predict a response rate

among breast cancer patients to Pak-1 inhibition? Are other cancers with Pak-1 overexpression susceptible to Pak inhibitor treatment? Thus far, only schwannomas and luminal breast cancers have been examined. Does therapeutically relevant Pak-1-inhibition require a combination approach in breast cancer, such as with Docetaxel? What other combination therapies are possible? Pak-1 has roles in promoting survival (suggesting co-dosing apoptotic activators such as ABT-263), proliferation (MEK, RAF inhibitors), and tamoxifen resistance in ER+ breast cancers (which simultaneous Pak-1-inhibitor dosing may reverse). Answering these and many other questions may soon be possible by using the newly-discovered Pak-1 selective inhibitors described above.

3.4 Methods

Protein Purification

An oligonucleotide containing the amino acid sequence of human PAK1 kinase domain (residues 249-545), with K299R and T423E mutations and codon-optimized for *E. coli* expression, was cloned into a pGEX6p-1 expression plasmid. This plasmid contains the coding sequence for Glutathione S-Transferase (GST) and a short linker sequence specific for Precision Protease downstream of the start codon and amino-terminal to the inserted Pak-1 expression sequence. This expression plasmid was transformed into *E-coli* BL21-Rosetta 2 cells. Growth conditions were optimized to maximize protein solubility by varying the IPTG concentration, growth temperature, and induction length of time. Protein was induced at 30°C with 1mM IPTG overnight. Cells were harvested, lysed, and lysate was resuspended in a previously published buffer,¹⁴⁷ bound to a glutathione column (GSTTrap, GE Healthcare), washed repeatedly, and eluted with 10mM

glutathione. The protein was then cleaved by Precision Protease, washed through the GST column to separate kinase from GST, and finally purified by Sephacryl S-100 (GE Healthcare) size-exclusion chromatography.

Wild-type Pak-4 (residues 291-591) oligonucleotide was similarly cloned and expressed in *E. coli* cells. Induction occurred at with 1mM IPTG at 37°C for 3 hours. Purification was conducted as described for Pak-1.

NMR measurements

All NMR measurements were collected on a Bruker DRX500 or 600 spectrometer equipped with a cryoprobe and a Bruker Sample Jet sample changer. Two-dimensional sensitivity-enhanced ¹H/¹⁵N- HSQC spectra were measured at 60μM protein concentration for 256 scans, while STD-NMR measurements were conducted at 10μM protein concentration with 8 scans.

Fluorescence Anisotropy Assay

FPA measurements were carried out in 384-well, black, flat-bottom plates (Greiner Bio-One) using the EnVision plate reader (PerkinElmer) with a G-factor of 0.81. All assays were conducted in assay buffer containing 20 mM TRIS pH 7.5, 50 mM NaCl, 3 mM DTT, and 2.5% final DMSO concentration. To measure the affinity of BODIPY-labeled ATP (Sigma) for Pak-1-KD, protein was titrated into a fixed concentration of 100nM BODIPY-ATP and incubated for 1 hour at room temperature. Anisotropy values were plotted in prism and fit by a one-site (Total) non-

linear binding model. Competition experiments were conducted by adding a saturating concentration of unlabeled ATP to pre-incubated 100nM BODIPY-ATP and 50 μ M Pak-1.

Kinase Activity Assay

To measure direct compound inhibition of kinase activity, we use the LANCE Ultra Time Resolved (TR)-FRET assay kit (Perkin Elmer). Total reaction volume is 10 μ L with all reactions taking place in a buffer of 25mM Tris, 120mM NaCl, 10mM MgCl₂, pH 8.0. Full-length GST-Pak-1 kinase (ProQinase) is first activated by incubating with 4 μ M ATP for three hours at 4^oC. A master mix of pre-activated Pak-1 and ATP is prepared in buffer such that the final Pak-1 and ATP concentrations are 9nM and 0.09 μ M, respectively (care being taken to account for the ATP already present due to Pak-1 activation). This master mix is aliquoted into a white Optiplate-384 (Perkin Elmer). Compounds are three-fold serially diluted in 10% DMSO at four-times the desired final concentration and added to the appropriate well (2.5% DMSO final concentration). Lastly, peptide substrate is added such that the final concentration is 50nM. Control reactions receive vehicle (DMSO); negative control reactions lack ATP and Pak-1. Indicated concentrations of Pak-1, ATP, and peptide substrate concentration were optimized to keep each component within the linear portion of their own dose-response curve.

Reaction proceeds for 20 minutes at room temperature. Quenching occurs with the addition of 10 μ L EDTA and anti-phosphate antibody solution such that the final concentrations are 10 μ M and 2nM, respectively. The plate equilibrates for one hour at room temperature and is then read on an Envision spectrometer (Perkin Elmer) with the following filters: Excitation UV320/340nm,

Emission Europium at 615nm and 205-APC at 665nm. Data is analyzed in Excel using Xcel Fit analysis software. IC₅₀ values are reported as K_s by the Cheng-Prusoff equation.

This assay is similarly run for Pak-4 as described above using 2.5nM Pak-4 and 0.25μM total ATP. Pre-activation with ATP is not required.

Cellular Mechanistic Assay

This assay quantifies direct inhibition of Pak-1 kinase activity in cells by measuring changes in phosphorylation at Pak-1-specific residues MEK site S298 or MERLIN S518. Cells are plated into 6-well dishes and grown to 80% confluency in medium containing 10% serum. To determine the time of maximal inhibition, compound was added to MDA-MB-468 cells at 80% confluency for 5, 15, 30, 60, or 300 minutes. Cells were lysed in denaturing SDS loading buffer with 10mM DTT and boiled at 90°C for 3 minutes. Samples were run on an SDS-PAGE gel and transferred to Immobilon-FL PVDF membrane (Millipore). Membrane was blotted in primary antibody against total Pak-1 kinase, total MEK (Cell Signaling), and phosphor-S298 MEK (Abcam), or to total MERLIN and posphoS518 MERLIN. Western blots are visualized on the Odyssey system (Licor). The ratio of phosphor-protein to total protein for compound-treated cells compared to control DMSO-treated cells indicates whether compound inhibited Pak-1 kinase activity. To determine compound dose-response curves, inhibitor or vehicle (DMSO) control was added for 30 minutes 37°C. Cell lysates were collected and analyzed as above. The percentage of phospho-protein to total protein is quantified and plotted in Prism (GraphPad) to determine IC₅₀.

Chapter 4

Discovery of Mcl-1 inhibitors and identification of sensitive cancer types

4.1 Introduction

One of the hallmarks of cancer is the evasion of programmed cell death, termed 'apoptosis'. The Bcl-2 family of proteins are important regulators of apoptosis. Clinical and pre-clinical evidence suggest that upregulation of one of these family members, Myeloid cell leukemia-1 (Mcl-1), is a common survival mechanism in response to oncogenic activation. Small-molecule inhibitors of other pro-survival Bcl-2 family members, such as ABT-263 and ABT-199, have achieved pre-clinical and clinical success at reducing tumor burden, but no Mcl-1 inhibitor has been clinically tested. In this chapter, I describe the discovery of specific small-molecule inhibitors of Mcl-1 for the treatment of cancer, and molecularly profile and predict which cancer types may respond to targeted Mcl-1 inhibition.

4.1.1 *Mechanisms of cell death*

Mammalian cells are constantly exposed to diverse extracellular and intracellular stressors, including growth factor and oxygen deprivation, DNA damage, oncogenic signaling, metabolic changes, and the addition of cytotoxic molecules. Each cell contains repair pathways to correct aberrant states arising from these events.^{190,191} Ultimately, a cell may be unable to fully repair the sustained damage and may proactively commit to death through a controlled and

active process. Alternatively, cells may instead passively die through an uncontrolled process. This choice – passive or active – has profound effects on both the cell and the surrounding tissue microenvironment.

The passive, uncontrolled process by which a cell dies is termed ‘necrosis.’¹⁹² Cells undergo necrosis after gross injury to the cell membrane or by the loss of intracellular ATP,¹⁹³ and this process is distinguished by morphological alterations that include plasma membrane swelling, disruption of mitochondria and organelle membranes, distended endoplasmic reticulum, and cytoplasmic blebs. Eventually this process culminates in the loss of membrane integrity, the release of cellular contents into the surrounding tissue, and finally cytokine-mediated inflammatory signaling to macrophages to stimulate the removal of necrotic cellular components.^{192,194} Necrosis is a passive process: no cellular mechanism controls the progression of death or the manner in which the cell is disposed. As such, necrosis does not require energy or operative cellular machinery, and therefore is most commonly employed by a patch of cells in response to a mechanical or toxic event, such as the loss of membrane integrity.

In contrast, an energy-rich cell with an intact membrane may choose to undergo a controlled cell death program. This process, coined “apoptosis” in 1972 (from the Greek words *apo*, ‘of, by, from’ and *ptosis*, ‘fall,’ pronounced ‘a-po-toe-sis’), is distinguished from necrosis by a cytological morphology of nuclear and cytoplasmic condensation, the disruption of the cell into distinct membrane-bound fractions, and the eventual phagocytosis of cellular constituents by macrophages, parenchymal cells, or neoplastic cells.^{194,195} This process requires active cellular machinery to regulate and execute discrete steps, and requires available energy to affect the response.¹⁹² Cells carefully audit for cellular damage and, in response to crossing a pre-

determined threshold, transition away from a pro-survival balance.^{196,197} The decision to execute apoptosis or necrosis is not always pre-determined: cells in a given population may undergo either apoptosis or necrosis despite receiving the same damaging stimuli.¹⁹⁴ These processes are not mutually exclusive; rather, they lie on a continuum where a cell may transition from a controlled apoptotic response to a necrotic response when the ATP concentration drops, cellular machinery is grossly inhibited, or the plasma membrane is disrupted by further damaging events.¹⁹²

Nevertheless, undergoing apoptosis rather than necrosis is usually advantageous to the organism. First, apoptosis reduces damage to the surrounding tissue. By carefully packaging up cellular components for phagocytosis, apoptosis prevents the release of inflammatory cytokines that might damage nearby cells through an inflammatory response.¹⁹² Second, apoptosis allows an organism to carefully control the cell population through selective weeding of unneeded cells. This process is highly utilized during development and in epithelial cell shedding. Third, apoptosis enables a cell to die in response to internal damage that is not severe enough to prevent cellular survival. For example, cancer-promoting events such as oncogene activation or DNA damage can be mitigated by pre-emptively removing the damaged cell from the population.^{11,192,198,199} Loss of the apoptotic response is one of the hallmarks of cancer.¹¹

Apoptosis is classified into three distinct pathways: intrinsic, extrinsic, and the granzyme pathway (Figure 4-1). The intrinsic pathway is activated in response to intra-cellular stimuli such as DNA damage, oncogenic overstimulation, viral infection, and other activities. While these signals may arise because of extra-cellular events (such as UV irradiation inducing DNA damage or AKT activation through aberrant cytokine stimulation), the direct activating stimuli for

apoptosis occur within the cell. In contrast, the extrinsic pathway is externally activated through direct binding of extracellular ligands to death receptors on the cell surface (such as Fas ligand binding to Fas cell-surface death receptor).^{192,200} The third mechanism, the granzyme pathway, is activated by cytotoxic T cell-mediated release and insertion of intracellular pore-forming perforin proteins, and the trafficking of serine proteases through these pores into the target cell.^{201,202} All apoptotic pathways converge to activate members of the caspase family of cysteine proteases, which terminates in activation of the cellular 'execution pathway' through the proteolytic cleavage of caspase-3. This results in DNA fragmentation, cleavage of cellular proteins, ligand expression for phagocytic bodies, and the formation of apoptotic bodies containing condensed organelles and chromatin, as described above.^{196,203}

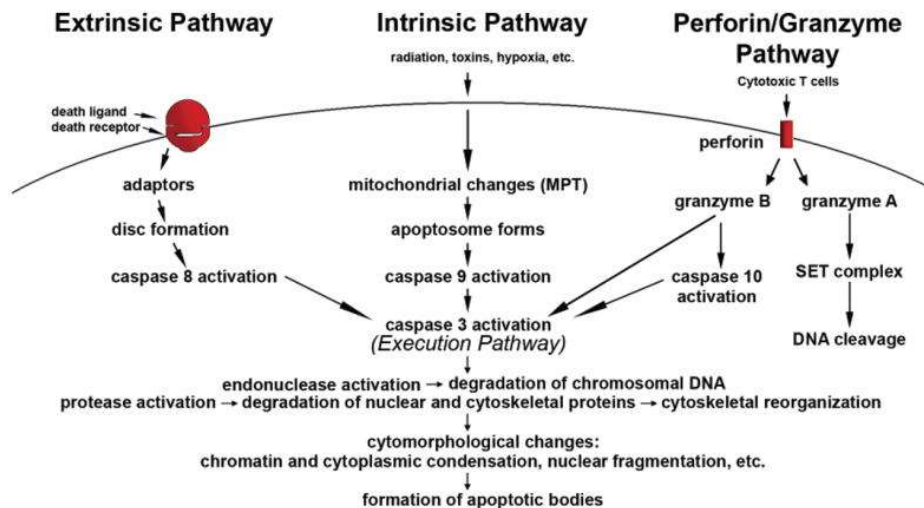


Figure 4-1: Apoptosis consists of the extrinsic, intrinsic, and perforin/granzyme pathways
 Apoptotic pathways all converge on the caspase-based execution pathway and activation of the serine protease caspase-3, which is responsible for most of the phenotypic traits exhibited by apoptotic cells, such as cellular blebbing, loss of adhesion, and packaging of cellular components. Figure from Elmore¹⁹²

4.1.2 *The Bcl-2 family of proteins regulate the intrinsic apoptotic pathway*

The intrinsic apoptotic pathway is controlled by a balance of pro-apoptotic and anti-apoptotic proteins in the B-cell CLL/lymphoma 2 (Bcl-2) family.²⁰⁴ Bcl-2 was originally discovered in 1984 in a chromosomal translocation in B cell follicular lymphoma.²⁰⁵ Over 20 mammalian genes with homology to this founding member were subsequently discovered, and all contain at least one of the four conserved α -helical Bcl-2 Homology (BH) domains present in Bcl-2 itself.²⁰⁶ This diverse protein family contains members that promote as well as those that inhibit apoptosis, and the interplay between pro- and anti-apoptotic members act as controls to determine whether apoptosis will occur. Briefly, activation of the intrinsic apoptotic cascade induces the expression or translocation of pro-apoptotic Bcl-2 family members to the mitochondria (termed “BH3-only proteins” by virtue of expressing only the third Bcl-2 homology domain).²⁰⁷ The BH3-only proteins subsequently trigger pore formation in the mitochondrial outer membrane via induced multimerization of the executioner proteins Bak or Bax by a process that leads to cytochrome c release and caspase-dependent apoptosis.²⁰⁸ Anti-apoptotic Bcl-2 family proteins, including Bcl-2, Bcl-xL, and Mcl-1, sequester pro-apoptotic members of the same family to inhibit apoptosis (Figure 4-2).¹⁹⁰

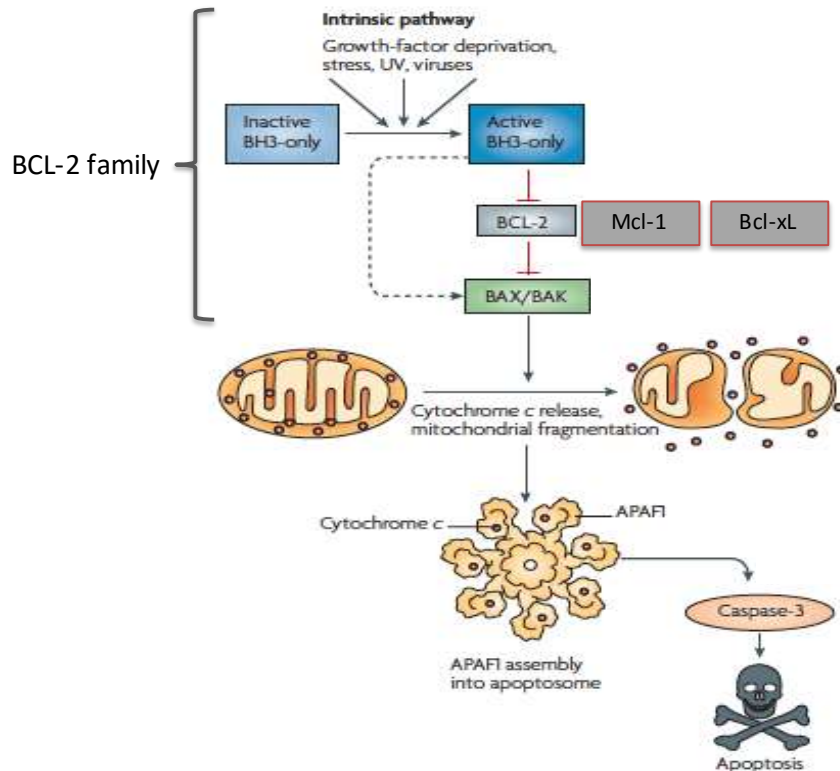


Figure 4-2: The Bcl-2 family of proteins regulates the intrinsic apoptotic cascade

Stimulating events activate BH3-only proteins, which then antagonize anti-apoptotic Bcl-2 family members such as Mcl-1 and Bcl-2. Pro-death executioner proteins Bax and Bak are thereby released from an inhibitory complex with these anti-apoptotic proteins, and thereby organize into pore-forming multimers in the mitochondrial outer membrane. This allows cytochrome c release, caspase activation, and an irreversible commitment to cell death. Adapted from Youle, *et al* 2008.²⁰⁷

4.1.3 BH3-only proteins activate apoptosis in response to diverse stimuli

Pro-apoptotic BH3-only proteins are essential initiators of apoptosis conserved from *C. elegans* to humans.²⁰⁹ Over ten distinct members have been characterized in mammalian cells.²¹⁰ These 'BH3-only proteins' are far more complex than their simplistic nomenclature would suggest, though each is distinguished by the expression of the third Bcl-2 homology (BH) domain near the carboxy-terminal end of the protein. This domain is short – it forms a single α -helical secondary structure when folded – and is comprised of four key conserved hydrophobic residues

(ϕ_1 – ϕ_4 , Figure 4-3).²¹¹ The size and organization of BH3-only proteins outside the BH3 domain is widely variable. Most, but not all, express a transmembrane-spanning helix at the carboxy-terminus that is used for membrane insertion into the mitochondrial outer membrane.^{212,213} Loss of this helix prevents mitochondrial localization and abrogates activity for some BH3-only proteins, such as Noxa.²¹⁴ These proteins are intrinsically unstructured until bound to multi-domain Bcl-2 family members.²¹⁵

heptad	A	b	c	d	e	f	g	A	b	c	d	e	f	g	A	b	c	d	e	f	g	A	b	c	d	e	f	g	A	
hsBim	E	P	A	D	M	R	P	E	I	W	I	A	Q	E	L	R	R	I	G	D	E	F	N	A	Y	Y	A	R	R	
hsBid	S	E	S	Q	E	D	I	I	R	N	I	A	R	H	L	A	Q	V	G	D	S	M	D	R	S	I	P	P	G	
hsPuma	R	G	E	E	E	Q	W	A	R	E	I	G	A	Q	L	R	R	M	A	D	D	L	N	A	Q	Y	E	R	R	
hsBad	A	P	P	N	L	W	A	A	Q	R	Y	G	R	E	L	R	R	M	S	D	E	F	V	D	S	F	K	K	G	
hsBmf	G	Q	W	Q	H	Q	A	E	V	Q	I	A	R	K	L	Q	C	I	A	D	Q	F	H	R	L	H	V	Q	Q	
hsHrk	L	G	L	R	S	S	A	A	Q	L	T	A	A	R	L	K	A	L	G	D	E	L	H	Q	R	T	M	W	R	
hsNoxa	A	R	A	P	A	E	L	E	V	E	C	A	T	Q	L	R	R	F	G	D	K	L	N	F	R	Q	K	L	L	
hsBik	S	L	E	C	M	E	G	S	D	A	L	A	L	R	L	A	C	I	G	D	E	M	D	V	S	L	R	A	P	
ceEGL-1	D	S	E	I	S	S	I	G	Y	E	I	G	S	K	L	A	A	M	C	D	D	F	D	A	Q	M	M	S	Y	
ceCED13	A	C	N	S	N	T	V	E	Y	N	I	G	R	K	L	T	V	M	C	D	E	F	D	S	E	L	M	S	Y	
								ϕ_1							ϕ_2								ϕ_3						ϕ_4	

Figure 4-3: Sequences of the BH3-motif of BH3-only proteins.

They key BH3-motif conserved sequences are boxed, and key binding hydrophobic residues is indicated by ϕ_1 – ϕ_4 . Adapted from Kvaisakul, *et al* 2014.

These proteins utilize two distinct mechanisms to activate apoptosis.²¹⁶ First, all BH3-only proteins are capable of binding to a subset of pro-survival Bcl-2 family members (Bcl-2, Bcl-xL, Mcl-1, and others). BH3 binding preferences of these grooves vary widely among Bcl-2 family members and have been extensively characterized (Figure 4-4).²¹⁷⁻²¹⁹ The BH3-only proteins Bim, Bid, and Puma are promiscuous – they bind to all known multi-domain Bcl-2 family members. Bad binds to Bcl-2, Bcl-xL, and Bcl-w, but not to the executioner proteins Bak and Bax, nor to Mcl-1 or A1/Bfl-1. Noxa uniquely binds to Mcl-1 and A1/Bfl-1, while Hrk uniquely binds to Bcl-xL.

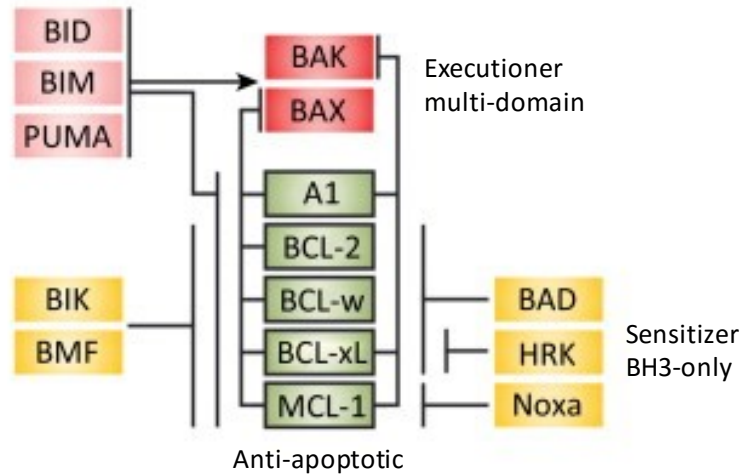


Figure 4-4: BH3-domain interactions among Bcl-2 family proteins

A surprising degree of BH3-binding specificity is present among Bcl-2 family members. Adapted from Moldoveanu *et al*, 2014.²¹⁹

As mentioned above, BH3-only proteins are activated in response to internal stressors such as oncogenic signaling, DNA damage, or viral infection. Each form of damage activates a different subset of BH3-only proteins. Mechanisms of activation involve at least threefold: increased expression, induced translocation to the mitochondria, and reduced degradation.²²⁰ For example, Noxa is a primary response element to P53 sensing of DNA damage, and its mRNA is highly upregulated after P53 activation.²²¹ Bim expression increases as well, such as by oncogenic myc activation,²²² but a common post-translational mechanism is translocation to the mitochondria from a cytosolic complex with dynein light chain DLC-1.²²³ Finally, the rate of protein degradation can be altered. Noxa activity in particular is heavily regulated by the rate of its degradation.²²⁴

4.1.4 Pro-survival Bcl-2 family members sequester pro-apoptotic proteins

In contrast to the BH3-only proteins, multi-domain Bcl-2 family members are characterized by a central, globular structure consisting of eight α -helices (Figure 4-5).²⁰⁶ N-terminal regulatory domains and a C-terminal membrane-tethering helix are not shown in Figure 4-5 but are crucial for their proper biological activity, as discussed below. The BH3 α -helical domain binds in a hydrophobic groove formed on top by the BH1, 2, and 3 helices, and on the bottom by the α 3 and α 4 helices.²⁰⁶ These BH3-domain interactions form the basis of antagonism between pro-survival and pro-death Bcl-2 family members.

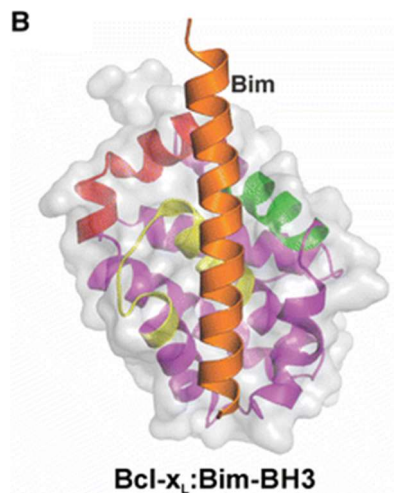


Figure 4-5: Structure of BH3 interactions with anti-apoptotic Bcl-2 proteins

The pro-survival Bcl-2 family members (exemplified here by Bcl-xL) contain eight α -helices (numbered α 1-8) and four “Bcl-2 homology” (BH) domains. Three of these domains form the binding pocket for antagonizing “BH3-only” proteins to bind: BH1, colored yellow; BH2, colored red; and BH3; colored green. BH4/ α 1 helix is colored purple and is located latitudinally across the structure behind the green BH3 and yellow BH1 helices.²¹¹ Adapted from Kvensakul 2014.

Multi-domain Bcl-2 family members are not functionally redundant: each possess distinct and highly specific binding preferences (Figure 4-4), tissue distribution, and post-translational modifications.²²⁵ For example, Mcl-1 is highly expressed in a variety of tissues, including prostate,

breast, endometrium, epidermis, stomach, intestine, colon, and the respiratory tract, but is notably absent from neuronal tissues in the brain or spinal cord.^{226,227} Expression of a particular pro-survival family members, such as Mcl-1, is commonly inversely correlated to the expression of another, such as Bcl-2. For example, Bcl-2 is highly expressed in brain neuronal tissues but not in cardiac or skeletal muscle, where Mcl-1 is highly utilized.²²⁶

Mcl-1 expression, degradation, and localization is uniquely regulated among the pro-survival Bcl-2 family members (Figure 4-6), and has been extensively reviewed elsewhere.²¹² Most control occurs due to numerous regulatory elements in the N-terminal region, which is significantly larger than other proteins in this family (350 residues compared to 239 residues in Bcl-2, for example). Efficient trafficking to the mitochondria from cytosolic reserves is highly dependent on localization signals present in the Mcl-1 N-terminal sequences, including internal EELD sequence and a mitochondrial import receptor TOM70 binding domain.^{212,228} In addition, Mcl-1 degradation is highly regulated. Mcl-1 is much more rapidly degraded *in vivo* than other pro-survival Bcl-2 family members (with a half-life of just 30-60 minutes, on average). Degradation is primarily mediated by the proteasome pathway using E3 ubiquitin ligases HUWE/MULE and b-TrCP/FBXW7. Their recruitment to Mcl-1 is modified by phosphorylation at several residues (Figure 4-6). For example, mutation of S162 to phospho-dead mutant abrogated mitochondrial localization despite continued expression of the C-terminal membrane-spanning helix. Indeed, Mcl-1 localized almost exclusively to the nucleus in this case.²²⁹ Upstream pathways may increase (GSK3B at S155 and S159) or decrease (ERK at T92 and T163) degradation. Finally, Mcl-1 anti-apoptotic activity is modified by phosphorylation in this large N-terminal region. The aforementioned GSK3B phosphorylation events at S155 and S159 also directly inhibit Bim

binding, thus freeing this BH3-only protein to induce apoptosis. In conclusion, Mcl-1 activity is uniquely regulated in response to cellular stressors. These provide unique avenues to control apoptotic activity in response to cellular stressors.

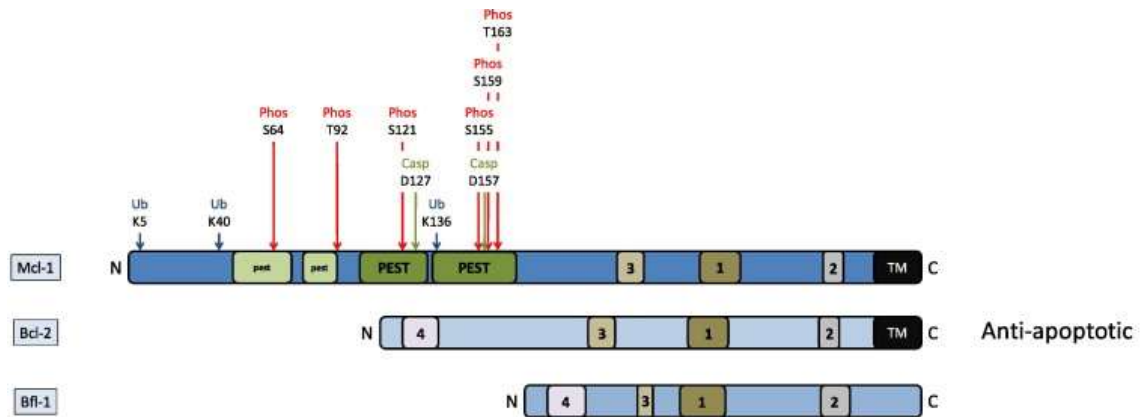


Figure 4-6: Mcl-1 is uniquely regulated through its N-terminus

The Mcl-1 N-terminal regulatory region is significantly larger than other pro-survival Bcl-2 family members, and it contains several regulatory elements controlling Mcl-1 localization, degradation, and apoptotic inhibitory activity. Adapted from Thomas, *et al* 2010.²¹²

4.1.5 Mcl-1 protein overexpression is implicated in cancer cell survival

Evasion of apoptosis is an irrevocable hallmark of cancer.¹¹ Cancer initiation and maintenance forces cells into tremendous metabolic, oncogenic, and hypoxic stress, and therefore requires the suppression of apoptotic signaling.^{190,230,231} In the absence of environmental or oncogenic stressors, multi-domain Bcl-2 family members such as Mcl-1, Bcl-2, and Bcl-2-like protein 1 isoform 1 (Bcl-xL), prevent apoptosis by sequestering pro-apoptotic Bcl-2 family members. Many cancer types aberrantly block oncogenic apoptotic signaling by increasing the steady-state expression of one or more of these proteins through genetic amplification, transcript upregulation, or reduced degradation.²⁰⁰ In particular, amplification of the gene encoding Mcl-1 is one of the most common genetic aberrations in human cancer.^{232,233}

It is commonly observed in cancers of the prostate, lung, pancreatic, breast, ovarian, melanoma, B-cell chronic lymphocytic leukemia, acute myeloid leukemia, and acute lymphoblastic leukemia.²³⁴ Overexpression in breast cancer is associated with a high tumor grade and poor survival.²³⁵ Mcl-1 overexpression is implicated as a resistance factor for multiple therapies used in the treatment of breast and other cancers,²³⁶ including microtubule-targeted agents paclitaxel and vincristine,²³⁷ and compounds that inhibit Bcl-2 and Bcl-xL.^{238,239}

Thus, Mcl-1 represents an important target for the treatment of many cancers. One of the key cancers that could be effectively targeted by an Mcl-1 inhibitor is breast cancer. Breast cancer is the second-most frequently diagnosed malignancy in U.S. women with 230,000 new cases and 40,000 deaths in 2011. The triple-negative breast carcinoma (TNBC) subtype, which does not express the estrogen receptor (ER) and progesterone receptor (PR), and lacks overexpression of human epidermal growth factor receptor-2 (HER2), afflicts nearly 15% of all breast cancer patients and remains refractory to rationally-targeted endocrine and HER2-directed therapies.^{240,241} The current standard of care for TNBC is radiation and neoadjuvant cytotoxic chemotherapy, and it carries a poor clinical prognosis.²⁴²⁻²⁴⁴ Thus, the development of novel rational targeted therapeutics such as an Mcl-1 inhibitor is a major unmet need. TNBC cells also require inhibition of the intrinsic apoptotic pathway for survival, and failure to account for increase apoptotic forcing is terminal.²⁴⁵ The MCL1 gene is the most common genetic amplification (after TP53) that occurs following neoadjuvant therapy in TNBC,²⁴⁶ and as described below, Mcl-1 is commonly upregulated in this cancer subtype.

Pre-clinical evidence suggests that Mcl-1 represents a promising target for the treatment of breast cancers.^{233,247,248} Multiple pre-clinical studies have demonstrated anti-proliferative

effects of RNAi mediated MCL-1 protein knockdown in a wide variety of cancer types.^{191,249-259} Mcl-1 knockdown reduces cell viability in a breast and lung cancer panel,²³³ and the volume of xenograft derived from breast cell lines is reduced following Mcl-1 silencing.²³² Small-molecule transcriptional repressors or post-translational destabilization of Mcl-1 phenocopy this effect.^{237,260-262}

The forced overexpression of Mcl-1 in transgenic mice has been reported to exhibit a high incidence of B-cell lymphoma,²⁶³ while Mcl-1 down-regulation using antisense oligonucleotides or siRNA has been shown to induce apoptosis in a number of cancer cell types.^{251,256} Doxycycline-inducible overexpression of the Mcl-1 antagonizing Bcl-2 homology domain 3 (BH3)-only protein Noxa, but not Bim, Puma, or tBid, synergizes with Bcl-2 and Bcl-xL inhibitor ABT-737 treatment in Jurkat J16 cells.²¹⁷ These data suggest that Mcl-1 expression selectively benefits tumor cell survival.

Likewise, Bcl-xL and Bcl-2 are also commonly amplified²³² and have been clinically implicated in driving tumor cell survival in multiple cancer types (ref). Bcl-xL been implicated in preventing various cancers from undergoing programmed cell death, including melanoma²⁶⁴ and colon cancer.^{265,266} In addition, in breast and lung tumors, Bcl-xL amplification correlates with a decreased sensitivity to transcriptional repressors.²³³

4.1.6 Therapeutic use of an Mcl-1 specific inhibitor

Enhanced dependency on anti-apoptotic Bcl-2 family member expression to avoid cell death in cancer cells suggest that neutralizing their function may be an effective strategy to combat cancer.²⁴⁷ Loss of anti-apoptotic protein function may restore apoptotic signaling,

enhance responses to anti-cancer chemotherapy, and improve the outcome of many cancer patients.²³⁶ Inhibitors developed for other pro-survival proteins, such as Bcl-2 and Bcl-xL, have proved highly effective at reducing cancer cell growth both *in vitro* and *in vivo*.²⁶⁷⁻²⁶⁹ The Bcl-2, Bcl-xL, and Bcl-w inhibitor ABT-737 reduces viability in small-cell lung cancer,⁸³ and the orally bioavailable derivative ABT-263 has shown phase-II clinical success at reducing tumor burden in SCLC and CLL as well.²⁷⁰ Therefore, targeted inhibition of Mcl-1 could also result in cell death in a subset of cancers, including TNBC. Further, Mcl-1 inhibition increase sensitivity to anticancer chemotherapy by weakening the apoptotic blockade, as has already been seen with transcriptional Mcl-1 repression by flavopiridol synergizing with ErbB1/ErbB2 inhibition.²⁴⁷

Another important utility of Mcl-1 inhibition is overcoming resistance to other Bcl-2 family inhibitors. Pre-clinical studies have suggested that resistance to Bcl-2 and Bcl-xL inhibitors is often the result of a compensatory increase in Mcl-1 expression to sequester pro-apoptotic proteins. Therefore, an Mcl-1 inhibitor will have therapeutic relevance not only as an agent in Mcl-1-dependent cancers, but will serve as a useful therapeutic in resistant tumors as well.^{239,271}

Effectively using these targeted therapeutics requires accurately predicting which anti-apoptotic proteins the tumor depends upon for survival. High expression of a pro-survival Bcl-2 family member does not necessarily correlate with the dependency on that protein to prevent apoptosis.²⁷²⁻²⁷⁴ Individual pro-survival Bcl-2 family proteins preferentially inhibit a subset of pro-apoptotic family members,²¹⁸ and cancer cells require a counterbalancing antagonist for whichever pro-apoptotic stimuli are present. Moreover, additional regulatory mechanisms, such as limiting trafficking to the mitochondria or reduced protein degradation, may alter activity regardless of the absolute protein level expressed.²¹² More accurate predictions use a multi-

protein index, such as the ratio of Mcl-1 to Bcl-xL to predict Mcl-1 dependency in small cell lung carcinoma,²⁵⁹ or the ratio of phospho-Bcl-2/(Mcl-1+Bcl-2) to predict sensitivity to the pan-Bcl-2 inhibitor S1 in leukemia.²⁷⁵

4.1.7 Publicly disclosed BH3-mimetic Mcl-1 inhibitors

A small-molecule BH3-mimetic capable of displacing endogenous BH3-domain containing proteins should antagonize the function of pro-survival Bcl-2 family members. Because these interactions are formed by protein-protein interactions (Figure 4-5), they are considered difficult to target with small molecules.⁶⁸ Differentiating the on-target activity of BH3 mimetics (apoptosis) from off-target activity (potentially also apoptosis) is critical for guiding compound SAR and future cellular and *in vivo* studies. Four criteria have been proposed to validate a putative BH3 mimetic.²⁷⁶ (1) Its biological activity must be dependent on the expression of Bax or Bak, without which the cell cannot undergo apoptosis through the intrinsic pathway. (2) The compound must achieve exquisite potency in the “subnanomolar and often low picomolar affinities” to demonstrate on-target cellular activity,²⁷⁷ a number derived from the observed activity (or lack thereof) for peptides and small-molecule inhibitors with weaker affinities. (3) Compound cytotoxic activity should be correlated with Bcl-2 family expression levels (e.g. increased expression of Mcl-1 confers resistance to ABT-737), and (4) treatment in an animal should result in the expected on-target toxic events (e.g. loss of platelets for Bcl-xL antagonists or loss of lymphocytes for Bcl-2 inhibitors). Many reported inhibitors fail to meet these criteria through equipotent killing of Bax/Bak deficient cells, such as obatoclax or gossypol^{278,279} and its derivatives, though both did progress to clinical testing. Other putative Mcl-1 inhibitors, such as

MIM1²⁸⁰ or a compound published by Abulwerdi *et al.*,²⁸¹ have weak binding affinity and mixed cellular data suggesting that not all activity is on-target.²⁸²

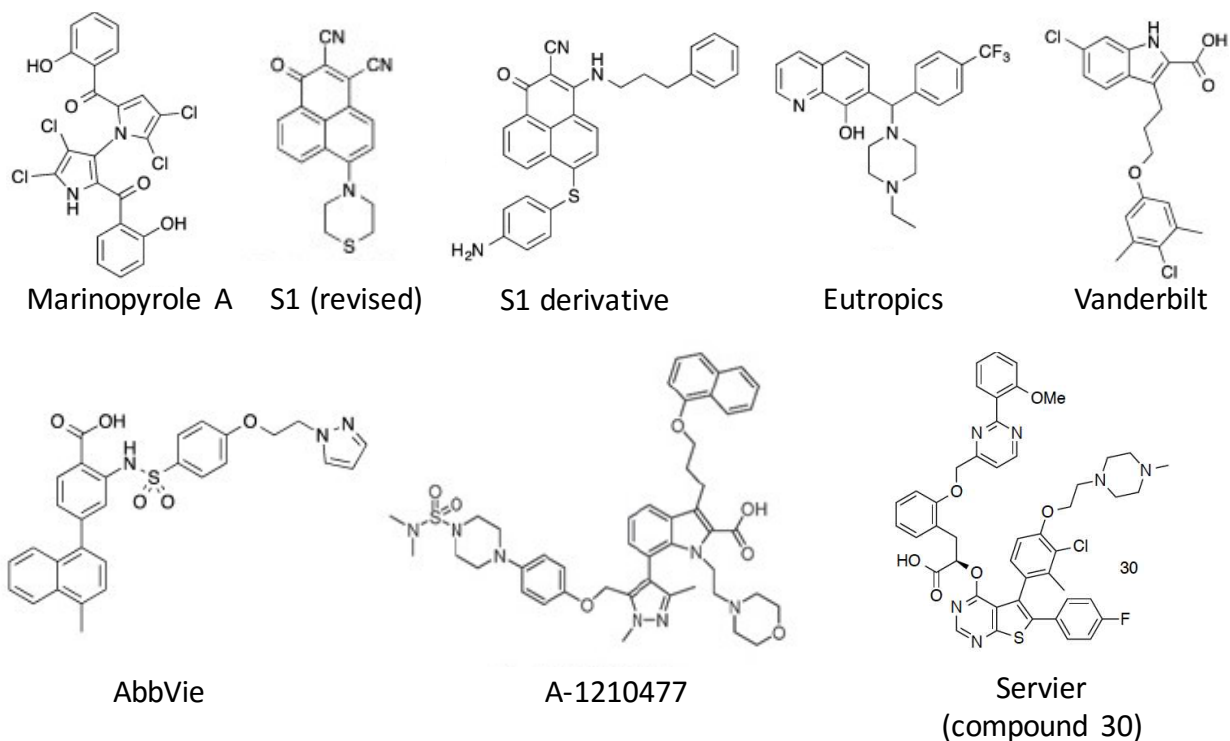


Figure 4-7: Compounds discussed in this introduction with reported Mcl-1 activity

Maritoclax (Marinopyrole A) binds to the Mcl-1 BH3-binding groove with such weak affinity (10 μ M) that it seemingly fails to meet the first criteria proposed by Lessene, *et al.* However, its reported mechanism is not simply BH3 antagonism, but rather induced Mcl-1 degradation through a proteasome-dependent mechanism.²⁸³ This finding has been both refuted^{284,285} and confirmed.^{286,287}

Zhang and colleagues have published a number of compounds around a central scaffold. These “S1” compounds and derivatives have reported Mcl-1 binding down to a reported 10nM affinity but no selectivity over Bcl-2 and Bcl-xL. The parent compound, S1, may induce apoptosis

through one of several mechanisms including the upregulation of Noxa (which induces Mcl-1 degradation)²⁸⁸ or the induction of autophagy.²⁸⁹

A high-throughput screen by Eutropics Pharmaceuticals identified compounds that bind to Mcl-1, and a counter-screen against Bcl-xL was used to sub-select for selective Mcl-1 binding compounds.²⁹⁰ Subsequent chemical optimization resulted in a 310nM IC₅₀ for Mcl-1 and 40μM for Bcl-xL. This compound dose-dependently reduced proliferation in Mcl-1 dependent cell lines, and this activity correlated with the degree of mitochondrial “priming” for apoptosis. However, the compound is not very potent.

AbbVie conducted a fragment-based screen against Mcl-1 and elaborated molecules based on two initial scaffolds. The most potent elaborated molecules, based on an aryl sulfonamide core, bound Mcl-1 with a 30nM affinity, though no cell-based activity was claimed. A second AbbVie report described the elaboration of an HTS hit that bound to Mcl-1 with 4.4μM affinity and was moderately selective against Bcl-2 and Bcl-xL. Using biochemical assays and x-ray crystallography, this initial lead was optimized to a molecule with a reported K_i of 480pM for A-1210477. This compound exhibited anti-proliferative activity in Mcl-1 dependent cell lines in multiple cancer types, dose-dependent disruption of Mcl-1/Bim complexes, and combinatorial activity with ABT-263.^{277,291,292}

Servier recently disclosed a series of Mcl-1 inhibitors in a patent application. These compounds were based on a thienopyrimidine core, and display low-nanomolar IC₅₀s on cell viability in the multiple myeloma cell line H929 and activity in animal models.

The Fesik group previously reported on the discovery of selective and high-affinity Mcl-1 inhibitors by a fragment-merging approach that bound with affinity of 55nM,⁹⁰ but only *in vitro*

biochemical data was reported because at that time the affinities were not sufficiently potent enough to warrant cellular investigation.²⁹¹

In this chapter, we report on a continuation of these initial studies⁹⁰ and describe my contributions to the discovery of small molecules that specifically impair the anti-apoptotic function of Mcl-1 and cause cell death in multiple cancers, including TNBCs. In addition, I have profiled the Mcl-1 and Bcl-xL dependencies in various cancer types, molecularly characterized that dependency, and developed predictions for selecting future cancer types, cell lines, and patients for inhibitor testing.

4.2 Results

4.2.1 Optimized a fluorescence-based assay to measure Mcl-1 inhibitors

We hypothesized that the discovery of a specific Mcl-1 inhibitor will have a positive therapeutic benefit in a subset of human cancers, including TNBC, which is refractory to currently available targeted therapeutics. To measure the affinity of our synthesized Mcl-1 inhibitors for the determination of compound SAR, a fluorescence polarization anisotropy (FPA) assay that had been previously developed in our lab by Dominico Vigil was re-optimized.⁹⁰ This assay functions by indirectly measuring the tumbling rate of molecules in solution. The tumbling rate slows with increased molecular mass. When excited by polarized light, slower-tumbling larger molecules will more often fluoresce in the same plane than smaller molecules. Therefore, the ratio of emitted light in the same plane to that in the opposite plane (called the anisotropy) roughly correlates with molecular size. Typically, a small fluorescently labeled probe peptide is used which can bind the protein with high affinity. Compound-mediated displacement of this probe will lower the

anisotropy in a dose-dependent fashion to determine an IC_{50} value for the inhibitor (Figure 4-8A).¹⁷⁵

In this assay, Mcl-1 is pre-incubated with a FITC-labeled peptide derived from the BH3 sequence of Bak. As expected, titrating Mcl-1 protein results in a dose-dependent increase in anisotropy; this interaction has a K_D of 17nM (Figure 4-8B). Addition of an Mcl-1 competitor to this solution dose-dependently reduces this anisotropy (Figure 4-8C). Because a competition-binding assay cannot measure an IC_{50} below the receptor concentration, the lower limit of detection for this assay is 15nM IC_{50} (corresponding to ~7nM K_i). To determine ligand selectivity, we further optimized this assay for use with pro-survival Bcl-2 family members Bcl-xL (Figure 4-8D) and Bcl-2 (not shown). All newly synthesized Mcl-1 inhibitors were subsequently measured using this assay for determination of compound K_i , with the IC_{50} converted to a K_i value by the method of Wang and colleagues.²⁹³

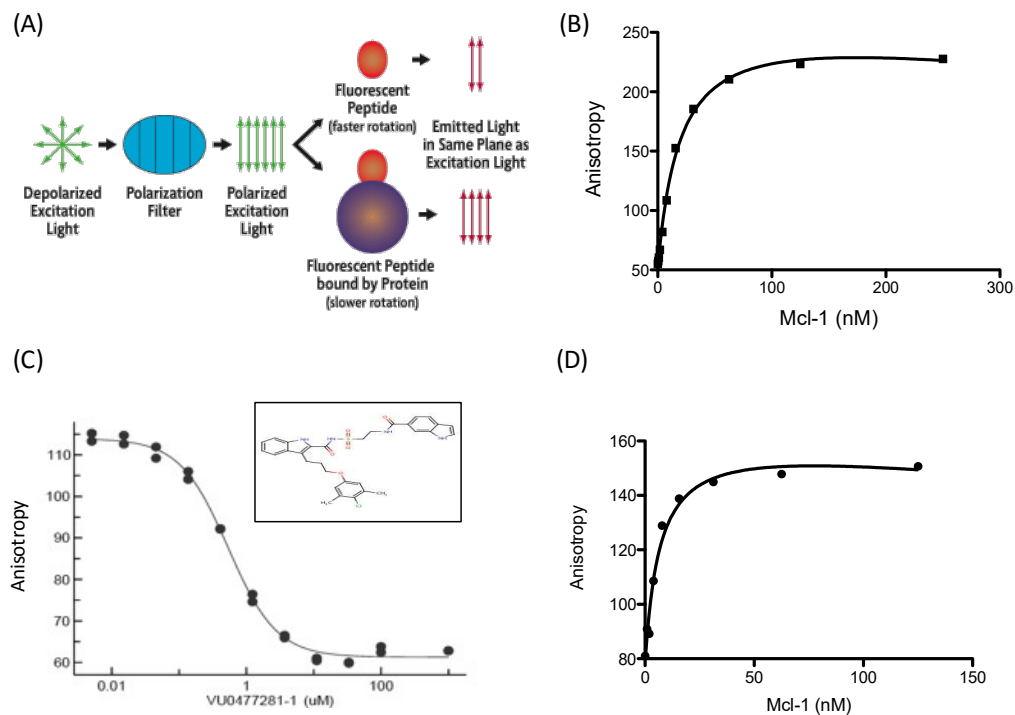


Figure 4-8: Optimization of the Mcl-1 FPA assay

(A) Schematic of an FPA assay.²⁹⁴ **(B)** Saturation binding curve for Mcl-1 and 10nM FITC-Bak peptide. The K_D for this interaction is 17nM. **(C)** Example competition binding experiment for VU0477281-1 displacing FITC-Bak peptide. 15nM Mcl-1 and 10nM FITC-Bak were used. The calculated K_i is 278nM (average of three independent experiments). **(D)** The K_D for the interaction between Bcl-xL and 5nM FITC-Bak peptide was determined to be 7.2nM in this saturation binding experiment (average of three independent experiments).

4.2.2 Discovery of slow-binding compounds

Most compounds rapidly achieved equilibrium within minutes of being added to the assay mixture (Figure 4-9A). The observed IC_{50} does not appreciably change for up to 20 hours, though the assay does degrade over that time as evidenced by an overall loss in signal. In contrast, the IC_{50} for a subset of compounds continued to improve even after 20 hours of incubation (Figure 4-9B), visible here as a leftward shift in the dose-response curve over time. The striking nature of this difference is observable when comparing the K_i values for VU0468562 and VU0475560

(Figure 4-9C). These time-dependent effects were not due to alterations in assay fluorescence through intrinsic compound fluorescence or quenching. Time-dependent compounds contain no obvious reactive center for covalent attachment to the protein or peptide, and addition of fresh reducing agent DTT has no effect, nor does altering the order of addition of Mcl-1, compound, and peptide probe (data not shown). In addition, these time-dependent compounds were not covalently binding to Mcl-1, as evidenced by no alteration in Mcl-1 mass before and after compound addition (Figure 4-9D).

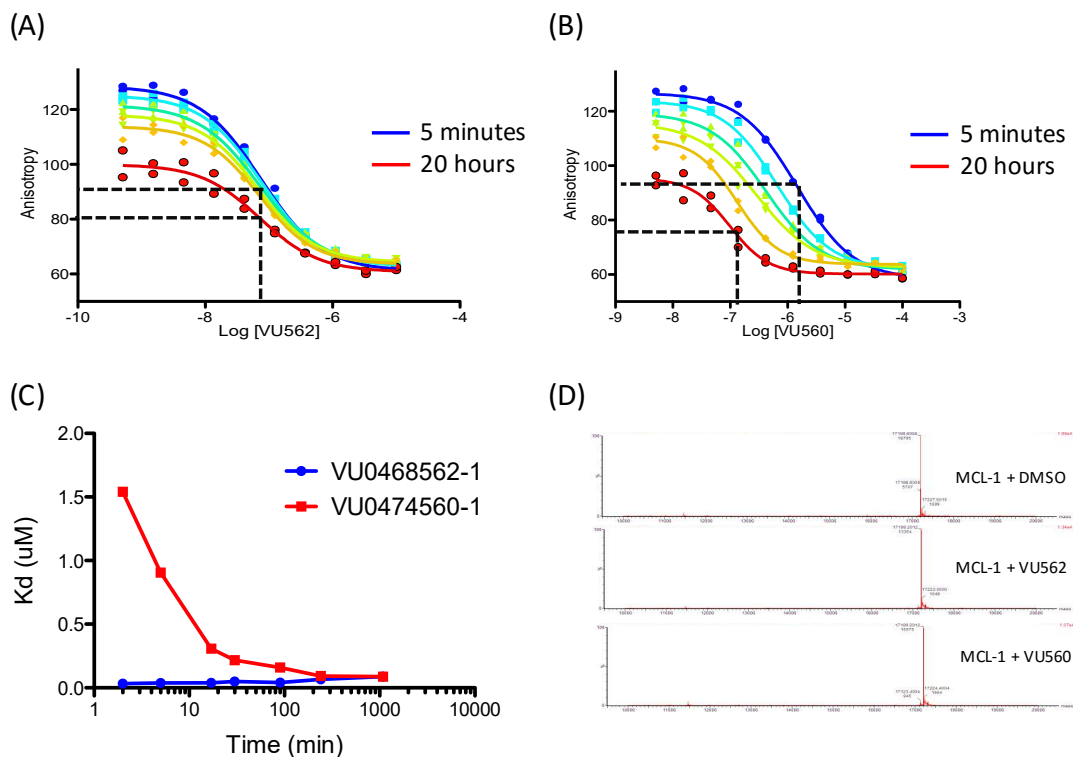


Figure 4-9: Some Mcl-1 inhibitors bind time-dependently

(A) Example competition binding curves for a fast-binding compound from 5 minutes to 20 hours. This behavior is typical of the majority of compounds. **(B)** Example competition binding curves for a slow-binding compound; the leftward shift with increasing time is clearly evident and indicates an apparent increase in potency. **(C)** The K_i value derived from each curve is plotted

over time. **(D)** Mass spectrometry analysis confirms that VU562 and VU560 do not bind covalently to Mcl-1, here indicated by no change in Mcl-1 protein mass through co-incubation with ligand.

A comprehensive survey of all synthesized compounds revealed clear SAR trends to predict time-dependent activity. Inclusion of a 4-substitution on the indole ring is the strongest predictor, and these substitutions may be electron donating (CH₃) or electron withdrawing (halide and trihalides). In contrast, substitutions at the indole 6-position (or no substitution at all) have no effect. A second predictor of time-dependency is a 2-acylsulfonamide substitution, whereas a carboxylic acid or hydrogen are not predictive. The combination of 4-substitution and 2-acylsulfonamide yield the strongest time-dependent compounds, as is the case for VU0475560 exemplified above. R-group substitutions off the ether linkage, such as naphthyl or dichloromethyl phenyl rings, have no effect. Based on these trends, we ceased our exploration of the 4-substituted indole series of compounds and carefully monitored all newly synthesized 2-acylsulfonamide compounds for time-dependency. Analysis of Mcl-1 co-crystallized with both time dependent and independent compounds does not reveal any obvious conformational changes or residue side chain rearrangements that would account for slow binding kinetics. All indications point to genuine slow binding kinetics for these compounds, though this hypothesis requires validation by directly measuring binding kinetics using an appropriate technology, such as SPR.

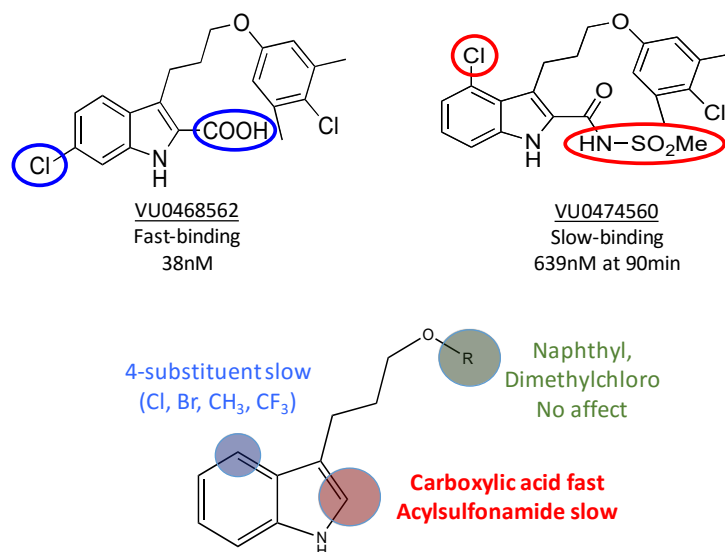


Figure 4-10: Summary of the SAR for time-dependent compound binding

4-indole substitutions and 2-acylsulfonamide substitutions are correlated with time-dependent binding, but different R substitutions coming off the ether linkage from the 2-indole position does not affect time dependency.

4.2.3 Development of assays to measure picomolar-affinity compound interactions

Clinically effective Mcl-1 inhibitors will likely require binding affinities in the picomolar range.²⁹¹ Because the FPA assay described in Friberg *et al*, 2013 can only detect interactions to 7nM, we sought to develop a new assay. AlphaScreen (Perkin-Elmer) is a homogenous, label-based assay that theoretically provides a higher signal/noise ratio than FPA and might enable highly sensitive affinity determination. In this assay, a labeled peptide and Mcl-1 are selectively bound by a 'donor' or 'acceptor' bead, respectively; photo-excitation of the donor beads caused a chemical release of singlet oxygen, which reacts with the acceptor bead to emit light (Figure 4-11).

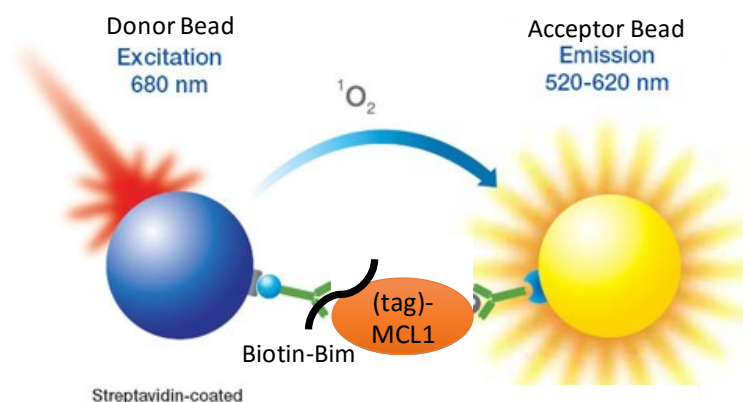


Figure 4-11: Schematic for the AlphaScreen assay

Binding interactions between two labeled components (here, biotinylated Bim peptide and HIS6-tagged Mcl-1 protein) bring two labeled beads together. Specific excitation of the donor bead at 680nm releases singlet oxygen, which reacts with the acceptor bead to release light at 520-620nm only when in close proximity.

This assay required a more potent Mcl-1-interacting peptide than the Bak-derived peptide used in the FPA assay. We initially chose a biotinylated peptide derived from the Bim BH3-domain sequence (Bim2, Table 4-1). We measured the affinity and binding kinetics of biotin-Bim2 peptide using surface plasmon resonance (SPR, Table 4-1). The K_D was determined to be 500pM, but the kinetic on- and off-rates were extremely slow (requiring 60 minutes to reach 95% bound). At that rate, equilibrium within the assay solution would require many hours of incubation time. Moreover, the peptide required the addition of non-ionic detergent (e.g. Tween-20) to solubilize it in solution. We therefore designed and had synthesized additional peptides to increase their binding kinetics and solubility. We first truncated the initial four residues in the hopes that this would lead to faster binding kinetics (Bim3). The peptide retained high potency and only slightly increased the kinetic binding rate. We next tested a Bim-derived peptide that was previously described (WEHI-Bim4).²⁹⁵ Although the binding rate of this peptide was faster, the addition of a detergent was required for reproducible activity. Finally, we truncated the N-terminal four

residues and C-terminal arginine to reduce potency and increase the binding kinetics and mutated an isoleucine to an alanine at the 6-position (Bim6 peptide). In crystal structures, the Ile points away from Mcl-1, and we hoped that transition of this amino acid to a less hydrophobic residue would increase its solubility without abolishing binding or reducing helicity. Indeed, binding kinetics for this peptide were further increased and detergent was no longer required for peptide solubilization.

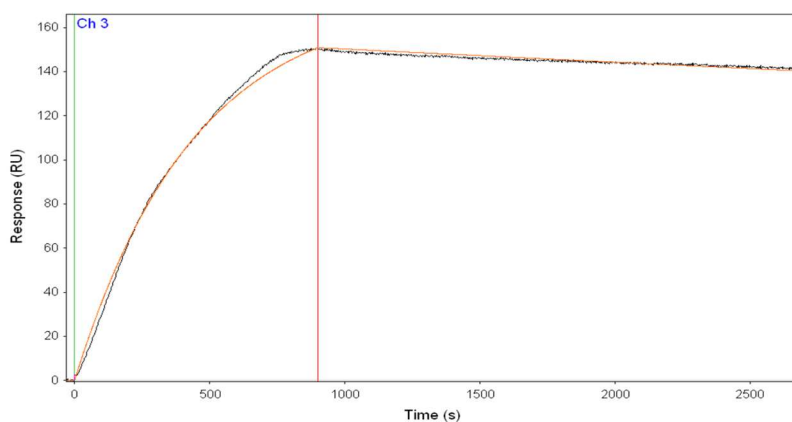


Figure 4-12: Biotin-Bim2 peptide has unsuitably slow binding kinetics

The binding kinetics of Biotin-Bim2 peptide, as measured by SPR, are extremely slow and are unsuitable for use in this assay. K_a is $0.71 \times 10^5 \text{ M}^{-1} \text{ s}^{-1}$, K_d is $0.44 \times 10^{-4} \text{ s}^{-1}$, and K_D is 500pM.

Peptide	Sequence	K_a ($E5 M^{-1}s^{-1}$)	K_d ($E-4 s^{-1}$)	KD(nM)	Comments
Bim2	DMRPEIWI A QELRRI GDEFNAYYARR	0.71	0.449	0.5	Slow kinetics High potency Insoluble Low fluorescence
Bim3	___EIWI A QELRRI GDEFNAYYARR	3.3	2.8	0.8	High potency Insoluble Low fluorescence
WEHI Bim4	DLRPEIRIAQELRRIG DEFNETYTRR	9.8	1.7	1.8	Insoluble
Bim6	___E A RIAQELRRI GDEFNETYTR_	1.7	6.1	3.5	Faster kinetics More soluble

Table 4-1: Bim peptide sequences developed for use in the AlphaScreen assay
Binding kinetics and affinities were all determined by SPR.

Unfortunately, AlphaScreen beads are themselves dependent on detergent for activity. No binding signal could be generated without the addition of a non-ionic detergent (Figure 4-13A). Indeed, this effect is dose-dependent. Lower detergent concentrations yield lower signal. The type of non-ionic detergent used is also significant. For example, oxyethylated fatty alcohol (C12E10) resulted in the highest signal, and Triton X-100 provided the lowest signal (Figure 4-13B). The reason for these differences is unknown and does not correlate with the CMC of each detergent. Ionic detergents such as CHAPS were ineffective.

We next tested the ability of this assay to accurately measure competitive compound binding. We titrated the Mcl-1 inhibitor VU0485530 into a mixture of Mcl-1 and Bim6 (1nM each) to determine its IC_{50} in a buffer containing Tween-20. Unfortunately, the value determined (1044nM) was found to be 150-fold higher than that measured using the FPA/Bak assay without Tween. Indeed, program compounds from multiple series displayed tens or a hundred-fold reduction in activity in the presence of detergent, and this intolerance for detergent was confirmed in the FPA/Bak assay supplemented with either Tween-20 or C12E10 (Figure 4-13D).

Therefore, because the AlphaScreen assay had an absolute requirement for detergent, and program compounds did not yet possess sufficient physical properties to tolerate detergent in solution, we chose to discontinue this assay.

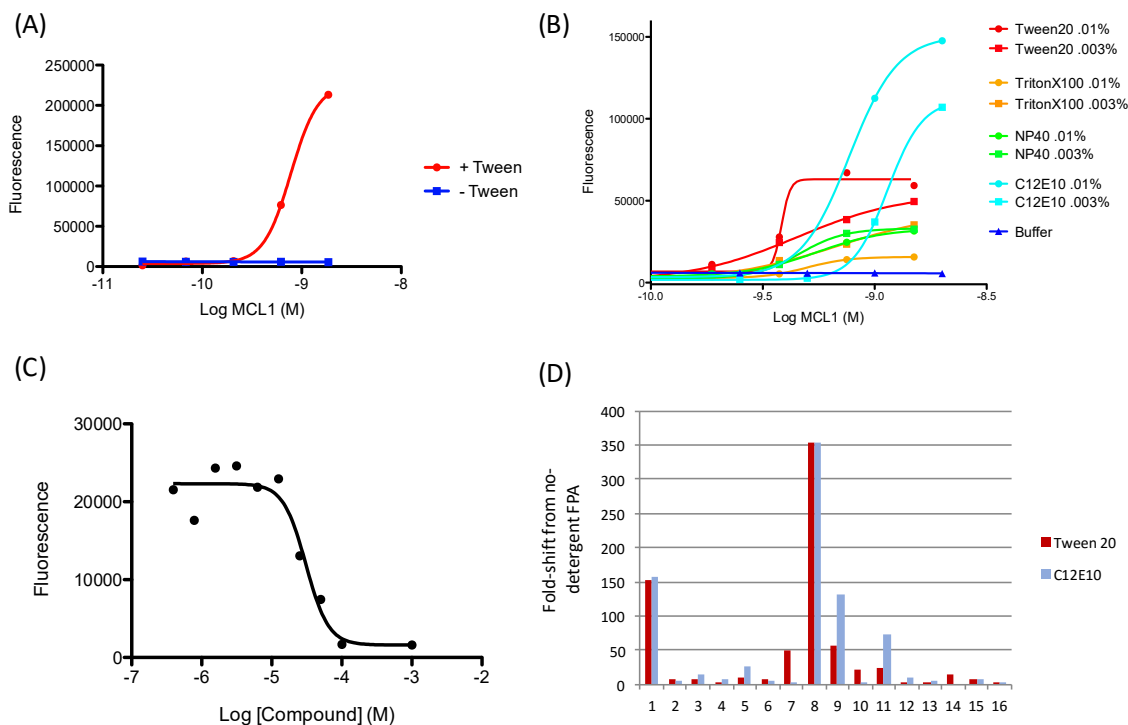


Figure 4-13: The Alphascreen assay requires detergent to produce signal

(A) Saturation binding curve for Biotin-Bim2 (1nM) binding to Mcl-1, with or without 0.01% TWEEN-20. No signal is obtained in the absence of this detergent. **(B)** Four diverse non-ionic detergents at two concentrations have differing effects on assay performance. As before, no signal is generated without detergent with this peptide and bead combination (blue line), but highest signal is generated using oxyethylated fatty alcohol (C12E10) at 0.01%. **(C)** Including detergent in the assay buffer significantly weakens compound affinity. Shown is an example competition binding curve for VU0485530 in the Alphascreen assay with 0.01% TWEEN-20. The K_i is calculated to be 1044nM; in FPA/Bak, the K_i is 7nM. **(D)** Sixteen diverse compounds selected to represent all series under active development at that time were analysed in the FPA/Bak assay in the presence of 0.007% TWEEN-20 or 0.01% C12E10 (both under their respective CMC). Shown is the fold-shift in K_i from a control run in the absence of detergent.

We were originally precluded from using the FITC-Bim2 peptide at low (1nM) concentrations in an FPA assay because of extremely low intrinsic fluorescence (Figure 4-14A). However, improvements made to the Bim probes for the AlphaScreen assay fortuitously resulted in a

significantly increased fluorescence that provided parity with the Bak peptide and made it possible to run an FPA assay using the FITC-labeled Bim6 probe. Indeed, a saturation-binding curve could be reliably measured for FITC-Bim6 even at a probe concentration of 31pM probe concentration. The K_D for the peptide/Mcl-1 interaction was determined to be 220pM (Figure 4-14B). For routine use, a 1nM peptide concentration was selected to provide reproducibly high signal. The lower limit of detection for an IC_{50} in a biochemical competition assay is the protein concentration, which in this case was selected to be 1.5nM. Therefore, by the equation of Wang *et al*,²⁹³ the lower limit of detection for the K_i is 200pM. We next tested whether binding is time-dependent; equilibrium had not been achieved 15 minutes post-addition, but the assay had stabilized by 2 and 6 hours (Figure 4-14C). An example of a dose-response competition curve for biotin-Bim6 is shown in Figure 4-14D, and the K_i was calculated to be equal to its SPR-derived number.

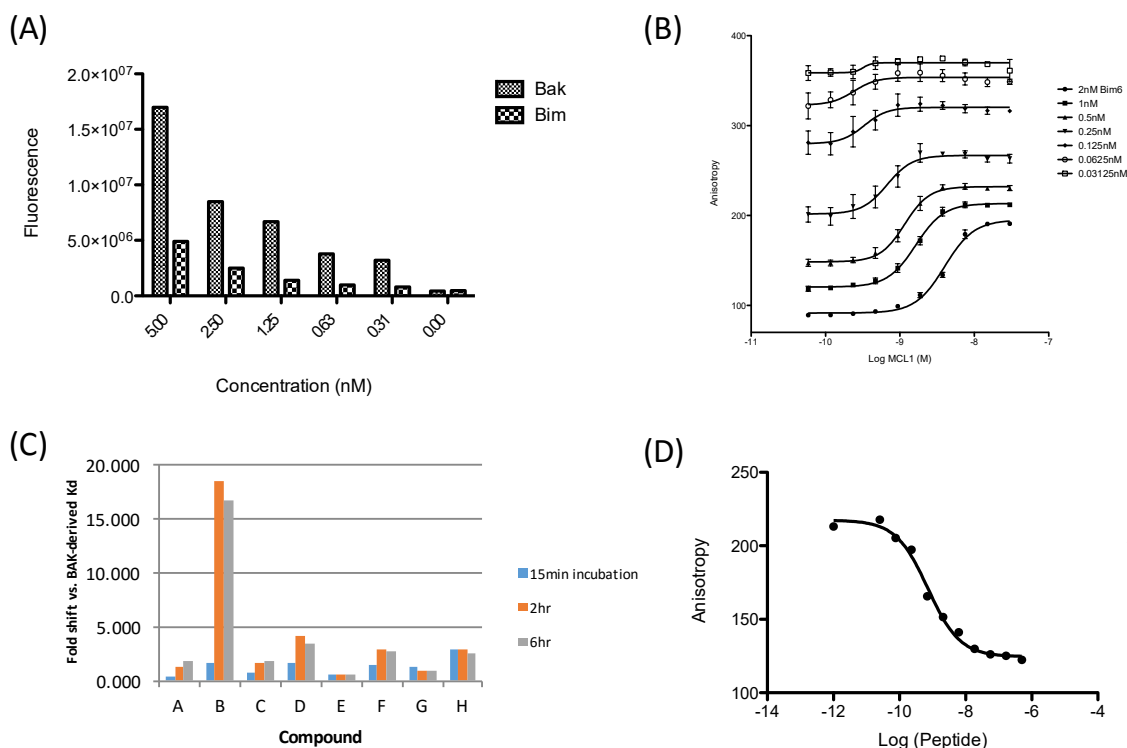


Figure 4-14: Development and optimization of the FPA/Bim6 assay

(A) Total fluorescence from the Bak and Bim2 probes; Bim2 yields significantly lower fluorescence and is just twice background at 1nM. **(B)** Improvements to peptide kinetics and solubility (Table 4-1) improved fluorescence efficiency, allowing saturation-binding curves with just 31pM peptide. **(C)** Compounds assayed with FPA/Bim6 reach equilibrium quickly, within 2 hours post-addition. **(D)** Example competition curve for Biotin-Bim6 peptide measured with FITC-Bim6 in FPA assay. The measured K_i value (6.2nm) agrees favorably with SPR-derived numbers (3.5nM).

Just one compound in Figure 4-14C showed a difference in K_i between the FPA/Bak and FPA/Bim6 assays. To determine whether other compounds were similarly divergent, we measured the K_i in FPA/Bak and the FPA/Bim6 assays for a diverse collection of 100 compounds spanning a range of affinities from different compound series. As seen in Figure 4-15A, most compounds agree between the Bim-based and Bak-based assays when detergent is not used, although several outliers are noted. Similarly, addition of 0.01% C12E10 to both assays shifted the K_i but retained the complementarity (Figure 4-15B). Outlier compounds, noted especially in the detergent-containing experiment, primarily contain a basic amine substituted off the 7-

position on the indole ring, although this determination is not absolutely predictive, as some basic-amine containing compounds fail to cause such substantial shifts. To illustrate this point, we removed basic-amine containing compounds from the series and replotted in Figure 4-15D; the correlation is nearly perfect and no outliers are present.

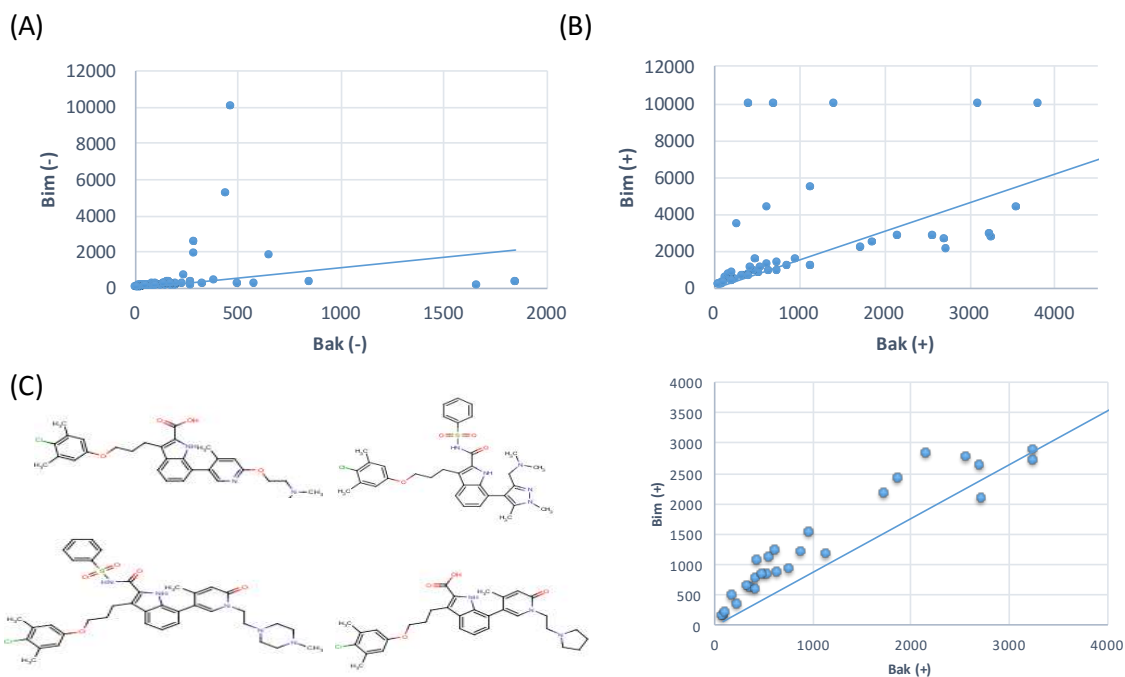


Figure 4-15: The FPA/Bak and FPA/Bim6 assays similarly measure most compounds

(A) Compound affinities that were measured in the FPA/Bim and FPA/Bak assays are similar (slope=1.16). Several outlier compounds measured weaker in the FPA/Bim6 assay. **(B)** With 0.01% C12E10 added to both assays, affinities continue to agree overall across this set of compounds but several more outliers are noted (slope = 1.55). **(C)** Outlier compounds are those containing a basic amine functional group on substitutions at the 7-position of the indole ring. **(D)** Removing basic-amine containing compounds at the indicated position resulted in a nearly 1:1 correlation between Bim/FPA and Bak/FPA derived numbers for Mcl-1 program compounds across diverse series (slope=0.889).

In conclusion, the FPA/Bim6 assay was able to reliably measure compounds with picomolar affinity without the need for non-ionic detergents, and continuity was maintained with previous results in the FPA/Bak assay. This assay was subsequently used to assay all newly synthesized program compounds for the determination of compound SAR.

4.2.4 BH3 profiling used to measure Mcl-1 dependency of cancer cell lines

Accurately and unambiguously determining whether a cell line depends on Mcl-1 for survival is critical to understanding whether program compounds kill cells by an on-target mechanism. In the absence of a specific and high-affinity Mcl-1 tool molecule, we chose BH3 profiling as the most accurate method to determine sensitivity to Mcl-1-specific BH3 mimetics. BH3 profiling has been used to predict the sensitivity of cell lines and patient derived hematologic cancer cells to Bcl-2 family inhibitors and to define the dependence on specific family members.^{296,297} This assay quantifies mitochondrial depolarization after administration of a BH3-derived peptide in digitonin-permeabilized whole cells. Peptides have differing binding specificities to Bcl-2 family members, which allows for a sophisticated dissection of the individual contributions of these proteins to prevent apoptosis.

We assembled a panel of hematologic cancer cell lines and interrogated them for sensitivity to a panel of BH3-derived peptides. The Bim peptide promiscuously binds anti-apoptotic BCL-2 family members and will interrogate how “primed for death” the cell is – that is, how easily the mitochondria depolarize at a given concentration of Bim peptide. Conversely, the Bad peptide is selective for anti-apoptotic proteins Bcl-2, Bcl-xL, and Bcl-w, while the MS-1 peptide is selective for Mcl-1.²⁹⁸ Use of these selective peptides specifically interrogates the contributions of these individual proteins to survival.

Results from the H929 multiple myeloma and K562 chronic myelogenous leukemia cell lines are exemplified in Figure 4-16A-B. Both respond to the Bim peptide, indicating that each contains an intact intrinsic apoptotic pathway with expression of Bak or Bax to depolarize the

mitochondria in response to pro-apoptotic signaling. However, H929 is strongly dependent on Mcl-1 for survival, as evidenced by a strong response to the Mcl-1 specific MS-1 peptide; whereas, K562 is completely resistant to this peptide even up to greater than 10 μ M. In contrast, H929 is highly resistant to the Bad peptide while K562 is sensitive to it. These results suggest that H929 would be strongly sensitive to small-molecule inhibition of Mcl-1, while K562 would be strongly resistant to such inhibition. This analysis was expanded across the panel to identify the most Mcl-1 dependent and resistant cell lines (Figure 4-16C). These data were subsequently used to interpret all program cellular assays, including proliferation, caspase activation, and co-immunoprecipitation.

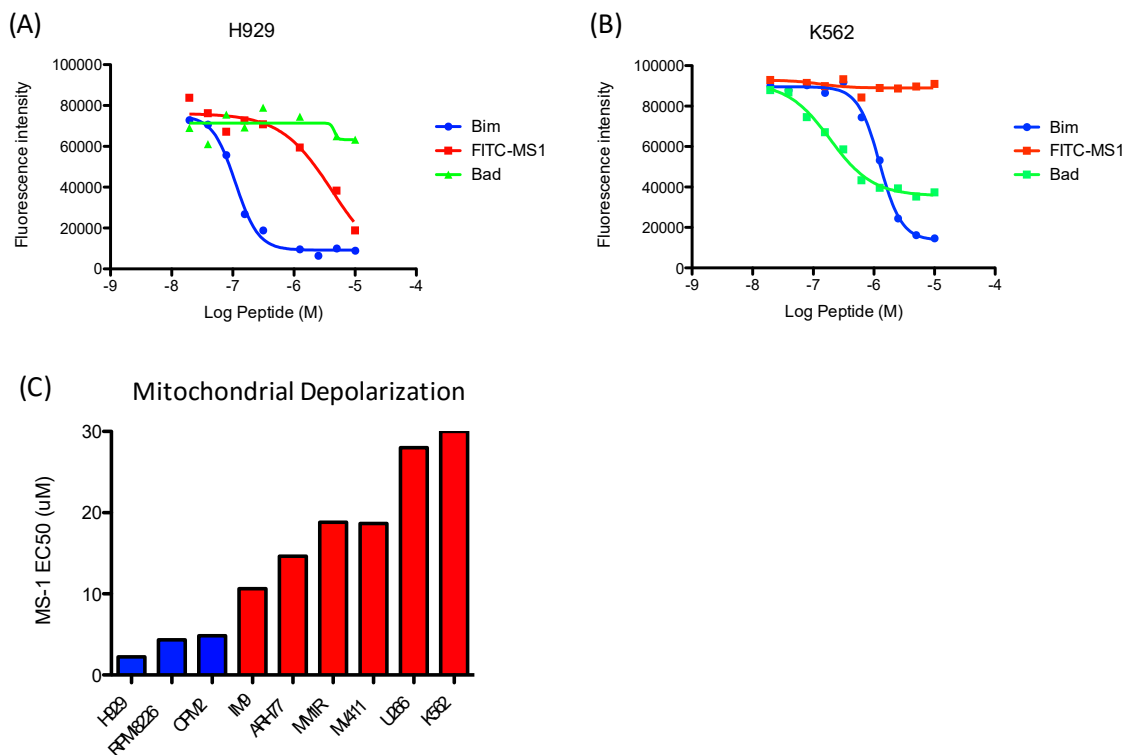


Figure 4-16: 'BH3 profiling' was used to determine Mcl-1 dependency status

(A-B) BH3 profiling was conducted on live H929 and K562 cells to determine their sensitivity to Bcl-2 family inhibition. Both responded to the Bim peptide, indicating an intact intrinsic apoptotic pathway, but only H929 responded to Mcl-1 specific peptide MS-1. In contrast, only K562 responded to the Bcl-2, Bcl-xL, and Bcl-w inhibitory Bad peptide. **(C)** This analysis was expanded

across a panel of hematologic cell lines. Mcl-1 dependent lines, where the MS-1 EC_{50} is below $10\mu\text{M}$, are shown in blue, while Mcl-1 resistant cell lines are shown in red.

4.2.5 *Developed assays to discriminate on-target and off-target activity in cells*

Loss of Mcl-1 protein function should selectively induce mitochondrial depolarization, caspase activation, and apoptosis only in Mcl-1 dependent cell lines while having, at worst, weak off-target activity in Mcl-1 independent cell lines. Further, Mcl-1 protein should be dose-dependently displaced from interacting partners Bim, Bak, and Noxa by the inhibitor compound. We profiled compound activity against all these effects to identify potent, on-target Mcl-1 inhibitors.

First, Mcl-1 inhibitors should only potently depolarize mitochondria in dependent cell lines. We used the mitochondrial depolarization assay described above to profile leading program compounds against Mcl-1 dependent and resistant cell lines. Some compounds, such as VU0658758 (FPA/Bim6 $K_i=0.55\text{nM}$) were non-selectively toxic with EC_{50} s of $> 10\mu\text{M}$; however, more recent compounds such as VU0659158 and VU0659159 (FPA/Bim6 $K_i=0.2\text{nM}$) depolarized mitochondria with EC_{50} s of 168nM and 747nM , respectively, in the Mcl-1 dependent H929 cell line and were significantly weaker in the Mcl-1 independent K562 line (Figure 4-17A-C). When mitochondria depolarization is compared with compound effect in cell proliferation experiments for the most recent compounds, a 1:1 correlation is observed in the H929 Mcl-1 dependent cells, suggesting that cell death is selectively due to Mcl-1-inhibition and subsequent apoptosis (Figure 4-18D). Of note, the low concentration of digitonin detergent used in this assay buffer does not affect compound binding in the FPA/Bim6 assay.

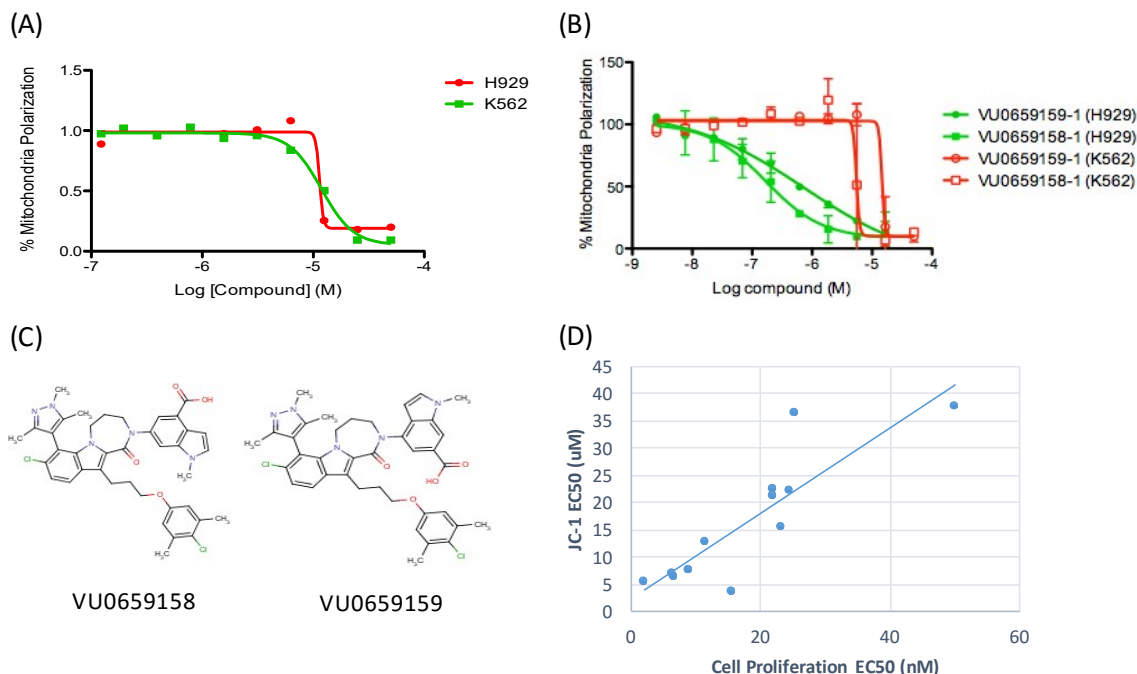


Figure 4-17: Mcl-1 inhibitors cause dose-dependent mitochondrial depolarization

(A) Not all compounds selectively depolarize mitochondria in Mcl-1 dependent cell lines. Some, such as VU0658758 (FPA/Bim6 $K_i=0.55\text{nM}$), depolarize both H929 and K562 cell lines with a 10-12 μM EC_{50} , suggesting off-target activity. (B) In contrast, VU0659158 and VU0659159 (C) are highly potent and selective for Mcl-1 dependent H929 mitochondria. (D) EC_{50} s for Mcl-1 inhibitors in the JC-1 mitochondria depolarization assay correlate with the loss in cell viability in a proliferation assay in Mcl-1-dependent cell line H929.

All potent Mcl-1 program compounds were characterized in multiple Mcl-1 dependent and resistant cell lines for their ability to induce caspase 3/7 activation as a consequence of activating the apoptotic cascade. Indeed, VU0659158 and VU0659159 selectively activated apoptosis in the H929 Mcl-1 dependent cell line, while the K562 Mcl-1 insensitive cell line was resistant (Figure 4-18A). Likewise, these compounds only reduced cell proliferation (as assayed by Cell Titer-Glo, which measures ATP content as a proxy for cell count) in H929 but not K562 cells (Figure 4-18B).

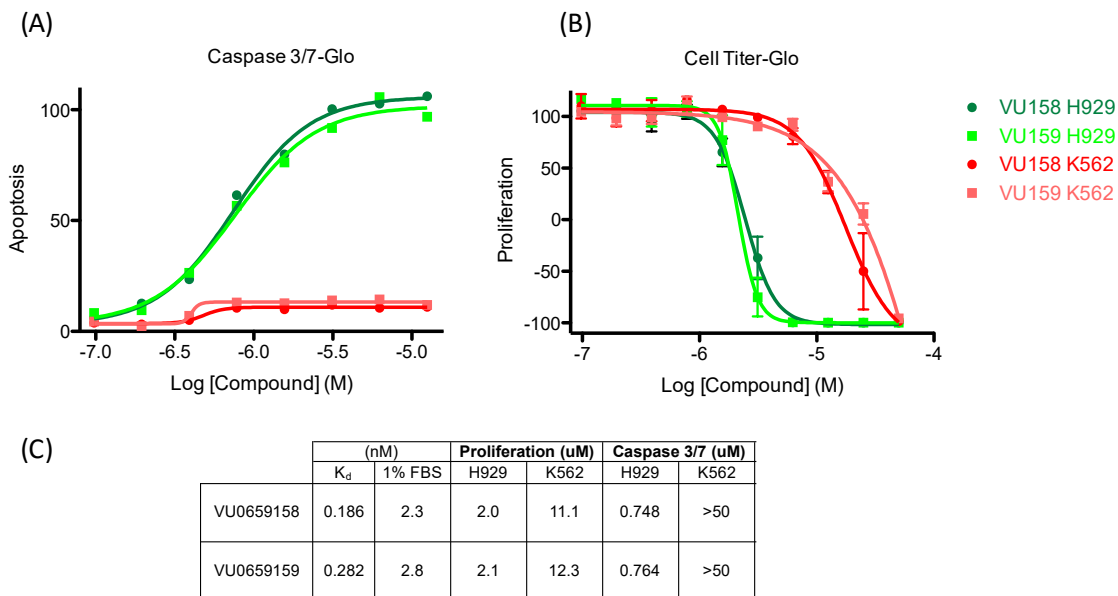


Figure 4-18: Mcl-1 inhibitors dose-dependently induce Caspase cleavage and cell death (A) VU0659158 and VU0659159 induce caspase 3/7 activation and (B) reduce proliferation selectively in the Mcl-1 dependent H929 cell line. These curves were generated by Carrie Browning. (C) Table of activities for these compounds.

A high-affinity Mcl-1 BH3 mimetic should disrupt interactions between Mcl-1 and other Bcl-2 family members. Thus, we sought to test whether our compounds could bind to endogenous cellular Mcl-1 and inhibit the binding of a peptide derived from pro-apoptotic proteins.²⁹⁹ Cell lysates from human chronic myelogenous leukemia K562 cells were incubated with biotin labeled MS-1, a peptide that binds specifically to Mcl-1.²⁹⁸ This peptide selectively pulls down cellular Mcl-1. As shown in Figure 4-19, the addition of VU0657538 blocks the ability of MS-1 to pulldown Mcl-1, demonstrating that the compound binds to cellular Mcl-1 and blocks the interaction with biotin MS-1 in a dose-dependent manner.

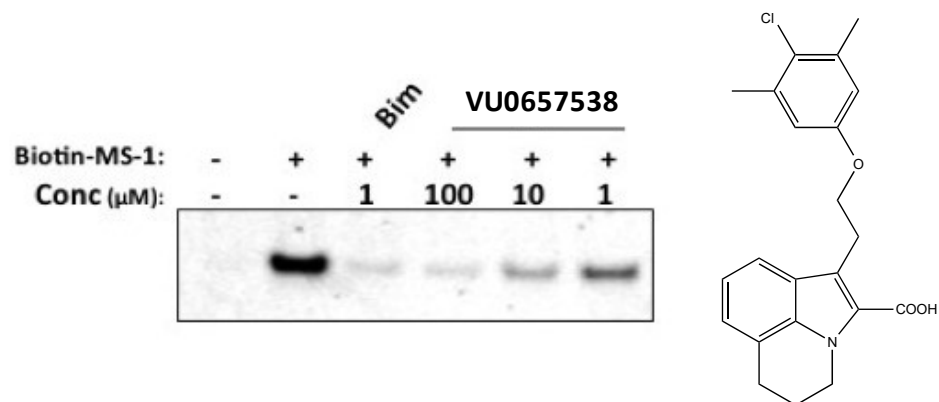


Figure 4-19: VU0657538 inhibits binding of biotin-MS-1 to Mcl-1 in cell lysates

K562 cell lysates were incubated with compound or a Bim-BH3 peptide positive control at indicated concentrations. Streptavidin-conjugated beads bound with biotin-MS-1 were incubated with the lysates to pull down cellular Mcl-1, which was visualized by Western blot.

To test whether Mcl-1 BH3-interactions are disturbed in a live cellular system, we dosed live H929 multiple myeloma cells with compounds for 90 minutes, lysed the cells, pulled down Mcl-1, and blotted for interacting partners Noxa or Bim. Unsurprisingly, weaker affinity compounds failed to disrupt this interaction even at 50μM concentrations (Figure 4-20). More potent compounds, such as VU0660117-1 and VU0660131-1, did exhibit sufficient potency and physical properties to show activity in this assay format (Figure 4-21). Finally, VU0659158 was found to potently disrupt the Mcl-1/Noxa complex in whole H929 cells (Figure 4-22).

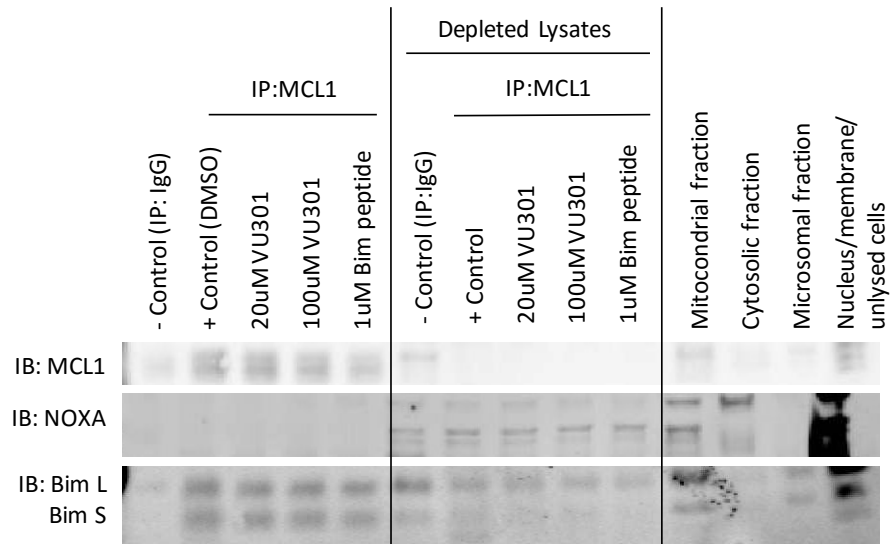


Figure 4-20: VU0516301-1 fails to disrupt Noxa or Bim in H929 cells

Cell lysate was incubated with the indicated compound concentration of VU0516301-1 (FPA/Bak $K_i=12.5nM$), then Mcl-1 was immunoprecipitated, washed, and western blotted. No disruption in Noxa or Bim was observed by compound. Additionally, the depleted lysates and sub-cellular fractions were probed as noted.

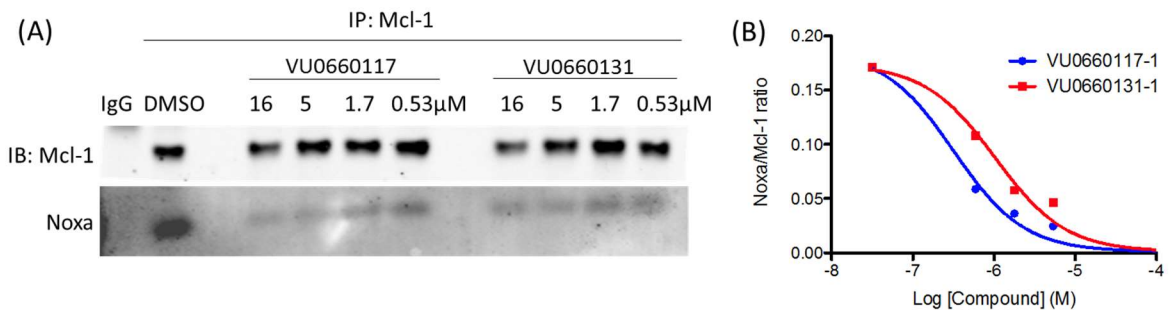


Figure 4-21: High affinity Mcl-1 inhibitors potently displace Noxa from cellular Mcl-1

VU0660117-1 (0.41nM K_i in FPA/Bim6) and VU0660131-1 (0.55nM K_i in FPA/Bim6) here show dose-dependent inhibition of Mcl-1/Noxa complexes in live cells after 90 minutes. **(A)** Western blot results from IgG control or Mcl-1 IP dosed with indicated concentration of compound in micromolar. **(B)** Band intensities from the western blot in (A) were quantified and plotted as the ratio of Noxa to Mcl-1. VU177 more potently displaces Noxa with an EC_{50} is 0.3 μM, while the EC_{50} for VU131 is 1.1 μM.

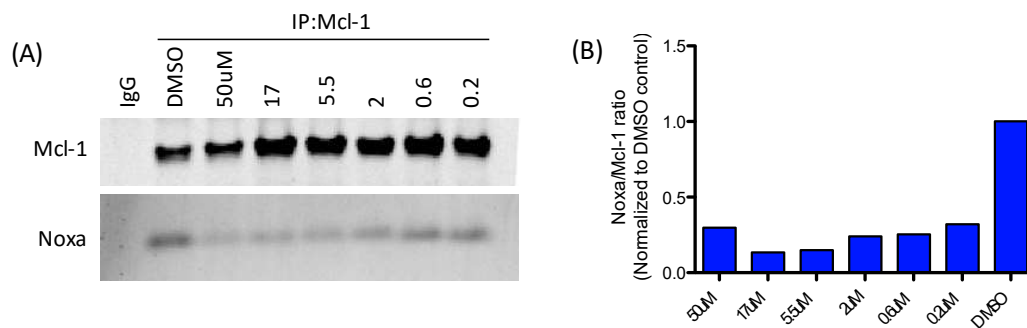


Figure 4-22: High affinity inhibitor VU0659158 potentially displaces Noxa from Mcl-1

(A) VU0659158-1 (FPA/Bim6 $K_i=0.2\text{nM}$) potentially disrupts the Mcl-1/Noxa interaction in whole H929 live cells in this co-immunoprecipitation experiment. **(B)** The western blot in (A) is quantified and normalized to the DMSO-treated control.

Compound-mediated disruption of Mcl-1/Bim complexes in whole cells was visualized using the DuoLink proximity ligation assay (PLA, Sigma). Whole cells were fixed, permeabilized, and probed with Mcl-1 and Bim antibodies, then visualized with a fluorescent conjugate antibody that recognizes two antibodies in close proximity. In this way, signal is only generated when Mcl-1 and Bim are in complex. As seen in Figure 23A, no appreciable signal is generated by Mcl-1 or Bim antibody alone (red), but the combination brightly stains (red; blue DAPI).

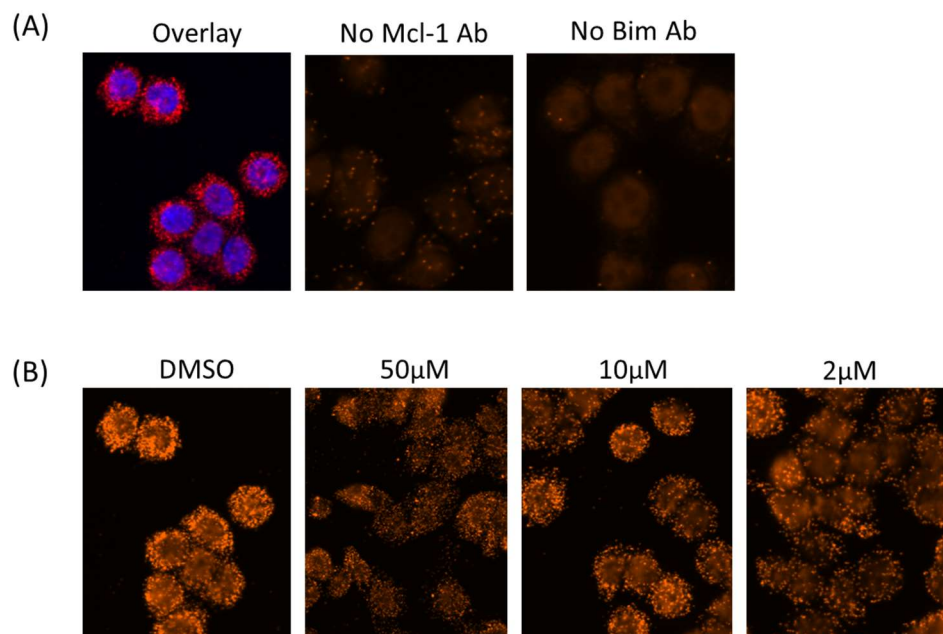


Figure 4-23: Duolink PLA assay visualizes disruption of Mcl-1/Bim complexes in live cells
(A) Mcl-1/Bim complexes (red) are brightly stained in this overlay with DAPI (blue). In contrast, no appreciable stain is evident when using only the Bim or Mcl-1 antibody. **(B)** Cells were dosed with the indicated concentration of VU0659158-1 or DMAO for 90 minutes, then harvested and stained as before. Mcl-1/Bim complexes are reduced in a dose-dependent manner.

4.2.6 *Mcl-1 protects a subset of TNBC cell lines from apoptosis*

Predicting whether Mcl-1 can protect a particular cancer cell from apoptosis is not trivial, and heretofore, no published study had interrogated whether Mcl-1 significantly protects TNBC cancers from death and whether an Mcl-1 inhibitor would prove efficacious in TNBC cancers, which currently lack rationally-targeted therapeutic options. Because Mcl-1 and Bcl-xL are frequently upregulated in human breast cancer, and based on their importance to prevent apoptosis in many cancer types, we hypothesized that some TNBC cell lines may depend on these proteins to prevent apoptosis, and that silencing one or both would reduce cell viability. To test this hypothesis, we silenced the expression of Mcl-1 or Bcl-xL using small-interfering RNAs (siRNA). We first validated our siRNA protocol: of the four unique motifs tested for each protein,

Mcl-1 motif-17 and Bcl-xL motif-14 reproducibly yielded the greatest knockdown of over 85% compared to non-silencing control (NSC) in MDA-MB-468 and MDA-MB-453 cells (Figure 4-24A-B). The NSC motif did not lower cell viability; however, silencing Mcl-1 expression substantially reduced the viability of MDA-MB-468 cells in a protein knockdown-dependent manner (Figure 4-24C-D). In contrast, silencing Bcl-xL had a smaller effect on both cell lines despite high protein knockdown (>90%).

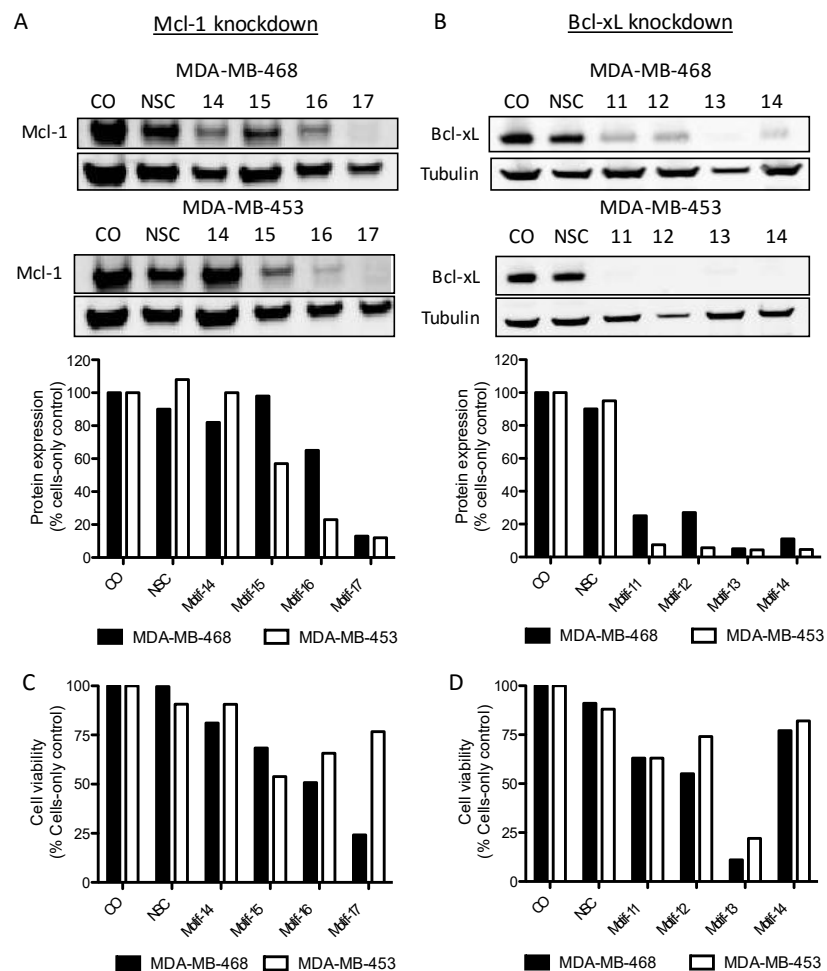


Figure 4-24: Mcl-1 and Bcl-xL protein expression was specifically silenced by siRNA transfection (A-B) Four separate siRNA oligonucleotides silenced Mcl-1 (A) or Bcl-xL (B) expression in the MDA-MB-468 and MDA-MB-453 cell lines. Knockdown efficiency was quantified by western blot, with percent knockdown equal to the Tubulin-normalized ratio of Mcl-1 expression in siRNA-treated cells compared to cells-only control. Mcl-1 motif-17 and Bcl-xL motif-14 yielded the highest percent knockdown. (C-D) Cell viability after Mcl-1 (C) or Bcl-xL (D) protein silencing was

quantified using Cell Titer-Glo, a luminescence assay which detects ATP as a proxy for viable cells in culture. Cell viability was reduced knockdown-dependently for Mcl-1 in the MDA-MB-468 cell line, but MDA-MB-453 was much less responsive. Despite highly efficient knockdown of Bcl-xL, cell viability was not dramatically reduced in either cell line. Cytotoxic effects from motif-13 were not related to the level of protein knockdown and are considered off-target.

We silenced Mcl-1 or Bcl-xL using these siRNAs in a panel of seventeen publicly available luminal and basal cell lines (Fig 1). Cell viability was measured after five days to allow for several population doublings, and knockdown efficiency was verified by western blot at the conclusion of the experiment (Table 4-2). Mcl-1 knockdown dramatically reduced proliferation by 60% or more in seven lines (blue, A). Four lines have an intermediate dependency on Mcl-1 (40-60% loss, cyan), and the remainder were largely insensitive (red). We observed increased caspase 3/7 activity after Mcl-1 siRNA transfection only in Mcl-1 dependent, but not independent, cell lines (Figure 1B, Figure 4-26). Similarly, using flow cytometry we observed an increase in apoptotic marker Annexin V staining after Mcl-1 knockdown only in dependent cell lines (Figure 4-27). These data suggest that a subset of our cell lines are solely dependent on Mcl-1 for survival, and reduced proliferation after Mcl-1 protein knockdown is caused by apoptotic induction.

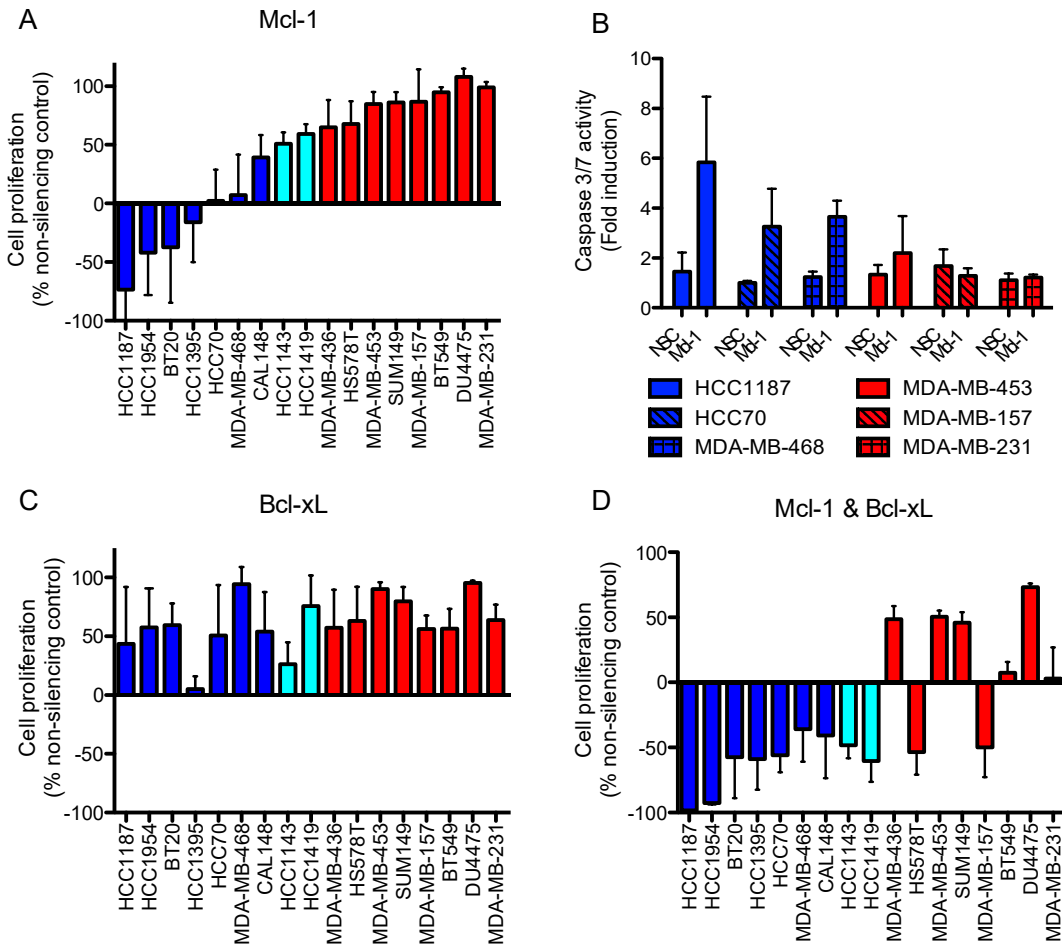


Figure 4-25: A subset of TNBC cell lines are solely dependent on Mcl-1 to evade apoptosis

(A) Mcl-1 expression was silenced by siRNA and cell proliferation was normalized as the ratio of siRNA-treated to non-silencing control (NSC) treated cells, subtracting each value by the initial cell count. With this scaling, 100% indicates knockdown has no effect on viability compared to NSC, 0% means no change in cell count, and negative values indicate cell death. A subset of lines are sensitive to Mcl-1 knockdown (cell viability reduced by 60% or more, blue). Two lines are intermediately sensitive (40–60% reduced viability, cyan), whereas the remainder are Mcl-1 loss insensitive (red). **(B)** Fold-induction of caspase 3/7 activity from untreated cells as measured by Caspase-Glo. Mcl-1 knockdown but not NSC siRNA induces caspase 3/7 activity in dependent, but not independent, cell lines after 24 h. **(C)** Bcl-xL expression was silenced by siRNA. Two lines are sensitive with >60% reduction in proliferation. In contrast, dually silencing Mcl-1 and Bcl-xL expression **(D)** reduces viability in most lines. Values are the mean of at least three independent experiments (error bars S.D.)

	Mcl-1			Bcl-xL		
	N=1	N=2	N=3	N=1	N=2	N=3
HCC1954	98	100	100	96	97	100
HCC1187	80	NA	NA	92	100	95
BT20	100	NA	NA	83	100	100
HCC1395	86	97	NA	93	94	97
MD468	95	80	96	91	81	99
HCC70	94	77	85	78	92	80
CAL148	91	95	93	72	85	88
HCC1143	85	77	97	92	85	95
HCC1419	85	100	80	70	95	92
MD436	95	96	100	98	94	93
HS578T	81	81	85	97	95	94
MD453	96.5	86	75	95.4	96	91
SUM149	100	99	94	75	96	91
MB157	81	84.3	92	94	83.3	92
BT549	73	88	88	90	80	94
DU4475	83	80	84	72	86	87
MD231	98	89	80	99	72	86

Table 4-2: Percent knockdown of Mcl-1 and Bcl-xL for experiments in Figure 4-25
 NA indicates insufficient cells remaining to quantify knockdown percentage.

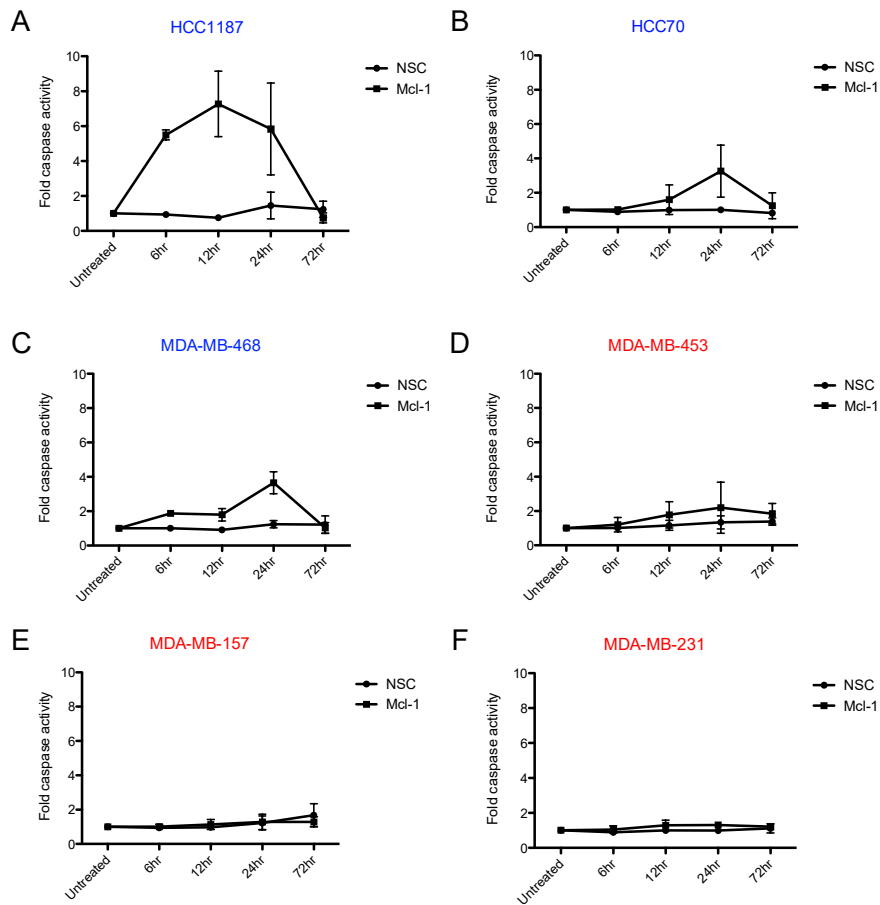


Figure 4-26: Mcl-1 protein silencing induces caspase activation

(A-F) Caspase activity increases after Mcl-1 protein knockdown only in Mcl-1 dependent cell lines. Mcl-1 siRNA or non-silencing control oligonucleotides were administered, and after 6, 12, 24, or

72 hours, caspase 3/7 enzymatic activity was measured by Caspase-Glo. Activity increases primarily in Mcl-1 dependent cell lines HCC1187, HCC70, and MDA-MB-468. Independent lines MDA-MB-453, MDA-MB-157, and MDA-MB-231 showed little or no caspase activity with Mcl-1 silencing. Points shown are the average of at least two independent experiments (error bars SEM). Mcl-1 knockdown efficiency was verified by western blot to be over 80%.

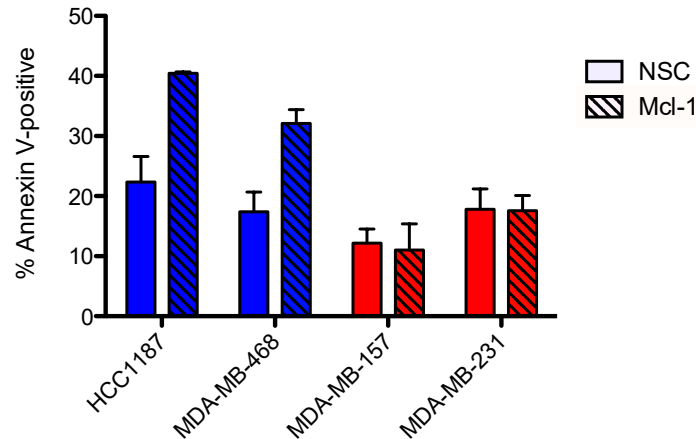


Figure 4-27: Annexin V-positive cells increases in Mcl-1 dependent lines after knockdown

Cells positive for Annexin V, a marker for apoptosis, increases only in Mcl-1 dependent cells (blue) 24 hours after siRNA-mediated knockdown of Mcl-1 (hashed bars) compared to non-silencing control siRNA (solid). Mcl-1 independent lines (red) show no corresponding increase in this apoptotic marker. Shown are means of at least two independent experiments (error bars SEM).

Two lines are intermediately sensitive (40-60% reduced viability, cyan), while the remainder are Mcl-1 loss insensitive (red). (B) Fold-induction of caspase 3/7 activity from untreated cells as measured by Caspase-Glo. Mcl-1 knockdown but not NSC siRNA induces caspase 3/7 activity in dependent, but not independent, cell lines after 24 hours. (C) Bcl-xL expression was silenced by siRNA. Two lines are sensitive with greater than 60% reduction in proliferation. In contrast, dually silencing Mcl-1 and Bcl-xL expression (D) reduces viability in most lines. Values are the mean of at least three independent experiments (error bars SD).

In contrast, siRNA silencing of Bcl-xL expression had only a modest effect on viability for most of the cell lines tested (Figure 4-25C). Only two of the seventeen lines qualify as sensitive under our criteria, one of which is also sensitive to Mcl-1 silencing (HCC1395). These data suggest that unlike Mcl-1, few of these TNBC lines depend solely on Bcl-xL for survival.

It is easy to envision that some TNBC cell lines may block apoptosis via protection from two or more pro-survival Bcl-2 family members. To test this, we silenced the expression of both Mcl-1 and Bcl-xL proteins with concurrent siRNA treatment. Knockdown of both proteins results in significantly more cell death across the TNBC panel than with knockdown of either protein alone (Figure 4-25D), including for cell lines insensitive to Mcl-1 knockdown.

4.2.7 BH3 profiling confirms the specific dependency on Mcl-1 for survival

We performed BH3 profiling on a subset of our TNBC panel to further elucidate the protective role of individual anti-apoptotic Bcl-2 family members. Treatment with 10 μ M of the highly potent and pan-Bcl-2 family antagonist Bim-BH3 peptide depolarized the mitochondria in all cell lines tested (A), verifying that they are sensitive to BH3-mediated antagonism. In contrast, treatment with the Mcl-1 specific peptide MS-1 (Figure 4-28B) at 100 μ M depolarized mitochondria only in the Mcl-1-dependent cell lines. The differing concentrations used reflect the lower activity of MS-1 and are consistent with prior concentrations used for this peptide and others in the literature.²⁹⁸ The Bad-BH3 peptide, which antagonizes Bcl-2 and Bcl-w in addition to Bcl-xL, depolarized mitochondria to a lesser extent than did the MS-1 peptide, which also agrees with the Bcl-xL siRNA results above (Figure 4-28C). Of note is the higher-than-expected response

to Bad-BH3 in MDA-MB-231 cells, though this is perhaps explained by the broad activity of Bad-BH3 to also antagonize other Bcl-2 family members.

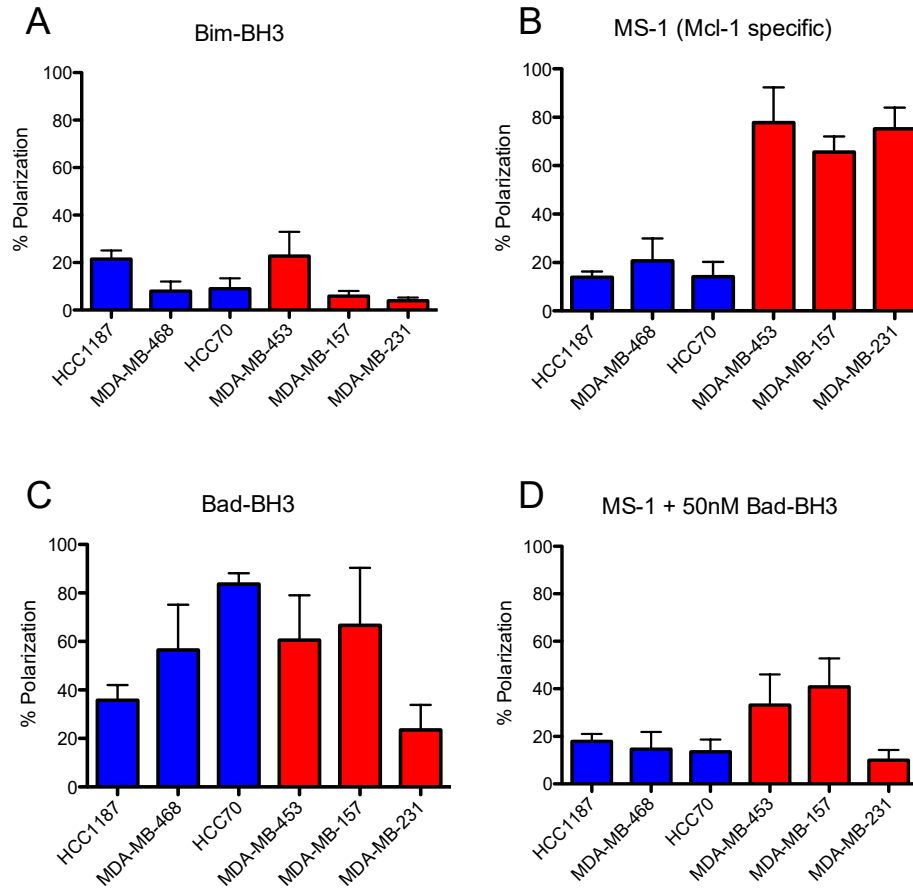


Figure 4-28: BH3 profiling confirms Mcl-1 dependency status

(A) Whole-cell treatment with 10 μ M Bim-BH3 peptide, a non-specific pro-survival Bcl-2 family antagonist, induced mitochondria depolarization in all cell lines tested. (B) In contrast, the Mcl-1 specific antagonist MS-1 at 100 μ M selectively depolarized mitochondria only in Mcl-1-dependent cell lines. (C) The Bad-BH3 peptide, which antagonizes Bcl-2 and Bcl-w in addition to Bcl-xL, depolarized mitochondria at 10 μ M strongly only in the MDA-MB-231 cell line. (D) Combined administration of 0.05 μ M Bad-BH3 peptide with MS-1 peptide as in (A) depolarized mitochondria more strongly. Shown are the mean of at least three independent experiments (Error bars SD).

Finally, we simulated our dual siRNA results by co-administering the MS-1 peptide and a sub-E10 dose (50 nM) of Bad-BH3, a concentration chosen to clearly demonstrate the synergistic effect of co-dosing. In agreement with our previous results, the mitochondria depolarization

increased compared to MS-1 peptide alone for the three Mcl-1 independent cell lines tested. The change in polarization for MDA-MB-453 exceeds that expected from our dual siRNA experiments, presumably due to the expanded binding profile of Bad-BH3. Not surprisingly, increasing the concentration of Bad-BH3 peptide to 1 μ M further sensitized these cell lines to MS-1 peptide (data not shown).

4.2.8 *Mcl-1 sequesters more Bim than Bcl-xL in Mcl-1 dependent cell lines*

Results from the BH3-profiling experiments suggest that Bcl-xL is failing to significantly protect these TNBC cells from apoptosis. To investigate the mechanism, we first considered whether Bcl-xL was not efficiently trafficking to the mitochondria; however, the mitochondrial fraction of Bcl-xL is actually higher than that of Mcl-1 (Figure 4-29A). Similarly, Bcl-xL phosphorylation at Serine 62 blocks BH3-domain binding, but no phosphorylation at this residue were noted (Figure 4-29A).³⁰⁰ Nevertheless, it is still possible that Mcl-1 is sequestering a larger percentage of pro-apoptotic proteins. To investigate this possibility, we immunoprecipitated Mcl-1 from the sensitive cell line H929 and ran a western blot. The fraction of Noxa which was pulled down with Mcl-1 is equivalent to the fraction in the input, indicating that all the Noxa in the cell is sequestered by Mcl-1 (as expected). Similarly, the ratio of Mcl-1/Bim is similar between the two fractions, indicating again that Mcl-1 is sequestering a majority of the Bim in this cell line. Thus, Bcl-xL plays only a minority role in sequestering pro-apoptotic Bim protein (Figure 4-29C-D). To directly answer this question, we immunoprecipitated Mcl-1, Bcl-xL, and Bim, and probed for each protein in a western blot. As expected, Mcl-1 and Bim reciprocally co-immunoprecipitated together, but Bcl-xL does not immunoprecipitate with Bim (Figure 4-29E).

These data suggest that the H929 cell line does not depend on Bcl-xL for survival despite expressing the protein. To directly test this hypothesis, we dosed H929 cells with the specific Bcl-xL inhibitor WEHI-539 and observed no mitochondrial depolarization or reduction in viability, while the Bim and MS-1 peptides powerfully depolarized the mitochondria.

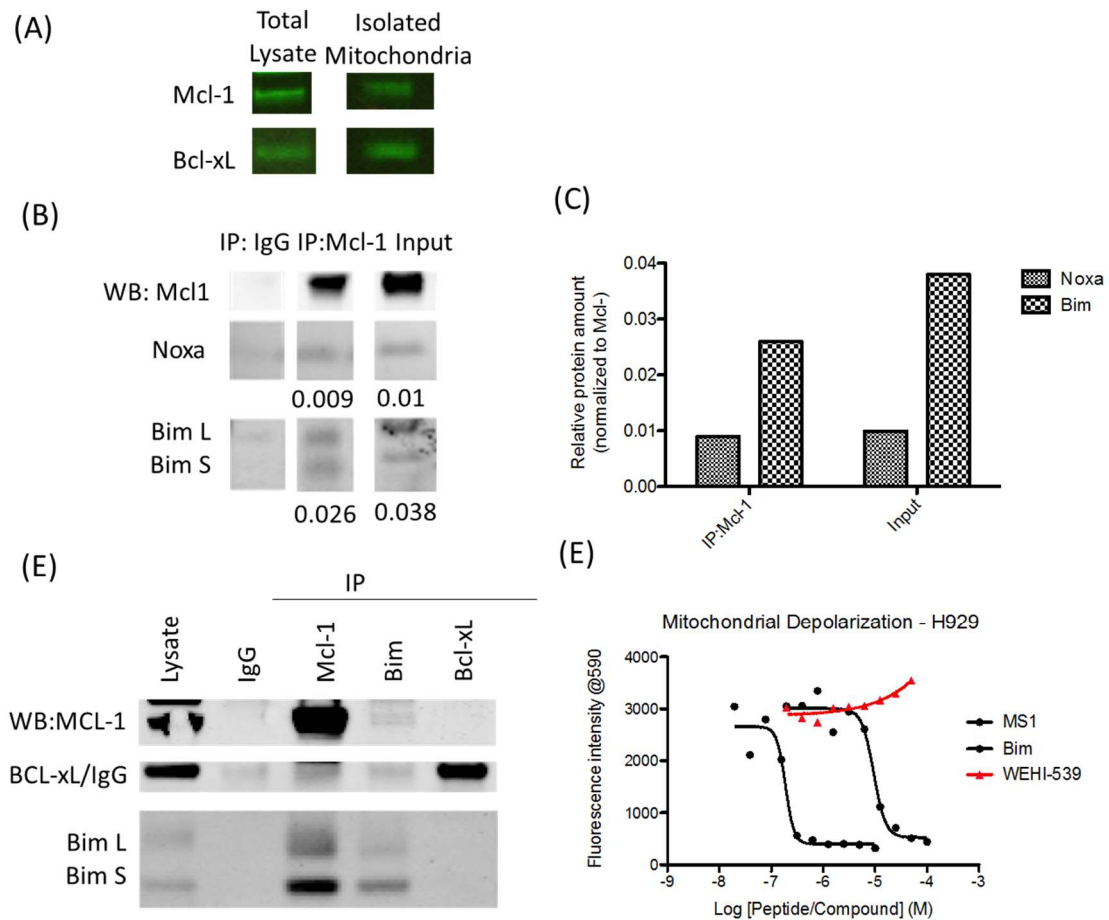


Figure 4-29: Mcl-1, but not Bcl-xL, primarily sequesters mitochondrial Bim

(A) Bcl-xL is efficiently trafficked to the mitochondria. Bcl-xL is clearly evident in western blot of isolated mitochondrial fractions, and the ratio of Bcl-xL to Mcl-1 is actually higher on the mitochondria than in total lysate, indicating that a higher percentage of Bcl-xL is mitochondrial-bound. **(B)** Bcl-xL is not inactivated by phosphorylation at Serine 62. **(C-D)** Mcl-1 is complexed with nearly all of the Noxa, and 2/3 of the Bim, in H929 cells (an Mcl-1 dependent cell line). **(E)** Mcl-1 is co-immunoprecipitated with Bim, and Bim co-immunoprecipitates with Mcl-1, but Bcl-xL is not capable of pulling down Bim. **(F)** As predicted, H929 cells are resistant to the Bcl-xL

inhibitor WEHI-539 in this mitochondria depolarization assay, but is highly responsive to the Mcl-1 specific peptide MS-1 and pan-inhibitor Bim.

4.2.9 *Mcl-1 knockdown overcomes resistance to Bcl-xL small-molecule inhibitors*

Because cell lines in our TNBC panel are largely resistant to Bcl-xL silencing, we reasoned these lines might also be resistant to the Bcl-xL specific small-molecule inhibitor WEHI-539,²⁹⁵ and that co-dosing with Mcl-1 knockdown might synergistically reduce viability. To test this hypothesis, we measured the viability IC₅₀ for WEHI-539 during concurrent treatment by NSC or Mcl-1 siRNA (Figure 4-30A). IC₅₀ values for NSC-treated cells are in the low micromolar range, indicating that these cells are not highly sensitive based on the potency observed for other Bcl-2 family inhibitors.³⁰¹ However, in combination with Mcl-1 knockdown, compound potency improves markedly across the panel, such as the 15-fold improvement for MDA-MB-157 cells (Figure 4-30B). We next tested whether Bcl-2 is an important survival factor by repeating the above experiment using the Bcl-2 specific inhibitor ABT-199.³⁰² Cells were insensitive to compound alone or in combination with Mcl-1 siRNA (Figure 4-30C,D). Finally, we repeated this experiment with ABT-263, a Bcl-2 and Bcl-xL dual inhibitor (Figure 4-30C, ref 30). As seen with WEHI-539, cells were largely resistant to compound alone but were extremely sensitive to combination with Mcl-1 silencing (Figure 4-30E-F). In summary, the Bcl-xL inhibitors ABT-263 and WEHI-539, but not the selective Bcl-2 inhibitor ABT-199, have an additive effect with Mcl-1 knockdown to reduce cell viability in these cell lines.

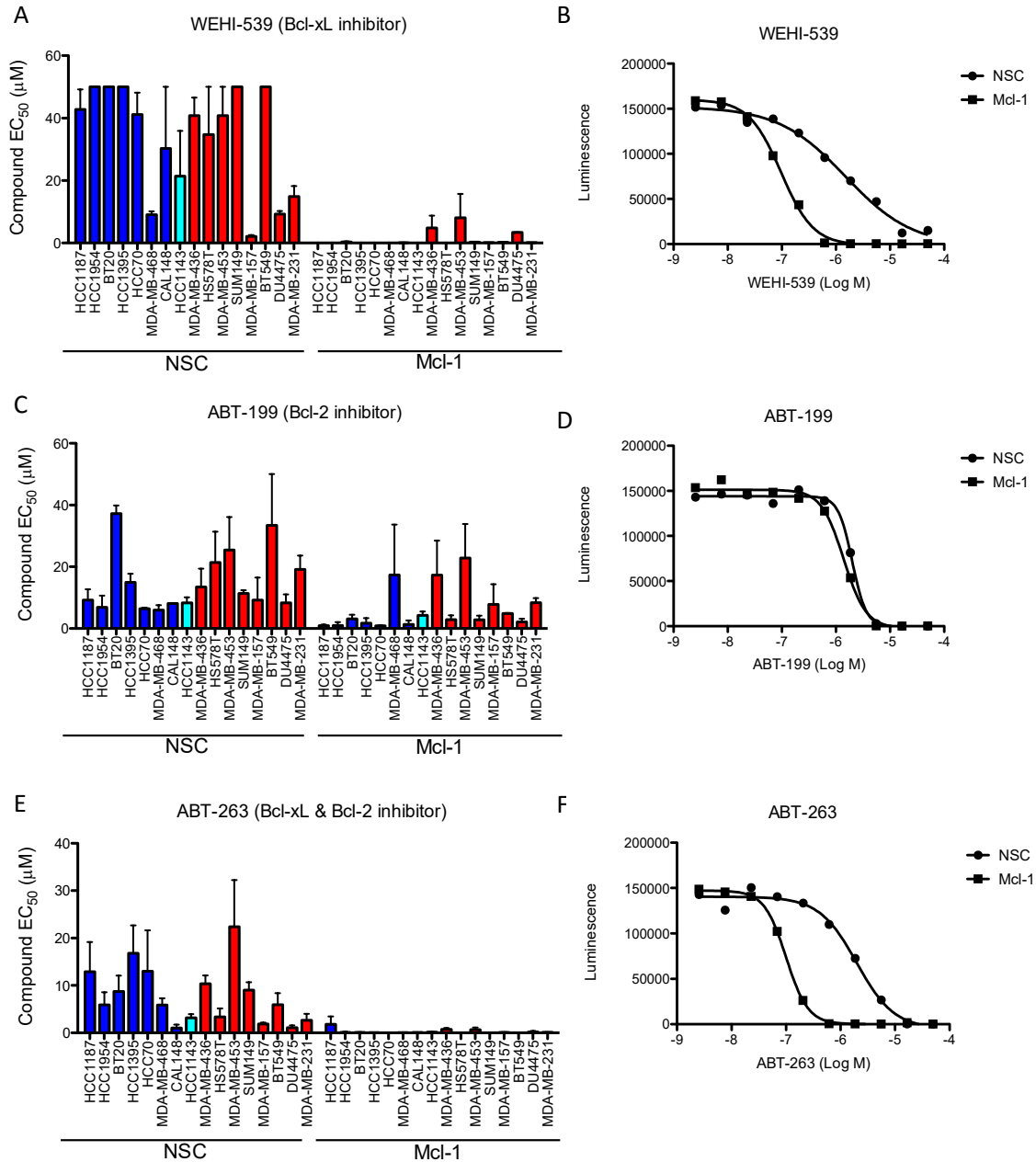


Figure 4-30: Bcl-2 and Bcl-xL inhibitors in combination with Mcl-1 silencing

Cells were treated with NSC or Mcl-1 siRNA, then dosed with compound to measure IC₅₀. (A) The observed IC₅₀ of the selective Bcl-xL inhibitor WEHI-539 is reduced dramatically across the panel when Mcl-1 is knocked out compared to NSC control. (B) Representative dose-response curves in MDA-MB-157 cells treated with WEHI-539. In contrast, cells remained resistant to ABT-199 (a Bcl-2 selective inhibitor) irrespective of Mcl-1 knockdown across the panel (C) and exemplified in MDA-MB-157 cells (D). (E) Cell lines are also resistant to dual inhibition of Bcl-xL and Bcl-2 by the inhibitor ABT-263 when dosed with NSC siRNA, but co-dosing ABT-263 with Mcl-1 siRNA decreases compound IC₅₀ similar to that observed with WEHI-539. Representative curves for

MDA-MB-157 are shown in F. Shown are the mean of at least two independent experiments (Error bars SEM).

4.2.10 Mcl-1 inhibitors powerfully synergize with Bcl-2 family inhibition

We next sought to expand these studies by examining co-dosing studies with a specific Mcl-1 small-molecule inhibitor and ABT-263. The EC₅₀ to activate caspase 3/7 improved markedly with co-administration of increasing doses of ABT-263 with VU0659158 in H929 cells, while co-administration of ABT-263 sensitized the Mcl-1 insensitive K562 cell line to Mcl-1 inhibition (Figure 4-31A-B). These results are consistent with our above findings, as well as the literature implicating Mcl-1 as a resistance factor for Bcl-xL and Bcl-2 inhibitors. The interaction between Mcl-1 and Bcl-xL/Bcl-2 inhibitors is extremely synergistic with a combination index of less than 0.1.³⁰³

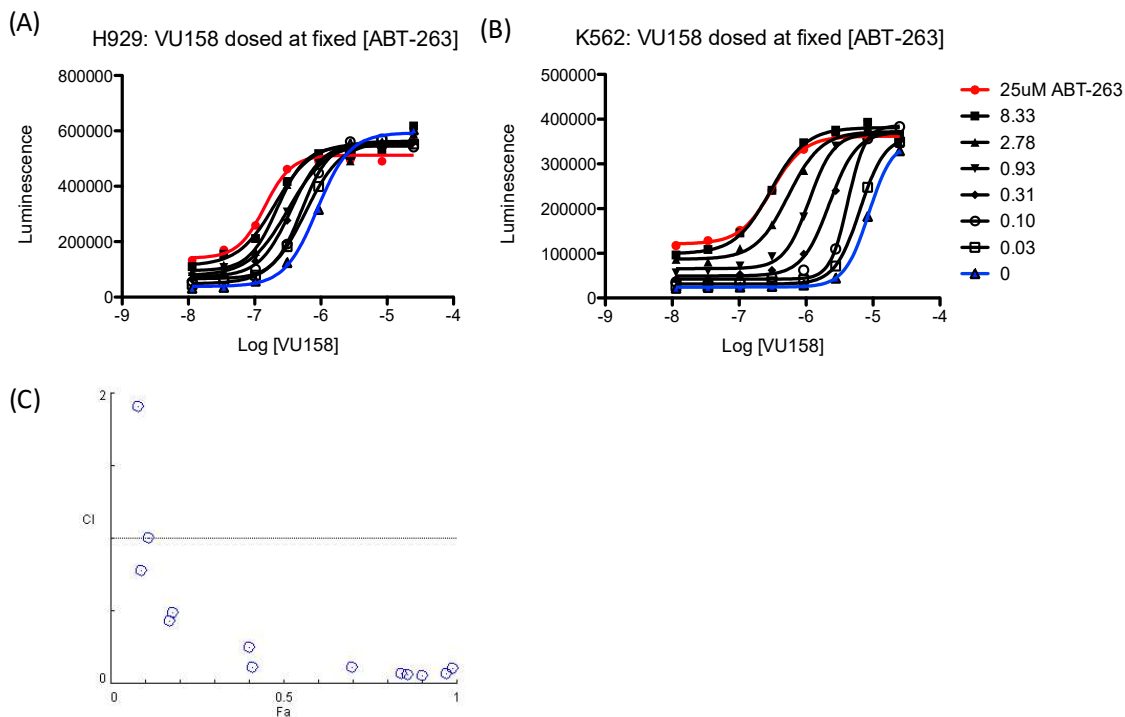


Figure 4-31: Mcl-1 inhibitors powerfully synergize with Bcl-2/Bcl-xL inhibitor ABT-263
Mcl-1 inhibitor VU0659158 was dosed at a fixed concentration of ABT-263 in H929 cells (A) or K562 cells (B) and the level of caspase 3/7 activity was measured with Caspase-Glo. Consistent with siRNA-based results, co-dosing a Bcl-xL/Bcl-2 inhibitor improved the activity of Mcl-1 inhibitor. (C) The interaction of VU0659158 with ABT-263 is highly synergistic with Combination Index (CI) less than 0.1. Fa; fraction active.

4.2.11 Bcl-2 family member mRNA or protein levels do not predict Mcl-1 dependency

Our siRNA, compound treatment, and BH3 profiling experiments all suggest a critical role for Mcl-1 to protect a subset of TNBC lines from apoptosis. Moreover, Mcl-1 has been shown to sequester a larger fraction of pro-apoptotic proteins than Bcl-xL in some cell lines. However, the determinants of this effect are not clear, nor was it clear why some (but not all) lines depended on Mcl-1 for survival. We found no correlation between mRNA expression and cell viability in these TNBC lines for Bcl-2 family members Mcl-1, Bcl-xL, Noxa, Bim, Bax, Bak, and Bax (Figure 4-32). Since steady-state protein expression might vary significantly from mRNA levels, we

additionally profiled each cell line by western blot (Figure 4-33) As expected, expression differed among the cell lines, particularly the levels of the BH3-only proteins Noxa and Bim as well as the anti-apoptotic proteins Bcl-2, Mcl-1, Bcl-xL. We found no significant correlation between Mcl-1 sensitivity and protein expression for anti-apoptotic Mcl-1, Bcl-xL, and Bcl-2 (Figure 4-34A-C), nor for the expression of BH3-only proteins Bim and Noxa (Figure 4-34D, E). Expression of pro-apoptotic executioner proteins Bak and Bax weakly correlated with Mcl-1 dependency, with an R^2 of 0.35 and 0.44, respectively ($p < 0.05$) (Figure 4-34F-G). Together, expression of single proteins at best only weakly correlates with Mcl-1 dependency.

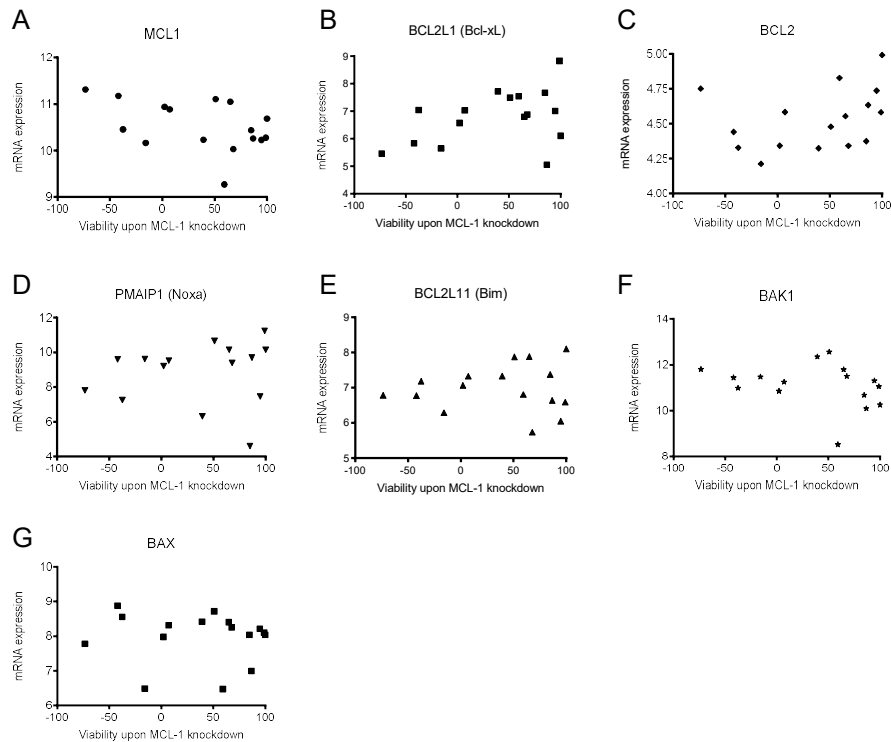


Figure 4-32: mRNA expression levels do not correlate with MCL-1 sensitivity

(A-G) mRNA expression levels for MCL1, BCL1L1 (Bcl-xL), BCL2, PMAIP1 (Noxa), BCL2L11 (Bim), BAK1, and BAX from the Broad-Novartis Cancer Cell Line Encyclopedia (CCLE) were examined for correlation with cell viability after Mcl-1 knockdown using linear regression. In each case, no statistically significant correlation was observed.

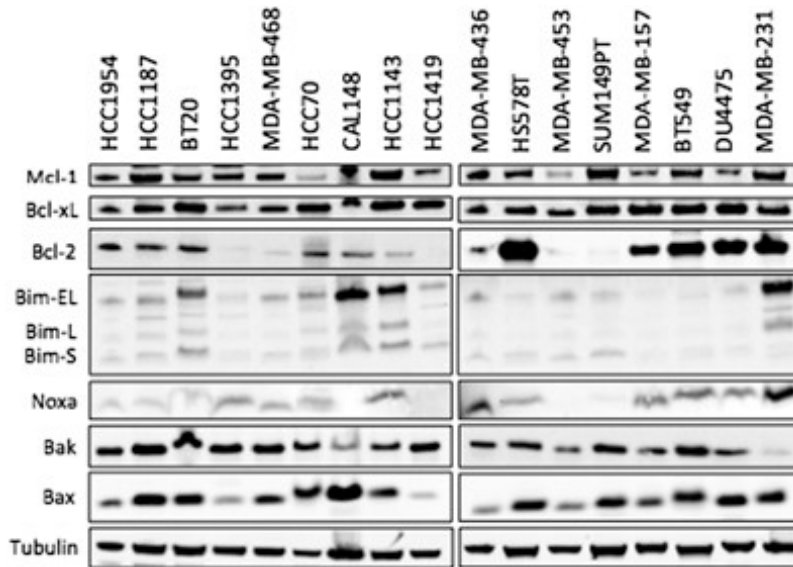


Figure 4-33: Bcl-2 family protein expression levels in the TNBC cell line panel
 Equal amount (18 μ g) of cell lysate was analyzed by western blot and probed for the indicated protein, with Tubulin as a loading control.

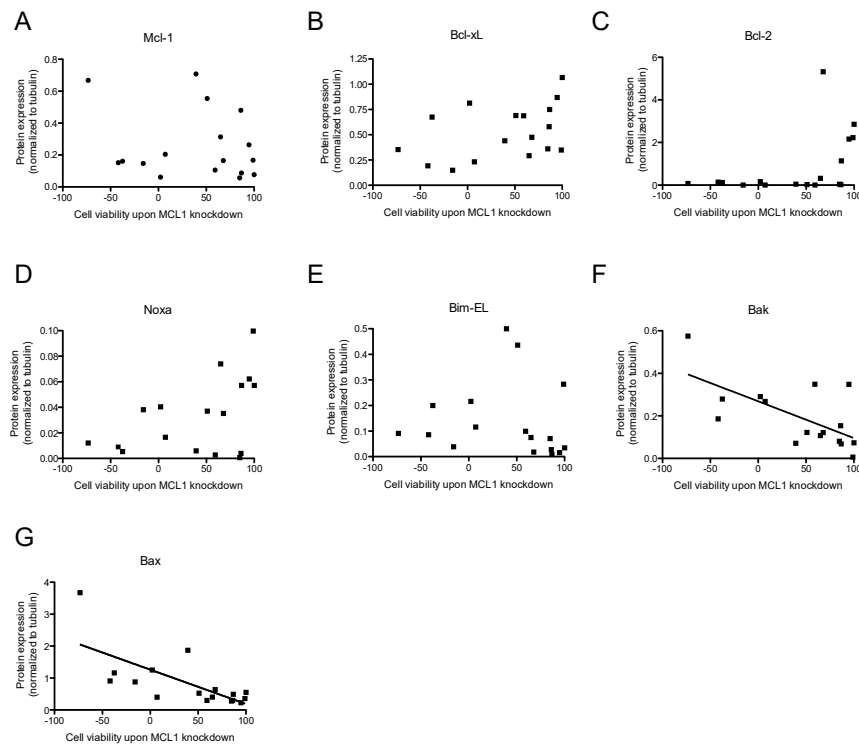


Figure 4-34: Bcl-2 family protein expression does not strongly correlate with Mcl-1 sensitivity
 (A-E) Tubulin-normalized protein expression levels for Mcl-1, Bcl-xL, Bcl-2, Noxa, and Bim do not significantly correlate with cell viability after Mcl-1 knockdown. (F-G) Expression of executioner

Bcl-2 family protein Bak and Bax correlates with Mcl-1 sensitivity with an R^2 of 0.34 and 0.44, respectively ($p < 0.05$).

4.2.12 A combined index of Bcl-2 family proteins better predicts Mcl-1 dependency

Since Bcl-2 proteins work in concert to regulate apoptosis, a more holistic approach for predicting survival dependency on Mcl-1 should include multiple protein expression levels. Using a multiple linear regression (**1**) where y is cell viability after Mcl-1 knockdown and $[protein]$ is the protein expression normalized to Tubulin from the western blot analysis, we used a least squares fit of equation 1 to obtain the constant factors b and m_{1-5} . Mcl-1 and Bcl-xL were included due to their role in singly or dually protecting the cell from apoptosis, as seen in Figures 1 and 2. Bak was chosen due to its mechanistic function to depolarize the mitochondria after Mcl-1 and Bcl-xL are antagonized and its significant correlation with Mcl-1 sensitivity in Figure 5. Bim and Noxa are important general and Mcl-1 specific antagonizing BH3-only proteins, respectively.

$$y = b + m_1*[Mcl-1] + m_2*[Bcl-xL] + m_3*[Noxa] + m_4*[Bim] + m_5*[Bak] \quad \mathbf{1}$$

$$y = 31.3 + 76.4*[Mcl-1] + 89.9*[Bcl-xL] + 336[Noxa] - 104*[Bim] - 230*[Bak] \quad \mathbf{2}$$

Using this equation, we predicted Mcl-1 sensitivity for each cell line and plotted it against the experimentally determined viability (Figure 4-35A). The resulting fit has an R^2 of 0.71 ($p < 0.001$). To identify the relative importance of each protein in the equation, we recalculated by singly removing each factor (Figure 4-36A-E). Removing Bak had the largest effect on R^2 , followed by Bcl-xL, Bim, Mcl-1, and Noxa respectively, which is consistent with our single-linear

regression showing Bak as the strongest individual predictor of sensitivity among these five proteins. We further tested this equation by replacing the least significant contributor (Noxa) with Bcl-2, but the quality of the fit decreased (Figure 4-36F).

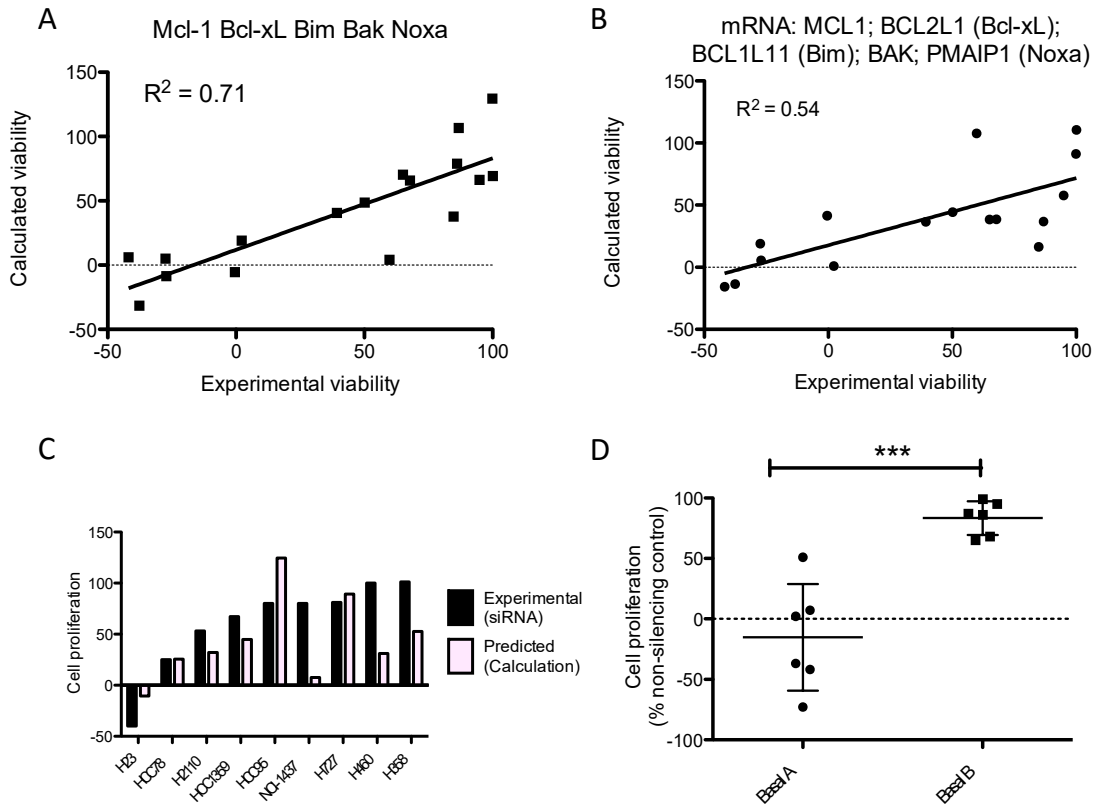


Figure 4-35: A combined index predicts sensitivity to Mcl-1 knockdown

(A) Multiple linear regression was used to fit Mcl-1, Bcl-xL, Bim, Bak, and Noxa protein expression to predict cell viability after Mcl-1 knockdown; the fit is plotted against experimental viability and a least-squares-fit linear regression line is drawn ($R^2=0.71$, $p<0.0001$). (B) Using mRNA expression values results in a weaker, but still significant, overall fit ($R^2=0.54$, $p<0.0001$). (C) Using this mRNA-derived index, we predicted Mcl-1 sensitivity in a panel of nine non-small-cell lung cancer cell lines, and compared those numbers to experimentally-determined viability after silencing Mcl-1 expression. (D) Grouping cell lines by subtype indicates that Basal A significantly correlates with Mcl-1 sensitivity, while Basal B subtyped cell lines are Mcl-1 insensitive (two-tailed t-test, $p<0.0004$, error bars SD).

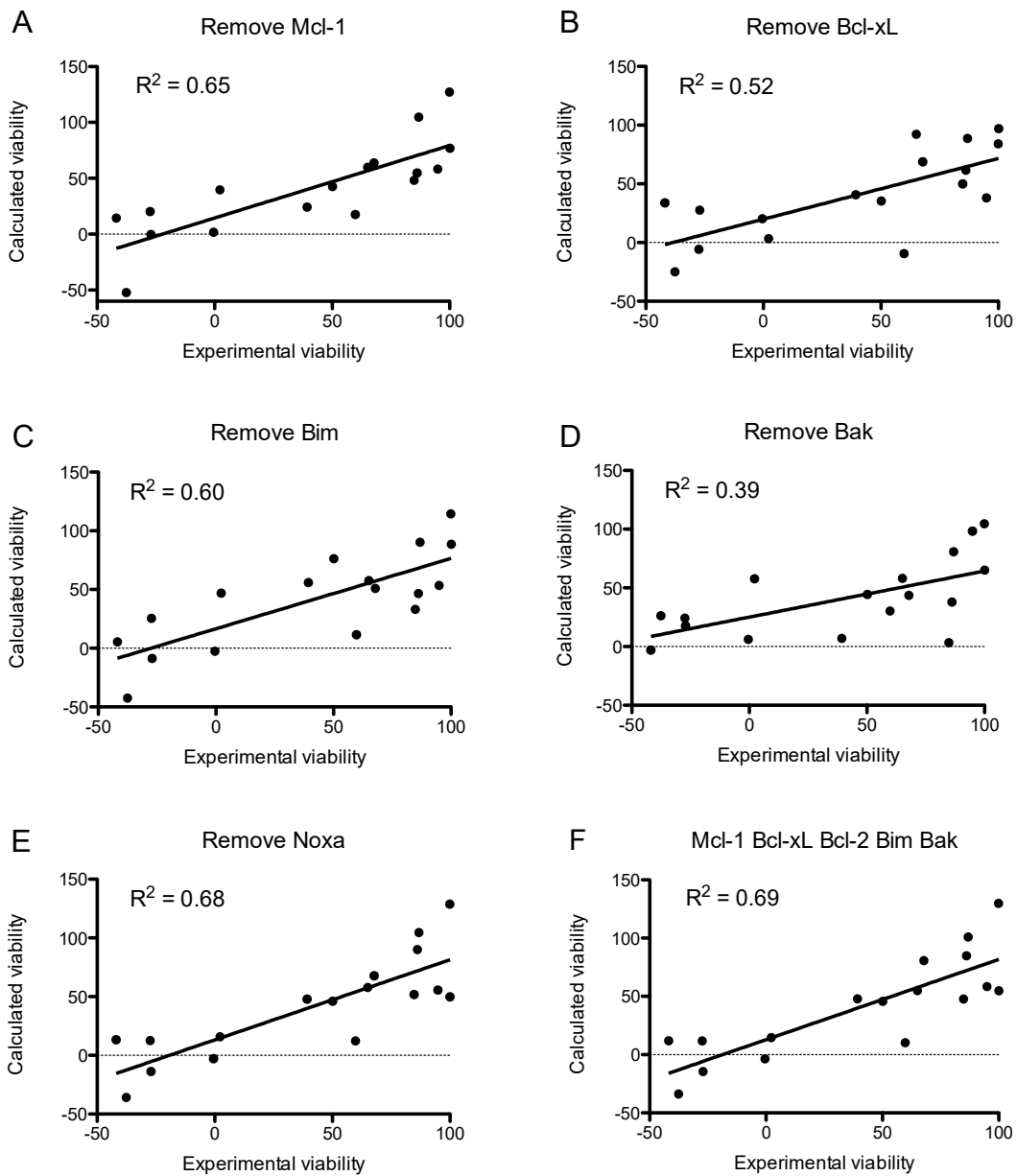


Figure 4-36: Bak most heavily contributes to the prediction algorithm

(A-E) Individual proteins were removed from the viability index to ascertain their influence on the goodness-of-fit. Bak has the most significant contribution, followed by Bcl-xL, Bim, Mcl-1, and Noxa, respectively. (F) Including the anti-apoptotic protein Bcl-2 in the multiple linear regression rather than Noxa does not improve the fit for our TNBC cell lines.

Coefficients depend on the protein's importance to predict viability and on the quantified western blot band intensity (e.g. the low-intensity Noxa bands result in a large coefficient). Therefore, this equation is highly dependent on uniform band staining between experiments, and necessitates a loading control to standardize results obtained under different conditions. Normalized mRNA expression is another metric that is often used as a surrogate for protein expression and is available for a large number of cancer cell lines in public databases (such as the CCLE), allowing rapid identification of more potentially sensitive cell lines for additional study. We tested whether mRNA levels predicted cell line sensitivity (Figure 4-35B). Although the goodness-of-fit and the slope both decreased, the overall R^2 was significant at 0.54 ($p < 0.001$) (Equation 3).

$$y = 675 - 52.5*[Mcl-1] + 22.6*[Bcl-xL] + 6.27[Noxa] + 0.158*[Bim] - 46.0*[Bak] \quad \mathbf{3}$$

We next tested whether the coefficients derived from TNBC cell lines would have predictive value in other cancer types. We silenced Mcl-1 expression in a panel of non-small cell lung cancer cell lines and compared their experimental viability to predictions based on equation 3. The equation correctly forecasted the dependency of seven out of the nine tested, including the identification of H23 and HCC78 as very sensitive and H358 and H727 as insensitive (Figure 4-35C). The equation incorrectly classified two cell lines as sensitive that the siRNA data revealed as insensitive. We then expanded our prediction across the entire CCLE dataset (Figure 4-37). As expected, we see a wide distribution of Mcl-1 sensitivities. The predicted most sensitive line is H929, which we identified in Figure 4-37 to be almost exclusively Mcl-1 dependent.

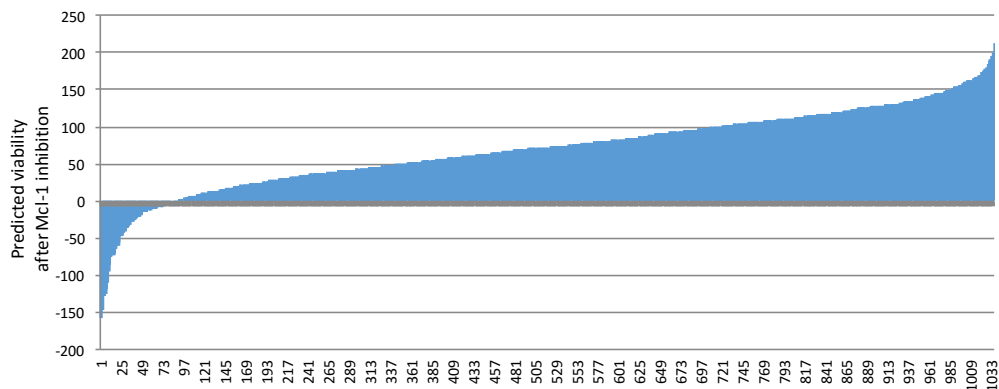


Figure 4-37: Prediction of Mcl-1 dependency in the CCLE

Mcl-1 dependency was predicted for each for each of 1,033 cell lines in the Broad-Novartis Cancer Cell Line Encyclopedia. Cell lines are ranked in order of most-to-least Mcl-1 dependent. Shown are the predicted viability in a five-day proliferation experiment if Mcl-1 was completely inhibited, with negative numbers indicating a loss of initial cells.

Finally, we examined whether Mcl-1 sensitive cell lines segregate to a particular subtype of TNBC. In confirmation of a previous report,²⁴⁸ we found that Mcl-1 sensitivity correlates with the Basal A TNBC subtype as defined by Neve *et al*,³⁰⁴ while the Basal B subtype is resistant (Figure 4-35D).

4.3 Discussion

Cancer cells often protect themselves from programmed cell death by upregulating anti-apoptotic members of the Bcl-2 protein family, or conversely, by reducing the expression of pro-death family members. Pharmacologically removing this apoptotic block can restore apoptosis and provides a useful therapeutic approach for treating tumors.³⁰¹ During my work as a graduate student at Vanderbilt, I helped to discover small molecules that specifically impair the anti-apoptotic function of Mcl-1 and cause cell death in multiple cancers, including TNBCs. Development of robust biochemical assays capable of measuring picomolar-affinity compounds was crucial for Mcl-1 drug discovery, without which no SAR would be revealed to guide

compound synthesis. The fluorescence polarization anisotropy assay developed with the Bim6 probe permitted measurements of compound affinity down to 200pM. The BH3 profiling assay accurately measured the Mcl-1 dependency of a panel of cell lines, and enabled us to select those lines most heavily dependent on Mcl-1 to investigate for on-target reductions in viability and activation of caspases. BH3 profiling also revealed cell lines that were completely independent of Mcl-1 for survival, which allowed us to measure off-target apoptotic toxicity for program compounds. In addition, the mitochondrial depolarization assay, co-immunoprecipitation, and proximity ligation assays allowed us to directly measure the ability of program compounds to induce disruption of the mitochondrial outer membrane and disruption of Mcl-1/Noxa, Mcl-1/Bim, or Mcl-1/Bak interactions (Figure 4-38). These assays were critical to guide compound synthesis, and have enabled the development of compounds with on-target cellular activity to disrupt Mcl-1/Noxa complexes, activate caspases, and reduce cell proliferation. Some of these compounds, like the exemplified compound VU0659158, have progressed to *in vivo* testing, while more recently synthesized compounds in the Fesik group have significantly improved binding affinities and in-cell activity compared to these exemplified compounds.

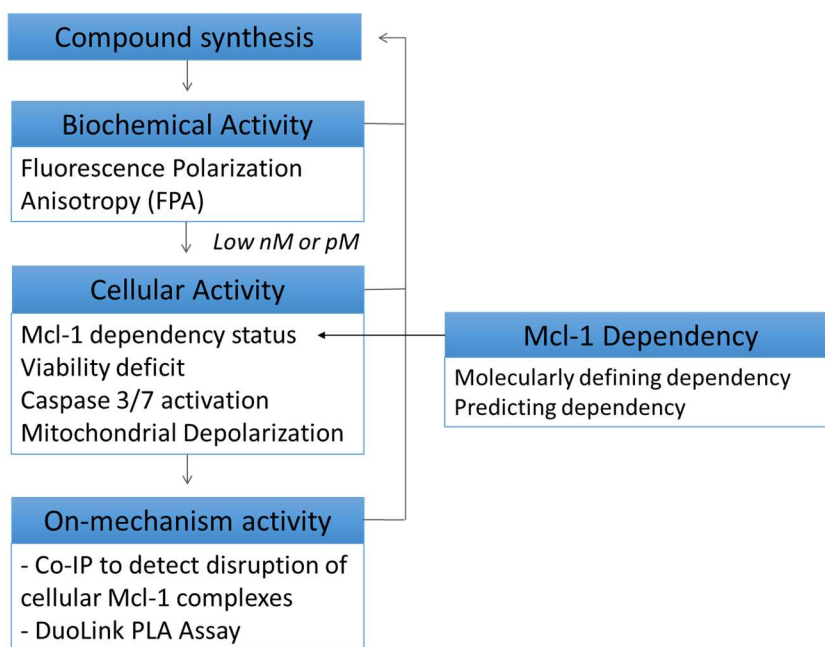


Figure 4-38: Mcl-1 program compound progression chart

All assays depicted in this figure (except Caspase 3/7 activation) were introduced and optimized by this author.

The protein(s) responsible for apoptotic protection can differ for individual tumors and cell lines and have important implications on the choice of treatment. Prior to these studies, it was unclear whether TNBC significantly relied upon Mcl-1 for survival. We found that a significant fraction of TNBC cell lines (41%) are dependent upon Mcl-1 for survival, as evidenced by dramatically reduced viability after Mcl-1 protein knockdown, Caspase 3/7 activation, Annexin V staining, and mitochondrial depolarization by an Mcl-1-specific peptide. In contrast, silencing Bcl-xL had only a modest effect in the TNBC cell lines examined. Strikingly, co-silencing both produced significantly increased cell death and reduced viability in the majority of cell lines, even those that were resistant to silencing either protein individually. These data have been further confirmed by other groups in breast cancer cell lines, including TNBC.²⁹²

Consistent with these results, the Bcl-xL inhibitor WEHI-539 was largely ineffective when used alone against TNBC cells lines, but potently killed cells in combination with Mcl-1

knockdown. Similarly, the dual Bcl-2 and Bcl-xL inhibitor ABT-263 was only mildly cytotoxic when used alone, indicating that Bcl-2 and Bcl-xL combined inhibition do not reduce viability, but in combination with Mcl-1 silencing is strongly cytotoxic. These results suggest that inhibition of Mcl-1 in TNBC could re-sensitize tumors following acquired resistance to Bcl-2 family chemotherapeutics, as is seen in other cancer types.^{238,239,305}

We next sought to understand why some (but not all) cell lines responded to Mcl-1 knockdown. Each cell line in this TNBC panel expresses the executioner proteins Bak, Bax, and BH3-only proteins, and their mitochondria depolarizes in response to Bim. These data suggest that intrinsic-pathway apoptotic blockade is due to antagonism by high levels of anti-apoptotic proteins (e.g. Mcl-1, Bcl-xL, etc).³⁰⁶ While alternate routes exist to block apoptosis without affecting Bcl-2 family proteins on the mitochondrion (such as by upregulating Inhibitors of Apoptosis proteins (IAPs), or by blocking BH3-only protein activation), the sensitivity of most cell lines to single Mcl-1, or combined Mcl-1 and Bcl-xL knockdown, suggests that these other mechanisms are underutilized. We observed high (albeit varied) levels of Mcl-1 and Bcl-xL and low levels of Bcl-2 protein expression across the TNBC cell line panel. While expression of a particular anti-apoptotic protein does not necessarily indicate a cell is dependent on it for survival,¹³⁻¹⁴ significant expression is likely a necessary precondition for the protein to be an important sensor of cell death stimuli and thus a viable target for therapeutic manipulation. Indeed, all Mcl-1, Bcl-xL, or dually sensitive cell lines expressed the requisite protein(s). Additionally, Bak and Bax protein levels significantly (albeit weakly) correlated with reduced viability after Mcl-1 knockdown, indicating their central importance to execute mitochondrial depolarization when anti-apoptotic Bcl-2 family antagonism is removed.

Cancer cells differ not just in the absolute expression levels of anti-apoptotic proteins, but also in their extent of pro-apoptotic protein activation. A cell line or tumor with higher pro-apoptotic activation is more “primed for death” and will require more anti-apoptotic proteins to survive.³⁰⁶ Therefore, it is not surprising that we saw no correlation of Mcl-1 protein or mRNA with Mcl-1 dependency because these fail to account for differences in cellular pro-apoptotic potential. Likewise, the extent of unbound anti-apoptotic proteins is also an important criteria to predict dependency. Over 40% of tested lines responded to Mcl-1 knockdown alone, but most of the insensitive lines required combined Mcl-1 and Bcl-xL knockdown to die, suggesting that these lines express additional anti-apoptotic proteins sufficient to sequester any released pro-apoptotic factors after Mcl-1 loss.²⁷⁴

Interestingly, knockdown of Bcl-xL alone had relatively little effect compared to Mcl-1 knockdown. While the two proteins have unique specificities for BH3-only proteins (e.g. Mcl-1 can bind Noxa but Bcl-xL can bind Bad), their overall anti-apoptotic mechanisms are similar. This discrepancy has been observed in other cancer types as well, including acute myeloid leukemia³⁰⁷ and estrogen receptor positive breast cancer.¹² The Bad-BH3 peptide, which antagonizes Bcl-2, Bcl-w, and Bcl-xL, depolarized mitochondria to a lesser extent than the Mcl-1 specific peptide. This suggests that in these cell lines the pool of Bcl-2, Bcl-w and Bcl-xL contributes marginally compared to Mcl-1 in protection against apoptotic induction. Perhaps Mcl-1 more actively sequesters pro-apoptotic proteins, with the bulk of Bcl-xL prevented from blocking apoptosis by localization or inactivation.

Because of these complications, we are unsurprised to find several previously published multi-protein indexes for predicting response to Bcl-2 family inhibitors.^{259,308} Our data suggests

that an additional metric for predicting dependency on a particular anti-apoptotic protein will consider the relative amounts of both pro- and anti-apoptotic proteins. We found that an index of five proteins (Mcl-1, Bcl-xL, Bim, Bak, and Noxa) could highly predict Mcl-1 sensitivity with an R^2 of 0.71. Since these predictions were based on *in vitro* experiments, their performance *in vivo* with complicating factors such as stroma and the associated microenvironment deserves further study.

Including Bcl-2 in the index did not improve our viability predictions in TNBC. The TNBC cell lines tested cells were resistant to the Bcl-2 specific inhibitor ABT-199 alone or in combination with Mcl-1 silencing, which suggests that Bcl-2 provides little anti-apoptotic protection in these cell lines. However, including Bcl-2 might make the equation more broadly applicable to other cancer types that do heavily rely on Bcl-2 to protect against apoptosis during Mcl-1 loss.

Our results suggest that a BH3-mimetic capable of inhibiting Mcl-1 interactions might prove efficacious as a single-agent therapeutic in some TNBC tumors; whereas, single-agent inhibition of Bcl-2 or Bcl-xL may be largely ineffective. In other TNBC tumors, combination therapy may be required. The highly significant correlation of Basal A subtype status to Mcl-1 dependency in these cell lines should be further investigated using patient-derived samples, and could prove to be an effective biomarker for clinical breast cancer patient selection. In other cancer types, an analysis of the protein or mRNA levels of Bcl-2 family members (e.g. Mcl-1, Bcl-xL, Bak, and Bim) may be useful in a multi-factorial expression as shown here to mechanistically predict which tumors are likely to respond to an Mcl-1 inhibitor across different tumor types.

The finding that Mcl-1 and Bcl-xL/Bcl-2 inhibition is powerfully synergistic suggests several intriguing possibilities. First, co-administration would improve the efficacy of an Mcl-1 inhibitor,

and may expand the number of tumors sensitive to an Mcl-1-targeting therapeutic. More excitingly, co-administering an Mcl-1 inhibitor with Bcl-xL inhibition may lower the efficacious threshold for Bcl-xL inhibition below the toxicity threshold for inducing thrombocytopenia (in humans, around 2-4 μ M of ABT-263). Simultaneous inhibition of Bcl-2, Bcl-xL, and Bcl-w by ABT-263 is tolerated by healthy cells at low micromolar concentrations; whether the addition of Mcl-1 inhibitors can be tolerated at sufficient concentrations to achieve a positive therapeutic outcome remains unexplored

In sum, the body of work in this Chapter was crucial to the discovery of specific and potent Mcl-1 inhibitors. Moreover, these data suggest criteria to select cancer types and patients with tumors that will most highly respond to an Mcl-1 inhibitor.

4.4 Methods

Cell lines & culture conditions

Cell lines were obtained from the American Type Culture Collection (ATCC, Manassas, VA, USA) except for Cal148 (obtained Deutsche Sammlung von Mikroorganismen und Zellkulturen GmbH, Braunschweig, Germany) and Sum149PT (obtained from Asterand, Detroit, MI, USA). Cells were cultured in recommended media.

Protein knockdown & cell viability

Protein expression was silenced using small-interfering RNA (siRNA). On-targetPLUS motifs specific to the 3'-UTR or ORF for Mcl-1 and Bcl-xL were obtained from Dharmacon (Thermo Scientific, Waltham, MA, USA). Cells were plated in antibiotic-free medium at 5000 cells/well in

a 96-well plate. After 24 hours, medium was replaced with siRNA-containing medium consisting of 0.01% Dharmafect I transfection reagent and 25 nM siRNA sequence specific to the target or non-silencing control (NSC) motif. Control wells received normal media. Cell viability was measured after five days using Cell Titer-Glo (Promega, Fitchburg, WI, USA), a fluorescent assay that produces signal corresponding to ATP concentration (a proxy for cell count). Signal was measured on the Spectramax M5 plate reader (Molecular Devices, Sunnyvale, CA, USA) averaged over five replicate wells. Conditions were optimized such that cell viability was reduced by the non-silencing control siRNA by no more than 30%, and protein knockdown was verified by western blot analysis using lysates collected at the conclusion of the experiment.

Flow Cytometry

Cells were plated in a 6-well dish at 100,000 cells/well. Non-silencing or Mcl-1 siRNA were dosed for 24 hours before collection and staining with fluorescein isothiocyanate conjugates of annexin V and propidium iodide (Life Technologies) and analyzed on a 5 Laser LSR II (BD Biosciences).

Western Blotting

Cell lysates were collected in RIPA buffer. Equal amount of lysate (18 μ g) was boiled in SDS protein loading buffer supplemented with 10mM DTT, separated by SDS-PAGE, transferred to Immobilon-FL PVDF membrane (Millipore, Billerica, MA, USA), and blotted for indicated protein. Antibodies for Mcl-1 (Y37), Bcl-xL (E18) obtained from Abcam (Cambridge, UK); Bcl-2 (50E3), Bak and Bax from Cell Signaling Technologies (Danvers, MA, USA); Bim (H-191) and Bad (C-7) from Santa Cruz Biotechnology (Dallas, TX, USA); Noxa and α -Tubulin (DM1A) from Millipore. Each was

used at a 1:1000 dilution. Blots were probed with species-appropriate IRDye-conjugated secondary antibodies (Licor, Lincoln, NE, USA) at 1:20,000 dilution and measured on the Licor Odyssey system. Quantification performed on the Licor Image Studio.

BH3 profiling

Synthetic peptides were ordered from Genscript. Sequences are as previously described for MS-1,²⁹⁸ Bim-BH3 and Bad-BH3.²⁹⁶ BH3 profiling was conducted and analyzed as described.²⁹⁶ Fluorescence was measured on a Biotek Cytation 3 after 1.5 hours. DMSO control was used for zero depolarization, and FCCP at 20 μ M was used for 100% depolarization. Normalized percent polarization is calculated as (Sample-FCCP)/(DMSO-FCCP). Compounds were run similarly and typically were conducted as 10-point, 3-fold dilution series.

Mcl-1 knockdown combination studies

Cells were plated in antibiotic free medium to a final count of 1000 cells/well in a 96-well plate and left for 24 hours. Non-silencing control or Mcl-1 siRNA were added as described above. After two days, compounds ABT-263, ABT-199, or WEHI-539 (SelleckChem, Houston, TX, USA) were added in ten-point, three-fold serial dilutions to a final DMSO concentration of 0.5%. Cell viability was quantified on day 5 by Cell Titer-Glo and read on the Spectramax M5 plate reader. Results shown are the average of two or more independent experiments.

Compound studies

Cells were plated in antibiotic free medium to a final count of 1000 cells/well in a 96-well plate and left for 24 hours. Compounds were plated in a ten-point, 3-fold dilution pattern with a final DMSO concentration of 0.5%. Three days after compound addition, cell viability or caspase activation was measured by addition of Cell Titer-Glo or Caspase-Glo (Promega) and read on the Biotek Cytation 3 plate reader.

mRNA expression data

Robust Multi-array Average-normalized mRNA expression data for each cell line (excluding Sum149, for which data was not available) was obtained from the Broad-Novartis Cancer Cell Line Encyclopedia (CCLE), available at <http://www.broadinstitute.org/ccle>.

Regression analysis

Linear regression and statistical analysis was performed in Prism (Graphpad Software, La Jolla, CA, USA). Multiple linear regression was performed using the LINEST function in Microsoft Excel 2010 (Redmond, WA, USA).

Fluorescence Polarization Anisotropy competition assays

Fluorescein isothiocyanate (FITC)-labeled FITC-Bak-BH3 peptide (FITC-AHx-GQVGRQLAIIGDDINR-NH₂) were purchased from GenScript and used without further purification. FPA measurements were carried out in 384-well, black, flat-bottom plates (Greiner Bio-One) using the Cytation 3 plate reader (Biotek). All assays were conducted in assay buffer containing 20 mM TRIS pH 7.5, 50 mM NaCl, 3 mM DTT, and 5% final DMSO concentration for the FPA/Bak assay. To measure

inhibition of the FITC-Bak-BH3 interaction with Bcl-2 family members, 10nM FITC-Bak-BH3 peptide was incubated with 15 nM Mcl-1. For IC₅₀ determination, compounds were diluted in DMSO in a 10-point, 3-fold serial dilution scheme, added to assay plates, and incubated for 1.5 hours at room temperature. The change in anisotropy was measured and used to calculate an IC₅₀ (inhibitor concentration at which 50% of bound peptide is displaced), by fitting the inhibition data using XLFit software (Guildford, UK), to a single-site binding model. This was converted into a binding dissociation constant (K_D) according to the formula⁵⁰:

$$K_D = [I]_{50} / ([L]_{50} / K_D^{\text{pep}} + [P]_0 / K_D^{\text{pep}} + 1)$$

where [I]₅₀ is the concentration of the free inhibitor at 50% inhibition, [L]₅₀ is the concentration of the free labeled ligand at 50% inhibition, [P]₀ is the concentration of the free protein at 0% inhibition and K_D^{pep} represents the dissociation constant of the FITC-labeled peptide probe.

A FITC-labeled peptide derived from the Bim-BH3 sequence (FITC-Bim6, FITC-Ahx-EARIAQELRRIGDEFNETYTR-NH₂) was similarly ordered from Genscript and used without further purification. Competition binding assays were conducted as described above for FPA/Bak, with the following modifications: 1nM FITC-Bim6 peptide and 1.5nM Mcl-1 protein were used, and final DMSO concentration was kept to 1%.

Biotin streptavidin pull-down experiment

Human chronic myelogenous leukemia K562 cells were grown in RPMI-8226 complete media, lysed in NP-40 buffer (150mM NaCl, 1% NP-40, 50mM Tris, pH 8.0), cleared by centrifugation, and incubated with indicated concentrations of compound or Bim-BH3 peptide (FITC-Ahx-

EARIAQLRRIGDEFNETYTR, Genscript) for 60 minutes at room temperature. Separately, Dynabeads M-280 streptavidin conjugated beads (Life Technologies) were incubated with biotin-Ahx-MS-1, an Mcl-1 specific peptide, for 30 minutes and washed four times with PBS plus 0.01% TWEEN-20. The loaded beads were then incubated with lysate at room temperature for ten minutes, washed twice, boiled in SDS-PAGE loading buffer, and analyzed by Western blot (Licor Odyssey) with an Mcl-1 specific antibody (Y37, Abcam).

Whole-cell Pull-down experiment

Human multiple myeloma H929 cells were grown in RPMI-8226 complete media with 10% serum and incubated with the indicated concentration of compound for indicated time. Cells were then collected, lysed in NP-40 buffer (150mM NaCl, 1% NP-40, 50mM Tris, pH 8.0) plus TWEEN-20 at 0.1%, and cleared by centrifugation. Separately, Protein-G Dynabeads (Life Technology) were incubated with Mcl-1 S-19 antibody (Santa Cruz) for 10 minutes at room temperature, cross-linked with 5mM BS₃ for 30 minutes, quenched with Tris-HCL for 15 minutes, and finally washed in NP-40 buffer. The collected cell lysate was then added to the washed beads and incubated for 10 minutes at room temperature, washed, and finally collected in SDS-PAGE loading buffer and heated at 70C for ten minutes. The samples were analyzed by Western blot (Licor Odyssey) and probed with an Mcl-1 specific antibody (Y37, Abcam), Noxa-specific antibody (Calbiochem), or Bim-specific antibody (Y36, Abcam).

Proximity Ligation Assay (PLA)

The PLA assay was conducted using the DuoLink In Situ reagent kit from Sigma, which includes pre-made solutions of Antibody Diluent, Wash Buffer A and B, and Blocking Buffer, as well as all ligation, amplification, and antibodies required to recognize the primary antibodies supplied by the user. Cells were plated in a clear bottom black Griner 384 well plates at 25,000 cells/well twenty-four hours prior to the start of the experiment. Cells were then treated with compound or DMSO control for 90 minutes, washed with PBS, fixed with 1% formaldehyde for 10 minutes, and permeabilized with 0.1% Triton X-100 for 5 minutes. Cells were then washed twice with PBS and incubated with 1x Blocking Buffer at 37°C for 30 minutes. Primary antibodies for rabbit Mcl-1 (S-19) and goat Bim (M-20) (Santa Cruz) were diluted 1:50 in 1x Antibody Diluent and incubated with shaking for 4 hours at room temperature. Cells were then washed twice with Wash Buffer A and incubated for 1 hour at 37°C with a 1:5 dilution of anti-Goat (plus) and anti-Rabbit (minus) PLA probes in Antibody Diluent. For the ligation reaction, the plate was washed twice in 1x Wash Buffer A for 5 minutes and incubated with 1x Ligation Stock and a 1:40 dilution of ligase for 30 minutes at 37°C and washed twice in 1x Wash Buffer A. For the amplification stage, Amplification Stock was diluted to 1x in water, supplemented with 1:80 dilution of polymerase, and incubated with cells for 100min at 37°C. Wells were finally washed twice with 1x Wash Buffer B for 10 minutes, then finally with 0.01x Wash Buffer B for 1 minute. To stain with DAPI, NucBlue Fixed Cell Stain (Life Technologies) was diluted to manufacturer's recommendations (2 drops/1mL) and added to each well for 5 minutes. Cells were then washed twice with PBS and filled to a final volume of 40uL PBS. Plates were read on the ImageXpress Micro XLS Widefield High-Content Analysis System (Molecular Devices) in the Vanderbilt University High-Throughput Screening

Core. Data analysis was conducted on the manufacturers imaging software by algorithmically determining the average stain intensity of each cell. Negative control wells (those lacking one of the primary antibodies) were used as negative controls to indicate background fluorescence.

Chapter 5

General conclusions

Despite remarkable advancements in cancer therapy in the last half century, malignant carcinomas remain the second largest cause of death in the United States.¹ Significant improvements in our basic understanding of cancer initiation and progression have led to testable hypotheses regarding which proteins may be irrevocably depended upon by these cancer cells for survival, but which are dispensable in healthy tissues. “Targeted therapeutics” designed to inhibit these oncogenes may be more efficacious than traditional chemotherapeutics, and may have significantly lower toxicities in non-cancerous cells as well.³

Successful targeted therapies require extensive pre-clinical validation of the protein target. Many highly validated proteins have been identified, including K-Ras and many of its downstream effectors, the BCR-ABL fusion oncogene, HER2/ErbB2 receptor tyrosine kinase, and estrogen receptor- α . Inhibitors have been developed against several of these exemplified targets, and many others, and many have achieved remarkable clinical success.

Still greater advancements in cancer therapy may be possible if small-molecule inhibitors are developed for highly-validated protein targets for which no inhibitor currently exists. Problematically, not all proteins are easily druggable.³⁰⁹ This thesis encompasses a significant body of work towards the discovery of new small-molecule inhibitors for three challenging protein targets, and the further validation of these targets as suitable objects for “targeted therapy.” The protein targets included in this dissertation include three areas in which a large body of pre-clinical experimental evidence exists, and for which no clinically-relevant small-molecule inhibitor had been discovered.

Ras is one of the most highly validated targets in cancer research, yet no small-molecule inhibitor for oncogenic Ras has yet been developed due to the extremely challenging nature of inhibiting protein-protein interactions with the Ras surface. In this thesis, the results of a fragment-based screen against K-Ras (G12D) in the active, GTP-bound form were disclosed. A team at Boehringer Ingelheim is actively refining the fragments identified in this screen with a significant chemical synthesis effort and x-ray crystallographic support. These efforts are a significant and reasonable starting point for the discovery of bona-fide K-Ras inhibitors, and we hope that this effort will lead to new Ras inhibitors suitable for use in humans, that the pre-clinical observations implicating Ras as a key oncogene driving survival in human cancer will be confirmed by dramatic responses in human patients.



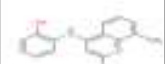















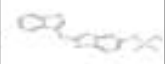
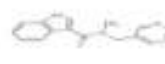




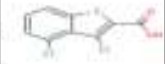
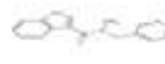
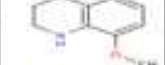

Pak-1 kinase has been demonstrated to drive cancer growth and motility, notably in breast cancer, and overexpression clinically correlates with increased tumor grade and a worse prognosis. No Pak-1 selective inhibitor had yet been disclosed when this project began, and engineering selectivity for Pak-1 over other Pak family kinases was predicted to be challenging. We sought to discover a specific small-molecule inhibitor of Pak-1 and initially conducted two fragment-based screens to identify chemical matter that bound to the Pak-1 kinase domain. Biochemical assays, x-ray crystallographic support, and aggressive chemical modification yielded molecules that bound to Pak-1 with 210nM affinity. We further identified methods of inducing selectivity for Pak-1 over the closely related Pak-4 kinase. We discontinued active discovery when several Pak-1-selective small molecules were disclosed starting in 2013 because our effort was no longer competitive, but the availability of these inhibitors is a significant benefit to the Pak-1 kinase research field. These small-molecules have not yet achieved clinical testing, so Pak-1

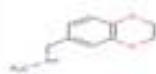
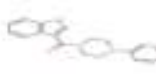
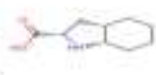

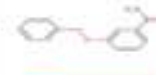
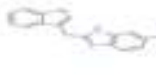


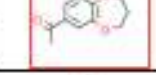
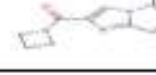







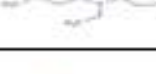



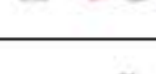






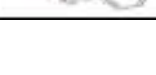

cannot be conclusively validated as a cancer target. However, all pre-clinical *in vitro* and *in vivo* evidence with these inhibitors continues to suggest that Pak-1 inhibition, alone or in combination with other agents, will be efficacious in select cancer types.


















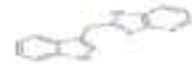










Finally, this thesis discloses our efforts to discover Mcl-1 inhibitors and to understand the cancer types most addicted to this oncogene. Several biochemical and cellular assays were developed to demonstrate inhibitor activity in multiple settings. These assays provided key details needed by the chemists to improve the affinity and activity of these compounds. We hope a carefully selected Mcl-1 inhibitor will be ready for IND-enabling studies in the near future. Moreover, this thesis expands our understanding of the mechanism by which cells depend on Mcl-1 for survival, and includes new methods to predict oncogenic dependency on Mcl-1. These advances may help select patient populations for future clinical trials of Mcl-1 inhibitors. All research disclosed in this thesis supports the hypothesis that a specific Mcl-1 inhibitor will be a beneficial therapeutic in a subset of cancer types, including TNBC breast cancers.


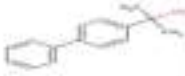










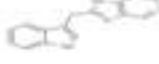







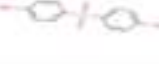




Appendix A



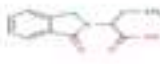



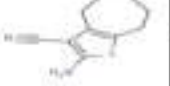





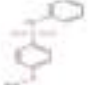
K-Ras-GTP-bound fragments identified in the fragment-based screen

Vanderbilt ID	Structure	Screen	SCORE	Vanderbilt ID	Structure	Screen	SCORE
VU0412845-1		Primary	3	VU0282080-2		Primary	2
VU0412946-1		Primary	3	VU0417512-1		Primary	2
VU0207708-4		Primary	3	VU0417483-1		Primary	2
VU0432387-2		Primary	3	VU0416116-1		Primary	2
VU0432438-1		Primary	3	VU0447186-1		Primary	2
VU0432440-1		Primary	3	VU0447310-1		Primary	2
VU0447089-2		Primary	3	VU0447313-1		Primary	2
VU0447282-1		Primary	3	VU0447854-1		Primary	2
VU0448430-1		Primary	3	VU0447885-1		Primary	2
VU0448142-1		Primary	3	VU0448366-1		Primary	2
VU0412497-1		Primary	2	VU0448369-1		Primary	2
VU0303474-2		Primary	2	VU0448417-1		Primary	2
VU0294685-2		Primary	2	VU0448366-1		Primary	2
VU0432771-1		Primary	2	VU0430214-1		Primary	2

Vanderbilt ID	Structure	Screen	SCORE	Vanderbilt ID	Structure	Screen	SCORE
VU0430587-1		Primary	2	VU0448506-1		Primary	1
VU0430315-1		Primary	2	VU0448429-1		Primary	1
VU0411234-1		Primary	2	VU0448430-1		Primary	1
VU0430277-1		Primary	2	VU0446851-1		Primary	1
VU0430214-1		Primary	2	VU0430524-1		Primary	1
VU0421867-1		Primary	2	VU0411362-1		Primary	1
VU0421801-1		Primary	2	VU0407351-1		Primary	1
VU0017882-2		Primary	2	VU0405915-1		Primary	1
VU0416790-1		Primary	1	VU0412636-1		Primary	1
VU0417561-1		Primary	1	VU0411915-1		Primary	1
VU0432968-1		Primary	1	VU0411114-1		Primary	1
VU0180998-4		Primary	1	VU0410933-1		Primary	1
VU0416972-1		Primary	1	VU0411398-1		Primary	1
VU0006194-3		Primary	1	VU0030524-4		Primary	1
VU0417852-1		Primary	1	VU0024679-5		Primary	1










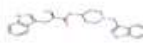













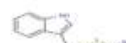














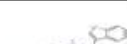
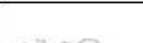
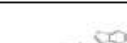
Vanderbilt ID	Structure	Screen	SCORE	Vanderbilt ID	Structure	Screen	SCORE
VU0430382-1		Primary	1	VU0011699-2		Counterscreen	3
VU0431238-1		Primary	1	VU0011509-2		Counterscreen	3
VU0431149-1		Primary	1	VU0406331-1		Counterscreen	3
VU0431108-1		Primary	1	VU0447104-1		Counterscreen	3
VU0422078-1		Primary	1	VU0055241-3		Counterscreen	3
VU0042202-2		Primary	1	VU0447089-1		Counterscreen	3
VU0013976-2		Primary	1	VU0447148-1		Counterscreen	3
VU0092346-2		Primary	1	VU0447098-1		Counterscreen	3
VU0010137-2		Primary	1	VU0432385-2		Counterscreen	3
VU0432441-1		Primary	1	VU0430640-1		Counterscreen	3
VU0448432-1		Primary	1	VU0447313-1		Counterscreen	3
VU0448487-1		Primary	1	VU0432439-1		Counterscreen	3
VU0448489-1		Primary	1	VU0447282-1		Counterscreen	3
VU0448505-1		Primary	1	VU0049995-2		Counterscreen	2

Vanderbilt ID	Structure	Screen	SCORE	Vanderbilt ID	Structure	Screen	SCORE
VU0406872-1		Counterscreen	2	VU0412466-1		Counterscreen	1
VU0412241-1		Counterscreen	2	VU0407741-1		Counterscreen	1
VU0447273-1		Counterscreen	2	VU0412055-1		Counterscreen	1
VU0315948-3		Counterscreen	2	VU0447160-1		Counterscreen	1
VU0433818-1		Counterscreen	2	VU0432441-1		Counterscreen	1
VU0447186-1		Counterscreen	2	VU0407482-1		Counterscreen	1
VU0432387-2		Counterscreen	2	VU0405937-1		Counterscreen	1
VU0012117-2		Counterscreen	1	VU0034402-2		Counterscreen	1
VU0162226-3		Counterscreen	1	VU0417771-1		Counterscreen	1
VU0412272-1		Counterscreen	1	VU0024434-2		Counterscreen	1
VU0118880-2		Counterscreen	1				
VU0407586-1		Counterscreen	1				
VU0417630-1		Counterscreen	1				
VU0411292-1		Counterscreen	1				
VU0015906-2		Counterscreen	1				

Vanderbilt ID	Structure	Screen	SCORE
VU0016932-5		Counterscreen	0
VU0416204-1		Counterscreen	0
VU0405979-1		Counterscreen	0
VU0085653-2		Counterscreen	0
VU0412157-1		Counterscreen	0
VU0410755-1		Counterscreen	0
VU0118450-2		Counterscreen	0
VU0406786-1		Counterscreen	0
VU0007058-2		Counterscreen	0
VU0408573-1		Counterscreen	0
VU0447092-1		Counterscreen	0
VU0406713-2		Counterscreen	0
VU0447090-1		Counterscreen	0

Appendix B

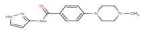
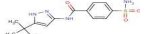
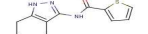
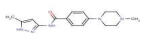
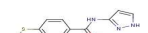

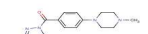

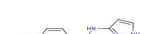
Affinities measured for compounds bound to K-Ras-GTP

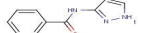
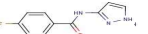
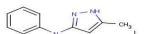
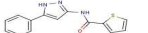
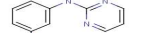
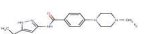
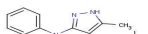

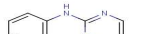
VU Number	Compound	Kd (uM)	VU Number	Compound	Kd (uM)	VU Number	Compound	Kd (uM)
VU0461459-1		178	VU0450250-1		1270	VU0450249-1		1430
VU0453493-1		310	VU0461533-1		1270	VU0461454-1		1430
VU0459618-1		678	VU0453647-1		1300	VU0460184-1		1440
VU0461527-1		945	VU0459550-1		1309	VU0452931-2		1480
VU0461493-1		959	VU0460240-1		1330	VU0450245-1		1500
VU0460004-1		973	VU0460001-1		1331	VU0453676-1		1660
VU0461491-1		1006	VU0461448-1		1355	VU0457015-1		1900
VU0460182-1		1020	VU0450246-1		1360	VU0207708-4		2000
VU0459907-1		1115	VU0453494-1		1360	VU0432438-1		1300
VU0453622-1		1170	VU0460244-1		1379	VU0294685-2		400
VU0460003-1		1190	VU0461526-1		1388	VU0448366-1		1600
VU0461477-1		1230	VU0461469-1		1398			
VU0461467-1		1252	VU0460008-1		1400			
VU0460009-1		1260	VU0461458-1		1410			
VU0461489-1		1260	VU0460007-1		1420			

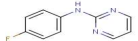
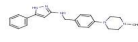
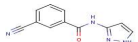
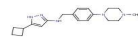
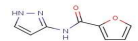
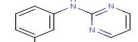
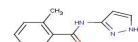
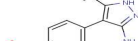
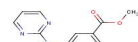
Appendix C

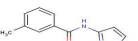
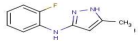
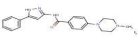
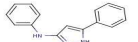
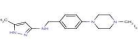
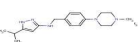
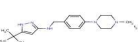


Structure	Vanderbilt.ID	Library	Pak-1	Pak-4
	VU0466177	Designed	1.70	1.35
	VU0467151	Designed	3.60	2.62
	VU0465672	Designed	5.05	0.36
	VU0466176	Designed	6.20	2.01
	VU0467149	Designed	8.70	3.60
	VU0465668	Designed	9.60	15.86
	VU0466171	Designed	13.10	17.20
	VU0467334	Designed	17.20	12.15
	VU0467153	Designed	19.00	5.22

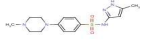
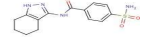
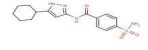
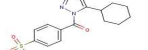
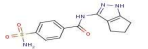
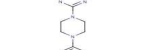
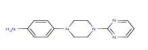
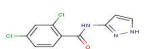
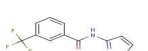
	VU0466178	Designed	22.70	4.42
	VU0466182	Designed	29.90	4.86
	VU0466181	Designed	37.00	
	VU0467733	Designed	41.00	10.43
	VU0463835	Designed	59.00	
	VU0456757	Designed	68.60	
	VU0459371	Designed	71.45	54.00
	VU0467147	Designed	89.00	27.50
	VU0458506	Designed	131.00	78.00

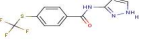
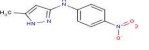
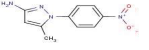
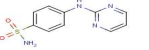
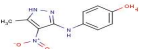
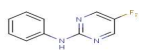
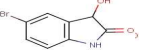
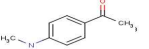
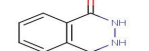
	VU0455693	Designed	139.00	21.00
	VU0467150	Designed	147.00	29.00
	VU0467152	Designed	161.00	41.90
	VU0465670	Designed	168.00	87.25
	VU0458503	Designed	194.00	76.00
	VU0459373	Designed	223.00	126.00
	VU0456756	Designed	242.70	176.00
	VU0466180	Designed	252.00	41.90
	VU0455591	Designed	287.00	176.00

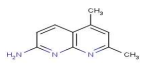
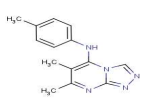
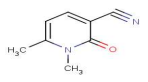
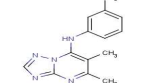
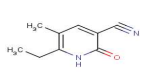
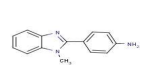
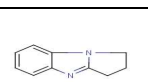
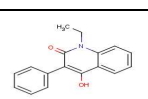
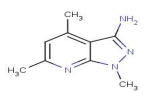
	VU0455588	Designed	294.00	129.00
	VU0455589	Designed	296.00	212.00
	VU0461498	Designed	302.00	266.00
	VU0466179	Designed	304.00	161.00
	VU0455694	Designed	309.00	245.00
	VU0465669	Designed	311.00	13.95
	VU0459370	Designed	327.50	397.00
	VU0455697	Designed	334.00	324.00
	VU0455696	Designed	342.00	284.00

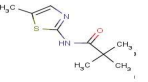
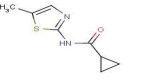
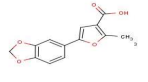
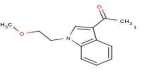
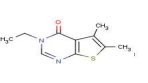
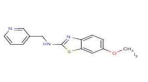
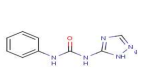
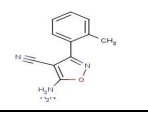
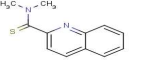
	VU0463812	Designed	346.00	258.00
	VU0466865	Designed	346.00	>400
	VU0455590	Designed	348.00	366.00
	VU0466868	Designed	377.00	225.00
	VU0458507	Designed	423.00	288.00
	VU0463811	Designed	451.00	310.00
	VU0458508	Designed	458.00	>600
	VU0459616	Designed	464.50	285.71
	VU0455695	Designed	467.00	400.00

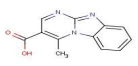
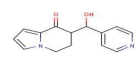
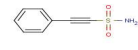
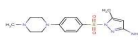
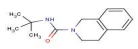
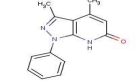
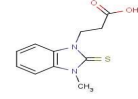
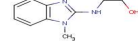
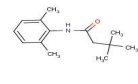
	VU0458501	Designed	490.50	493.51
	VU0459615	Designed	522.00	400.00
	VU0465671	Designed	>400	5.36
	VU0466869	Designed	>400	201.50
	VU0466864	Designed	>400	>400
	VU0466866	Designed	>400	>400
	VU0466867	Designed	>400	>400
	VU0466870	Designed	>400	>400
	VU0466871	Designed	>400	>400

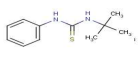
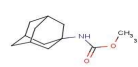
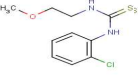
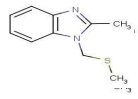
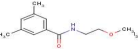
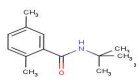
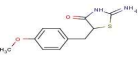
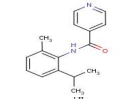
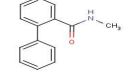
	VU0466872	Designed	>400	>400
	VU0467148	Designed	>400	>400
	VU0467331	Designed	>400	9.31
	VU0467332	Designed	>400	>400
	VU0467333	Designed	>400	>400
	VU0203451	Designed	>600	>600
	VU0456758	Designed	>600	>600
	VU0458505	Designed	>600	>600
	VU0458502	Designed	>600	>600

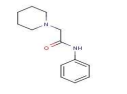
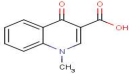
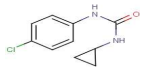
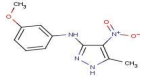
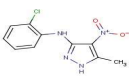
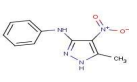
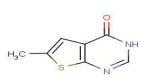
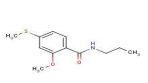
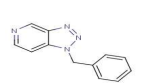
	VU0458504	Designed	>600	>600
	VU0459372	Designed	>600	>600
	VU0459617	Designed	>600	>600
	VU0462884	Designed	>600	324.00
	VU0463797	Designed		
	VU0463810	Designed		
	VU0060618	First site	90.50	131.00
	VU0085117	First site	100.25	199.00
	VU0118844	First site	227.00	

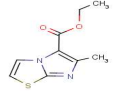
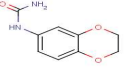
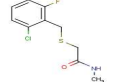
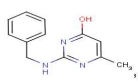
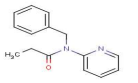
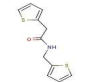
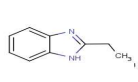
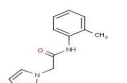
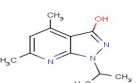
	VU0065941	First site	271.50	436.00
	VU0416773	First site	295.50	359.00
	VU0408790	First site	379.50	445.00
	VU0417271	First site	392.00	482.00
	VU0408792	First site	401.00	446.00
	VU0209271	First site	573.00	>1500
	VU0433265	First site	577.05	741.00
	VU0226787	First site	617.00	533.00
	VU0417646	First site	646.50	635.00

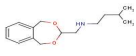
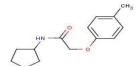
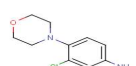
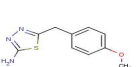
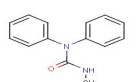
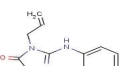
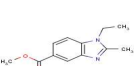
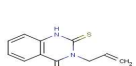
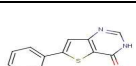
	VU0408230	First site	679.00	783.00
	VU0408260	First site	700.00	NOFIT
	VU0412960	First site	826.50	841.00
	VU0407615	First site	841.50	1251.00
	VU0164975	First site	885.00	743.00
	VU0410942	First site	1223.00	>1500
	VU0433702	First site	1243.50	629.00
	VU0178718	First site	1280.00	617.00
	VU0220499	First site	>1500	>1500

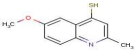
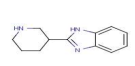
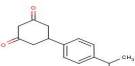
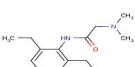
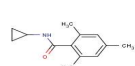
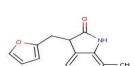
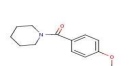
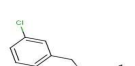
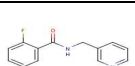
	VU0411936	First site	>1500	1375.00
	VU0430338	First site	>1500	>1500
	VU0406180	First site		
	VU0466873	First site	>400	
	VU0044832	First site		
	VU0041348	First site		
	VU0053334	First site		
	VU0022511	First site		
	VU0035714	First site		

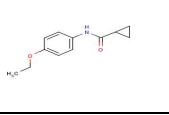
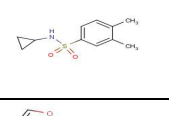
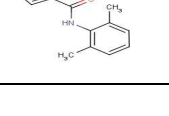
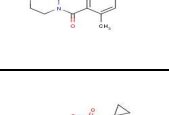
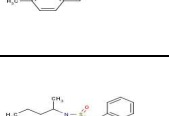
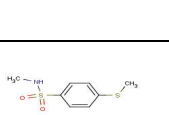
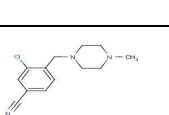
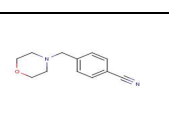

	VU0042202	First site		
	VU0008407	First site		
	VU0037613	First site		
	VU0016783	First site		
	VU0050880	First site		
	VU0051853	First site		
	VU0014239	First site		
	VU0001806	First site		
	VU0050715	First site		

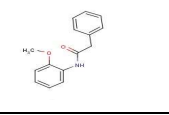
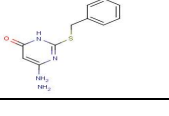
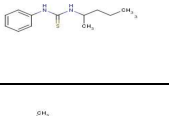
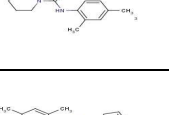
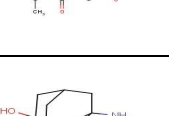
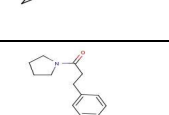
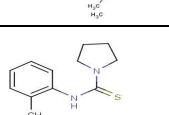
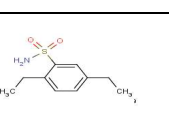

	VU0049179	First site		
	VU0035519	First site		
	VU0041939	First site		
	VU0030127	First site		
	VU0030273	First site		
	VU0030442	First site		
	VU0094120	First site		
	VU0247375	First site		
	VU0248365	First site		

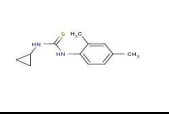
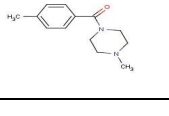
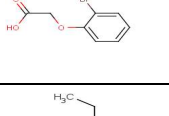
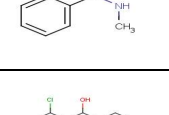
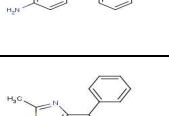
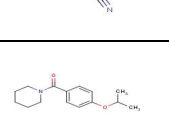
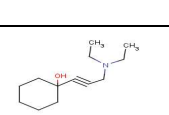
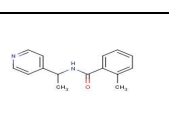

	VU0240580	First site		
	VU0156272	First site		
	VU0178547	First site		
	VU0128364	First site		
	VU0162613	First site		
	VU0178589	First site		
	VU0170482	First site		
	VU0219954	First site		
	VU0247030	First site		

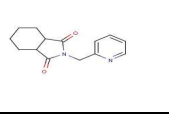
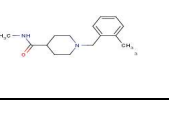
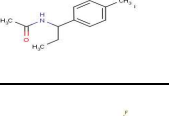
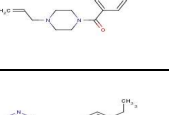
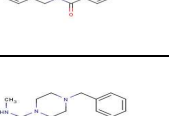
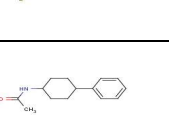
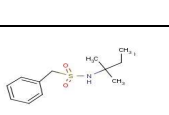
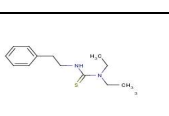

	VU0262965	First site		
	VU0087874	First site		
	VU0176877	First site		
	VU0194525	First site		
	VU0209310	First site		
	VU0309373	First site		
	VU0085635	First site		
	VU0127934	First site		
	VU0092122	First site		

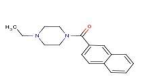
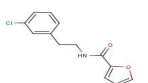
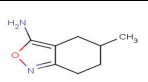
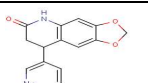
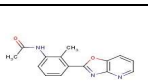
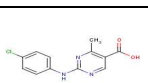
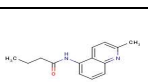
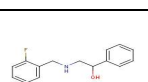
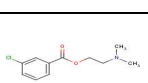
	VU0118958	First site		
	VU0408537	First site		
	VU0408776	First site		
	VU0407996	First site		
	VU0407824	First site		
	VU0408647	First site		
	VU0406722	First site		
	VU0408055	First site		
	VU0408675	First site		

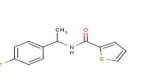
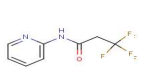
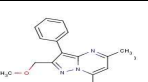
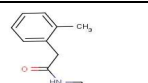
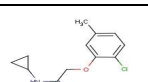
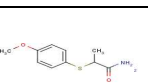
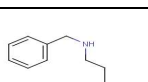
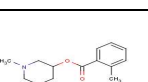
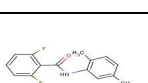
	VU0406935	First site		
	VU0407846	First site		
	VU0406319	First site		
	VU0407823	First site		
	VU0408085	First site		
	VU0406728	First site		
	VU0407352	First site		
	VU0407017	First site		
	VU0407000	First site		

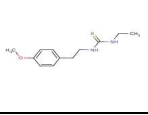
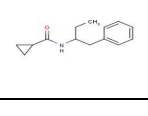
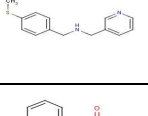
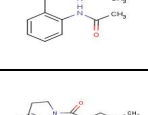
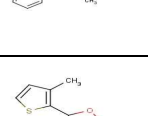
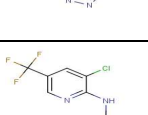
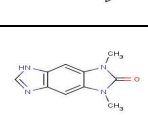
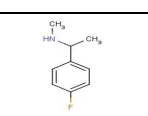

	VU0406311	First site		
	VU0407180	First site		
	VU0407294	First site		
	VU0407946	First site		
	VU0407958	First site		
	VU0406110	First site		
	VU0407158	First site		
	VU0406929	First site		
	VU0407374	First site		

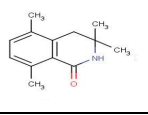
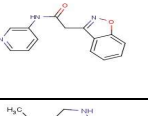
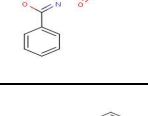
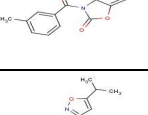
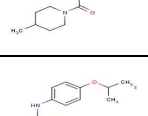
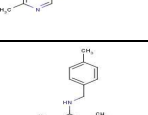
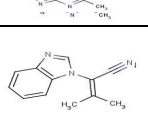
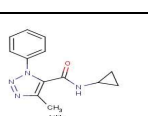

	VU0407003	First site		
	VU0406437	First site		
	VU0405886	First site		
	VU0406999	First site		
	VU0408616	First site		
	VU0407640	First site		
	VU0408172	First site		
	VU0406072	First site		
	VU0407829	First site		

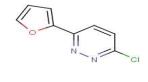
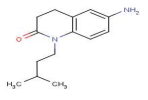
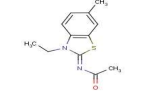
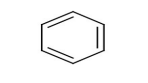
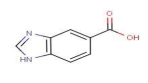
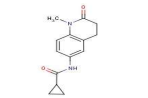
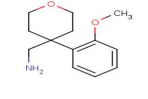
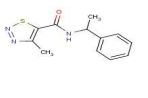
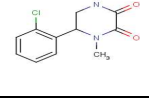
	VU0407731	First site		
	VU0408483	First site		
	VU0408762	First site		
	VU0408000	First site		
	VU0407468	First site		
	VU0407027	First site		
	VU0407524	First site		
	VU0407256	First site		
	VU0407173	First site		

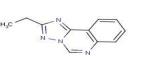
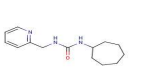
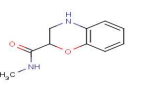
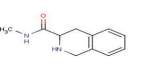
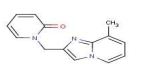
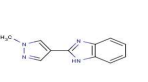
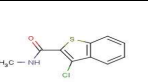
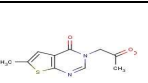
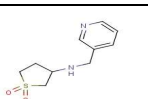
	VU0411708	First site		
	VU0410732	First site		
	VU0411971	First site		
	VU0411249	First site		
	VU0413131	First site		
	VU0412186	First site		
	VU0411180	First site		
	VU0411034	First site		
	VU0412827	First site		

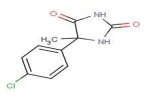
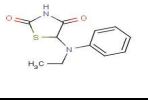
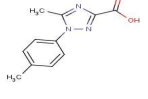
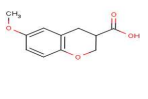
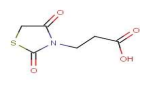
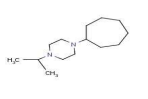
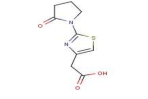
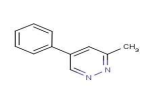
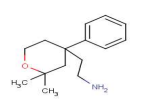
	VU0412042	First site		
	VU0413005	First site		
	VU0412073	First site		
	VU0412169	First site		
	VU0411685	First site		
	VU0412237	First site		
	VU0412455	First site		
	VU0410727	First site		
	VU0410552	First site		

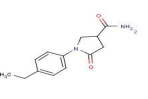
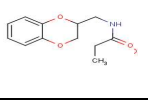
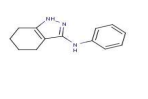
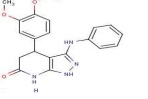
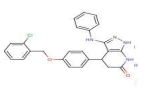
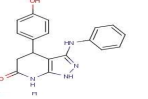
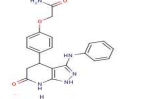
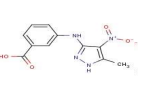
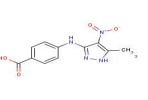
	VU0412995	First site		
	VU0410950	First site		
	VU0411163	First site		
	VU0410595	First site		
	VU0412752	First site		
	VU0413795	First site		
	VU0416412	First site		
	VU0416498	First site		
	VU0417488	First site		

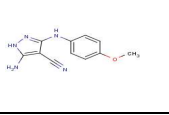
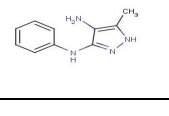
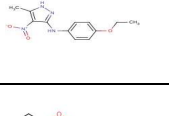
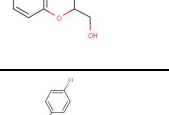
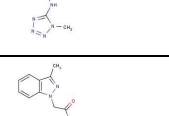
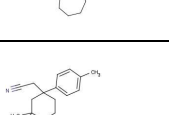
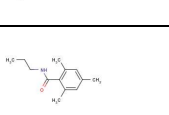
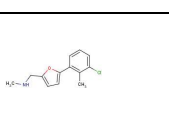

	VU0417580	First site		
	VU0417721	First site		
	VU0417235	First site		
	VU0417252	First site		
	VU0416461	First site		
	VU0416889	First site		
	VU0417272	First site		
	VU0415911	First site		
	VU0416835	First site		

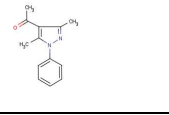
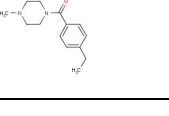
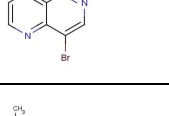
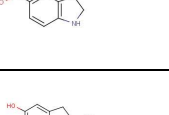
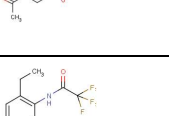
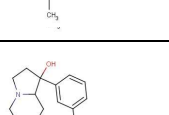
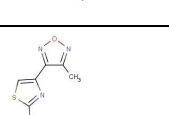
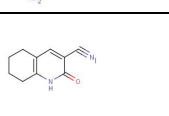

	VU0421419	First site		
	VU0421684	First site		
	VU0421265	First site		
	VU0421055	First site		
	VU0421344	First site		
	VU0421722	First site		
	VU0421698	First site		
	VU0421809	First site		
	VU0421569	First site		

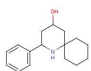
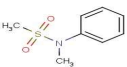
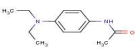
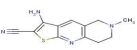
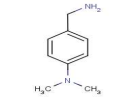
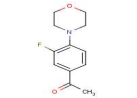
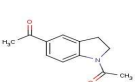
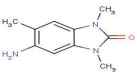
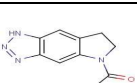
	VU0430240	First site		
	VU0430374	First site		
	VU0430252	First site		
	VU0430521	First site		
	VU0430498	First site		
	VU0430390	First site		
	VU0430393	First site		
	VU0431162	First site		
	VU0431257	First site		

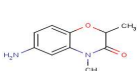
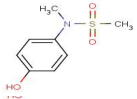
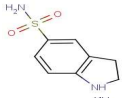
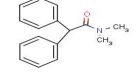
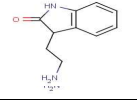
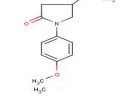
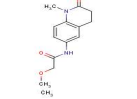
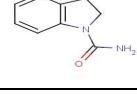
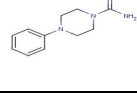
	VU0431103	First site		
	VU0433466	First site		
	VU0433008	First site		
	VU0432739	First site		
	VU0432814	First site		
	VU0433439	First site		
	VU0433209	First site		
	VU0433277	First site		
	VU0433035	First site		

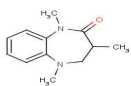
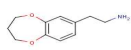
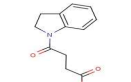
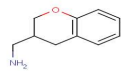
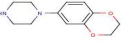
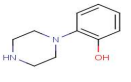
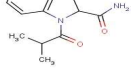
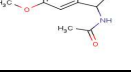
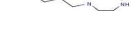
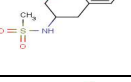
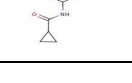
	VU0432862	First site		
	VU0433527	First site		
	VU0463883	First site		
	VU0463887	First site		
	VU0463888	First site		
	VU0463889	First site		
	VU0463890	First site		
	VU0463891	First site		
	VU0463892	First site		

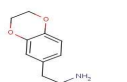
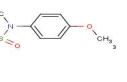
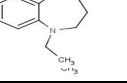
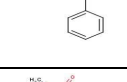
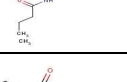
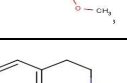
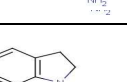
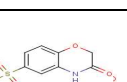

	VU0463893	First site		
	VU0463919	First site		
	VU0463942	First site		
	VU0052316	First site		
	VU0027407	First site		
	VU0417833	First site		
	VU0406701	First site		
	VU0407986	First site		
	VU0411292	First site		

	VU0004591	First site		
	VU0408426	First site		
	VU0421403	First site		
	VU0433064	First site		
	VU0431084	First site		
	VU0407098	First site		
	VU0411740	First site		
	VU0301954	First site		
	VU0408789	First site		

	VU0406535	First site		
	VU0053155	First site/ Second site	>1500	>1500
	VU0406618	First site/ Second site	525.33	510.00
	VU0407779	First site/ Second site	344.00	464.00
	VU0085250	Second site	163.00	117.00
	VU0005234	Second site	295.00	203.00
	VU0431163	Second site	449.00	332.00
	VU0432929	Second site	561.00	351.00
	VU0417826	Second site	>1500	311.00

	VU0432902	Second site	>1500	628.00
	VU0406329	Second site	>1500	1345.00
	VU0432916	Second site	>1500	>1500
	VU0406066	Second site		
	VU0430557	Second site		
	VU0433151	Second site		
	VU0421724	Second site		
	VU0118751	Second site		
	VU0416551	Second site		

	VU0137633	Second site		
	VU0432717	Second site		
	VU0117985	Second site		
	VU0430234	Second site		
	VU0433100	Second site		
	VU0413533	Second site		
	VU0421855	Second site		
	VU0407405	Second site		
	VU0432944	Second site		
	VU0417178	Second site		
	VU0421704	Second site		

	VU0432638	Second site		
	VU0407212	Second site		
	VU0070832	Second site		
	VU0430074	Second site		
	VU0417185	Second site		
	VU0433360	Second site		
	VU0433267	Second site		
	VU0415876	Second site		
	VU0431259	Second site		

REFERENCES

- 1 Howlader N, N. A., Krapcho M, Garshell J, Miller D, Altekruse SF, Kosary CL, Yu M, Ruhl J, Tatalovich Z, Mariotto A, Lewis DR, Chen HS, Feuer EJ, Cronin KA (eds). SEER Cancer Statistics Review, 1975-2012, National Cancer Institute.
- 2 Smith, B. D., Smith, G. L., Hurria, A., Hortobagyi, G. N. & Buchholz, T. A. Future of Cancer Incidence in the United States: Burdens Upon an Aging, Changing Nation. *J Clin Oncol* **27**, 2758-2765, doi:10.1200/Jco.2008.20.8983 (2009).
- 3 Weinstein, I. B. Cancer. Addiction to oncogenes--the Achilles heal of cancer. *Science* **297**, 63-64, doi:10.1126/science.1073096 (2002).
- 4 Weinstein, I. B. Disorders in cell circuitry during multistage carcinogenesis: the role of homeostasis. *Carcinogenesis* **21**, 857-864 (2000).
- 5 Druker, B. J. Imatinib as a paradigm of targeted therapies. *Adv Cancer Res* **91**, 1-30, doi:10.1016/S0065-230X(04)91001-9 (2004).
- 6 Arteaga, C. L. *et al.* Treatment of HER2-positive breast cancer: current status and future perspectives. *Nat Rev Clin Oncol* **9**, 16-32, doi:10.1038/nrclinonc.2011.177 (2012).
- 7 Sharma, S. V., Bell, D. W., Settleman, J. & Haber, D. A. Epidermal growth factor receptor mutations in lung cancer. *Nat Rev Cancer* **7**, 169-181, doi:10.1038/nrc2088 (2007).
- 8 Ashworth, A., Lord, C. J. & Reis-Filho, J. S. Genetic interactions in cancer progression and treatment. *Cell* **145**, 30-38, doi:10.1016/j.cell.2011.03.020 (2011).
- 9 Arteaga, C. L. Progress in breast cancer: overview. *Clin Cancer Res* **19**, 6353-6359, doi:10.1158/1078-0432.CCR-13-2549 (2013).
- 10 Haber, D. A., Gray, N. S. & Baselga, J. The evolving war on cancer. *Cell* **145**, 19-24, doi:10.1016/j.cell.2011.03.026 (2011).
- 11 Hanahan, D. & Weinberg, R. A. The hallmarks of cancer. *Cell* **100**, 57-70 (2000).
- 12 Bourne, H. R., Sanders, D. A. & McCormick, F. The GTPase superfamily: conserved structure and molecular mechanism. *Nature* **349**, 117-127, doi:10.1038/349117a0 (1991).
- 13 Wennerberg, K., Rossman, K. L. & Der, C. J. The Ras superfamily at a glance. *J Cell Sci* **118**, 843-846, doi:10.1242/jcs.01660 (2005).
- 14 Colicelli, J. Human RAS superfamily proteins and related GTPases. *Sci STKE* **2004**, RE13, doi:10.1126/stke.2502004re13 (2004).
- 15 Vigil, D., Cherfils, J., Rossman, K. L. & Der, C. J. Ras superfamily GEFs and GAPs: validated and tractable targets for cancer therapy? *Nat Rev Cancer* **10**, 842-857, doi:10.1038/nrc2960 (2010).
- 16 Milburn, M. V. *et al.* Molecular switch for signal transduction: structural differences between active and inactive forms of protooncogenic ras proteins. *Science* **247**, 939-945 (1990).
- 17 Neil, G. A. & Bruce, W. R. Experimental approaches to colon cancer prevention in humans. *Gastroenterol Clin North Am* **17**, 917-930 (1988).
- 18 Bos, J. L., Rehmann, H. & Wittinghofer, A. GEFs and GAPs: critical elements in the control of small G proteins. *Cell* **129**, 865-877, doi:10.1016/j.cell.2007.05.018 (2007).
- 19 Guo, X., Schrader, K. A., Xu, Y. & Schrader, J. W. Expression of a constitutively active mutant of M-Ras in normal bone marrow is sufficient for induction of a malignant

- mastocytosis/mast cell leukemia, distinct from the histiocytosis/monocytic leukemia induced by expression of activated H-Ras. *Oncogene* **24**, 2330-2342, doi:10.1038/sj.onc.1208441 (2005).
- 20 Neal, S. E., Eccleston, J. F., Hall, A. & Webb, M. R. Kinetic analysis of the hydrolysis of GTP by p21N-ras. The basal GTPase mechanism. *J Biol Chem* **263**, 19718-19722 (1988).
- 21 Schweins, T. *et al.* Substrate-assisted catalysis as a mechanism for GTP hydrolysis of p21ras and other GTP-binding proteins. *Nat Struct Biol* **2**, 36-44 (1995).
- 22 Scheffzek, K. *et al.* The Ras-RasGAP complex: structural basis for GTPase activation and its loss in oncogenic Ras mutants. *Science* **277**, 333-338 (1997).
- 23 Bernardis, A. & Settleman, J. GAPs in growth factor signalling. *Growth Factors* **23**, 143-149, doi:10.1080/08977190500130480 (2005).
- 24 Cichowski, K., Santiago, S., Jardim, M., Johnson, B. W. & Jacks, T. Dynamic regulation of the Ras pathway via proteolysis of the NF1 tumor suppressor. *Genes Dev* **17**, 449-454, doi:10.1101/gad.1054703 (2003).
- 25 McGillicuddy, L. T. *et al.* Proteasomal and genetic inactivation of the NF1 tumor suppressor in gliomagenesis. *Cancer Cell* **16**, 44-54, doi:10.1016/j.ccr.2009.05.009 (2009).
- 26 Boguski, M. S. & McCormick, F. Proteins regulating Ras and its relatives. *Nature* **366**, 643-654, doi:10.1038/366643a0 (1993).
- 27 Maertens, O. & Cichowski, K. An expanding role for RAS GTPase activating proteins (RAS GAPs) in cancer. *Adv Biol Regul* **55**, 1-14, doi:10.1016/j.jbior.2014.04.002 (2014).
- 28 Ehrhardt, A., Ehrhardt, G. R., Guo, X. & Schrader, J. W. Ras and relatives--job sharing and networking keep an old family together. *Exp Hematol* **30**, 1089-1106 (2002).
- 29 Bar-Sagi, D. & Feramisco, J. R. Microinjection of the ras oncogene protein into PC12 cells induces morphological differentiation. *Cell* **42**, 841-848 (1985).
- 30 Simon, M. A., Bowtell, D. D., Dodson, G. S., Laverty, T. R. & Rubin, G. M. Ras1 and a putative guanine nucleotide exchange factor perform crucial steps in signaling by the sevenless protein tyrosine kinase. *Cell* **67**, 701-716 (1991).
- 31 Han, M. & Sternberg, P. W. let-60, a gene that specifies cell fates during *C. elegans* vulval induction, encodes a ras protein. *Cell* **63**, 921-931 (1990).
- 32 Karnoub, A. E. & Weinberg, R. A. Ras oncogenes: split personalities. *Nat Rev Mol Cell Bio* **9**, 517-531, doi:DOI 10.1038/nrm2438 (2008).
- 33 Pai, E. F. *et al.* Structure of the guanine-nucleotide-binding domain of the Ha-ras oncogene product p21 in the triphosphate conformation. *Nature* **341**, 209-214, doi:10.1038/341209a0 (1989).
- 34 Rensland, H. *et al.* Substrate and product structural requirements for binding of nucleotides to H-ras p21: the mechanism of discrimination between guanosine and adenosine nucleotides. *Biochemistry* **34**, 593-599 (1995).
- 35 Vetter, I. R. & Wittinghofer, A. The guanine nucleotide-binding switch in three dimensions. *Science* **294**, 1299-1304, doi:10.1126/science.1062023 (2001).
- 36 Wittinghofer, A. & Vetter, I. R. Structure-function relationships of the G domain, a canonical switch motif. *Annu Rev Biochem* **80**, 943-971, doi:10.1146/annurev-biochem-062708-134043 (2011).
- 37 Stephen, A. G., Esposito, D., Bagni, R. K. & McCormick, F. Dragging ras back in the ring. *Cancer Cell* **25**, 272-281, doi:10.1016/j.ccr.2014.02.017 (2014).

- 38 Willumsen, B. M., Christensen, A., Hubbert, N. L., Papageorge, A. G. & Lowy, D. R. The p21 ras C-terminus is required for transformation and membrane association. *Nature* **310**, 583-586 (1984).
- 39 Jackson, J. H. *et al.* Farnesol modification of Kirsten-ras exon 4B protein is essential for transformation. *Proc Natl Acad Sci U S A* **87**, 3042-3046 (1990).
- 40 Casey, P. J., Solski, P. A., Der, C. J. & Buss, J. E. p21ras is modified by a farnesyl isoprenoid. *Proc Natl Acad Sci U S A* **86**, 8323-8327 (1989).
- 41 Schaber, M. D. *et al.* Polyisoprenylation of Ras in vitro by a farnesyl-protein transferase. *J Biol Chem* **265**, 14701-14704 (1990).
- 42 Fivaz, M. & Meyer, T. Reversible intracellular translocation of KRas but not HRas in hippocampal neurons regulated by Ca²⁺/calmodulin. *J Cell Biol* **170**, 429-441, doi:10.1083/jcb.200409157 (2005).
- 43 Paz, A., Haklai, R., Elad-Sfadia, G., Ballan, E. & Kloog, Y. Galectin-1 binds oncogenic H-Ras to mediate Ras membrane anchorage and cell transformation. *Oncogene* **20**, 7486-7493, doi:10.1038/sj.onc.1204950 (2001).
- 44 Lopez-Alcala, C. *et al.* Identification of essential interacting elements in K-Ras/calmodulin binding and its role in K-Ras localization. *J Biol Chem* **283**, 10621-10631, doi:10.1074/jbc.M706238200 (2008).
- 45 Mitin, N., Rossman, K. L. & Der, C. J. Signaling interplay in Ras superfamily function. *Curr Biol* **15**, R563-574, doi:10.1016/j.cub.2005.07.010 (2005).
- 46 Fernandez-Garcia, B. *et al.* p73 cooperates with Ras in the activation of MAP kinase signaling cascade. *Cell Death and Differentiation* **14**, 254-265, doi:DOI 10.1038/sj.cdd.4401945 (2007).
- 47 Dower, N. A. *et al.* RasGRP essential for mouse thymocyte differentiation and TCR signaling. *Nat Immunol* **1**, 317-321 (2000).
- 48 Mitin, N., Rossman, K. L. & Der, C. J. Signaling interplay in Ras superfamily function. *Current Biology* **15**, R563-R574, doi:DOI 10.1016/j.cub.2005.07.010 (2005).
- 49 Repasky, G. A., Chenette, E. J. & Der, C. J. Renewing the conspiracy theory debate: does Raf function alone to mediate Ras oncogenesis? *Trends Cell Biol* **14**, 639-647, doi:10.1016/j.tcb.2004.09.014 (2004).
- 50 McCormick, F. & Wittinghofer, A. Interactions between Ras proteins and their effectors. *Curr Opin Biotechnol* **7**, 449-456 (1996).
- 51 Zhang, X. F. *et al.* Normal and oncogenic p21ras proteins bind to the amino-terminal regulatory domain of c-Raf-1. *Nature* **364**, 308-313, doi:10.1038/364308a0 (1993).
- 52 Rodriguez-Viciana, P., Warne, P. H., Vanhaesebroeck, B., Waterfield, M. D. & Downward, J. Activation of phosphoinositide 3-kinase by interaction with Ras and by point mutation. *EMBO J* **15**, 2442-2451 (1996).
- 53 Malliri, A. *et al.* Mice deficient in the Rac activator Tiam1 are resistant to Ras-induced skin tumours. *Nature* **417**, 867-871, doi:10.1038/nature00848 (2002).
- 54 Mitin, N. Y. *et al.* Identification and characterization of rain, a novel Ras-interacting protein with a unique subcellular localization. *J Biol Chem* **279**, 22353-22361, doi:10.1074/jbc.M312867200 (2004).
- 55 Cox, A. D. & Der, C. J. Ras family signaling: therapeutic targeting. *Cancer Biol Ther* **1**, 599-606 (2002).

- 56 Vogelstein, B. *et al.* Cancer genome landscapes. *Science* **339**, 1546-1558, doi:10.1126/science.1235122 (2013).
- 57 Pylayeva-Gupta, Y., Grabocka, E. & Bar-Sagi, D. RAS oncogenes: weaving a tumorigenic web. *Nat Rev Cancer* **11**, 761-774, doi:10.1038/nrc3106 (2011).
- 58 Prior, I. A., Lewis, P. D. & Mattos, C. A comprehensive survey of Ras mutations in cancer. *Cancer Res* **72**, 2457-2467, doi:10.1158/0008-5472.CAN-11-2612 (2012).
- 59 Gremer, L., Gilsbach, B., Ahmadian, M. R. & Wittinghofer, A. Fluoride complexes of oncogenic Ras mutants to study the Ras-RasGap interaction. *Biol Chem* **389**, 1163-1171, doi:10.1515/BC.2008.132 (2008).
- 60 Buhrman, G., Kumar, V. S., Cirit, M., Haugh, J. M. & Mattos, C. Allosteric modulation of Ras-GTP is linked to signal transduction through RAF kinase. *J Biol Chem* **286**, 3323-3331, doi:10.1074/jbc.M110.193854 (2011).
- 61 Buhrman, G., Holzapfel, G., Fetcs, S. & Mattos, C. Allosteric modulation of Ras positions Q61 for a direct role in catalysis. *Proc Natl Acad Sci U S A* **107**, 4931-4936, doi:10.1073/pnas.0912226107 (2010).
- 62 Samatar, A. A. & Poulidakos, P. I. Targeting RAS-ERK signalling in cancer: promises and challenges. *Nat Rev Drug Discov* **13**, 928-942, doi:10.1038/nrd4281 (2014).
- 63 Aguirre, A. J. *et al.* Activated Kras and Ink4a/Arf deficiency cooperate to produce metastatic pancreatic ductal adenocarcinoma. *Genes Dev* **17**, 3112-3126, doi:10.1101/gad.1158703 (2003).
- 64 Johnson, L. *et al.* Somatic activation of the K-ras oncogene causes early onset lung cancer in mice. *Nature* **410**, 1111-1116, doi:10.1038/35074129 (2001).
- 65 Haigis, K. M. *et al.* Differential effects of oncogenic K-Ras and N-Ras on proliferation, differentiation and tumor progression in the colon. *Nat Genet* **40**, 600-608, doi:10.1038/ng.115 (2008).
- 66 Chin, L. *et al.* Essential role for oncogenic Ras in tumour maintenance. *Nature* **400**, 468-472, doi:10.1038/22788 (1999).
- 67 Podsypanina, K., Politi, K., Beverly, L. J. & Varmus, H. E. Oncogene cooperation in tumor maintenance and tumor recurrence in mouse mammary tumors induced by Myc and mutant Kras. *Proc Natl Acad Sci U S A* **105**, 5242-5247, doi:10.1073/pnas.0801197105 (2008).
- 68 Arkin, M. R. & Wells, J. A. Small-molecule inhibitors of protein-protein interactions: progressing towards the dream. *Nat Rev Drug Discov* **3**, 301-317, doi:10.1038/nrd1343 (2004).
- 69 Cox, A. D., Fesik, S. W., Kimmelman, A. C., Luo, J. & Der, C. J. Drugging the undruggable RAS: Mission possible? *Nat Rev Drug Discov* **13**, 828-851, doi:10.1038/nrd4389 (2014).
- 70 Willumsen, B. M., Norris, K., Papageorge, A. G., Hubbert, N. L. & Lowy, D. R. Harvey murine sarcoma virus p21 ras protein: biological and biochemical significance of the cysteine nearest the carboxy terminus. *EMBO J* **3**, 2581-2585 (1984).
- 71 Whyte, D. B. *et al.* K- and N-Ras are geranylgeranylated in cells treated with farnesyl protein transferase inhibitors. *J Biol Chem* **272**, 14459-14464 (1997).
- 72 Rowell, C. A., Kowalczyk, J. J., Lewis, M. D. & Garcia, A. M. Direct demonstration of geranylgeranylation and farnesylation of Ki-Ras in vivo. *J Biol Chem* **272**, 14093-14097 (1997).

- 73 Uehling, D. E. & Harris, P. A. Recent progress on MAP kinase pathway inhibitors. *Bioorg Med Chem Lett*, doi:10.1016/j.bmcl.2015.07.093 (2015).
- 74 Yu, B. & Luo, J. Synthetic lethal genetic screens in Ras mutant cancers. *Enzymes* **34 Pt. B**, 201-219, doi:10.1016/B978-0-12-420146-0.00009-3 (2013).
- 75 Ostrem, J. M., Peters, U., Sos, M. L., Wells, J. A. & Shokat, K. M. K-Ras(G12C) inhibitors allosterically control GTP affinity and effector interactions. *Nature* **503**, 548-551, doi:10.1038/nature12796 (2013).
- 76 Sun, Q. *et al.* Discovery of small molecules that bind to K-Ras and inhibit Sos-mediated activation. *Angew Chem Int Ed Engl* **51**, 6140-6143, doi:10.1002/anie.201201358 (2012).
- 77 Maurer, T. *et al.* Small-molecule ligands bind to a distinct pocket in Ras and inhibit SOS-mediated nucleotide exchange activity. *Proc Natl Acad Sci U S A* **109**, 5299-5304, doi:10.1073/pnas.1116510109 (2012).
- 78 Erlanson, D. A. Introduction to fragment-based drug discovery. *Top Curr Chem* **317**, 1-32, doi:10.1007/128_2011_180 (2012).
- 79 Scott, D. E., Coyne, A. G., Hudson, S. A. & Abell, C. Fragment-based approaches in drug discovery and chemical biology. *Biochemistry* **51**, 4990-5003, doi:10.1021/bi3005126 (2012).
- 80 Wang, F., Fesik, S. Discovery of inhibitors of protein-protein interactions using fragment-based methods. (2015).
- 81 Bollag, G. *et al.* Clinical efficacy of a RAF inhibitor needs broad target blockade in BRAF-mutant melanoma. *Nature* **467**, 596-599, doi:10.1038/nature09454 (2010).
- 82 Woodhead, A. J. *et al.* Discovery of (2,4-dihydroxy-5-isopropylphenyl)-[5-(4-methylpiperazin-1-ylmethyl)-1,3-dihydrois oindol-2-yl]methanone (AT13387), a novel inhibitor of the molecular chaperone Hsp90 by fragment based drug design. *J Med Chem* **53**, 5956-5969, doi:10.1021/jm100060b (2010).
- 83 Oltersdorf, T. *et al.* An inhibitor of Bcl-2 family proteins induces regression of solid tumours. *Nature* **435**, 677-681, doi:10.1038/nature03579 (2005).
- 84 Harner, M. J., Frank, A. O. & Fesik, S. W. Fragment-based drug discovery using NMR spectroscopy. *J Biomol NMR* **56**, 65-75, doi:10.1007/s10858-013-9740-z (2013).
- 85 Kobayashi, M. *et al.* Target immobilization as a strategy for NMR-based fragment screening: comparison of TINS, STD, and SPR for fragment hit identification. *J Biomol Screen* **15**, 978-989, doi:10.1177/1087057110375614 (2010).
- 86 Fink, T. & Reymond, J. L. Virtual exploration of the chemical universe up to 11 atoms of C, N, O, F: Assembly of 26.4 million structures (110.9 million stereoisomers) and analysis for new ring systems, stereochemistry, physicochemical properties, compound classes, and drug discovery. *J Chem Inf Model* **47**, 342-353, doi:DOI 10.1021/ci600423u (2007).
- 87 Hann, M. M., Leach, A. R. & Harper, G. Molecular complexity and its impact on the probability of finding leads for drug discovery. *J Chem Inf Comp Sci* **41**, 856-864, doi:DOI 10.1021/ci000403i (2001).
- 88 Keseru, G. M. & Makara, G. M. The influence of lead discovery strategies on the properties of drug candidates. *Nature Reviews Drug Discovery* **8**, 203-212, doi:DOI 10.1038/nrd2796 (2009).
- 89 Scott, D. E. *et al.* Using a Fragment-Based Approach To Target Protein-Protein Interactions. *Chembiochem* **14**, 332-342, doi:DOI 10.1002/cbic.201200521 (2013).

- 90 Friberg, A. *et al.* Discovery of potent myeloid cell leukemia 1 (Mcl-1) inhibitors using fragment-based methods and structure-based design. *J Med Chem* **56**, 15-30, doi:10.1021/jm301448p (2013).
- 91 Shuker, S. B., Hajduk, P. J., Meadows, R. P. & Fesik, S. W. Discovering high-affinity ligands for proteins: SAR by NMR. *Science* **274**, 1531-1534 (1996).
- 92 O'Connor, C. & Kovrigin, E. L. Assignments of backbone (1)H, (1)(3)C and (1)(5)N resonances in H-Ras (1-166) complexed with GppNHp at physiological pH. *Biomol NMR Assign* **6**, 91-93, doi:10.1007/s12104-011-9332-3 (2012).
- 93 Ito, Y. *et al.* Regional polysterism in the GTP-bound form of the human c-Ha-Ras protein. *Biochemistry* **36**, 9109-9119, doi:10.1021/bi970296u (1997).
- 94 Reich, H. Structure Determination Using NMR. (2015).
- 95 Vo, U., Embrey, K. J., Breeze, A. L. & Golovanov, A. P. (1)H, (1)(3)C and (1)(5)N resonance assignment for the human K-Ras at physiological pH. *Biomol NMR Assign* **7**, 215-219, doi:10.1007/s12104-012-9413-y (2013).
- 96 Buhrman, G. *et al.* Analysis of binding site hot spots on the surface of Ras GTPase. *J Mol Biol* **413**, 773-789, doi:10.1016/j.jmb.2011.09.011 (2011).
- 97 Hajduk, P. J., Huth, J. R. & Fesik, S. W. Druggability indices for protein targets derived from NMR-based screening data. *J Med Chem* **48**, 2518-2525, doi:10.1021/jm049131r (2005).
- 98 Hwang, M. C., Sung, Y. J. & Hwang, Y. W. The differential effects of the Gly-60 to Ala mutation on the interaction of H-Ras p21 with different downstream targets. *J Biol Chem* **271**, 8196-8202 (1996).
- 99 Ong, C. C. *et al.* p21-activated kinase 1: PAK'ed with potential. *Oncotarget* **2**, 491-496 (2011).
- 100 Arias-Romero, L. E. & Chernoff, J. A tale of two Paks. *Biol Cell* **100**, 97-108, doi:10.1042/BC20070109 (2008).
- 101 Ma, Q. L., Yang, F., Frautschy, S. A. & Cole, G. M. PAK in Alzheimer disease, Huntington disease and X-linked mental retardation. *Cell Logist* **2**, 117-125, doi:10.4161/cl.21602 (2012).
- 102 Kelly, M. L. & Chernoff, J. Mouse models of PAK function. *Cell Logist* **2**, 84-88, doi:10.4161/cl.21381 (2012).
- 103 Allen, J. D. *et al.* p21-activated kinase regulates mast cell degranulation via effects on calcium mobilization and cytoskeletal dynamics. *Blood* **113**, 2695-2705, doi:10.1182/blood-2008-06-160861 (2009).
- 104 Chiang, Y. T. & Jin, T. p21-Activated protein kinases and their emerging roles in glucose homeostasis. *Am J Physiol Endocrinol Metab* **306**, E707-722, doi:10.1152/ajpendo.00506.2013 (2014).
- 105 Ke, Y., Lei, M., Wang, X. & Solaro, R. J. Novel roles of PAK1 in the heart. *Cell Logist* **2**, 89-94, doi:10.4161/cl.21497 (2012).
- 106 Rudolph, J., Crawford, J. J., Hoeflich, K. P. & Wang, W. Inhibitors of p21-activated kinases (PAKs). *J Med Chem* **58**, 111-129, doi:10.1021/jm501613q (2015).
- 107 Zenke, F. T., King, C. C., Bohl, B. P. & Bokoch, G. M. Identification of a central phosphorylation site in p21-activated kinase regulating autoinhibition and kinase activity. *J Biol Chem* **274**, 32565-32573 (1999).

- 108 Sells, M. A. & Chernoff, J. Emerging from the PAK: The p21-activated protein kinase family. *Trends in Cell Biology* **7**, 162-167, doi:Doi 10.1016/S0962-8924(97)01003-9 (1997).
- 109 Dummler, B., Ohshiro, K., Kumar, R. & Field, J. Pak protein kinases and their role in cancer. *Cancer Metastasis Rev* **28**, 51-63, doi:10.1007/s10555-008-9168-1 (2009).
- 110 Gatti, A., Huang, Z., Tuazon, P. T. & Traugh, J. A. Multisite autophosphorylation of p21-activated protein kinase gamma-PAK as a function of activation. *J Biol Chem* **274**, 8022-8028 (1999).
- 111 Walter, B. N. *et al.* Cleavage and activation of p21-activated protein kinase gamma-PAK by CPP32 (caspase 3). Effects of autophosphorylation on activity. *J Biol Chem* **273**, 28733-28739 (1998).
- 112 Puto, L. A., Pestonjamp, K., King, C. C. & Bokoch, G. M. p21-activated kinase 1 (PAK1) interacts with the Grb2 adapter protein to couple to growth factor signaling. *J Biol Chem* **278**, 9388-9393, doi:10.1074/jbc.M208414200 (2003).
- 113 Manser, E. *et al.* PAK kinases are directly coupled to the PIX family of nucleotide exchange factors. *Mol Cell* **1**, 183-192 (1998).
- 114 Rosenberger, G. & Kutsche, K. AlphaPIX and betaPIX and their role in focal adhesion formation. *Eur J Cell Biol* **85**, 265-274, doi:10.1016/j.ejcb.2005.10.007 (2006).
- 115 Bokoch, G. M. *et al.* A GTPase-independent mechanism of p21-activated kinase activation. Regulation by sphingosine and other biologically active lipids. *J Biol Chem* **273**, 8137-8144 (1998).
- 116 Abo, A. *et al.* PAK4, a novel effector for Cdc42Hs, is implicated in the reorganization of the actin cytoskeleton and in the formation of filopodia. *EMBO J* **17**, 6527-6540, doi:10.1093/emboj/17.22.6527 (1998).
- 117 Baskaran, Y., Ng, Y. W., Selamat, W., Ling, F. T. & Manser, E. Group I and II mammalian PAKs have different modes of activation by Cdc42. *EMBO Rep* **13**, 653-659, doi:10.1038/embor.2012.75 (2012).
- 118 Ha, B. H. *et al.* Type II p21-activated kinases (PAKs) are regulated by an autoinhibitory pseudosubstrate. *Proc Natl Acad Sci U S A* **109**, 16107-16112, doi:10.1073/pnas.1214447109 (2012).
- 119 King, H., Nicholas, N. S. & Wells, C. M. Role of p-21-activated kinases in cancer progression. *Int Rev Cell Mol Biol* **309**, 347-387, doi:10.1016/B978-0-12-800255-1.00007-7 (2014).
- 120 Wang, Z. *et al.* p21-activated kinase 1 (PAK1) can promote ERK activation in a kinase-independent manner. *J Biol Chem* **288**, 20093-20099, doi:10.1074/jbc.M112.426023 (2013).
- 121 Higuchi, M., Onishi, K., Kikuchi, C. & Gotoh, Y. Scaffolding function of PAK in the PDK1-Akt pathway. *Nat Cell Biol* **10**, 1356-1364, doi:10.1038/ncb1795 (2008).
- 122 Ong, C. C. *et al.* Targeting p21-activated kinase 1 (PAK1) to induce apoptosis of tumor cells. *Proc Natl Acad Sci U S A* **108**, 7177-7182, doi:10.1073/pnas.1103350108 (2011).
- 123 Kumar, R., Gururaj, A. E. & Barnes, C. J. p21-activated kinases in cancer. *Nat Rev Cancer* **6**, 459-471, doi:10.1038/nrc1892 (2006).
- 124 Balasenthil, S. *et al.* p21-activated kinase-1 signaling mediates cyclin D1 expression in mammary epithelial and cancer cells. *J Biol Chem* **279**, 1422-1428, doi:10.1074/jbc.M309937200 (2004).

- 125 Ye, D. Z. & Field, J. PAK signaling in cancer. *Cell Logist* **2**, 105-116, doi:10.4161/cl.21882 (2012).
- 126 Whale, A. D., Dart, A., Holt, M., Jones, G. E. & Wells, C. M. PAK4 kinase activity and somatic mutation promote carcinoma cell motility and influence inhibitor sensitivity. *Oncogene* **32**, 2114-2120, doi:10.1038/onc.2012.233 (2013).
- 127 Fawdar, S. *et al.* Targeted genetic dependency screen facilitates identification of actionable mutations in FGFR4, MAP3K9, and PAK5 in lung cancer. *Proc Natl Acad Sci U S A* **110**, 12426-12431, doi:10.1073/pnas.1305207110 (2013).
- 128 Radu, M., Semenova, G., Kosoff, R. & Chernoff, J. PAK signalling during the development and progression of cancer. *Nat Rev Cancer* **14**, 13-25 (2014).
- 129 Huynh, N., Liu, K. H., Baldwin, G. S. & He, H. P21-activated kinase 1 stimulates colon cancer cell growth and migration/invasion via ERK- and AKT-dependent pathways. *Biochim Biophys Acta* **1803**, 1106-1113, doi:10.1016/j.bbamcr.2010.05.007 (2010).
- 130 Arias-Romero, L. E. *et al.* A Rac-Pak signaling pathway is essential for ErbB2-mediated transformation of human breast epithelial cancer cells. *Oncogene* **29**, 5839-5849, doi:10.1038/onc.2010.318 (2010).
- 131 Park, E. R., Eblen, S. T. & Catling, A. D. MEK1 activation by PAK: a novel mechanism. *Cell Signal* **19**, 1488-1496, doi:10.1016/j.cellsig.2007.01.018 (2007).
- 132 Wang, R. A., Mazumdar, A., Vadlamudi, R. K. & Kumar, R. P21-activated kinase-1 phosphorylates and transactivates estrogen receptor-alpha and promotes hyperplasia in mammary epithelium. *EMBO J* **21**, 5437-5447 (2002).
- 133 Liotta, L. A. Tumor invasion and metastases--role of the extracellular matrix: Rhoads Memorial Award lecture. *Cancer Res* **46**, 1-7 (1986).
- 134 Ayala, I. *et al.* Multiple regulatory inputs converge on cortactin to control invadopodia biogenesis and extracellular matrix degradation. *J Cell Sci* **121**, 369-378, doi:10.1242/jcs.008037 (2008).
- 135 Dummler, B. & Field, J. Amplifying Pak kinases. *Cancer Biol Ther* **7**, 1803-1805 (2008).
- 136 Sells, M. A., Pfaff, A. & Chernoff, J. Temporal and spatial distribution of activated Pak1 in fibroblasts. *J Cell Biol* **151**, 1449-1458 (2000).
- 137 Sipes, N. S. *et al.* Cdc42 regulates extracellular matrix remodeling in three dimensions. *J Biol Chem* **286**, 36469-36477, doi:10.1074/jbc.M111.283176 (2011).
- 138 Schurmann, A. *et al.* p21-activated kinase 1 phosphorylates the death agonist bad and protects cells from apoptosis. *Mol Cell Biol* **20**, 453-461 (2000).
- 139 Shrestha, Y. *et al.* PAK1 is a breast cancer oncogene that coordinately activates MAPK and MET signaling. *Oncogene* **31**, 3397-3408, doi:10.1038/onc.2011.515 (2012).
- 140 Wang, Z. *et al.* Rac1 is crucial for Ras-dependent skin tumor formation by controlling Pak1-Mek-Erk hyperactivation and hyperproliferation in vivo. *Oncogene* **29**, 3362-3373, doi:10.1038/onc.2010.95 (2010).
- 141 Wang, R. A., Zhang, H., Balasenthil, S., Medina, D. & Kumar, R. PAK1 hyperactivation is sufficient for mammary gland tumor formation. *Oncogene* **25**, 2931-2936, doi:10.1038/sj.onc.1209309 (2006).
- 142 Callow, M. G. *et al.* Requirement for PAK4 in the anchorage-independent growth of human cancer cell lines. *J Biol Chem* **277**, 550-558, doi:10.1074/jbc.M105732200 (2002).

- 143 Tang, Y. *et al.* Kinase-deficient Pak1 mutants inhibit Ras transformation of Rat-1 fibroblasts. *Mol Cell Biol* **17**, 4454-4464 (1997).
- 144 Bostner, J. *et al.* Amplification of CCND1 and PAK1 as predictors of recurrence and tamoxifen resistance in postmenopausal breast cancer. *Oncogene* **26**, 6997-7005, doi:10.1038/sj.onc.1210506 (2007).
- 145 Holm, C. *et al.* Association between Pak1 expression and subcellular localization and tamoxifen resistance in breast cancer patients. *J Natl Cancer Inst* **98**, 671-680, doi:10.1093/jnci/djj185 (2006).
- 146 Goc, A. *et al.* P21 activated kinase-1 (Pak1) promotes prostate tumor growth and microinvasion via inhibition of transforming growth factor beta expression and enhanced matrix metalloproteinase 9 secretion. *J Biol Chem* **288**, 3025-3035, doi:10.1074/jbc.M112.424770 (2013).
- 147 Lei, M. *et al.* Structure of PAK1 in an autoinhibited conformation reveals a multistage activation switch. *Cell* **102**, 387-397 (2000).
- 148 Lei, M., Robinson, M. A. & Harrison, S. C. The active conformation of the PAK1 kinase domain. *Structure* **13**, 769-778, doi:10.1016/j.str.2005.03.007 (2005).
- 149 Zhang, J., Yang, P. L. & Gray, N. S. Targeting cancer with small molecule kinase inhibitors. *Nat Rev Cancer* **9**, 28-39, doi:10.1038/nrc2559 (2009).
- 150 Xing, L., Rai, B. & Lunney, E. A. Scaffold mining of kinase hinge binders in crystal structure database. *J Comput Aided Mol Des* **28**, 13-23, doi:10.1007/s10822-013-9700-4 (2014).
- 151 Cohen, P. & Alessi, D. R. Kinase drug discovery--what's next in the field? *ACS Chem Biol* **8**, 96-104, doi:10.1021/cb300610s (2013).
- 152 Noble, M. E., Endicott, J. A. & Johnson, L. N. Protein kinase inhibitors: insights into drug design from structure. *Science* **303**, 1800-1805, doi:10.1126/science.1095920 (2004).
- 153 Dar, A. C. & Shokat, K. M. The evolution of protein kinase inhibitors from antagonists to agonists of cellular signaling. *Annu Rev Biochem* **80**, 769-795, doi:10.1146/annurev-biochem-090308-173656 (2011).
- 154 Liu, Y. & Gray, N. S. Rational design of inhibitors that bind to inactive kinase conformations. *Nat Chem Biol* **2**, 358-364, doi:10.1038/nchembio799 (2006).
- 155 Cohen, P. Protein kinases--the major drug targets of the twenty-first century? *Nat Rev Drug Discov* **1**, 309-315, doi:10.1038/nrd773 (2002).
- 156 Schindler, T. *et al.* Structural mechanism for STI-571 inhibition of abelson tyrosine kinase. *Science* **289**, 1938-1942 (2000).
- 157 Ohren, J. F. *et al.* Structures of human MAP kinase kinase 1 (MEK1) and MEK2 describe novel noncompetitive kinase inhibition. *Nat Struct Mol Biol* **11**, 1192-1197, doi:10.1038/nsmb859 (2004).
- 158 Knight, Z. A. & Shokat, K. M. Features of selective kinase inhibitors. *Chem Biol* **12**, 621-637, doi:10.1016/j.chembiol.2005.04.011 (2005).
- 159 Karaman, M. W. *et al.* A quantitative analysis of kinase inhibitor selectivity. *Nature Biotechnology* **26**, 127-132, doi:DOI 10.1038/nbt1358 (2008).
- 160 Maksimoska, J. *et al.* Targeting Large Kinase Active Site with Rigid, Bulky Octahedral Ruthenium Complexes. *Journal of the American Chemical Society* **130**, 15764-+, doi:DOI 10.1021/ja805555a (2008).

- 161 Guo, C. X. *et al.* Discovery of Pyrroloaminopyrazoles as Novel PAK Inhibitors. *Journal of Medicinal Chemistry* **55**, 4728-4739, doi:DOI 10.1021/jm300204j (2012).
- 162 Murray, B. W. *et al.* Small-molecule p21-activated kinase inhibitor PF-3758309 is a potent inhibitor of oncogenic signaling and tumor growth. *Proc Natl Acad Sci U S A* **107**, 9446-9451, doi:10.1073/pnas.0911863107 (2010).
- 163 Licciulli, S. *et al.* FRAX597, a small molecule inhibitor of the p21-activated kinases, inhibits tumorigenesis of neurofibromatosis type 2 (NF2)-associated Schwannomas. *J Biol Chem* **288**, 29105-29114, doi:10.1074/jbc.M113.510933 (2013).
- 164 Staff, E. Genentech Buys Afraxis Compound Rights for Up to \$187.5M. *Genetic Engineering & Biotechnology News* (2013). <<http://www.genengnews.com/gen-news-highlights/genentech-buys-afraxis-compound-rights-for-up-to-187-5m/81247918/>>.
- 165 Ong, C. C. *et al.* Small molecule inhibition of group I p21-activated kinases in breast cancer induces apoptosis and potentiates the activity of microtubule stabilizing agents. *Breast Cancer Res* **17**, 59, doi:10.1186/s13058-015-0564-5 (2015).
- 166 Chow, H.-Y. D., B.; Duron, S. G.; Campbell, D. A.; Ong, C. & C.; Hoeflich, K. P. C., L.-S.; Welling, D. B.; Yang, Z.-J.; Chernoff, J. Unpublished.
- 167 patent, A. Patent.
- 168 Abdel-Magid, A. F. PAK1: A Therapeutic Target for Cancer Treatment. *Acs Medicinal Chemistry Letters* **4**, 431-432, doi:DOI 10.1021/ml400101g (2013).
- 169 McCoull, W. *et al.* Identification and optimisation of 7-azaindole PAK1 inhibitors with improved potency and kinase selectivity. *Medchemcomm* **5**, 1533-1539, doi:DOI 10.1039/c4md00280f (2014).
- 170 Viaud, J. & Peterson, J. R. An allosteric kinase inhibitor binds the p21-activated kinase autoregulatory domain covalently. *Molecular Cancer Therapeutics* **8**, 2559-2565, doi:Doi 10.1158/1535-7163.Mct-09-0102 (2009).
- 171 Tsai, J. *et al.* Discovery of a selective inhibitor of oncogenic B-Raf kinase with potent antimelanoma activity. *Proc Natl Acad Sci U S A* **105**, 3041-3046, doi:10.1073/pnas.0711741105 (2008).
- 172 Pirruccello, M. *et al.* A dimeric kinase assembly underlying autophosphorylation in the p21 activated kinases. *J Mol Biol* **361**, 312-326, doi:10.1016/j.jmb.2006.06.017 (2006).
- 173 Begley, D. W., Moen, S. O., Pierce, P. G. & Zartler, E. R. Saturation transfer difference NMR for fragment screening. *Curr Protoc Chem Biol* **5**, 251-268, doi:10.1002/9780470559277.ch130118 (2013).
- 174 Mayer, M. & Meyer, B. Characterization of ligand binding by saturation transfer difference NMR spectroscopy. *Angew Chem Int Edit* **38**, 1784-1788, doi:Doi 10.1002/(Sici)1521-3773(19990614)38:12<1784::Aid-Anie1784>3.0.Co;2-Q (1999).
- 175 Souza-Fagundes, E. M. *et al.* A high-throughput fluorescence polarization anisotropy assay for the 70N domain of replication protein A. *Anal Biochem* **421**, 742-749, doi:10.1016/j.ab.2011.11.025 (2012).
- 176 Ha, B. H., Morse, E. M., Turk, B. E. & Boggon, T. J. Signaling, Regulation, and Specificity of the Type II p21-activated Kinases. *J Biol Chem* **290**, 12975-12983, doi:10.1074/jbc.R115.650416 (2015).

- 177 Anastassiadis, T., Deacon, S. W., Devarajan, K., Ma, H. & Peterson, J. R. Comprehensive assay of kinase catalytic activity reveals features of kinase inhibitor selectivity. *Nat Biotechnol* **29**, 1039-1045, doi:10.1038/nbt.2017 (2011).
- 178 Davis, M. I. *et al.* Comprehensive analysis of kinase inhibitor selectivity. *Nat Biotechnol* **29**, 1046-1051, doi:10.1038/nbt.1990 (2011).
- 179 Becattini, B. & Pellecchia, M. SAR by ILOEs: An NMIR-based approach to reverse chemical genetics. *Chem-Eur J* **12**, 2658-2662, doi:DOI 10.1002/chem.200500636 (2006).
- 180 Murray, B. W. *et al.* Small-molecule p21-activated kinase inhibitor PF-3758309 is a potent inhibitor of oncogenic signaling and tumor growth. *P Natl Acad Sci USA* **107**, 9446-9451, doi:DOI 10.1073/pnas.0911863107 (2010).
- 181 Beeser, A., Jaffer, Z. M., Hofmann, C. & Chernoff, J. Role of group A p21-activated kinases in activation of extracellular-regulated kinase by growth factors. *J Biol Chem* **280**, 36609-36615, doi:10.1074/jbc.M502306200 (2005).
- 182 Coles, L. C. & Shaw, P. E. PAK1 primes MEK1 for phosphorylation by Raf-1 kinase during cross-cascade activation of the ERK pathway. *Oncogene* **21**, 2236-2244, doi:10.1038/sj.onc.1205302 (2002).
- 183 Frost, J. A., Xu, S., Hutchison, M. R., Marcus, S. & Cobb, M. H. Actions of Rho family small G proteins and p21-activated protein kinases on mitogen-activated protein kinase family members. *Mol Cell Biol* **16**, 3707-3713 (1996).
- 184 Kissil, J. L., Johnson, K. C., Eckman, M. S. & Jacks, T. Merlin phosphorylation by p21-activated kinase 2 and effects of phosphorylation on merlin localization. *J Biol Chem* **277**, 10394-10399, doi:10.1074/jbc.M200083200 (2002).
- 185 Xiao, G. H., Beeser, A., Chernoff, J. & Testa, J. R. p21-activated kinase links Rac/Cdc42 signaling to merlin. *J Biol Chem* **277**, 883-886, doi:10.1074/jbc.C100553200 (2002).
- 186 Alfthan, K., Heiska, L., Gronholm, M., Renkema, G. H. & Carpen, O. Cyclic AMP-dependent protein kinase phosphorylates merlin at serine 518 independently of p21-activated kinase and promotes merlin-ezrin heterodimerization. *J Biol Chem* **279**, 18559-18566, doi:10.1074/jbc.M313916200 (2004).
- 187 Curry, J. E. *et al.* (Google Patents, 2009).
- 188 Traut, T. W. Physiological concentrations of purines and pyrimidines. *Mol Cell Biochem* **140**, 1-22 (1994).
- 189 Zhao, Z. S. & Manser, E. Do PAKs make good drug targets? *F1000 Biol Rep* **2**, 70, doi:10.3410/B2-70 (2010).
- 190 Adams, J. M. & Cory, S. The Bcl-2 apoptotic switch in cancer development and therapy. *Oncogene* **26**, 1324-1337, doi:1210220 [pii] 10.1038/sj.onc.1210220 (2007).
- 191 Akgul, C. Mcl-1 is a potential therapeutic target in multiple types of cancer. *Cell Mol Life Sci* **66**, 1326-1336, doi:10.1007/s00018-008-8637-6 (2009).
- 192 Elmore, S. Apoptosis: a review of programmed cell death. *Toxicol Pathol* **35**, 495-516, doi:10.1080/01926230701320337 (2007).
- 193 Zeiss, C. J. The apoptosis-necrosis continuum: insights from genetically altered mice. *Vet Pathol* **40**, 481-495 (2003).
- 194 Kerr, J. F., Wyllie, A. H. & Currie, A. R. Apoptosis: a basic biological phenomenon with wide-ranging implications in tissue kinetics. *Br J Cancer* **26**, 239-257 (1972).

- 195 Hengartner, M. O. The biochemistry of apoptosis. *Nature* **407**, 770-776, doi:10.1038/35037710 (2000).
- 196 Wyllie, A. H. "Where, O death, is thy sting?" A brief review of apoptosis biology. *Mol Neurobiol* **42**, 4-9, doi:10.1007/s12035-010-8125-5 (2010).
- 197 Leveille, F. *et al.* Suppression of the intrinsic apoptosis pathway by synaptic activity. *J Neurosci* **30**, 2623-2635, doi:10.1523/JNEUROSCI.5115-09.2010 (2010).
- 198 Vaux, D. L., Cory, S. & Adams, J. M. Bcl-2 gene promotes haemopoietic cell survival and cooperates with c-myc to immortalize pre-B cells. *Nature* **335**, 440-442, doi:10.1038/335440a0 (1988).
- 199 Kerr, J. F., Winterford, C. M. & Harmon, B. V. Apoptosis. Its significance in cancer and cancer therapy. *Cancer* **73**, 2013-2026 (1994).
- 200 Czabotar, P. E., Lessene, G., Strasser, A. & Adams, J. M. Control of apoptosis by the BCL-2 protein family: implications for physiology and therapy. *Nat Rev Mol Cell Biol* **15**, 49-63, doi:10.1038/nrm3722 (2014).
- 201 Brunner, T. *et al.* Fas (CD95/Apo-1) ligand regulation in T cell homeostasis, cell-mediated cytotoxicity and immune pathology. *Semin Immunol* **15**, 167-176 (2003).
- 202 Trapani, J. A. & Smyth, M. J. Functional significance of the perforin/granzyme cell death pathway. *Nat Rev Immunol* **2**, 735-747, doi:10.1038/nri911 (2002).
- 203 Shalini, S., Dorstyn, L., Dawar, S. & Kumar, S. Old, new and emerging functions of caspases. *Cell Death Differ* **22**, 526-539, doi:10.1038/cdd.2014.216 (2015).
- 204 Cory, S. & Adams, J. M. The Bcl2 family: regulators of the cellular life-or-death switch. *Nat Rev Cancer* **2**, 647-656, doi:10.1038/nrc883 (2002).
- 205 Tsujimoto, Y., Finger, L. R., Yunis, J., Nowell, P. C. & Croce, C. M. Cloning of the chromosome breakpoint of neoplastic B cells with the t(14;18) chromosome translocation. *Science* **226**, 1097-1099 (1984).
- 206 Petros, A. M., Olejniczak, E. T. & Fesik, S. W. Structural biology of the Bcl-2 family of proteins. *Biochim Biophys Acta* **1644**, 83-94, doi:10.1016/j.bbamcr.2003.08.012 (2004).
- 207 Youle, R. J. & Strasser, A. The BCL-2 protein family: opposing activities that mediate cell death. *Nat Rev Mol Cell Biol* **9**, 47-59, doi:10.1038/nrm2308 (2008).
- 208 Danial, N. N. & Korsmeyer, S. J. Cell death: critical control points. *Cell* **116**, 205-219 (2004).
- 209 Conradt, B. & Horvitz, H. R. The *C. elegans* protein EGL-1 is required for programmed cell death and interacts with the Bcl-2-like protein CED-9. *Cell* **93**, 519-529 (1998).
- 210 Aouacheria, A., Brunet, F. & Gouy, M. Phylogenomics of life-or-death switches in multicellular animals: Bcl-2, BH3-Only, and BNip families of apoptotic regulators. *Mol Biol Evol* **22**, 2395-2416, doi:10.1093/molbev/msi234 (2005).
- 211 Kvensakul, M. & Hinds, M. G. The structural biology of BH3-only proteins. *Methods Enzymol* **544**, 49-74, doi:10.1016/B978-0-12-417158-9.00003-0 (2014).
- 212 Thomas, L. W., Lam, C. & Edwards, S. W. Mcl-1; the molecular regulation of protein function. *FEBS Lett* **584**, 2981-2989, doi:10.1016/j.febslet.2010.05.061 (2010).
- 213 Wilfling, F. *et al.* BH3-only proteins are tail-anchored in the outer mitochondrial membrane and can initiate the activation of Bax. *Cell Death Differ* **19**, 1328-1336, doi:10.1038/cdd.2012.9 (2012).
- 214 Weber, A., Auslander, D. & Hacker, G. Mouse Noxa uses only the C-terminal BH3-domain to inactivate Mcl-1. *Apoptosis* **18**, 1093-1105, doi:10.1007/s10495-013-0868-9 (2013).

- 215 Hinds, M. G. *et al.* Bim, Bad and Bmf: intrinsically unstructured BH3-only proteins that undergo a localized conformational change upon binding to prosurvival Bcl-2 targets. *Cell Death Differ* **14**, 128-136, doi:10.1038/sj.cdd.4401934 (2007).
- 216 Shamas-Din, A., Brahmabhatt, H., Leber, B. & Andrews, D. W. BH3-only proteins: Orchestrators of apoptosis. *Biochim Biophys Acta* **1813**, 508-520, doi:10.1016/j.bbamcr.2010.11.024 (2011).
- 217 Rooswinkel, R. W., van de Kooij, B., Verheij, M. & Borst, J. Bcl-2 is a better ABT-737 target than Bcl-xL or Bcl-w and only Noxa overcomes resistance mediated by Mcl-1, Bfl-1, or Bcl-B. *Cell Death Dis* **3**, e366, doi:10.1038/cddis.2012.109 (2012).
- 218 Chen, L. *et al.* Differential targeting of prosurvival Bcl-2 proteins by their BH3-only ligands allows complementary apoptotic function. *Mol Cell* **17**, 393-403, doi:10.1016/j.molcel.2004.12.030 (2005).
- 219 Moldoveanu, T., Follis, A. V., Kriwacki, R. W. & Green, D. R. Many players in BCL-2 family affairs. *Trends Biochem Sci* **39**, 101-111, doi:10.1016/j.tibs.2013.12.006 (2014).
- 220 Bouillet, P. & Strasser, A. BH3-only proteins - evolutionarily conserved proapoptotic Bcl-2 family members essential for initiating programmed cell death. *J Cell Sci* **115**, 1567-1574 (2002).
- 221 Oda, E. *et al.* Noxa, a BH3-only member of the Bcl-2 family and candidate mediator of p53-induced apoptosis. *Science* **288**, 1053-1058 (2000).
- 222 Kelly, P. N. & Strasser, A. The role of Bcl-2 and its pro-survival relatives in tumourigenesis and cancer therapy. *Cell Death Differ* **18**, 1414-1424, doi:10.1038/cdd.2011.17 (2011).
- 223 Puthalakath, H., Huang, D. C., O'Reilly, L. A., King, S. M. & Strasser, A. The proapoptotic activity of the Bcl-2 family member Bim is regulated by interaction with the dynein motor complex. *Mol Cell* **3**, 287-296 (1999).
- 224 Ploner, C., Kofler, R. & Villunger, A. Noxa: at the tip of the balance between life and death. *Oncogene* **27 Suppl 1**, S84-92, doi:10.1038/onc.2009.46 (2008).
- 225 Sorenson, C. M. Bcl-2 family members and disease. *Biochim Biophys Acta* **1644**, 169-177, doi:10.1016/j.bbamcr.2003.08.010 (2004).
- 226 Krajewski, S. *et al.* Immunohistochemical analysis of Mcl-1 protein in human tissues. Differential regulation of Mcl-1 and Bcl-2 protein production suggests a unique role for Mcl-1 in control of programmed cell death in vivo. *Am J Pathol* **146**, 1309-1319 (1995).
- 227 Yang, T., Kozopas, K. M. & Craig, R. W. The intracellular distribution and pattern of expression of Mcl-1 overlap with, but are not identical to, those of Bcl-2. *J Cell Biol* **128**, 1173-1184 (1995).
- 228 Chou, C. H., Lee, R. S. & Yang-Yen, H. F. An internal EELD domain facilitates mitochondrial targeting of Mcl-1 via a Tom70-dependent pathway. *Mol Biol Cell* **17**, 3952-3963, doi:10.1091/mbc.E06-04-0319 (2006).
- 229 Thomas, L. W. *et al.* Serine 162, an essential residue for the mitochondrial localization, stability and anti-apoptotic function of Mcl-1. *PLoS One* **7**, e45088, doi:10.1371/journal.pone.0045088 (2012).
- 230 Willis, S. N. *et al.* Apoptosis initiated when BH3 ligands engage multiple Bcl-2 homologs, not Bax or Bak. *Science* **315**, 856-859, doi:10.1126/science.1133289 [pii] 10.1126/science.1133289 (2007).
- 231 Lowe, S. W. & Lin, A. W. Apoptosis in cancer. *Carcinogenesis* **21**, 485-495 (2000).

- 232 Beroukhim, R. *et al.* The landscape of somatic copy-number alteration across human
cancers. *Nature* **463**, 899-905, doi:10.1038/nature08822 (2010).
- 233 Wei, G. *et al.* Chemical genomics identifies small-molecule MCL1 repressors and BCL-xL
as a predictor of MCL1 dependency. *Cancer Cell* **21**, 547-562,
doi:10.1016/j.ccr.2012.02.028 (2012).
- 234 Quinn, B. A. *et al.* Targeting Mcl-1 for the therapy of cancer. *Expert Opin Investig Drugs*
20, 1397-1411, doi:10.1517/13543784.2011.609167 (2011).
- 235 Ding, Q. *et al.* Myeloid cell leukemia-1 inversely correlates with glycogen synthase kinase-
3beta activity and associates with poor prognosis in human breast cancer. *Cancer Res* **67**,
4564-4571, doi:10.1158/0008-5472.CAN-06-1788 (2007).
- 236 Rodriguez-Nieto, S. & Zhivotovsky, B. Role of alterations in the apoptotic machinery in
sensitivity of cancer cells to treatment. *Curr Pharm Des* **12**, 4411-4425 (2006).
- 237 Wertz, I. E. *et al.* Sensitivity to antitubulin chemotherapeutics is regulated by MCL1 and
FBW7. *Nature* **471**, 110-114, doi:10.1038/nature09779 (2011).
- 238 van Delft, M. F. *et al.* The BH3 mimetic ABT-737 targets selective Bcl-2 proteins and
efficiently induces apoptosis via Bak/Bax if Mcl-1 is neutralized. *Cancer Cell* **10**, 389-399,
doi:10.1016/j.ccr.2006.08.027 (2006).
- 239 Tahir, S. K. *et al.* Influence of Bcl-2 family members on the cellular response of small-cell
lung cancer cell lines to ABT-737. *Cancer Res* **67**, 1176-1183, doi:10.1158/0008-5472.CAN-
06-2203 (2007).
- 240 Carey, L. A. Directed therapy of subtypes of triple-negative breast cancer. *Oncologist* **16**
Suppl 1, 71-78, doi:10.1634/theoncologist.2011-S1-71 (2011).
- 241 Schmadeka, R., Harmon, B. E. & Singh, M. Triple-negative breast carcinoma: current and
emerging concepts. *Am J Clin Pathol* **141**, 462-477, doi:10.1309/AJCPQN8GZ8SILKGN
(2014).
- 242 Hudis, C. A. & Gianni, L. Triple-negative breast cancer: an unmet medical need. *Oncologist*
16 Suppl 1, 1-11, doi:10.1634/theoncologist.2011-S1-01 (2011).
- 243 Dent, R. *et al.* Triple-negative breast cancer: clinical features and patterns of recurrence.
Clin Cancer Res **13**, 4429-4434, doi:10.1158/1078-0432.CCR-06-3045 (2007).
- 244 McCarthy, N., Mitchell, G., Bilous, M., Wilcken, N. & Lindeman, G. J. Triple-negative breast
cancer: making the most of a misnomer. *Asia Pac J Clin Oncol* **8**, 145-155,
doi:10.1111/j.1743-7563.2012.01533.x (2012).
- 245 O'Toole, S. A. *et al.* Therapeutic targets in triple negative breast cancer. *J Clin Pathol* **66**,
530-542, doi:10.1136/jclinpath-2012-201361 (2013).
- 246 Balko, J. M. *et al.* Molecular profiling of the residual disease of triple-negative breast
cancers after neoadjuvant chemotherapy identifies actionable therapeutic targets.
Cancer Discov **4**, 232-245, doi:10.1158/2159-8290.CD-13-0286 (2014).
- 247 Mitchell, C. *et al.* Inhibition of MCL-1 in breast cancer cells promotes cell death in vitro
and in vivo. *Cancer Biol Ther* **10**, 903-917, doi:10.4161/cbt.10.9.13273 (2010).
- 248 Petrocca, F. *et al.* A genome-wide siRNA screen identifies proteasome addiction as a
vulnerability of basal-like triple-negative breast cancer cells. *Cancer Cell* **24**, 182-196,
doi:10.1016/j.ccr.2013.07.008 (2013).

- 249 Boisvert-Adamo, K., Longmate, W., Abel, E. V. & Aplin, A. E. Mcl-1 is required for melanoma cell resistance to anoikis. *Mol Cancer Res* **7**, 549-556, doi:7/4/549 [pii] 10.1158/1541-7786.MCR-08-0358 (2009).
- 250 Chen, W. *et al.* Acquired activation of the Akt/cyclooxygenase-2/Mcl-1 pathway renders lung cancer cells resistant to apoptosis. *Mol Pharmacol* **77**, 416-423, doi:mol.109.061226 [pii] 10.1124/mol.109.061226 (2010).
- 251 Chetoui, N. *et al.* Down-regulation of mcl-1 by small interfering RNA sensitizes resistant melanoma cells to fas-mediated apoptosis. *Mol Cancer Res* **6**, 42-52, doi:10.1158/1541-7786.MCR-07-0080 (2008).
- 252 Hauck, P., Chao, B. H., Litz, J. & Krystal, G. W. Alterations in the Noxa/Mcl-1 axis determine sensitivity of small cell lung cancer to the BH3 mimetic ABT-737. *Mol Cancer Ther* **8**, 883-892, doi:8/4/883 [pii] 10.1158/1535-7163.MCT-08-1118 (2009).
- 253 Keuling, A. M. *et al.* RNA silencing of Mcl-1 enhances ABT-737-mediated apoptosis in melanoma: role for a caspase-8-dependent pathway. *PLoS One* **4**, e6651, doi:10.1371/journal.pone.0006651 (2009).
- 254 Konopleva, M. *et al.* Mechanisms of apoptosis sensitivity and resistance to the BH3 mimetic ABT-737 in acute myeloid leukemia. *Cancer Cell* **10**, 375-388, doi:S1535-6108(06)00313-8 [pii] 10.1016/j.ccr.2006.10.006 (2006).
- 255 Lucas, K. M. *et al.* Modulation of NOXA and MCL-1 as a strategy for sensitizing melanoma cells to the BH3-mimetic ABT-737. *Clin Cancer Res* **18**, 783-795, doi:1078-0432.CCR-11-1166 [pii] 10.1158/1078-0432.CCR-11-1166 (2012).
- 256 Moulding, D. A. *et al.* Apoptosis is rapidly triggered by antisense depletion of MCL-1 in differentiating U937 cells. *Blood* **96**, 1756-1763 (2000).
- 257 Qin, J. Z., Xin, H., Sitailo, L. A., Denning, M. F. & Nickoloff, B. J. Enhanced killing of melanoma cells by simultaneously targeting Mcl-1 and NOXA. *Cancer Res* **66**, 9636-9645, doi:66/19/9636 [pii] 10.1158/0008-5472.CAN-06-0747 (2006).
- 258 Thallinger, C. *et al.* Mcl-1 antisense therapy chemosensitizes human melanoma in a SCID mouse xenotransplantation model. *J Invest Dermatol* **120**, 1081-1086, doi:12252b [pii] 10.1046/j.1523-1747.2003.12252.x (2003).
- 259 Zhang, H. *et al.* Mcl-1 is critical for survival in a subgroup of non-small-cell lung cancer cell lines. *Oncogene* **30**, 1963-1968, doi:10.1038/onc.2010.559 (2011).
- 260 Xu, H. & Krystal, G. W. Actinomycin D decreases Mcl-1 expression and acts synergistically with ABT-737 against small cell lung cancer cell lines. *Clin Cancer Res* **16**, 4392-4400, doi:1078-0432.CCR-10-0640 [pii] 10.1158/1078-0432.CCR-10-0640 (2010).
- 261 Olberding, K. E. *et al.* Actinomycin D synergistically enhances the efficacy of the BH3 mimetic ABT-737 by downregulating Mcl-1 expression. *Cancer Biol Ther* **10**, 918-929, doi:13274 [pii] 10.4161/cbt.10.9.13274 (2010).
- 262 Inuzuka, H. *et al.* Mcl-1 ubiquitination and destruction. *Oncotarget* **2**, 239-244, doi:242 [pii] (2011).
- 263 Zhou, P. *et al.* MCL1 transgenic mice exhibit a high incidence of B-cell lymphoma manifested as a spectrum of histologic subtypes. *Blood* **97**, 3902-3909 (2001).
- 264 Heere-Ress, E. *et al.* Bcl-X(L) is a chemoresistance factor in human melanoma cells that can be inhibited by antisense therapy. *Int J Cancer* **99**, 29-34 (2002).

- 265 Colak, S. *et al.* Decreased mitochondrial priming determines chemoresistance of colon cancer stem cells. *Cell Death Differ* **21**, 1170-1177, doi:10.1038/cdd.2014.37 (2014).
- 266 Zhang, H. *et al.* Genomic analysis and selective small molecule inhibition identifies BCL-XL as a critical survival factor in a subset of colorectal cancer. *Mol Cancer* **14**, 126, doi:10.1186/s12943-015-0397-y (2015).
- 267 Billard, C. BH3 mimetics: status of the field and new developments. *Mol Cancer Ther* **12**, 1691-1700, doi:10.1158/1535-7163.MCT-13-0058 (2013).
- 268 Gandhi, L. *et al.* Phase I study of Navitoclax (ABT-263), a novel Bcl-2 family inhibitor, in patients with small-cell lung cancer and other solid tumors. *J Clin Oncol* **29**, 909-916, doi:10.1200/JCO.2010.31.6208 (2011).
- 269 Vogler, M., Dinsdale, D., Dyer, M. J. & Cohen, G. M. Bcl-2 inhibitors: small molecules with a big impact on cancer therapy. *Cell Death Differ* **16**, 360-367, doi:10.1038/cdd.2008.137 (2009).
- 270 Rudin, C. *et al.* Patient Outcome and Exploratory Analysis from a Phase 2a Study of Navitoclax (Abt-263) in Patients with Advanced/Relapsed Small Cell Lung Cancer (SclC). *J Thorac Oncol* **6**, S644-S645 (2011).
- 271 Yecies, D., Carlson, N. E., Deng, J. & Letai, A. Acquired resistance to ABT-737 in lymphoma cells that up-regulate MCL-1 and BFL-1. *Blood* **115**, 3304-3313, doi:10.1182/blood-2009-07-233304 (2010).
- 272 Vaillant, F. *et al.* Targeting BCL-2 with the BH3 mimetic ABT-199 in estrogen receptor-positive breast cancer. *Cancer Cell* **24**, 120-129, doi:10.1016/j.ccr.2013.06.002 (2013).
- 273 Goldsmith, K. C. *et al.* BH3 response profiles from neuroblastoma mitochondria predict activity of small molecule Bcl-2 family antagonists. *Cell Death Differ* **17**, 872-882, doi:10.1038/cdd.2009.171 (2010).
- 274 Morales, A. A. *et al.* Distribution of Bim determines Mcl-1 dependence or codependence with Bcl-xL/Bcl-2 in Mcl-1-expressing myeloma cells. *Blood* **118**, 1329-1339, doi:10.1182/blood-2011-01-327197 (2011).
- 275 Zhang, Z. *et al.* An antiapoptotic Bcl-2 family protein index predicts the response of leukaemic cells to the pan-Bcl-2 inhibitor S1. *Br J Cancer* **108**, 1870-1878, doi:10.1038/bjc.2013.152 (2013).
- 276 Lessene, G., Czabotar, P. E. & Colman, P. M. BCL-2 family antagonists for cancer therapy. *Nat Rev Drug Discov* **7**, 989-1000, doi:10.1038/nrd2658 (2008).
- 277 Levenson, J. D. *et al.* Potent and selective small-molecule MCL-1 inhibitors demonstrate on-target cancer cell killing activity as single agents and in combination with ABT-263 (navitoclax). *Cell Death Dis* **6**, e1590, doi:10.1038/cddis.2014.561 (2015).
- 278 Lei, X. *et al.* Gossypol induces Bax/Bak-independent activation of apoptosis and cytochrome c release via a conformational change in Bcl-2. *FASEB J* **20**, 2147-2149, doi:10.1096/fj.05-5665fje (2006).
- 279 Vogler, M. *et al.* Different forms of cell death induced by putative BCL2 inhibitors. *Cell Death Differ* **16**, 1030-1039, doi:10.1038/cdd.2009.48 (2009).
- 280 Cohen, N. A. *et al.* A competitive stapled peptide screen identifies a selective small molecule that overcomes MCL-1-dependent leukemia cell survival. *Chem Biol* **19**, 1175-1186, doi:10.1016/j.chembiol.2012.07.018 (2012).

- 281 Abulwerdi, F. *et al.* A novel small-molecule inhibitor of mcl-1 blocks pancreatic cancer growth in vitro and in vivo. *Mol Cancer Ther* **13**, 565-575, doi:10.1158/1535-7163.MCT-12-0767 (2014).
- 282 Varadarajan, S. *et al.* Evaluation and critical assessment of putative MCL-1 inhibitors. *Cell Death Differ* **20**, 1475-1484, doi:10.1038/cdd.2013.79 (2013).
- 283 Doi, K. *et al.* Discovery of Marinopyrrole A (Maritoclax) as a Selective Mcl-1 Antagonist that Overcomes ABT-737 Resistance by Binding to and Targeting Mcl-1 for Proteasomal Degradation. *Journal of Biological Chemistry* **287**, 10224-10235, doi:DOI 10.1074/jbc.M111.334532 (2012).
- 284 Eichhorn, J. M., Alford, S. E., Hughes, C. C., Fenical, W. & Chambers, T. C. Purported Mcl-1 inhibitor marinopyrrole A fails to show selective cytotoxicity for Mcl-1-dependent cell lines. *Cell Death & Disease* **4**, doi:ARTN e880 DOI 10.1038/cddis.2013.411 (2013).
- 285 Varadarajan, S. *et al.* Maritoclax and dinaciclib inhibit MCL-1 activity and induce apoptosis in both a MCL-1-dependent and -independent manner. *Oncotarget* **6**, 12668-12681 (2015).
- 286 Opferman, J. *Personal communication.*
- 287 Pandey, M. K. *et al.* Proteasomal degradation of Mcl-1 by maritoclax induces apoptosis and enhances the efficacy of ABT-737 in melanoma cells. *PLoS One* **8**, e78570, doi:10.1371/journal.pone.0078570 (2013).
- 288 Albershardt, T. C. *et al.* Multiple BH3 mimetics antagonize antiapoptotic MCL1 protein by inducing the endoplasmic reticulum stress response and up-regulating BH3-only protein NOXA. *J Biol Chem* **286**, 24882-24895, doi:10.1074/jbc.M111.255828 (2011).
- 289 Zhong, J. T. *et al.* The BH3 mimetic S1 induces autophagy through ER stress and disruption of Bcl-2/Beclin 1 interaction in human glioma U251 cells. *Cancer Lett* **323**, 180-187, doi:10.1016/j.canlet.2012.04.009 (2012).
- 290 Richard, D. J. *et al.* Hydroxyquinoline-derived compounds and analoguing of selective Mcl-1 inhibitors using a functional biomarker. *Bioorg Med Chem* **21**, 6642-6649, doi:10.1016/j.bmc.2013.08.017 (2013).
- 291 Bruncko, M. *et al.* Structure-guided design of a series of MCL-1 inhibitors with high affinity and selectivity. *J Med Chem* **58**, 2180-2194, doi:10.1021/jm501258m (2015).
- 292 Xiao, Y. *et al.* MCL-1 Is a Key Determinant of Breast Cancer Cell Survival: Validation of MCL-1 Dependency Utilizing a Highly Selective Small Molecule Inhibitor. *Mol Cancer Ther*, doi:10.1158/1535-7163.MCT-14-0928 (2015).
- 293 Nikolovska-Coleska, Z. *et al.* Development and optimization of a binding assay for the XIAP BIR3 domain using fluorescence polarization. *Analytical Biochemistry* **332**, 261-273, doi:10.1016/j.ab.2004.05.055 (2004).
- 294 Motif, A. *FP Diagram Animated*,
<http://www.activemotif.com/images/products/FP_diagram_animated.gif> (
- 295 Lessene, G. *et al.* Structure-guided design of a selective BCL-X(L) inhibitor. *Nat Chem Biol* **9**, 390-397, doi:10.1038/nchembio.1246 (2013).
- 296 Ryan, J. & Letai, A. BH3 profiling in whole cells by fluorimeter or FACS. *Methods* **61**, 156-164, doi:10.1016/j.ymeth.2013.04.006 (2013).

- 297 Certo, M. *et al.* Mitochondria primed by death signals determine cellular addiction to antiapoptotic BCL-2 family members. *Cancer Cell* **9**, 351-365, doi:10.1016/j.ccr.2006.03.027 (2006).
- 298 Foight, G. W., Ryan, J. A., Gulla, S. V., Letai, A. & Keating, A. E. Designed BH3 peptides with high affinity and specificity for targeting Mcl-1 in cells. *ACS Chem Biol* **9**, 1962-1968, doi:10.1021/cb500340w (2014).
- 299 Abulwerdi, F. A. *et al.* 3-Substituted-N-(4-hydroxynaphthalen-1-yl)arylsulfonamides as a novel class of selective Mcl-1 inhibitors: structure-based design, synthesis, SAR, and biological evaluation. *J Med Chem* **57**, 4111-4133, doi:10.1021/jm500010b (2014).
- 300 Eichhorn, J. M., Sakurikar, N., Alford, S. E., Chu, R. & Chambers, T. C. Critical role of anti-apoptotic Bcl-2 protein phosphorylation in mitotic death. *Cell Death Dis* **4**, e834, doi:10.1038/cddis.2013.360 (2013).
- 301 Tse, C. *et al.* ABT-263: a potent and orally bioavailable Bcl-2 family inhibitor. *Cancer Res* **68**, 3421-3428, doi:10.1158/0008-5472.CAN-07-5836 (2008).
- 302 Souers, A. J. *et al.* ABT-199, a potent and selective BCL-2 inhibitor, achieves antitumor activity while sparing platelets. *Nat Med* **19**, 202-208, doi:10.1038/nm.3048 (2013).
- 303 N, C. T. M. CompuSyn for Drug Combinations: PC Software and User's Guide: A Computer Program for Quantitation of Synergism and Antagonism in Drug Combinations, and the Determination of IC50 and ED50 and LD50 Values. *ComboSyn Inc, Paramus, (NJ)* (2005).
- 304 Neve, R. M. *et al.* A collection of breast cancer cell lines for the study of functionally distinct cancer subtypes. *Cancer Cell* **10**, 515-527, doi:10.1016/j.ccr.2006.10.008 (2006).
- 305 Tromp, J. M. *et al.* Tipping the Noxa/Mcl-1 balance overcomes ABT-737 resistance in chronic lymphocytic leukemia. *Clin Cancer Res* **18**, 487-498, doi:10.1158/1078-0432.CCR-11-1440 (2012).
- 306 Deng, J. *et al.* BH3 profiling identifies three distinct classes of apoptotic blocks to predict response to ABT-737 and conventional chemotherapeutic agents. *Cancer Cell* **12**, 171-185, doi:10.1016/j.ccr.2007.07.001 (2007).
- 307 Glaser, S. P. *et al.* Anti-apoptotic Mcl-1 is essential for the development and sustained growth of acute myeloid leukemia. *Genes Dev* **26**, 120-125, doi:10.1101/gad.182980.111 (2012).
- 308 Al-Harbi, S. *et al.* An antiapoptotic BCL-2 family expression index predicts the response of chronic lymphocytic leukemia to ABT-737. *Blood* **118**, 3579-3590, doi:10.1182/blood-2011-03-340364 (2011).
- 309 Hajduk, P. J., Huth, J. R. & Tse, C. Predicting protein druggability. *Drug Discov Today* **10**, 1675-1682, doi:10.1016/S1359-6446(05)03624-X (2005).